# NOTE TO USERS

# A STUDY OF HAND-HANDLE INTERACTIONS AND HAND-ARM

# BIODYNAMIC RESPONSE TO VIBRATION

Yasser Saed Aldien

A Thesis

in

The department

of

Mechanical and Industrial Engineering

Presented in Partial Fulfillment of the Requirements
for the Degree of Doctor of Philosophy at
Concordia University
Montreal, Quebec, Canada

September, 2005

Library and
Archives Canada

Bibliothèque et
Archives Canada

Published Heritage
Branch

Direction du
Patrimoine de l'édition

395 Wellington Street
Ottawa ON K1A 0N4
Canada

395, rue Wellington
Ottawa ON K1A 0N4
Canada

# Canada

# ABSTRACT

## A STUDY OF HAND-HANDLE INTERACTIONS AND HAND-ARM BIODYNAMIC RESPONSE TO VIBRATION

Yasser Saed Aldien, Ph.D.
Concordia University, 2005

Hand-arm vibration syndrome (HAVS) is the term often used for the symptoms associated with prolonged occupational exposure to hand-arm vibration arising from hand-held power tools. The human hand and arm response to vibration has been widely investigated in terms of force-motion relationships at the hand-handle interface. Owing to the complex nature of the biological system, the reported data suggest inconsistent contributions due to various intrinsic and extrinsic factors. Furthermore, the injury risk posed by exposure to hand-tool vibration is strongly related to the hand-handle contact force. This dissertation research concerns with the study of hand-handle interactions under static and dynamic grasping of different handles, and characterization of hand-arm biodynamic response to vibration. The hand-handle interactions in static grasping task were characterized for various hand force combinations through measurement of interface pressure distributions using a flexible capacitive pressure sensing grid. The pressure peaks were assessed in view of known pressure discomfort threshold and sustained pressure values. The results suggest that pressure developed in the thenar eminence, when grasping a large size handle, could exceed the discomfort threshold. The hand-forces were defined in terms of independent grip and push forces, and hand-handle coupling and contact forces. The measured data were used to propose regression models for estimating contact force and interface peak pressure from directly measurable grip and push forces as a function of the handle size.

iii

The biodynamic responses of the human hand-arm system exposed to $x_h$- and $z_h$-axes vibration were characterized in terms of driving-point mechanical impedance and dissipated power. The experiments were designed to study the influences of various intrinsic and extrinsic factors, namely handle geometry, posture, magnitude and direction of vibration and hand forces. Both biodynamic responses were found to be better correlated with the coupling force below 200 Hz, and with the contact force at higher frequencies under $z_h$-axis of vibration. Apart from the experimental observations, the high significance of majority of the main factors was supported by multi-factor ANOVA. The effects of handle size, and push and grip forces on the biodynamic responses of the human hand-arm exposed to vibration were observed to be more significant for the extended forearm posture than that for the bent-elbow posture. The effects were far more significant for the extended arm posture, which revealed considerably higher coupling with the vibrating handle. This posture also resulted in considerably higher power absorption than the bent forearm posture. The spectra of power dissipated showed strong influences of direction and magnitude of vibration, and posture. The results further showed that the frequency content of the dissipated energy differ considerably from the current frequency-weighting function.

A new approach for modeling the hand-arm system is proposed on the basis of both the *DPMI* and absorbed power responses. Four different model structures are proposed and analyzed to characterize the biodynamic responses as function of hand forces. The two and three-DOF model structures were found to provide reasonably good predictions of both responses over a wide range of hand forces.

# ACKNOWLEDGEMENT

# TABLE OF CONTENTS

# LIST OF FIGURES

xvii

# LIST OF TABLES

# LIST OF ABBREVIATIONS

| | | | |
|---|---|---|---|
| $A_c$ | Interface contact area | g | Gram |
| ANOVA | Analysis of variance | $G_{Fv}$ | Cross spectral density of force and velocity. |
| $APMS$ | Apparent mass | $G_{vv}$ | Power spectral density of velocity |
| $a_{h,w}$ | Frequency-weighted acceleration | HAV | Hand-arm vibration |
| $c$ | Damping coefficient | HTV | Hand transmitted vibration |
| $CF$ | Coupling force | Hz | Hertz |
| $CFR$ | Contact force ratio | ISO | International Standards Organization |
| $CFZ_j$ | Contact force in zone $J$ | kg | Kilogram |
| COV | Coefficients of variation | kPa | kilo Pascal |
| $D$ | Handle diameter | m | meter |
| DOF | Degrees-of-freedom | $m$ | mass |
| $DPMI$ | Derive-point mechanical impedance | N | Newton |
| $F$ | Dynamic force at driving point | $PDT$ | Pressure discomfort threshold |
| $F_c$ | Contact force | $PPT$ | Pressure pain threshold |
| $F_g$ | Grip force | $r^2$ | Correlation coefficient |
| $F_p$ | Push force | SD | Standard deviation |

| | |
|---|---|
| *SP* | Sustained pressure |
| W | Watt |
| $x_h, y_h, z_h$ | Directions of vibration |
| $Z$ | Hand zone |
| $\Delta A$ | Sensor area |
| $\phi_h$ | Roll motion |
| $\theta_h$ | Yaw motion |
| $\varphi_h$ | Pitch motion |
| $\omega$ | Circular frequency |
| $\xi$ | Damping ratio |
| $\sigma$ | Standard Deviation |

# CHAPTER 1

## INTRODUCTION AND SCOPE OF THE DISSTERATION

1.1    General

In 1862 a French physician, Dr. Maurice Raynaud, identified a condition, presently referred to as "Raynaud's phenomenon", where an episodic spasm or intermittent constriction of peripheral vessels of an extremity in which a blanching of the fingertips occurred with exposure to the cold. Dr. Alice Hamilton in 1911 reported similar symptoms among workers exposed to vibrating tools in North America. This study concluded that exposure to combinations of vibration and cold temperatures, and poor workplace ergonomics were responsible for the vibration white fingers disorder, and that the affected areas are asymmetrically distributed on the hands (Brammer, 1984; Pelmear et al., 1998). The operators of hand-held power tools such as pneumatic drills, jackhammers, asphalt breakers, power chain saws, chipping tools, concrete vibrators, sanders; angle grinders and riveters, which are commonly used in several industries, are exposed to comprehensive levels of hand-transmitted vibration (HTV) arising from the tool-work piece-hand interactions. These high amplitude vibrations predominate in a wide frequency range, 10-2000 Hz, and are often limited to the hand-arm of the operators. Continual use of vibrating hand tools can cause several kinds of injuries to the hands and arms, which are collectively known as hand-arm vibration syndrome (HAVS) or as Raynaud's phenomenon of occupational origin (Gemme and Taylor, 1983).

The symptoms of HAVS develop in a gradual manner, and involve a number of years of occupational exposure to hand-transmitted vibration. The occupational vibration is a difficult hazard to recognize in its first stage, and is not as apparent as other potential

workplace hazards, such as toxic chemicals or fumes. A considerable lapse of time may exist between the first use of vibrating tool and the first appearance of any of the symptoms, which is designated as the latent period (Miyashita et al., 1983; Fridén, 2001). The most common and serious among the diseases caused by prolonged vibration exposure could be the vibration white finger (VWF) disease.

A study conducted by National Institute for Occupational Safety and Health – NIOSH- (1989) estimated that approximately 1.45 million workers in the USA were subject to some risks for developing HAVS. The prevalence of HAVS ranged from 6% to 100%, with an average of approximately 50%. In Canada, an estimate reported by National Research Council (1984) indicated that approximately 200,000 workers were exposed to hand-arm vibration. A study was performed in northern Ontario to determine the prevalence of hand-arm vibration syndrome (HAVS) in 617 workers at a base metal mine. Workers who were employed at the mine between 1989 and 1994 and who continued to live within a 100 km radius of the mine were sent a self-reported questionnaire to identify individuals with possible vibration-induced symptoms in their upper extremities. Of the 162 workers who attended a medical examination, 50% were diagnosed with HAVS and 26% showed other multiple afflictions e.g., both HAVS and carpal tunnel syndrome (CTS). None of the vibration-induced symptoms were reported in the 35% of the workers (Hill et al., 2001).

Operation of some of the hand tools demands high hand forces or hand-handle contact force, which is known to be one of the primary factors that increase the risk of cumulative trauma disorders (Radwin et al., 1987; Rempel et al.; 1992; Reidel, 1995). Many studies have suggested that the contact force between the hand and a tool handle

2

affect the severity of exposure to the hand-transmitted vibration and hand-wrist cumulative trauma disorders (Fransson and Winkel, 1991; Pyykkö et al., 1976; Radwin et al., 1987). High contact forces impose high stresses on the anatomical structure of the hand, which may be strongly affected by many factors, such as working posture, grip and push forces, handle size and hand-handle interface pressure. Existence of a high pressure on the surface of the hand, arising from grasping and guiding a tool handle, could cause a sense of discomfort or pain under sustained loading, which is often a limiting factor during work and may lead to potential impending tissue damage (Muralidhar and Bishu, 2000; Johansson et al., 1999). High local pressure at the hand surface could also cause impaired blood circulation in the hand of the operator of hand power tools.

In view of the potentially severe health effect of hand-arm exposure to vibration, extensive efforts have been made to study the phenomenon and the major contributory factors (Gemne, 1997; Fridén, 2001; ISO-5349, 2001; Gurram et al. 1995; Burström, 1994). The studies have concentrated in medical aspects and hand-arm syndromes etiology, dose-response standards, and biodynamic response of the human hand-arm system under vibration in order to develop better assessment methods and prevention strategies. These studies have clearly established the strong roles of many contributing factors related to the tool design, operating conditions and physiology. The effects of most of these contributing factors, however, have not been clearly quantified. This dissertation research concerns with the study of the effects of various tool and operating conditions related factors on the hand-handle contact force/pressure, and biodynamic responses of the hand-arm system in terms of driving-point mechanical impedance and

3

dissipated energy. The factors include the handle size and shape, grip and push forces, operating hand-arm posture, and magnitude of hand-transmitted vibration.

In this chapter the related reported studies on symptoms of prolonged exposure to hand-arm vibration, factors affecting the hand transmitted vibration (HTV), the risk assessment of HTV, the relationship between contact force and musculoskeletal loads, hand-arm biodynamic response to vibration and mathematical biodynamic modeling of human hand-arm system are briefly reviewed, to formulate the scope of the dissertation research.

## 1.2    Symptoms of Prolonged Exposure to Hand-Transmitted Vibration

Many epidemiological and clinical studies have focused on the effects and consequences of prolonged exposure to hand-transmitted vibration (Brammer et al., 1982). The term hand-arm vibration (HAV) syndrome is commonly used to refer to signs and symptoms associated with exposure to hand-transmitted vibration, these symptoms could be grouped under four categories as: (a) Vascular disorders; (b) Bone and joint disorders; (c) Neurological disorders; and (d) Muscular effects. These symptoms, arising from exposure to vibration and/or cold, are known to affect the performance and dexterity of the workers in an adverse manner, and in some cases the affected worker are forced to change their professions.

### 1.2.1    Vascular disorders

Although HAVS relates to the disorders of the peripheral neurological and vascular systems, musculoskeletal structure, bones and joints, and the central nervous system, the vascular component is the most easily observed component. The vascular effects and

4

symptoms of hand-transmitted vibration have been most widely investigated, studied and documented over the other components, while some disorders and symptoms associated with HAVS have been the subjects of discussions and debates whether they are directly associated with vibration exposure or other work conditions. The reported studies have clearly established that vascular disorders are definitely related to vibration impinging into the hand-arm system (Griffin, 1990; Bovenzi, 1997; Chetter et al. 1997). All the components of the HAVS, however, appear to be coupled in their mechanisms, and occur in a certain sequence with varying degree of severity, depending on the nature of vibration exposure and individual's conditions (Bovenzi, 1990).

The vascular symptoms in the reported studies have used many synonyms to describe vibration-induced vascular disorders, namely, dead or white finger, Raynaud's phenomenon of occupational origin, and, more recently, vibration-induced white finger (VWF) (Bovenzi et al., 2000). The vascular symptoms are the most thoroughly investigated symptoms related to HAV (Palmer et al. 2001). Clinically, VWF is characterized by episodes of white or pale fingers caused by spastic closure of the digital arteries (Bovenzi, 1993). Blanching is generally accompanied by numbness and reduced sensitivity of one or more fingers. These attacks are particularly common in the morning when metabolic activity is low, and tend to be more frequent in winter (Chetter et al., 1997). In the early stages, many of the symptoms of vibration syndrome, fatigue and muscular pain in the arms and shoulders will disappear shortly after a worker stops using the types of tools, which transmit vibration to the hands and arms (Griffin, 1990). With continued exposure to vibration the attacks tend to become more frequent, prolonged, and eventually could occur in all seasons. The fingers exposed to most vibration are affected

5

first, but all the fingers may gradually become affected at the late stage (Fridén, 2001). The attacks are usually triggered by cold and last from 5 to 30 to 40 minutes. A complete loss of tactile sensitivity may be experienced during an attack (Bovenzi, 1997). During VWF attacks, blood flow to the affected segments of the fingers is reduced or completely shut-off by contraction of the muscles, resulting in severe pain (Pyykkö, 1986).

A grading scale for the classification of VWF has been proposed at the Stockholm Workshop (1987), which clarifies the stages of VWF on the basis of frequency and severity of repeated attacks (Pelmear et al., 1998). Occasional white finger attacks affecting the tips and middle region of one or more fingers are referred to as stages 1 and 2 that relate to presence of mild and moderate symptoms (Table 1.1). More frequent attacks affecting all phalanges of most fingers are termed as more severe symptoms, classified as stage 3. Stage 4 is distinguished by the presence of trophic skin changes (Pelmear et al., 1998). In the recovery phase, commonly accelerated by warmth or local massage, redness may appear in the affected fingers as a result of a reactive increase of blood flow in the cutaneous vessels. Trophic skin changes may rarely occur in the later stages (Chetter et al., 1997).

1.2.2  Bone and joint disorders

Injuries to bones, such as cysts, vacuoles and an over-representation of carpal bone vacuoles, scaphoid fracture non-union and wrist joint arthrosis after long-term exposure to vibration have been reported by several investigators (Gemne and Srarste, 1987; Bovenzi, 1990; Gemne, 1997). Gemne and Srarste (1987) have conducted an extensive meta-analysis of the documented radiological bone and joint pathology in the hand and arms of workers using vibrating tools, and concluded that use of low frequency

6

pneumatic percussive tools (dominant vibration frequency lower that 40 Hz) may cause higher than normal prevalence of wrist and elbow osteroarthrosis. On the other hand, some investigators have claimed that the changes observed after vibration exposure are the same as those found due to the ageing process and to heavy manual work (Taylor et al., 1984).

Table 1.1. The Stockholm Workshop classification scale for VWF.

| Stage | Grade | Description |
|-------|-------|-------------|
| 0 | none | No attacks |
| 1 | Mild | Occasional attacks affecting only the tips of one or more fingers. |
| 2 | Moderate | Occasional attacks affecting finger tips and middle of the finger and rarely also the finger parts close to the palm. |
| 3 | Severe | Frequent attacks affecting most fingers |
| 4 | Very Severe | Same symptoms as in stage 3 with degenerate skin changes in the finger |

1.2.3 Muscular effects

Vibration-exposed workers may complain of muscle weakness and pain in the hands and arms. In some individuals, muscle fatigue can cause a work disability. Some work-related disorders have been reported in vibration-exposed workers, such as tendinitis and tenosynovitis in the upper limbs, and Dupuytren's contracture, a disease of the fascial tissue of the palm of the hand. These disorders seem to be related to ergonomic stress factors arising from heavy manual work, and the association with hand-transmitted

vibration is not conclusive (Bovenzi, 1990). There is overwhelming evidence that long-term exposure to vibration may cause muscular dysfunction, as evidenced by both reduced muscle force and endurance (Pyykkö, 1986). Banister and Smith (1972) showed that the users of vibrating tools suffer from significant decrease in manipulative skill and grip strength. A recent study (Necking et al., 2004) has shown that thenar muscles are affected by long-term vibration exposure from hand-held tools. The observed muscular abnormalities could explain the common subjective experience of hand weakness reported by those affected be HAVS. The observed muscle necrosis, fibrosis and structural disorganization are suggestive of direct muscle damage (Necking et al., 2004).

Electromyography (EMG- the graphing of electrical activity of a muscle) techniques have been used for better understanding of skeletal muscle responses to work tasks, estimation of muscle loading with activity and intramuscular pressure generation, and to comprehend the development of muscle fatigue (Li, 2002), and to study the activities of various hand-arm muscles under different static and dynamic conditions (Gurram el al., 1995). The EMG relates to the stress state of a muscle and provides significant insight to the muscle dynamics under different loading conditions. EMG in percent of maximal voluntary contraction (%MVC) has been employed for comparing the consequences of major work conditions (Moore and Garg, 1994; Lee and Jiang, 1999).

Operation of some of the power hand tools demands high grip, push or hand-handle contact force, which is known to be one of the primary factors that increase the muscular disorders. High contact forces impose high stresses on the anatomical structure of the hand, which may be strongly affected by many factors, such as working posture, weight of the tool, grip and push forces, handle size, individual work habits and hand-handle

interface pressure (Björing et al., 2002). Existence of a high pressure on the surface of the hand, arising from grasping and guiding a tool handle, could cause a sense of discomfort or pain under sustained loading, which is often a limiting factor during work and may lead to potential impending tissue and muscle damage (Muralidhar and Bishu, 2000). The grasping and guiding of a tool handle yields highly uneven distribution of forces at the hand surface (Gurram et al. 1995), which could vary considerably with hand and handle sizes, push and grip forces and nature of vibration.

## 1.2.4 Neurological disorders

There is clear evidence that work with vibratory tools can result in a wide variety of neurological disorders (Bovenzi, 1997; Nilsson and Lundström 2001). The sensory manifestations of HAVS include episodic tingling, numbness, paraesthesiae, poor co-ordination and, quite commonly, the pain. In the more advanced stages, intermittently or persistently reduced sensory perception, tactile discrimination and manipulative dexterity can occur (Fridén, 2001). Numbness, which occurs with the blanching of the fingers, may persist with decreased tactile and temperature sensitivity to a lesser or greater degree between attacks in subjects more severely affected with the neurological rather than the vascular component (Pelmear et al., 1998). Vibration-exposed workers may exhibit increased vibratory, thermal and tactile thresholds in clinical examinations (Bovenzi, 1997). It has been suggested that continuous vibration exposure can not only depress the excitability of skin receptors but also induce pathological changes in the digital nerves, such as perineural oedema, followed by fibrosis and nerve fibre loss (Bovenzi, 1990). However, there are currently no established means of predicting neurological disorders from the severity of exposures to hand-transmitted vibration (Griffin, 1990).

## 1.3    Contact Force and Musculoskeletal Problems

The operators of power hand-tools apply different levels of push and/or grip forces to the tool handle depending on the nature of the task, body posture and the type of tool. The grip force $F_g$ is the clamp-like force exerted by the hand when enclosing a handle, which is compensated within the hand by a gripping action acting in the opposite direction towards a dividing plane. The push force $F_p$ is the force exerted by the hand away from the operator's shoulder towards the work surface, which is not compensated within the contacting surface of the hand.

The working draft ISO/CD 15230 (2004), Reidel (1995) and Kaulbars (1996) define the hand-handle coupling force as a direct summation of the push and grip forces. While the contact force is defined as the sum of the distributed normal force at the hand–handle interface surrounding the handle as shown in Figure 1.1. The grip and push forces are simply the summation of the vector projections of the distributed contact force components along a specific axis of the handle at two different sides of the handle, as shown in the Figure. The resultant hand-handle contact force could be considered as a good measure of the hand force.
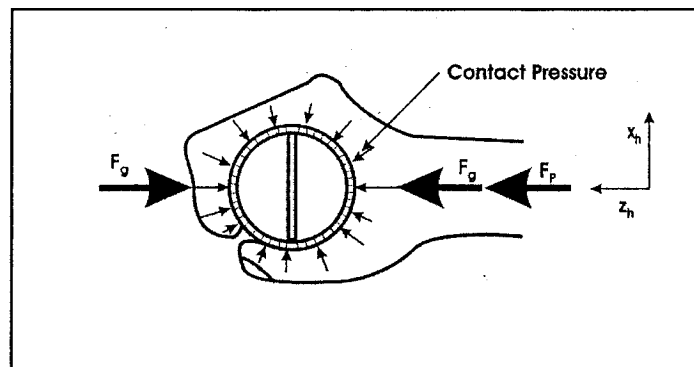


Figure 1.1: Definition of grip, push and contact forces.

10

There are many work related factors which could promote the development of musculoskeletal disorders such as job assignment, duration of vibration exposure, work style, repetitive hand/wrist flexion or extension on the affected side, high force hand/wrist tasks, awkward hand-arm posture, regular use of vibrating hand tools and anthropometric mismatches (Bernard, 1997). Kilbom et al. (1993) described three critical task demands that should be identified for ergonomic evaluations, when using hand-powered tools: (1) force requirements, (2) precision requirements, and (3) duration of a given task. National Research Council report (2001) has concluded that the work-related musculoskeletal disorders are associated with one or more work-related risk factors (force, posture and motion, vibration, and cold). Operation of some of the hand-held power tools demands high grip and push forces or hand-handle contact force, which is known to be one of the primary factors that increase the risk of cumulative trauma disorders (Radwin et al., 1987; Rempel et al., 1992; Reidel, 1995). The carpal tunnel syndrome (CTS) is one of the most known occupationally-related musculoskeletal disorders, which comprises a group of symptoms in the hand that arise from the presence of high pressure on one of the nerves which passes through the palm side of the wrist. The early symptoms are similar to those of the white finger and consist of tingling in the fingers. For the most part, only the thumb, index, and middle fingers are affected in CTS. Later, symptoms can progress to numbness. Pain in the wrist and fingers, clumsiness and muscle atrophy of the hand may also develop.

The literature relating occupational factors to the development of CTS has been widely reviewed by many authors (Armstrong et al. 1993; Kuorinka and Forcier 1995; Moore, 1992). Most of the reviews have concluded that work factors are one of the

important causes of CTS. According to a NIOSH (1997) review of thirty studies on the occupational factors associated with CTS, there is strong evidence of a positive association between exposure to a combination of occupational risk factors (e.g., force and repetitive work, force and posture) and CTS. Additionally, the review indicated that there is evidence of a positive association between CTS and either work-related repetition or force alone.

Chiang et al. (1993) studied 207 workers from eight fish processing factories in Taiwan. CTS was defined on the basis of symptoms and positive physical examination findings, while ruling out systemic diseases and injuries. CTS prevalence for the overall study group was 14.5%. The study found that the hand forceful work is statistically significant in predicted CTS. Roquelaure et al. (1997) evaluated non-occupational and occupational factors associated with CTS of the 65 identified cases. The medical history and household activities of the workers, the ergonomic and organizational characteristics of the job were analyzed. Exertion of force was statistically associated with CTS, and it was concluded that a number of risk factors accumulated by the workers form the major determinant of CTS. A review of several epidemiologic studies involving relationships between different work factors and hand/wrist tendonitis suggests strong evidence of an association between work requiring forceful exertions, in combination with other job risk factors, and hand/wrist tendonitis (Rosecrance and Cook, 1998). EMG has been the major quantitative measure of muscular efforts in studying the cumulative trauma disorders (CTS). Electromyography measurements have been extensively used to estimate the hand force, grip strength and optimum handle size (Ayoub and Presti, 1971).

The mechanisms leading to risk of hand-wrist cumulative trauma disorders have not been identified. High contact forces impose high stresses on the anatomical structure of the hand, which may be strongly affected by many factors, such as working posture, weight of the tool, grip and push forces, handle size, individual work habits and hand-handle interface pressure. Many studies have suggested that the contact force between the hand and a tool handle affect the severity of exposure to the hand-transmitted vibration and hand-wrist cumulative trauma disorders (Fransson and Winkel, 1991; Pyykkö et al., 1976; Radwin et al., 1987). While the majority of the studies on assessment of hand-tool operators have emphasized the consideration of overall contact force (Reidel, 1995; Kaulbars, 1996; ISO-5349-1, 2001; ISO/WC-15230; 2004), a direct measurement of contact force has not yet advanced for applications to power tools (Welcome et al., 2004)

Other studies have suggested that the perception of discomfort, fatigue and loss of productivity is related to concentration of localized forces at the hand-handle interface, as opposed to the total contact force (Gurram et al. 1995). Existence of a high pressure on the surface of the hand, arising from grasping and guiding a tool handle, could cause a sense of discomfort or pain under sustained loading, which is often a limiting factor during work and may lead to potential impending tissue damage. Sensitivity of the hand to externally applied pressures has been investigated using an algometer to establish the pressure-discomfort (*PDT*) and pressure-pain threshold (*PPT*) (Muralidhar and Bishu, 2000; Fransson-Hall and Kilbom, 1993; Johansson et al., 1999).

The grasping and guiding of a tool handle yields highly uneven distribution of forces at the hand surface (Gurram et al. 1995), which could vary considerably with hand and handle sizes, push and grip forces, and nature of vibration. Only a few studies have

attempted to study the distributed hand forces at the hand-handle interface and its dependence on the handle size, and grip and push forces that could serve as a vital basis for the design of handles. Limited efforts in the area have most likely been attributed to lack of reliable measurement methods (Fellows and Freivalds 1991, Gurram et al. 1995).

## 1.4 Hand Transmitted Vibration and Biodynamic Response

While a definite relationship between the nature of hand-transmitted vibration and disorders, and the injury mechanism have not been established, it is agreed that onset of these disorders can be reduced by decreasing the magnitude of hand-transmitted vibration. A quantitative relationship between the vibration exposure and the development of HAVS has been standardized in terms of a frequency weighting and dose-response relation (ISO-5349-1, 2001). The relationship between the vibration exposure and resulting injuries can be alternatively explored through characterization of the biodynamic response of the human hand-arm under HTV. The biodynamic response of the human hand and arm to HTV forms an essential basis for effective evaluations of the exposures, vibration attenuation mechanisms and potential injury mechanism (Dong et al., 2001).

## 1.4.1 Characterization of HAV

Vibration is the oscillatory form of motion, which characterized by its frequency components and magnitude, in terms of displacement, velocity or acceleration. Alternatively, the force that causes the motion could also be used to describe the mechanical vibration. The biodynamic response of the human hand-arm system to vibration has been investigated using a variety of motion parameters. It has been

14

proposed that the motion parameter could be correlated with the injury that may be caused by the vibration (Griffin, 1990). Most studies on hand-arm vibration are thus based upon the acceleration, which has been associated directly with the force and is believed to have strong relation with the physical damages caused by HTV. In addition, the transmitted vibration to the hand and tool can be conveniently measured in terms of acceleration, which exhibits appropriate sensitivity for the ranges of frequencies and magnitudes of major concern. The hand and arm response to vibration is thus frequently described in terms of acceleration in the standards (NIOSH, 1989; ISO-5349, 2001; ACGIH, 1998).

The human hand-arm possesses complex inertial and viscoelastic properties, and it exhibits motions along the six degrees of freedom (DOF): translational motions along the orthogonal axes ($x_h$, $y_h$ and $z_h$), and rotational motions along the roll ($\phi_h$), yaw ($\theta_h$), and pitch ($\varphi_h$) axes, as shown in Figure 1.2. The hand-arm response characteristics to vibration along the three translational axes have been the main focus of different studies, whereas the rotational motions have been ignored. Two orthogonal coordinate systems are, however, used to describe the direction of the vibration. The basicentric system is defined with reference to the tool, while the biodynamic system is defined with reference to the hand. In practice, the basicentric coordinate system is used (ISO-8727, 1997; ISO 5349-1, 2001).

15
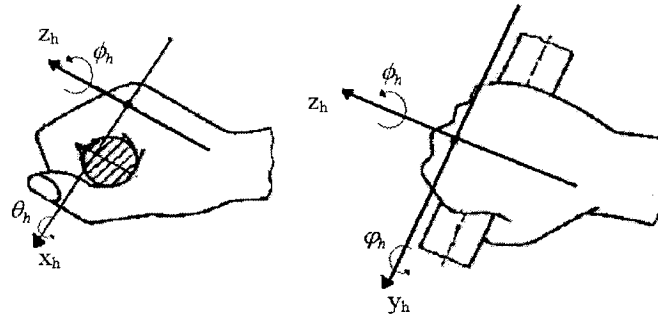
Figure 1.2: The basicentric coordinates at the hand-handle interface (ISO-8727, 1997).

1.4.2 Risk assessments of HAV exposure

Various guidelines proposed by different organizations suggest that vibration exposure be expressed in terms of root mean square (rms) acceleration in $m/s^2$ in the 1/3 octave band spectrum with center frequencies ranging from 6.3 Hz to 1250 Hz. Figure 1.3 illustrates a comparison of threshold limits of rms acceleration levels recommended by the British Standard Institute (BSI-6842, 1987), American National Standard Institute (ANSI-S3.34, 1986), and American Conference of Government Industrial Hygienists (ACGIH, 1990), for different periods of exposure during a work day. Acceleration levels that fall below a recommended curve for a given exposure time are considered to be acceptable. The standards do not specify safe exposure levels in terms of acceleration and exposure duration; however, the standards are intended for providing guidance for protecting a majority of workers from serious impairment due to vibration related diseases (Gurram, 1993).
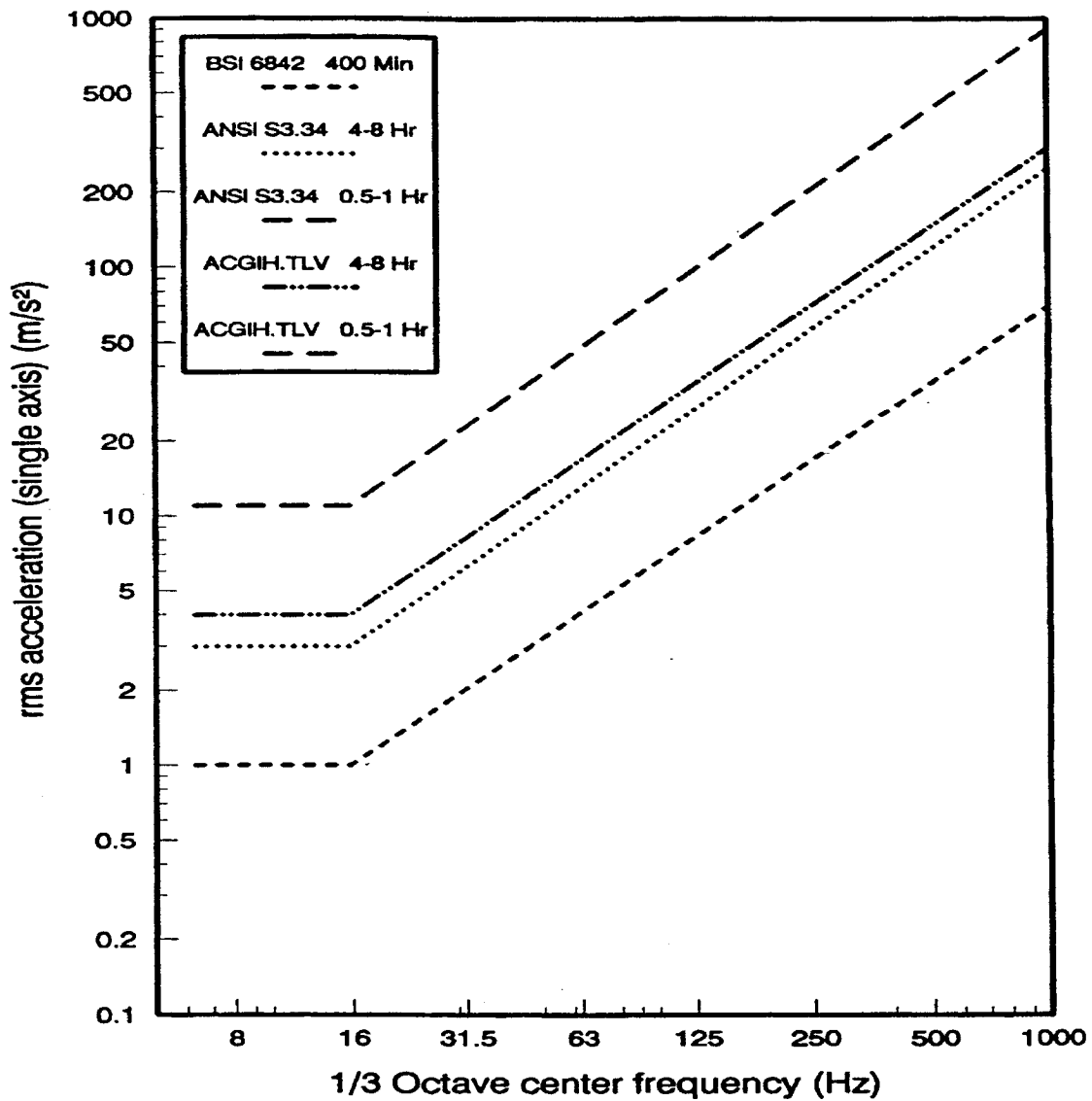
Figure 1.3: Hand-Arm vibration exposure limits recommended by different organizations (Gurram, 1993).

Little is known about the pathological basis of the vibration syndrome or the influence of specific attributes of vibration, i.e. the vibration level and the frequency components. Epidemiological evidence, however, show a positive correlation between the total exposure time and the severity of vibration white fingers, which suggest that the trauma could be cumulative (Griffin, 1990). Although symptoms of the hand-arm

17

vibration have been documented in many occupations, only a few dose-response relationships have been derived from epidemiological data (Burström, 1990). The establishment of a quantitative relation between the vibration exposure and the development of the vibration syndrome was achieved by frequency-weighting of the measured vibration with a function based on a contour of equinoxious frequencies (Gierke, 1971). This contour was established by combination of vibration amplitudes and frequencies that correspond to equal risk for causing VWF disease. By using this frequency-weighting procedure it was possible to develop a fairly good relationship between the vibration exposure and early stage of the vibration syndrome (Brammer, 1992; Burström, 1990).

The relationship between the potential risk and the measured acceleration has been thoroughly discussed in the NIOSH publication, "Criteria for Recommended Standard" (NIOSH 1989). This document proposes that unweighted frequency should be used as the basis for prevention and that the measurement range should be extended to 5000 Hz. The frequency-unweighted concept assumes that the severity of pathophysiologic effects from exposure to vibration is proportional to acceleration and is frequency independent.

Measurements and risk assessment of hand-arm transmitted vibration are currently based on ISO-5349-1 (2001). The magnitude, frequency and the duration of the vibration exposure are considered as the most important variables for the risk assessment. The standard specifies general methods for measuring and reporting the hand-transmitted vibration exposure, and provides guidance for risk evaluation on the basis of frequency-weighted acceleration, daily exposure time and dose-response relationship. It does not define the limits of safe exposure, and recommends the use of vector sum of rms

18

accelerations measured along the three orthogonal directions ($x_h$, $y_h$, $z_h$). The frequency weighting function defined in ISO-5349-1 (2001) suggests that a greater risk of injury is associated with vibration in the 6.3 to 16 Hz frequency range. The magnitude of the weighting function decreases at a rate of 6 dB/octave at frequencies above 16 Hz, as shown in Figure 1.4. The standard thus implies that the vibration risk decreases with increase in the frequency of hand-transmitted vibration. The frequency range of application of the measured values to the prediction of vibration injury is limited to the octave bands centered from 8 Hz to 1000 Hz.
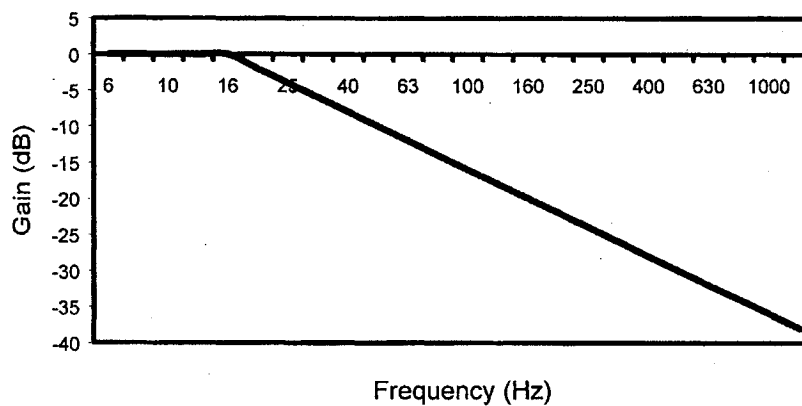


Figure 1.4: Frequency weighting function defined in standard ISO-5349 (2001).

The dose-response relationship, presented in the annexes to ISO-5349-1, is based on the dosage of frequency-weighted energy equivalent acceleration for a period equivalent to 8 hours of daily exposure, A(8), which defines the onset of potential vascular symptoms in the form of finger blanching. The relation between average latency interval for finger blanching and a single value of frequency-weighted acceleration has been estimated. Figure 1.5 illustrates the relationships between the equivalent daily vibration exposure, A(8), and the exposure duration in years ($D_y$) to produce finger blanching in 10% of the exposed population. The standard does not distinguish in the risk assessment

for vibration types, i.e. impact and non-impact vibrations. Moreover, the standard does not attempt to account for some other significant factors, such as coupling forces, handle size, the variation in musculoskeletal loading and working posture.

ISO-5349 standard has been subjected to many criticisms regarding the frequency-weighting function, daily and lifetime exposures, as well as for lack of considerations of other significant factors, such as coupling forces (Burström, 1990; Dong et al., 2001). While some studies have suggested that the dose-effect relationship overestimates the potential health risks (Louda et al., 1994; Walker et al., 1986), others have shown that it underestimates the risk of prevalence of HAVS (Nelson and Griffin, 1993; Pelmear et al., 1990).

It has also been reported that the weighting function was originally established on the basis of experimental data on discomfort sensation, which is related to acute sensory effect rather than chronic peripheral vascular functions (Miwa, 1968). Other studies have reported that the recommended weighting function is neither based on physiological nor the pathological effects of vibration, with only minimal consideration of the biodynamic response to vibration (Griffin, 1990). Furthermore, the subjective data used in deriving the function was measured only up to 300 Hz, while the values at higher frequencies were based upon extrapolations. Consequently, many concerns have been raised regarding the foundation of the current weighting function (Dong et al., 2001).

20
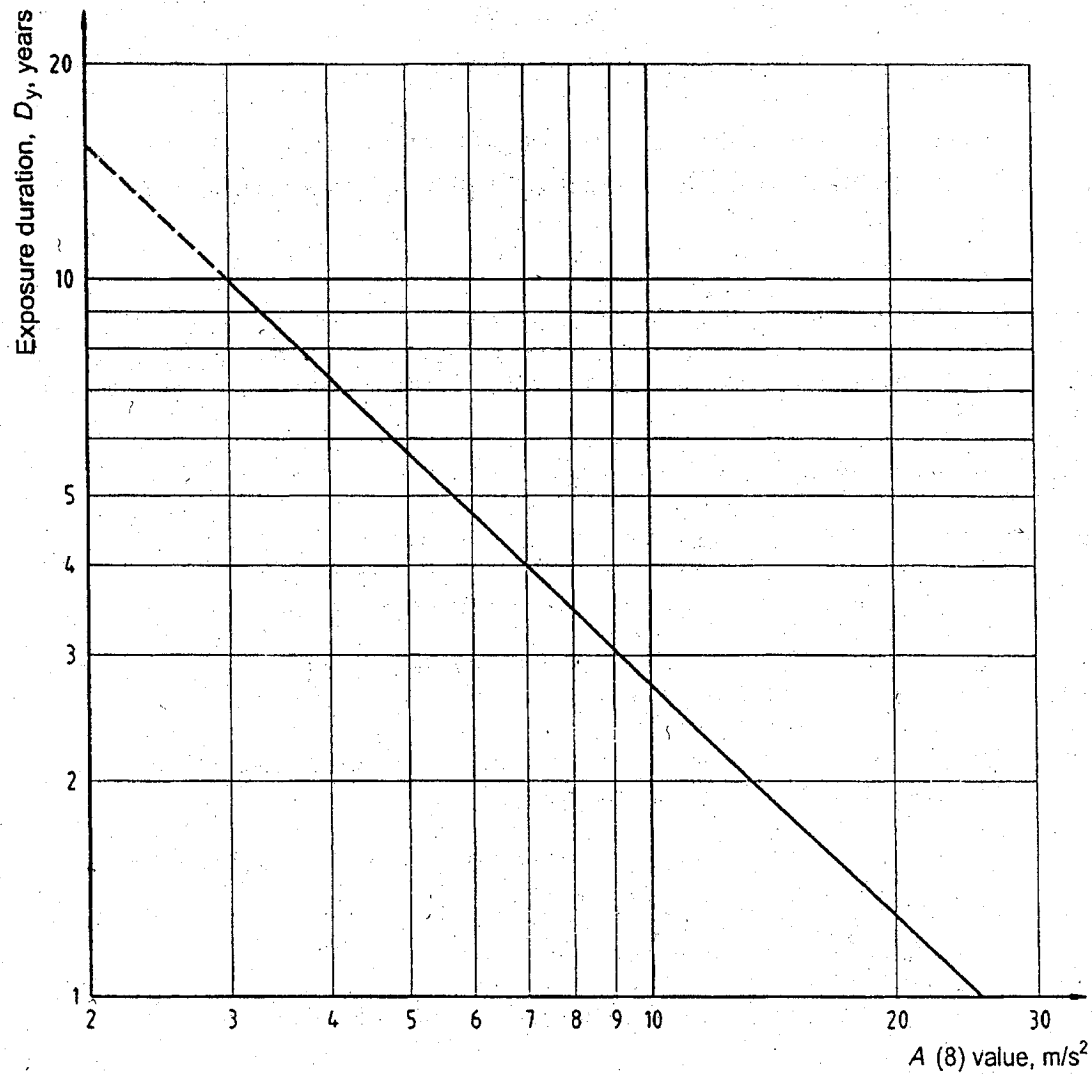
Figure 1.5: Vibration exposure for predicted 10% prevalence of vibration-induced white finger in a group of exposed persons (ISO-5349, 2001)

The American Conference of Governmental Industrial Hygienists (ACGIH, 1998) has recommended daily limits of exposure to frequency-weighted acceleration on the basis of frequency weightings defined in the ISO-5349-1 (Threshold Limit Values -TLV). The workers should not be exposed to vibration in excess of these limits. The TLVs are applied for assessing the exposure of the hand under a dominant vibration direction, i.e., $x_h$, $y_h$, or $z_h$. If the total daily exposure along one or more axes exceeds the total daily

exposure, then the TLV has been exceeded. The recommended TLV values are summarized in Table 1.2.

Table 1.2: (ACGIH) recommendation's limits for exposure of the hand to vibration.

| Total daily exposure duration | TLV of the dominant, frequency-weighted (rms), component acceleration which shall not be exceeded $m/s^2$ |
|---|---|
| 4 hours and less than 8 | 4 |
| 2 hours and less than 4 | 6 |
| 1 hour and less than 2 | 8 |
| Less than 1 hour | 12 |

The absorption of mechanical energy into the hand-arm system has been suggested as an alternate approach to develop a relationship between the vibration exposure and injury (Burström, 1990). An epidemiological study has shown that the prevalence of vibration induced white finger could be related to the amount of energy absorbed by the operators hand and arm (Lidström, 1977). It has been reported that the absorbed power by the human hand-arm system could serve as a better measure for the risk assessment of hand-transmitted vibration than the frequency-weighted rms acceleration, as recommended in ISO-5349-1 (Burström, 1990; Burström and Lundström, 1988).

1.5 Biodynamic Response to Vibration

Many studies have been conducted on assessment of symptoms of HAVS, whereas only little knowledge is gained on the pathological basis of vibration syndrome. While the efforts have evolved into standardized measurements and reporting methods, and important dose-response relationship, definite relationships between the nature of HTV and the disorders, and the injury mechanism do not yet exist. It is, however, generally

agreed that onset of these disorders can be reduced by decreasing the magnitude of HTV (Griffin, 1990; Gurram, 1993; Dong et al., 2001).

Only limited efforts have been made to explore mechanisms to reduce vibration at the source. The design of vibration attenuation mechanisms for power tools is quite challenging due to complexities associated with the compact designs and dynamics of the coupled system formed by the human hand-arm and the tool. The magnitude and frequency range, and direction of HTV are strongly related to many tool design and operating factors in a highly complex manner. The vibration generated by a tool is further strongly affected by its interactions with the human hand and arm, coupling force, working posture and various ergonomic design factors. The control of vibration caused by operation of a hand-held power tool thus necessitates knowledge of its dynamic behavior and dynamic interaction of the components within a tool, and most of all the biodynamic and energy absorption behavior of the human hand and arm.

The human hand and arm response to vibration has been widely investigated in terms of biodynamic responses, which forms an essential basis for effective evaluations of the vibration exposure, vibration attenuation mechanisms and possibly the potential injury mechanisms. The reported studies on biodynamic response and their finding could be grouped into three categories (Dong et al., 2001):

a- The transmission of hand vibration to different segments of the body, such as the finger, wrist, elbow, shoulder and head;

b- The force-motion response of the hand-arm system, expressed in terms of driving-point mechanical impedance (*DPMI*), apparent mass (*APMS*) or dynamic compliance; and

c- The absorption of vibration energy in the operator's hand.

1.5.1  Vibration transmission characteristics of the hand-arm system

A study of vibration transmissibility characteristics of the hand-arm system exposed to HTV can provide significant insight into relative motions of various components of the hand-arm, design of vibration isolators, resonance behavior of the hand-arm system and assessments of vibration attenuation performance of protective devices, such as anti-vibration gloves.  Although many studies have investigated the vibration attenuation performance of protective devices, only limited efforts have been made to study the vibration transmission through the hand arm system. This may be attributed to lack of appropriate sensors and measurement methodologies. Few investigators have attempted to study the biodynamic response of the hand-arm in terms of its vibration transmissibility for the purpose of quantifying the nature of vibration transmitted to different segments of the hand and arm (Cherian, 1994; Reynolds and Angevine, 1977; Kattel and Fernandez, 1999). The transmissibility studies have been generally limited to frequencies up to 1250 Hz (Dong et al., 2001).

The majority of these studies were performed using miniature and sub-miniature accelerometers attached to the skin. The measurement of vibration transmitted to different segments of the hand and upper limbs poses some difficulties in attaching the transducers to the flexible skins. The relative deformations of the skin and sensor mass could yield possible contaminating effects on the measured response. Non-contacting Laser Vibrometers or Laser Doppler Velocimeters (LDV) has also been employed in a few studies to measure the vibration transmitted to the hand-arm system (Gurram, 1993; Sörensson and Lundström, 1992). Laser vibrometers, however, have significant limitations in situations involving non-axial movement of the object and effective

24

measurement can be performed only when (i) the measurement location remains in the immediate vicinity of the central axis of the vibrometer's leaser beam, and (ii) the principal direction of movement is along the axis of the laser beam. The use of such vibrometers is therefore limited to laboratory applications only (Dong et al. 2001).

The vibration transmission characteristics of the human hand-arm system have been derived in the laboratory under controlled conditions and deterministic vibration (Sörensson and Burström, 1997; Cherian 1994; Reynolds and Angevine 1977). Few studies have also performed these measurements in the field during tool operation to assess the vibration performance of different tools and protective devices (Kattel and Fernandez, 1999). Different studies have invariably concluded that magnitudes of vibration transmitted to the hand-arm structure decrease with increasing frequency and the distance from the vibration source. Less than 10% of vibration at frequencies above 250 Hz is transmitted to the wrist and beyond, and vibration at frequencies below 100 Hz can be effectively transmitted to the forearms (Dong et al. 2001). Vibration at frequencies below 40 Hz can be transmitted to the forearm and upper arm without any noticeable attenuation (Sörensson and Lundström, 1992). The resonant-peak values of vibration transmitted to the phalanges reported in different studies differ remarkably. The peak values of transmitted vibration, however, have been reported to occur in the 80 to 200 Hz frequency range (Reynolds and Angevine, 1977; Sörensson and Lundström, 1992). These studies have further concluded that HTV above 200 Hz is primarily limited to the hands and fingers. For the vast majority of the hand-held power tools usage, the hands are considered to absorb most of the energy associated with HTV.

## 1.5.2 Driving-point mechanical impedance

The driving-point mechanical impedance $(Z)$ is widely used to describe the dynamic properties of the complex hand-arm system. It is defined as the ratio of the driving force $(F)$ to the velocity $(\dot{X})$ measured at the driving point. The dynamic responses of the hand-arm system to HTV could be expressed in different terms, such as mechanical compliance (the ratio of driving-point displacement to the driving force, $X/F$) or accelerance (ratio of driving-point acceleration to the driving force, $\ddot{X}/F$) or apparent mass (ratio of driving force to acceleration, $F/\ddot{X}$) or mechanical impedance.

The driving-point mechanical impedance $(DPMI)$, apparent mass $(APMS)$ or compliance may be related to the amount of mechanical energy transferred from power tools to the biological structure in contact with the tool (Reynolds, 1977). Even though the $DPMI$ may not directly relate to tissue loading and dynamics of the musculoskeletal structure of the hand-arm system, the $DPMI$ modulus and phase fully describe the overall mass-spring-damper-like behavior of the hand-arm system (Burström, 1990). Consequently, the measured response could allow for the analysis of effective masses, spring constants and damping factors as functions of the operating conditions and other individual variables. The $DPMI$ can also be effectively applied to estimate the amount of mechanical energy dissipated by the hand-arm structure under a specified hand tool vibration spectrum (Burström, 1990).

The driving-point mechanical impedance characteristics describing the biodynamic response of the hand-arm system have been extensively investigated under a wide range of vibration excitations and test conditions (Burström, 1997; Mishoe and Suggs, 1977;

Burström, 1990; Gurram et al., 1995; Cronjager and Hesse 1990; Kihlberg, 1995; Lundström and Burström, 1989; Jandák, 1989; Jandák, 1998; Daikoku and Ishikawa, 1989). Although hand-arm biodynamic responses have been measured on human subjects under carefully controlled conditions, remarkable differences exist among the data reported in different studies. These differences could be partly attributed to differences in experimental and measurement techniques employed. Moreover, the test conditions employed in these studies varied considerably, specifically with respect to the magnitude and frequency ranges of vibration excitation, handle size, grip force and posture. The lower and upper limits of frequency of excitation employed in these studies ranged from 2-20 Hz to 200-2000 Hz, respectively. Although the most of these studies have employed sinusoidal excitations, some studies have measured the biodynamic response of the hand-arm system under broad-band random and impulsive type excitations (Gurram, 1995; Burström, 1997; Kihlberg, 1995; Jandák, 1998).

Large differences among the reported biodynamic response data have been further attributed to the potential dependence of the biodynamic response on various contributory factors, such as grip and feed forces, postures, anthropometric parameters, individual differences and the inherent non-linear dynamic properties of the biological materials (Burström, 1997; Gurram; 1993). On the basis of a synthesis of data reported under comparable test conditions, the ISO 10068 (1998) has defined the standardized ranges of free mechanical impedance of human hand-arm system at its driving point in three translational axis ($x_h$, $y_h$ and $z_h$). These include the frequency range of 20-500 Hz, grip forces in the 25-50 N range and elbow angle close to $90°$ degree. The ranges of idealized values of the biodynamic response in the ISO-10068 (1998) represent a synthesis of the

widely varying datasets reported by different investigators. The ranges of the *DPMI* data, therefore, appear as wide envelopes of magnitude and phase values. Peak variations in the impedance magnitude about the mean are as high as 69%, 69% and 63%, for the $x_h$, $y_h$ and $z_h$ directions, respectively.

Furthermore, the maximum frequency of the standardized data in ISO-10068 (1998) is only 500 Hz, which may be considered to be too low in view of the characteristics of HTV. Additionally, the idealized ranges do not address the role of various contributory factors, such as grip force, push force, hand posture, shoulder abduction, elbow angle, handle geometry and individual differences. This is attributed to lack of available data and the use of inconsistent test conditions employed by different investigators. Despite the noteworthy differences, all studies agreed on the strong dependency of mechanical impedance on frequency and direction of vibration and the grip force.

## 1.5.3   Absorption of vibration power

An epidemiological study has shown that the prevalence of vibration induced white finger could be related to the amount of energy absorbed by the operators (Lidström, 1977). A study conducted by Reynolds and Angevine (1977) suggested the existence of a positive correlation between the subjective annoyance data and energy absorption in the hand and arm. Within related context, a reasonably good correlation between the power absorbed by the human body exposed to whole-body vibration and the subjective sensation of discomfort has also been reported (Pradko et al., 1965). It has been suggested that energy dissipation in the hand could provide a good correlation with the vibration damage to the hand-arm system (Cundiff, 1976; Burström, 1990; Burström and Lundström, 1994). In addition, it has been reported that the power absorbed by the human

hand-arm system is perhaps a better estimate of the vibration dosage than the frequency-weighted acceleration, as recommended in the ISO 5349-1 for the risk assessment of HTV (Burström and Lundström, 1988; Burström, 1990).

The power method can effectively account for the contributions due to various intrinsic and extrinsic factors, such as the grip force, hand-arm posture and individual differences, since the measure of power is derived from the vibratory force measured at the hand-tool interface during tool operation. This is an important advantage since the hand forces are known to vary considerably as a function of the amplitude of acceleration due to increased muscle contraction and tonic vibration reflex (Radwin et al., 1987). Unlike the *DPMI*, which is almost independent of the vibration magnitude, significantly higher magnitudes of absorbed power are obtained under higher vibration magnitudes. Considering the risks associated with HTV are mostly related to sensitivity of vibration and exposure duration, the absorbed power approach would serve as a better measure of the potential risk.

From a physical point of view, the power generated in the hand-arm system can be of two forms: reactive and active. The reactive power, attributed to the potential and kinetic energies stored in the elastic tissues of the hand-arm system, does not contribute directly to the net flow of energy between the handle and the hand-arm system. On the other hand, the active component of the power is directly related to the net flow of energy from the handle to the hand. Hand-arm system is a highly damped system (Reynolds and Soedel, 1972); its damping ability results in absorption the energy due to heating effect in the tissues. It is likely to assume that most of the energy probably is absorbed due to the relative motion between different tissues, muscles and skeletal structure of the hand and

29

arm. This motion leads to the absorption of heat and if the motion is too powerful, physical damage or modification of the system may occur (Reynolds and Keith, 1977).

## 1.5.4   Factors affecting the hand transmitted vibration and biodynamic response

The characteristics of the hand transmitted vibration and the human biodynamic response to vibration exposure are influenced by many extrinsic and intrinsic variables. The extrinsic variables include frequency, amplitude and direction of vibration, duration of the exposure, coupling force, grip type and grip pressure distributions. The intrinsic variables include the hand-arm posture, body size, anthropometrics characteristics and age (Griffin, 1990; Sörensson, 1998; Burström, 1994, 1997).

### Extrinsic factors

Direction of vibration is an important factor since human hand-arm system exhibits varying sensitivity to vibration along different axes (ISO-10068, 1998; Burström; 1997, Gurram et al., 1995; Kihlberg, 1995). The reported studies on clinical assessments and biodynamic responses have invariably concluded that hand-arm response to vibration is strongly affected by the frequency of vibration (ISO-5349-1, 2001; Burström, 1997; Pelmear and al., 1990; Griffin, 1990). The results of the clinical studies suggest that the peripheral vascular and neural effects are generally sensitive to vibration below 700 Hz (Dong et al., 2001). While the dominant frequencies of vibration generated by various power tools lie in the 25-320 Hz (Gurram, 1993). The reported cases of VWF are typically associated with tools having dominant vibration frequencies in the 25-250 Hz range. Owing to the most important effect of the vibration magnitude, the hand-arm

response to vibration is generally characterized in terms of acceleration (ANSI-S3.34, 1986; BSI-6842, 1987; ACGIH, 1990; ISO-5349, 2001).

The type of vibration excitation may also influence the biodynamic responses of human hand-arm system. However, there have been relatively few studies to quantify such effects (Dong et al, 2001). Based on the *DPMI* response of four male subjects under both sinusoidal and random excitations, Gurram (1993) concluded that the biodynamic response of hand-arm system differs under different types of vibration, particularly at frequencies above 200 Hz. The study performed by Kihlberg (1995) under impulsive and harmonic excitations, on the other hand, did not show a significant influence of these types of vibration excitation on the *DPMI*, dissipated energy, or transfer function of the hand-arm system. In follow up study a strong association was found between the development of finger blanching and the use of impulsive tools (Pelmear et al., 1995).

The coupling force at the hand-handle interface, often considered as a combination of grip and push forces, permits the flow of vibration energy from the tool into the hand, and consequently it presumes to affect the biodynamic response of hand-arm system considerably. It has been generally agreed that the coupling force has an obvious effect on the severity of vibration transmission (Griffin, 1990; Hartung et al., 1993). The magnitude of biodynamic response of human hand-arm, measured in terms of mechanical impedance, increases with the increasing of grip force (Mishoe and Suggs, 1977; Burström, 1990; Gurram, 1993). Some other studies have concluded that the biodynamic response of the human hand-arm is relatively less sensitive to variations in the push force (Bernard, 1990; Jandák, 1998). It is widely reported that the contact force between the hand and a tool handle affects the severity of exposure to HTV and hand-wrist

cumulative trauma disorders (Fransson and Winkel, 1991; Pyykkö et al., 1976; Radwin et al., 1987). Unlike the coupling force, the contact force is defined as the sum of normal components (perpendicular to the vibrating surface) of the distributed static forces acting between the hand and the vibrating surface (ISO/CD 15230, 2004; Welcome el al., 2004).

Considering that the hand-handle contact force depends upon the effective contact area of the hand-handle interface and thus the handle size, the biodynamic response of the hand-arm system would be expected to be influenced by the handle dimensions and geometry. However, only a single study has thus far considered the effect of handle size on the hand-arm biodynamic response to vibration (Reynolds and Falkenberg, 1984). The study reported the measured dynamic compliance of the hand-arm system for two different handle diameters (19 and 38 mm) for a group of 75 foundry workers. The results showed that both the phase and magnitude of the compliance vary with the handle diameter, while no attempt was made to quantify the effect of the handle size. Moreover, the influence of handle size on the mechanical dissipated power in the human hand-arm has not been attempted.

Intrinsic factors

The intrinsic factors such as muscle tension, body posture, hand size, gender, individual factors, age and weight are also known to influence the characteristics of the HTV and the biodynamic response of the human hand-arm to vibration. The effects of some of these factors have been investigated in a few studies. While their contributions have not been quantified, the effects of most of the intrinsic variables are considered to be of minor importance (Reynolds, 1977).

Variations in body posture, however, is considered as an important factor affecting the HTV especially in the low frequency range, i.e. less that 100 Hz (Burström, 1997), but it has not been quantitatively considered in the exposure evaluations. Gripping of tools with elevated arm posture or working with extended arms can cause increasing loading of the hand-arm muscles, leading to fatigue, soreness and pain (Freivalds, 2004). A vast number of studies have established that static forces generated by the human hand are strongly influenced by the hand-arm posture (Kattel et al., 1996; Marley et al., 1993; Kuzala and Vargo, 1992). The reported studies have clearly shown the effect of posture on the static hand forces, which could be related to variations in the muscle force capacity resulting from muscle length associated with upper limb posture (Danuta, 2003). Donati et al. (1992) observed changes in the activities of the triceps brachii under vibration exposure with variations in the hand-arm posture. Only a few studies have investigated the influence of hand-arm posture effect on the dynamic response of the hand-arm system in terms of *DPMI.* (Burström, 1990, 1997; Cronjäger and Hesse, 1989; Burström and Lundström, 1994). These studies have concluded that variations in the hand-arm posture affect the biodynamic responses, while the response trends do not vary considerably. The influence of the hand-arm posture on the absorbed power has also been investigated by Burström and Lundström (1988, 1994) and Burström (1994).

The size of the hand and arm may further affect the coupled hand-tool dynamics and the biodynamic response of the hand-arm system (Burström, 1990). Considering similar contact area, the magnitude of vibration transmitted to a particular location of the hand may vary with variations in the hand size. The variations in stiffness, mass density and damping ratio of the skin and other tissues of different individuals may further affect the

33

characteristics of HTV (Dong et al., 2001). The severity of individual factors may be influenced by biological susceptibility to vibration, agents affecting the peripheral circulation, such as low temperature, noise, smoking and medication. Furthermore, earlier disease or prior injuries to the fingers or hands as well as working methods can influence the severity of the effects from vibration (Griffin, 1990).

Gender effect on the biodynamic response has been reported in a few studies. The driving-point impedance magnitude, for female subjects was found to be 20% lower than those for the males subjects (ISO-10068, 1998). Power absorption was found to be 40% larger in males than in females under sinusoidal vibration (Burström, 1994). Similar values (25 to 40 % lower for females) have been also reported under random vibration (Sörensson and Burström, 1996). Another study has reported substantially smaller differences in the absorbed power of male and female subjects, ranging from 10 to 20 % (Burström and Lundström, 1994). Given that absorption is strongly correlated with sizes/volumes of anthropometric structures, the anthropometric differences between males and females may account for the observed differences, more than the biological tissue differences for the same size (Burström, 1994). Age has also been reported to have significant role in the energy absorption, the absorbed energy increase by approximately 1% per year of age (Burström, 1994). Another study concluded that the transmission of vibration from handle to hand increases for light weight operator (Toppila et al., 1997).

1.6    Biodynamic Modeling of the Human Hand-Arm System

The vibration transmission characteristics and the biodynamic response of the human hand-arm system to vibration of power tools are widely investigated in both the laboratory and the field. Owing to the complex nature of the tool vibration and the

coupled hand-tool system dynamics, such assessment methodologies require repetitive measurements involving representative human subject samples and test conditions. Such measurement-based methodologies are also known to pose considerable complexities in the data analysis due to relatively large inter- and intra-subject variability (Dong el al., 2001). In view of the expected contributions due to dynamics of the operator's hand and arm, and the effect of many intrinsic and extrinsic variables, assessment methods that either eliminate or reduce the involvement of human operators are considered highly desirable.

Biodynamic models of human hand-arm system have thus been proposed to represent the hand-arm system in coupling with the tool. The applications of biodynamic models of the human hand and arm offer considerable potential to carry out assessments through both analytical and experimental analyses, where the involvement of human subjects could be considerably reduced (Kinne and Melzig-Thiel, 1996; Jahn and Hesse, 1986). The hand-arm vibration (HAV) models, when integrated with the analytical model of a power tool, could permit efficient evaluations of the tool design factors and vibration attenuation devices. A number of biodynamic models of the human hand and arm have been proposed to study the vibration amplitude and power flow in the coupled hand, tool and work piece system; the potential performance benefit of vibration attenuation mechanisms; and to develop test rigs and hand-arm simulators for the assessment of vibration transmission performance of different tools (Byström et al., 1982; Cherian et al., 1996; Mishoe and Suggs; 1977, ISO-10068, 1998; Daikoku and Ishikawa, 1989).

Although the models provide little insight into the pathological changes caused by HTV, they serve as effective tools to study the effects of direction and magnitude of

vibration on the HTV (Abrams, 1971; Reynolds and Falkenberg, 1984). The majority of the reported models are mechanical equivalent models comprising lumped mass, stiffness and damping elements, where the lumped parameter values are identified upon curve fitting of the measured data. Multi-parameter non-linear-programming-based optimization techniques have also been used to identify the model parameters by minimizing a weighted error function of the *DPMI* magnitude and phase response (Gurram et al., 1995). However, since the model parameters are identified upon fitting a single target response function, the methodology could result in a multitude of model structures and associated parameter combinations that can be found to satisfy the required response, specifically when a multi-DOF model structure is considered. The uniqueness of the model structure and parameters could be considerably enhanced when additional constraints on target functions are introduced and/or more when multiple target response functions are used, i.e. *DPMI* and power absorption. Gurram (1993) employed a constrained multi-parameter optimization to minimize a weighted function of both the magnitude and phase response in an attempt to improve the uniqueness of the solution. A set of limit constraints was defined to achieve model parameters within the known bounds. The total mass considered in the model was constrained to lie within the range of mean values of the human hand-arm system.

A number of biodynamic models, ranging from simple single-degree-of-freedom (DOF) to four-DOF, have been developed to characterize the biodynamic response of the human hand-arm system in terms of *DPMI* or vibration transmissibility (Rakheja et al., 2002). The hand-arm vibration (HAV) models, invariably, are comprised of linear and time-invariant inertial, restoring and dissipative elements, such that linear analytical

methods may be used. The models, therefore, do not adequately represent the biomechanical properties of the human hand and arm (Dong et al, 2001). Furthermore, the reported models characterize the biodynamic behavior of the hand and arm under uncoupled vibration along three orthogonal axes ($x_h$, $y_h$, $z_h$) defined in ISO-5349 (2001), and they are usually applicable under specific conditions of grip and push forces, arm position, body posture, and characteristics of vibration excitation (Rakheja et al., 2002).

Rakheja et al. (2002) evaluated twelve different models in terms of their driving-point mechanical impedance modulus and phase responses. They examined the suitability of the reported models for realizing a mechanical simulator and for their applicability to the analyses of coupled hand-tool systems. The relative evaluations were performed using these performance three criteria. These included the ability of the model to characterize *DPMI* of the human hand-arm system within the range of idealized values presented in ISO-10068 (1998); the magnitude of model deflection under a static push force; and the vibration properties of the human hand-arm system evaluated in terms of natural frequencies and damping ratios. The study concluded that the majority of the models could not be applied for the development of a mechanical hand-arm simulator or assessment of dynamic behavior of the coupled hand-tool system. The higher order models, with three and four-DOF, in general resulted in impedance characteristics within the range of idealized values, but revealed excessive static deflections. On the other hand, the majority of the lower order models resulted in reasonable static deflections but relatively poor agreement with the idealized values of *DPMI*.

Although the validity of each model in predicting the biodynamic response acquired in the particular study has been well established, considerable differences were obvious

among the various models, which could be partly attributed to wide variations among the reported biodynamic response data and test conditions employed in different studies (Rakheja et al., 2002). The biodynamic models of human hand-arm have been invariably derived on the basis of mean response of a population of subjects under specific conditions. The strong dependency of the *DPMI* response on different factors, as evidenced from the data reported in the literature (Dong et al., 2001), would limit the applications of the proposed models. While most of the investigations on biodynamic response of human hand-arm to vibration recognize the influence of hand forces on the biodynamic response, only one reported model has attempted to identify grip force dependent parameters (Gurram et al., 1995). The development of a hand-arm biodynamic model with considerations of the grip and push forces variations, and postural effect, has not been attempted.

## 1.7   Scope and Objectives of the Dissertation Research

In the 80 years following the Hamilton's historical study, a large number of investigations have contributed to the advancements in understanding of the HTV. These include the standardized measurement and reporting methods, dose-response relationship, and clinical objective assessment methods of symptoms. The onset of vascular, neural and musculoskeletal disorders among the operators of hand-held power tools has been directly related to the magnitude of hand-transmitted vibration, a number of test methods have been proposed to evaluate the relative vibration characteristics of different tools and vibration attenuation mechanisms in the laboratory under controlled conditions. In view of the expected significant contributions due to the dynamics of the operator's hand and arm, and the effects of many intrinsic and extrinsic variables, it is desirable to thoroughly

characterize the biodynamic behavior of the operators' hand and arm, which when integrated with the model of the tool could yield significant design information. The biodynamic response of the human hand-arm to hand-transmitted vibration (HTV) forms an essential basis for effective evaluations of exposures, vibration attenuation mechanisms and potential injury mechanism. In addition, the relationships between the vibration exposure and resulting injuries could be explored through characterization of the biodynamic response of the human-hand arm under hand-transmitted vibration.

Many investigators have extensively evaluated the biodynamic responses under a wide range of test conditions to enhance understanding of the transmission of source vibration to the hand-arm system. Although the *DPMI* and absorbed power characteristics have been, invariably, measured under controlled test conditions, large differences exist among the human hand-arm biodynamic responses data reported in different studies. These discrepancies may be attributed to the multitude of test conditions employed by individual investigators; the complexity associated with the human hand and arm; the lack of standardized measurement and reporting methods; and strong dependencies of the mechanical impedance and absorbed power on grip force, push force, hand-arm posture, handle size and shape, and vibration characteristics. The lack of unanimity among the reported data has raised serious concerns pertaining to validity of the biodynamic response data and developed models associated with them. Further investigations on the characterization of biodynamic response of the hand-arm system are therefore vital to improve upon the existing standards (ISO-5349, 2001; ISO-10068, 1998).

There are many factors that determine or affect the transmission of tool vibration into the hand and arm. Many of them have not been sufficiently understood to enable them to be incorporated in the standard methods. No study has investigated the influence of handle size and shape in conjunction with variations in different contributory factors on the biodynamic response of the hand-arm system exposed to vibration neither in term of driving point mechanical impedance nor in power absorption. More data are needed to achieve more clear understanding of the human hand-arm response to vibration. The hand-arm biodynamic response to vibration is undoubtedly complex due to wide variations in conditions and contributory factors affecting the hand-arm response to vibration. Consequently, there is a need for a single study to be carried under carefully control test conditions to fully investigate the contributions of various factors that affect the HTV. The responses measured under a practical ranges of hand forces, handle sizes, hand-arm postures and vibration spectra would further contribute to enhancement of the corresponding standards.

Biodynamic models of human hand and arm have been proposed as attractive means to characterize the vibration amplitude and power flow in the coupled hand, tool and work piece system. However, Rakheja et al. (2002) concluded that a vast majority of these models cannot be applied for development of a hand-arm simulator or the assessment of dynamic behavior of the coupled hand-tool system. The lack of applications of hand-arm vibration models may be partly attributed to wide variations among the reported biodynamic responses data and test conditions employed in different studies. The models are valid only in the vicinity of the selected test condition.

The biodynamic response measured under representative conditions are expected to yield the necessary database for developing a more reliable model. A biodynamic model which could be capable of describing hand-arm response under a range of hand forces (push and grip) is needed. Applicable hand-arm vibration model, when integrated with the analytical model of power tools, could permit efficient evaluations of the tool design factors and to analyze the potential performance benefits of vibration attenuation devices.

The most serious effects of prolonged exposure to HTV is vibration white finger (VWF), which might be related to impaired blood circulation and blanching of affected fingers and parts of the hand. It was hypothesized that local concentration of contact pressure together with the hand-transmitted vibration may be related to causation of VWF (Gurram 1993, Nerem 1977). High grip, push or hand-handle contact force is also known to be one of the primary factors that increase the risk of cumulative trauma disorders. There is a need to investigate the dependence of localized pressure peaks in magnitude and location on the hand surface upon the handle size, and magnitudes of grip and push forces. The distribution of pressure and the contact force in the hand-handle interface and its association with the handle size could lead to advancement of knowledge on the handle size issue and to enhancement of the understanding of the biodynamic response of the human hand-arm, while operating power tools. The hand-handle interface contact force is known to affect the HTV and the biodynamic response of the hand and arm in a significant manner. The measurement of contact force, however, is quite complex in field application. A need thus exists to identify alternate methodologies for estimating the contact force from directly measurable quantities, such as push and grip forces.

41

### 1.7.1 Objective of the dissertation research

The overall objective of this dissertation research is to contribute towards development of improved assessment methods, and attainment of safer hand-held power tools and work environment through systematic analytical and experimental investigations on biodynamic response of human hand-arm system to hand-transmitted vibration, and dynamic interaction between the hand and the tool. The specific objectives of the proposed research are as follows:

a) To characterize the force-motion relationship at the hand-handle interface under a range of representative vibration and operating conditions, through laboratory measurement on a handle vibration simulator.

b) To evaluate biodynamic responses of the human hand-arm system in terms of *DPMI* and power absorption into hand and arm under selected vibration and operating conditions.

c) Attempt to quantify the dependence of the hand-arm *DPMI* and absorbed power responses on the handle size, hand forces (grip and push) imparted on the handle, coupling and contact forces developed at the hand-handle interface, and the hand-arm posture.

d) Investigate the statistical significance of various contributory factors, namely the magnitude of vibration, frequency of vibration, handle size, grip and push forces on hand-arm biodynamic responses to vibration.

e) Study the hand-handle interface pressure distribution for different handle sizes under different hand force combinations and develop methods that provide objective means to assess the magnitudes and locations of high pressure peaks that may cause pressure-induced discomfort and pain, and thereby the stresses imposed on the hand.

f) Obtain relationship between the contact force, and the directly measurable grip and push forces and examine the effect of the handle geometry on the contact force.

g) Develop multi-DOF lumped-parameter biodynamic models of the human hand and arm using the mean measured data, expressed in terms of *DPMI* magnitude and phase, and the absorbed power, and demonstrate the validity of the models for a range of grip and push forces, and hand-arm posture.

42

## 1.7.2 Thesis organization

This thesis research is divided into seven chapters. Chapter 2 is devoted to describe the experimental procedures and experiment set-up for measuring the contact force and pressure distribution under static conditions, and the biodynamic responses of the human hand-arm exposed to random vibration. The data analysis methods for deriving the; *DPMI* and absorbed power characteristics are presented. The chapter also summarizes the statistical analyses to study the significance of various contributory factors on the contact pressure and on the biodynamic responses.

The relationships between the coupling, contact forces, push and grip forces are explored in chapter 3 through the analysis of the measured contact pressure data. The data are analyzed to study the role of handle size on the contact force. The localized pressure peaks are derived in different zones of the hand surface, which are assessed in view of the known pressure discomfort threshold (*PDT*) and the sustained pressure (*SP*) values. Chapter 4 is devoted to discuss and analyze the measurements of hand-arm biodynamic response in term of driving point mechanical impedance (*DPMI*). The measured impedance data are analyzed to derive the intra-subject variability and mean trends. The data are employed to investigate the influence of handle size and shape, grip force, push force, coupling and contact forces, vibration intensity and hand-arm posture on the *DPMI*. Statistical analyses are performed to verify the significance of the studied factors on the mechanical impedance. Chapter 5 studies the biodynamic response in terms of power absorption into the hand and arm. The data are utilized to examine the influence of different studied factors on the absorbed power. Further, the influence of vibration frequency on the absorbed power and the amount of total absorbed power within different

frequency bands are investigated under different test conditions. The absorbed power characteristics of the hand-arm system are correlated with the coupling and contact forces to enhance an understanding of their contributions. The merits of the absorbed power measure relative to the *DPMI* are further discussed.

Chapter 6 reviews the human hand-arm model and their capability to be applied for the development of a mechanical hand-arm simulator or the assessment of dynamic behavior of the coupled hand-tool system. The mean measured data, expressed in terms of *DPMI* magnitude and phase, and the absorbed power are used to develop different multi-DOF lumped-parameter models using multi parameters optimization techniques. The model parameters are identified as functions of the hand forces and the validity of the proposed models is examined for the range of hand forces and two different postures. The conclusions derived from this dissertation and the suggestion for future works and investigations are presented in chapter 7.

# CHAPTER 2

## EXPERIMENTAL SET UP AND DATA ANALYSIS

### 2.1    General

Objective methods for characterizing the biodynamic responses of the human hand-arm system are reasonably well established. The methods, invariably, involve measurements of force and acceleration at the hand-handle interface, using a simulated handle subject to either harmonic or broad-band random vibration (Bylund and Burström, 2003; Jandák, 1998; Burström, 1997; Gurram et al., 1995; Burström and Lundström, 1994). The measured data are applied to characterize the force-motion relationships in the form of driving-point mechanical impedance (*DPMI*) or apparent mass (*APMS*) or dynamic compliance or power absorbed. Significant differences, however, exist in the experiment design employed in different studies, which translate into major differences in experiment set up, instrumentation; analyses methods and experiment design factor.

Owing to the strong dependence of various responses measures on the hand grip and push forces; coupling and contact forces; direction, frequency and magnitude of vibration and hand-arm posture, a through experiment design should consider combinations of all these contributory factors. Furthermore, large inter-subject variability of the measured data would require a representative sample size and application of sound analyses tools, in order to attain results that could provide meaningful interpretations of the measured response trends, and the role of various contributory factors. Owing to the high frequency components of tool vibration, the design of simulated handle and its support fixture resonant frequencies also posses some challenges in realizing the fixture resonant frequency well above the frequency range of vibration, namely 1000 Hz.

In contrast to the biodynamic response, the experimental methods for characterizing the hand-handle contact forces and pressure distributions are still evolving. The International Standard Organization has recently completed a draft document defining the hand-handle interface forces, including grip, push, coupling and contact forces, and method of their measurements (ISO-15230, 2004). The measurement of hand-handle contact forces and interface pressure poses many complexities due to requirement of large number of thin sensors and flexible sensing elements that do not alter considerably. A number of resistive and capacitive pressure sensing grids have evolved during the past decade for such applications (Welcome et al., 2004; Gurram et al., 1995). These comprise of large number of thin and flexible sensing elements could be conveniently applied to the handle surface to capture the hand-handle interface pressure distribution. The large number of sensors however tends to limit the measurements to either static or low frequency vibration.

This chapter describes the experimental set ups for characterizing the biodynamic response to vibration along the $x_h$- and $z_h$-axis (Figure 1.2), and hand-handle interface forces and the experiment designs. The experiments were performed in two stages involving the biodynamic and interface pressure measurements. The first stage of experiment was performed in the IRSST laboratory, using a number of simulated handles. Seven participants were employed in these experiments to study the hand-arm biodynamic response to vibration with six different handles exposed to two levels of broadband random vibration along the $z_h$ and $x_h$- axes under different grip and push forces combinations. The second stage of experiments was partly carried out at NIOSH laboratory and partly in the IRSST laboratory. A total of ten adult male subjects

participated in the experiments to measure static hand/handle contact force and contact pressure distributions over the hand surface as functions of the grip and push forces, and the handle size. The static hand-handle contact forces are evaluated for each combination of grip and push forces through measurement of pressure distribution at the hand-handle interface, to formulate relationships among the grip, push and contact forces as a function of the handle size. The correlation between hand-arm biodynamic response and both the coupling and contact forces are further exploded. Linear correlations and multiple regressions are performed to study the influence of some of the contributory factors on the human hand-arm biodynamic responses and on static contact force and peak pressure. The results are used to identify a proper definition of hand force which may be more correlated to the human hand-arm biodynamic responses to vibration. Linear multiple regressions have been applied to build some practically usable relations concerning hand/handle interface contact force and peak pressure magnitude. ANOVA statistical analyses using SPSS software are also carried out to reveal the significance of different studied contributory factors on the static contact force, peak pressure and biodynamic measures.

## 2.2   Hand-Arm Biodynamic Response Measurements

This component of the dissertation work is devoted to measure and study the biodynamic responses of the hand-arm system exposed to broadband random excitations along the $x_h$- and $z_h$-axes in terms of both the *DPMI* and the absorbed power and to examine the influence of various contributory factors, such as the vibration intensity, excitation frequency, hand-arm posture, grip and push forces, coupling and contact forces and the handle size, in view of both the biodynamic measures of the hand-arm system.

2.2.1    Test variables

Six instrumented handles were designed and instrumented to provide measures of the static and dynamic hand-handle forces and hand-arm *DPMI* and absorbed power responses. Three of the handles were cylindrical (30, 40 and 50 mm diameter) and the other three handles were semi-elliptical (30x38, 30x46 and 30x54 mm). The elliptical handles were built by placing rectangular inserts (8, 16 and 24 mm) between the two halves of the 30 mm cylindrical handle. Each cylindrical handle consisted of two aluminium semi-circular sections, which were joined together through two Kistler 9212 force sensors for measuring the grip force. Handles size and weights are given in Table 2.1, the three different cylindrical handles and the three rectangular inserts are shown in Fig 2.1. A PCB SEN026 tri-axial accelerometer was also mounted within one of the semi-circular section of the handle to measure the handle acceleration. The handle was mounted on an Unholtz-Dickie electrodynamic shaker system with 890 N force capacity through a support fixture and two Bruël & Kjær 8200 force transducers to measure the static and dynamic push force, as illustrated in Figure 2.2 and Figure 2.3. Figure 2.2 shows the pictorial views of the instrumented handle and the support, while Figure 2.3 demonstrates the exploded view of the handle and support.

Table 2.1: Handles size and weight

| Shape | Diameter (mm) | Weight (g) | Circumference(mm) |
|---|---|---|---|
| Cylindrical | 30 | 308.65 | 94.29 |
| Cylindrical | 40 | 440.88 | 125.71 |
| Cylindrical | 50 | 668.78 | 157.14 |
| Elliptical | 30x38 | 359.41 | 110.29 |
| Elliptical | 30x46 | 439.77 | 126.29 |
| Elliptical | 30x54 | 517.2 | 142.29 |
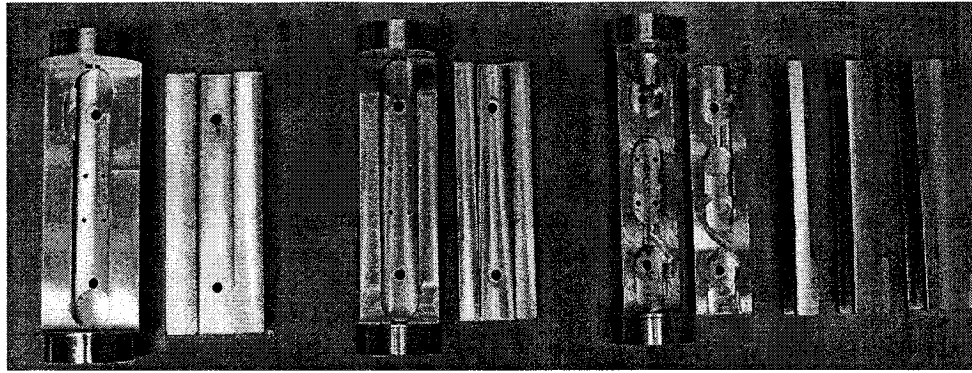
Figure 2.1: The different handles and inserts used in the experiments.



(a)                                      (b)
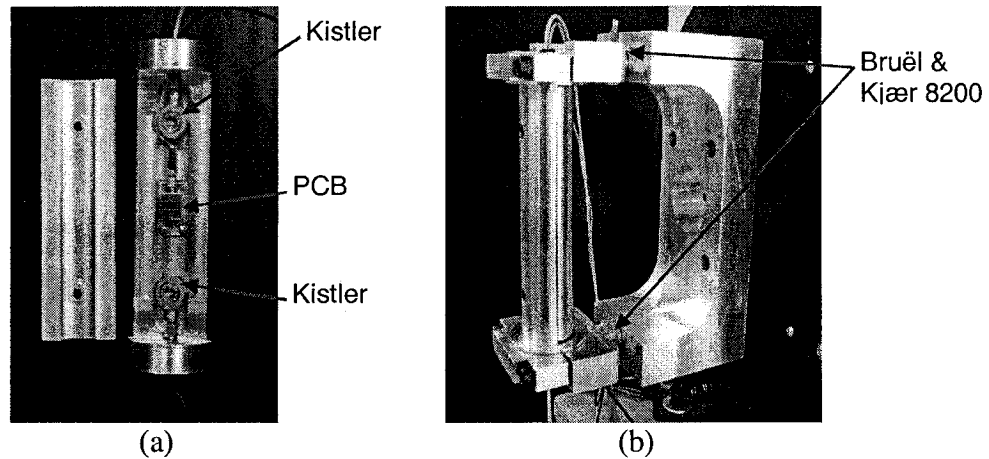
Figure 2.2 : Pictorial views of the instrumented handle (a) and the support (b).

Seven healthy male subjects were employed in this experiment. The anthropometrical data of the test participants are shown in Table 2.2, where the dimensions of the dominant right hands were measured, as shown in Figure 2.4.

Table 2.2: The anthropometrical data of the participants

| Subject | Hand Length (cm) | Hand Circumference (cm) | Hand Width (cm) | Hand Thickness (cm) | Arm Length (cm) |
|---|---|---|---|---|---|
| 1 | 20 | 22.5 | 10 | 3.5 | 44.4 |
| 2 | 17 | 22 | 10.5 | 3.7 | 47.9 |
| 3 | 19 | 21 | 10 | 3.5 | 50.5 |
| 4 | 19 | 21 | 10.5 | 3.6 | 43.5 |
| 5 | 21.3 | 23 | 11 | 3.5 | 49.5 |
| 6 | 19.26 | 21.9 | 10.4 | 3.6 | 47.3 |
| 7 | 19.9 | 22.0 | 10.6 | 3.4 | 47.1 |
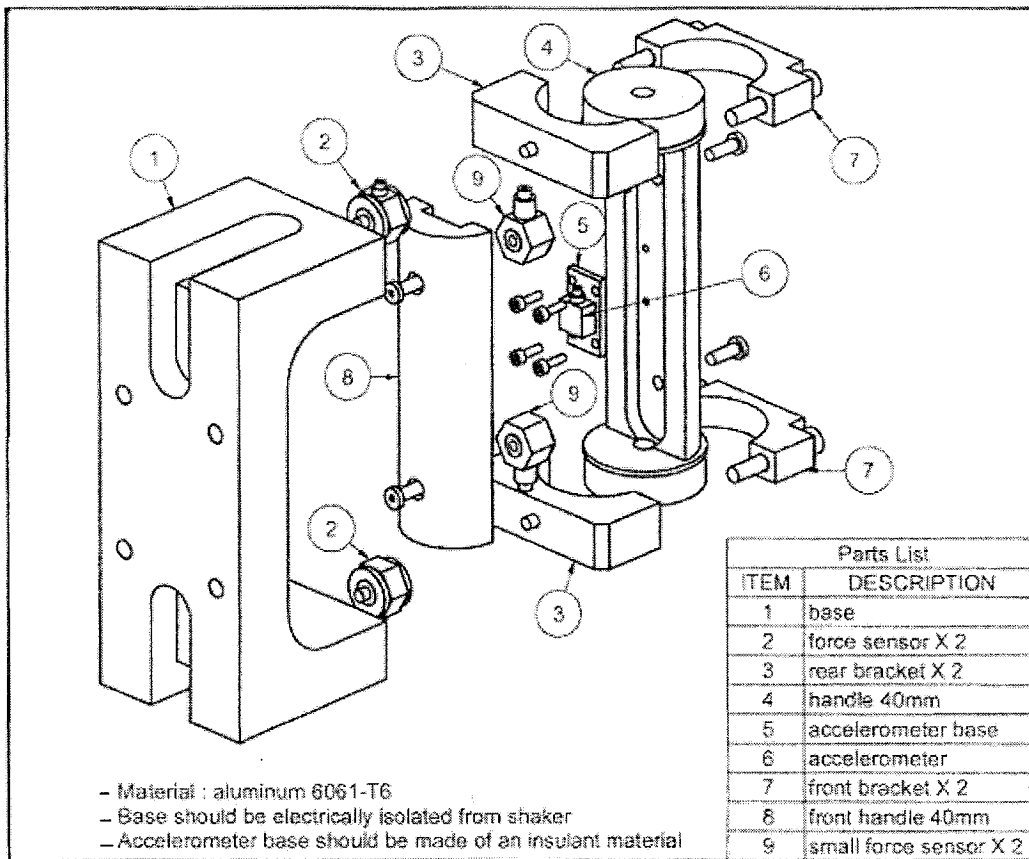
Figure 2.3: Exploded view of the instrumented handle (40 mm) and the support.
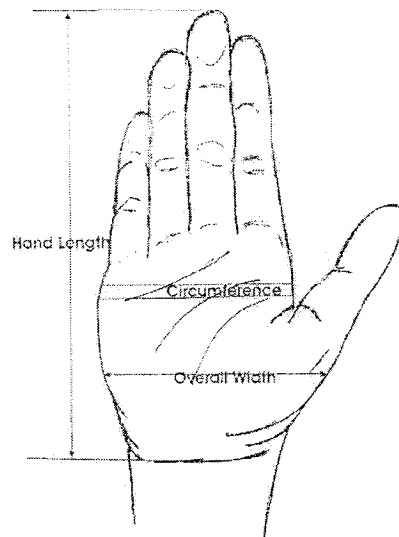


Figure 2.4: Dimension of a subject's hand.

Direction and magnitude of vibration

Measurements were undertaken under two different levels of broadband random vibration with constant acceleration power spectral density in the 8–1000 Hz frequency range to study the influence of vibration magnitude on the biodynamic responses of human hand-arm system exposed to vibration. The overall frequency-weighted rms acceleration ($a_{h,w}$) were computed following the ISO 5349-1 (2001) standard as $a_{h,w}$ = 2.5 m/s$^2$ for the lower spectrum and $a_{h,w}$ = 5.0 m/s$^2$ for the higher spectrum. The acceleration signal was fed back to the vibration closed-loop feedback controller to maintain constant acceleration spectra no matter what hand forces or any other test variables were applied. Two axes of vibration were considered in this study, $z_h$ and $x_h$-axes according to ISO 5349 (2001) (Figure 1.2). These two axes are more important from practical view point. The $y_h$-axis has not been considered in this research work, since the vibration along this axis (transverse direction) is not practically realistic. Figure 2.5 shows pictures for a worker using vibrated power tools, where the axes of vibration are very close to $z_h$ and $x_h$-axes as defined in the ISO-5349 (2001).

For both axes two hand-arm postures were considered in this test to study the effect of the posture on the biodynamic response of the human hand-arm exposed to vibration in both terms; *DPMI* and absorbed power and the significance of hand-arm posture in conjunction with the variations in the hand forces and handle sizes. The two different postures consisting in bent forearm with elbow angle of 90° (posture *P1*)and extended forearm with elbow angle of 180° (posture *P2*), with wrist being in the neutral position for both postures.

Figure 2.6 shows the schematic representations of the two postures (*P1* and *P2*).

51
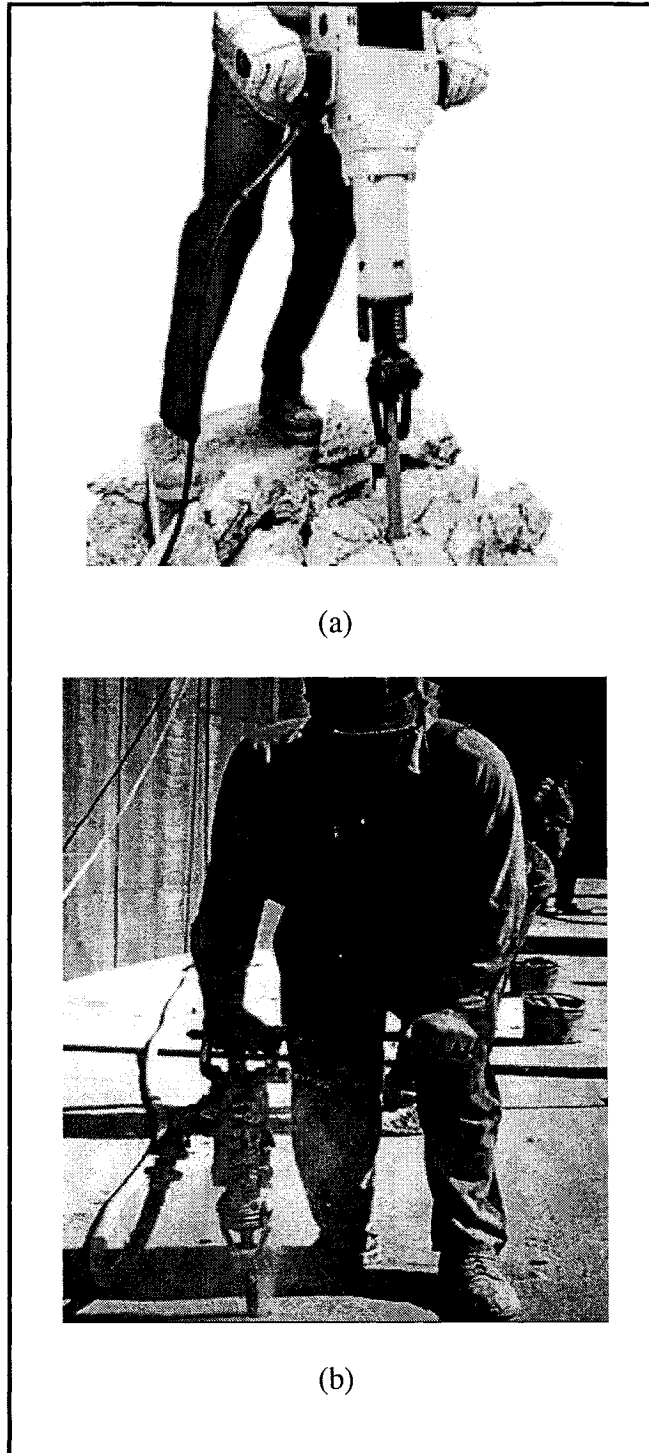
Figure 2.5: Workers using vibrated tools under two vibration axes: (a) $x_h$-axis; and (b) $z_h$ axis.
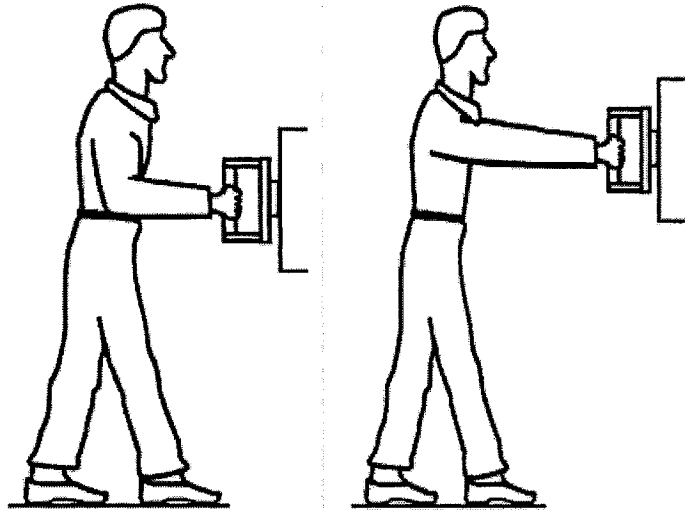
Figure 2.6: Schematic representations of the postures employed: (a) posture *P1*; and (b) posture *P2*.

The experiments have involved different test conditions under the two employed vibration axes; $z_h$ and $x_h$-axes. The handle with its support structure and push force sensors were mounted on an electro-dynamic vibration exciter, oriented along the $z_h$ and $x_h$-axes, while the grip force sensors integrated within the handle were oriented along the $z_h$-axis under both axes. Three levels of push and grip forces were used under both axes, while the grip force were the same (10, 30 and 50 N) for both axes, the push force levels were (25, 50 and 75 N) under $z_h$ -axis while (0, 25 and 50 N) under $x_h$-axis. Some subjects faced difficulties in applying high push force in $x_h$-axis. Six handles have been used in studying the biodynamic response of hand-arm under $z_h$-axis to verify the effect of handle size and shape in contact force and both biodynamic response measures. However, only cylindrical handles were employed in $x_h$-axis to examine the influence of handle diameter on the biodynamic responses at this axis. Table 2.3 summarizes the test matrix and the range of experimental conditions considered in this experiment.

Table 2.3: Test matrix and conditions considered in the experiment.

| Factor | $x_h$ | | $z_h$ | |
|---|---|---|---|---|
| | Levels | Details | Levels | Details |
| Subjects | - | 7 | - | 7 |
| Trails | - | 2 | - | 2 |
| Frequency range | - | 8 to 1000 Hz | - | 8 to 1000 Hz |
| Vibration level | 2 | 2.5 and 5 m/s$^2$ rms weighted | 2 | 2.5 and 5 m/s$^2$ rms weighted |
| Handle size | 3 | 30, 40, 50 mm diameter | 6 | 30, 40, 50 mm and 30x38, 30x48, 30x54 mm |
| Hand-arm posture | 2 | Posture $P1$: 90° flexion elbow  Posture $P2$: 180° flexion elbow | 2 | Posture $P1$: 90° flexion elbow  Posture $P2$: 180° flexion elbow |
| Grip force ($F_g$) | 3 | 10, 30 and 50 N | 3 | 10, 30 and 50 N |
| Push force ($F_p$) | 3 | 0, 25 and 50 N | 3 | 25, 50 and 75 N |

## 2.2.2    Method and experimental procedures

The total contact force between the hand and the handle was first evaluated for the seven participants with six different handles and nine grip/push force combinations (same as given in Table 2.3 along the $z_h$-axis) using the *NOVEL* PLIANCE system. The system comprised a flexible pressure sensing mat with a 16X11 matrix of capacitive pressure sensors in the same procedures and techniques applied in section 2.3.2 where the details and explanations are presented. For each measurement, the subject was given adequate time to adjust the grip and push forces to the specified values by monitoring the displayed forces. The measured grip and push forces, as well as the pressure distribution, were averaged over a 10 seconds period. The static force measurements performed while the handles were installed on the electro-dynamic shaker in a horizontal plane to permit gripping of the handle along the $z_h$-axis, and the subjects implemented the posture $P1$ (bent forearm with elbow angle of 90° and neutral wrist position). The purpose of the contact force measurements was to investigate the relationships between the hand arm biodynamic responses to vibration and the coupling and contact forces to verify the more

54

proper definition of hand forces which more related and correlated to hand-arm biodynamic responses.

The measurements of force-motion characteristics at the hand-handle interface were performed using the six different handles under $z_h$-axis vibration and three cylindrical handles $x_h$-axis. Each handle was instrumented for direct acquisition of the driving-point excitation and force response, and monitoring of the mean grip and push forces. Cylindrical handle consisted of two aluminum semi-circular sections, which were joined together through two Kistler 9212 force sensors for measuring the grip force. For semi-elliptical handles, the rectangular plates with different widths were inserted between the two halves of 30 mm cylindrical handle to attain the three different semi-elliptical handles. The driving-point acceleration is measured using a PCB SEN026 tri-axial accelerometer located within one of the semi-circular section of the handle. Each handle was mounted on an Unholtz-Dickie electrodynamic shaker system with 890 N force capacity through a support fixture and two Bruël & Kjær 8200 force transducers to measure the static and dynamic push force. The handle with its support structure and push force sensors were oriented along the $x_h$-axis and $z_h$-axis as shown in Figure 2.7, while the grip force sensors integrated within the handles were oriented always along the $z_h$-axis.

The reported data on the *DPMI* of the human hand arm suggest that the apparent mass of the human hand reduces to considerably small values at higher frequencies (Bernard, 1990). The measurement of *DPMI* or apparent mass thus requires a highly sensitive and accurate measurement system.

55
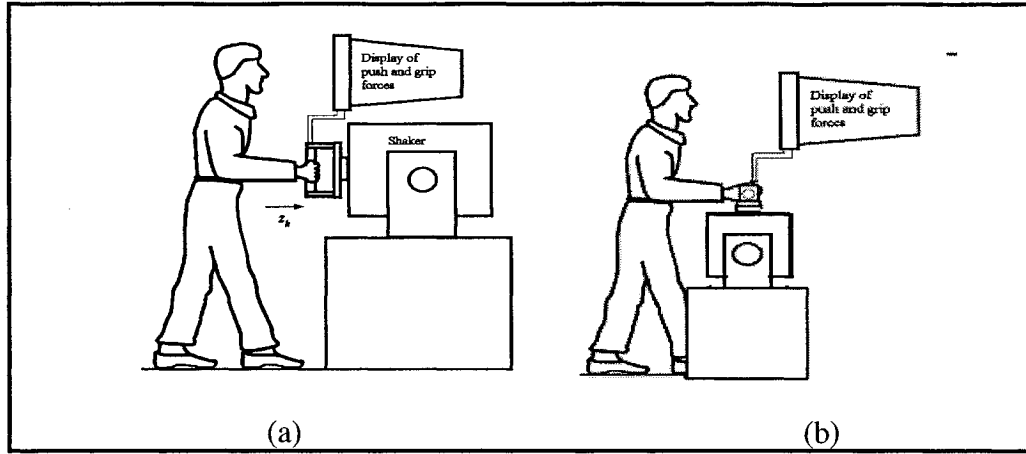
Figure 2.7: Two orientations of the handle and its support: (a) $z_h$-axis; (b) $x_h$-axis.

The systems ability to measure small variations in the mass with high accuracy is thus investigated through measurement of the apparent mass of the 40 mm handle and that of the handle with a small mass of 42 g rigidly attached to it. The mass value obtained from the difference between the measured apparent masses of the handle with and without the added mass revealed nearly constant mass and phase response close to zero, as shown in Figure 2.8. These results suggest that the *DPMI* measurements are accurate both in magnitude and phase, noting that the mass magnitude has a variation of less than 8 % and that the phase is very closed to zero, considering that the human hand-arm apparent mass magnitude is at least larger than 100 g in the frequency range of interest (8 – 1000 Hz).

The biodynamic responses measurements were undertaken under two different levels of broadband random vibration with constant acceleration power spectral density in the 8–1000 Hz frequency range. The overall frequency-weighted rms acceleration ($a_{h,w}$) were computed following the ISO 5349-1 (2001) standard as $a_{h,w}$ = 2.5 m/s$^2$ for the lower spectrum and $a_{h,w}$ = 5.0 m/s$^2$ for the higher spectrum. Each subject was advised to grip the mounted handle using his right hand. For each measurement, the subject was given

adequate time to adjust the grip and push forces to the specified values by monitoring the displayed forces.
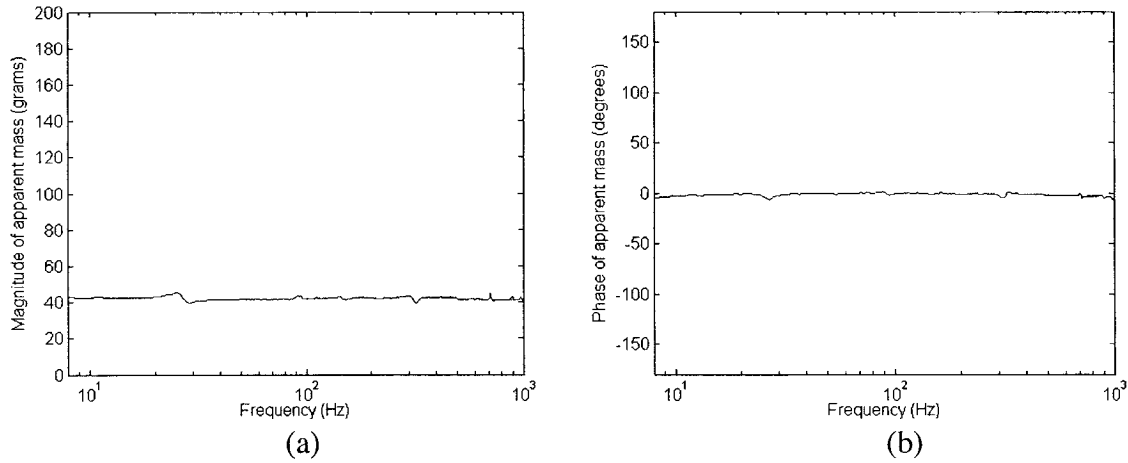


Figure 2.8: Measured apparent mass magnitude and phase response of the handle and support structure with an additional 42 g mass: (a) magnitude; (b) phase.

The synthesized vibration was applied to the hand-handle system along the specific vibration axes and the resulting dynamic force and handle acceleration were acquired in a multi-channel data acquisition and analysis system (Brüel & Kjær Pulse system). The data corresponding to each measurement were acquired over a period of seven seconds (25 averages using a Hanning window and an overlap of 75%) while the subjects were asked to maintain the push and grip forces near the required values. The measured grip and push forces, sampled at a rate of 4 samples/s, were displayed to the subject on a computer screen. The test was repeated if the subject, for any reason, failed to maintain the specified grip and/or push forces. Each experiment was performed twice to verify and ensure reasonable repeatability; the average value of both trials was used in the data analysis. The test orders were randomized to minimize the potential bias. The maximum daily exposure of a subject, however, was limited to 30 minutes. Figure 2.9 shows the biodynamic experimental measurement. The measurements were performed under two

different postures to examine the influence of hand-arm posture on the biodynamic responses of the hand-arm system exposed to vibration.
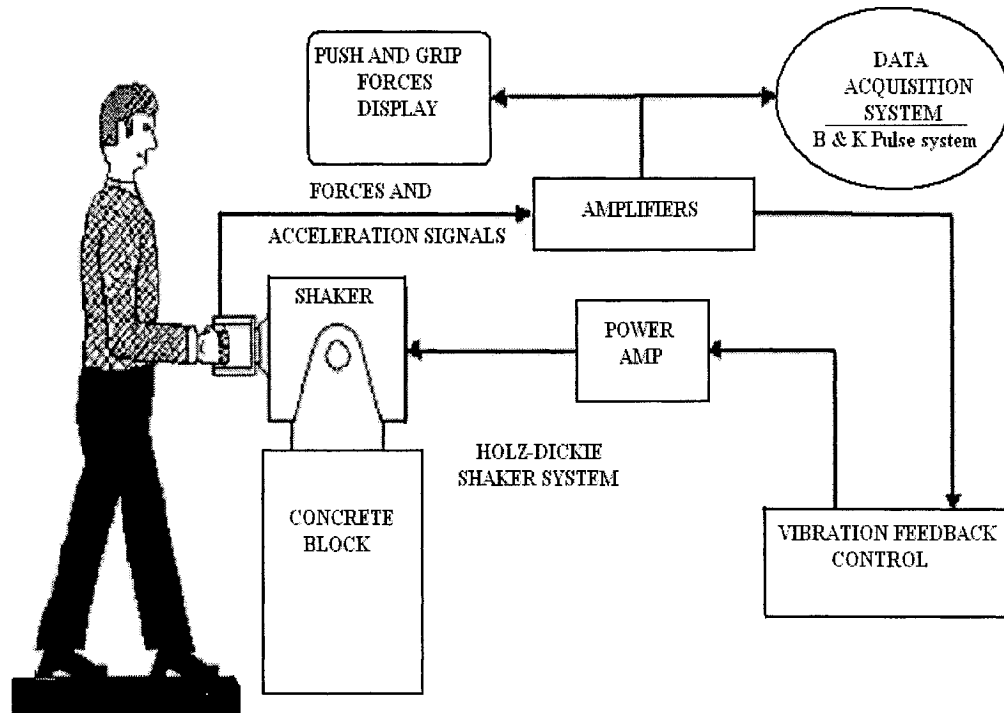


Figure 2.9: Hand-arm biodynamic response measurement.

### 2.2.3    Data analyses

The measured data were analyzed to derive the biodynamic responses of the hand-arm system exposed to $x_h$ and $z_h$ axes vibration, in terms of both the *DPMI* and the absorbed power. Both responses were evaluated in the 8-1000 Hz frequency range, while the absorbed power data corresponding to center frequency of each of the one-third octave bands are presented. The results were analyzed to identify important trends in view of the various factors considered such as; the handle size, vibration intensity, hand grip and push forces, and hand-arm posture.

58

The biodynamic response could be expressed in terms of apparent mass (*APMS*), driving point mechanical impedance (*DPMI*) as well as absorbed power. The apparent mass (*APMS*) for the hand-arm system exposed to vibration can be computed from:

$$APMS(j\omega) = \frac{F(j\omega)}{A(j\omega)}$$ 
(2.1)

where $F$ is the driving force, $A$ is the acceleration at the driving point, $\omega$ is the circular frequency of vibration and $j = \sqrt{-1}$.

The driving-point mechanical impedance (*DPMI*) is calculated as:

$$DPMI(j\omega) = \frac{F(j\omega)}{V(j\omega)}$$ 
(2.2)

where $V$ is the velocity measured at the driving point.

For random vibration, the driving point mechanical impedance is computed as following (Thomson, 1993):

$$DPMI(j\omega) = \frac{G_{Fv}(j\omega)}{G_{vv}(j\omega)}$$ 
(2.3)

where $G_{Fv}$ is the cross-spectrum of the dynamic force and handle velocity, both measured at the driving-point, and $G_{vv}$ is the auto-spectrum of the velocity measured at the handle.

The driving-point mechanical impedance of the handle and the supporting structure alone was subtracted from the *DPMI* of the hand-handle measured during the tests to account for the inertia effect of the handle and the supporting structure.

The power flowing into hand-arm system from vibrated handle at the hand/handle interface can be calculated from;

$$P(t) = F(t) \cdot V(t) \qquad\qquad (2.4)$$

where $F(t)$ and $V(t)$ are the dynamic force and velocity at the driving point, respectively.

From a physical point of view, the power generated in the hand-arm system can be of two forms: reactive and active. The reactive power, attributed to the potential and kinetic energies stored in the elastic tissues of the hand-arm system, does not contribute directly to the net flow of energy between the handle and the hand-arm system and thus there is no energy dissipation. On the other hand, the active component of the power is directly related to the net flow of energy from the handle to the hand. This form of energy is dissipated through the viscous elements of the hand-arm system, where it is converted into work and heat (Reynolds, 1977).

The power can be expressed in the frequency domain, which can be obtained by calculating the cross-spectrum of the driving force and velocity (Bendat and Piersol, 1986). Since there is phase difference between the driving force and the handle velocity, the cross-spectrum is normally complex, which can be generally expressed as follows:

$$P(\omega) = C(\omega) - jQ(\omega) \qquad\qquad (2.5)$$

where the real component, $C$, is the coincident spectral density function (co-spectrum) and the imaginary component, $Q$, is the quadrature spectral density function (quad-spectrum) (Bendat and Piersol, 1986).

The real component reflects the energy dissipated in the hand-arm system per unit time due to the friction at the interface between the hand and tool handle and the internal friction in the tissues of the hand-arm system. This component is usually termed absorbed

power. The imaginary component reflects the combination of the kinetic energy due to system inertia and the potential energy from the elasticity of the tissues. This portion of power may return back to the handle through the hand-handle interactions. The absorbed power by hand-arm system exposed to random vibration could be thus expressed in the frequency spectrum as:

$$P_{abs}(\omega) = \text{Re}[G_{Fv}(j\omega)] \qquad\qquad (2.6)$$

where $G_{Fv}$ is the cross-spectrum of the measured force and velocity, $\omega$ is the angular frequency, "Re" refers to real part and $j = \sqrt{-1}$. The absorbed power could be indirectly computed from driving point impedance measurement and handle velocity $v(j\omega)$ (Burström, 1990) as;

$$P_{abs}(\omega) = \text{Re}[DPMI(j\omega)]\,|v(j\omega)|^2 \qquad\qquad (2.7)$$

The measured data were analyzed to express the magnitudes of absorbed power corresponding to center frequency of each of the one-third octave bands in the 8-1000 Hz frequency range. The total absorbed power was then computed through summation of power values within each of the one-third octave bands. The total absorbed power in any frequency range is simply the summation of power in the third octave bands within this range.

The cancellations of the handle mass and damping effects can be achieved by using either a time-domain method or a frequency domain method. According to previous studies (McConnell, 1995) the frequency domain method is superior. The cancellation

61

formula was derived based on a measurement system model proposed by McConnell, which is expressed as follows:

$$P(\omega) = P_{hh}(\omega) - P_h(\omega) \qquad\qquad ( 2.8)$$

where $P_{hh}$, is the absorbed power measured in a subject test griping the vibrated handle, and $P_h$ is the power absorption measured with the handle alone (without any hand coupling).

Despite the strong dependence of the biodynamic responses upon individual differences (Burström, (1990), Burström and Lundström, (1989)), the inter-subject variability of the measured *DPMI* data has been reported in a single study (Gurram et al., 1995), while no such efforts have been made for the measured absorbed power. The comparisons of the mean *DPMI* (magnitude and phase) and absorbed power responses of individual subject, obtained in this research work revealed considerable scatter in the data for the considered axes in this study (chapters 4 and 5). However, in spite of the considerable scatter in the *DPMI* and absorbed power data obtained for the individuals under different test conditions, both the measures reveal definite common trends in the 8-1000 Hz frequency range. The mean values of the measured data could thus be used to study the important trends emphasizing the effects of individual factors. The mean value of absorbed power is simply the average of the absorbed power measured of each participant. While for the measured drive point mechanical impedance (*DPMI*), the mean value should be obtained by averaging the real and the imaginary parts separately as following:

$$MDPMI_{real} + MDPMI_{imag} = \sum_1^n DPMI_{real} + \sum_1^n DPMI_{imag} \qquad (2.9)$$

where *MDPMI* is the mean drive point mechanical impedance, the notations real and imag indicate the real and imaginary parts respectively and n is the number of the test subjects which is 7 in this test.

## 2.3    Static Contact Force and Pressure Distribution

The primary motivation for this component of the dissertation research drives from the need to define relationships between the grip and push forces and static contact force as the function of the handles size, and to study the hand-handle interface pressure distributions for different handle sizes under varying of magnitude of hand forces imparted on the handle. While the hand-handle contact force is known to influence the human hand-arm response to vibration and the stresses imposed on the biological structure (Reidel, 1995; Fransson and Winkel, 1991; Radwin et al., 1987), the measurement of contact force under vibration exposure or tool operation remains a formidable task. The targeted relationships between the contact force, and the grip and push forces. Moreover, such relations could provide an estimate of the peak pressure and thus means to assess the pressure-induced discomfort and pain sensation on the basis of known values of pressure discomfort threshold (*PDT*) and pressure pain threshold (*PPT*) values (Muralidhar and Bishu, 2000; Fransson-Hall and Kilbom, 1993; Johansson et al., 1999). The measured data are thus further analyzed to determine the magnitude and locations of pressure peaks at the hand surface for the ranges of handle size and forces considered. The working draft ISO/CD 15230 (2004) defines the hand-handle coupling force as a direct summation of the push and grip forces. While the contact force is

defined as the sum of the distributed normal force at the hand–handle interface surrounding the handle. The definitions of the hand forces are explored in detail in section 1.3.

In this study, instrumented handles were designed to measure both the grip and push forces imparted by the hand. A capacitive pressure-sensing grid is applied on the handle surface to measure the interface pressure distribution under static conditions.

### 2.3.1 Test variables

Three handles of circular cross-section (30 mm, 40 mm and 48 mm diameter), split along the length, were developed and instrumented in the NIOSH laboratory to measure the handgrip force. The measurements were performed under 5 different magnitudes of grip force (0, 15, 30, 50 and 75 N) and 4 different levels of push forces (0, 25, 50 and 75N). A total of 10 male adult subjects were employed in the study. The experimental design for each subject was a three-factor factorial type. The factors included handle diameter with three levels, grip force ($F_g$) with five levels and push force ($F_p$) with four levels and two repetitions (3x5x4x2). The test variables for this experiment are summarized in Table 2.4.

Table 2.4: Test variables considered in the study.

| Factor | Levels (number) | Details |
|---|---|---|
| Subjects | 10 | - |
| Handle size | 3 | 30, 40, 48 mm diameter |
| Hand-arm posture | 1 | 90° flexion elbow |
| Grip force ($F_g$) | 5 | 0, 15, 30, 50 and 75 N |
| Push force ($F_p$) | 4 | 0, 25, 50 and 75 N |

Table 2.5 summarizes the age, height and hand sizes of the test subjects, where the dimensions of the dominant right hands were measured, as shown in Figure 2.4. The hand volume was measured using water displacement method. The hand size of each subject was further derived in accordance with EN 420 (1994). With regards to the anthropometric data reported from several studies of US military personnel, the hand size of the test subjects would lie between the 75th and 90th percentile (NASA, 1078).

Table 2.5: Age, height, weight and hand sizes of the test subjects.

|  | Minimum | Maximum | Mean | Std. Deviation |
|---|---|---|---|---|
| Age | 18 | 60 | 30.2 | 4.87 |
| Height (m) | 1.77 | 1.9 | 1.84 | 0.04 |
| Weight (kg) | 63.5 | 127 | 86 | 17.65 |
| Hand length (cm) | 17.5 | 22 | 19.68 | 1.189 |
| Hand circumference (cm) | 20 | 25 | 22.46 | 1.331 |
| Overall hand width (cm) | 10.5 | 12 | 11.05 | 0.522 |
| Hand thickness (cm) | 4.5 | 5.5 | 4.88 | 0.44 |
| Hand volume (cm$^3$) | 345 | 525 | 429.6 | 54 |
| Hand size (EN420, 1994) | 9 | 10-11 | 9 | - |

2.3.2   Method and experimental procedures

A test fixture, comprising an instrumented handle and associated mounting, was designed to perform measurements of hand-handle interface pressure and contact force distributions. Three handles of circular cross-section (30 mm, 40 mm and 48 mm diameter), were employed in this test. Each handle integrated two force sensors (Kistler 9212) and a summing circuit was used to derive the grip force. The calibration data revealed linear force measuring characteristics of the handles in the 0 to 100 N ranges, irrespective of the position of the applied load along the span of the handle. Each handle was installed on an electro-dynamic shaker in a horizontal plane to permit gripping of the

65

handle along the $z_h$-axis using a mounting bracket. It should be noted that the shaker was merely used to provide a support for the test handle, since the concerned pressure distribution and forces are measured under the static condition alone. A Kistler force plate (Kistler 9286AA) was used to measure the push force imparted by the hand on the handle during experiments at the NIOSH laboratory. Alternate experiments were also performed at the IRSST laboratory using different handle design that integrated both grip and push force sensors within the fixture. Both the push and grip force signals were conditioned and displayed on a computer screen at a refresh rate of 1 sample/s for monitoring and control purposes.

Distribution of contact force/pressure:

The hand-handle interface contact pressure distributions were acquired using the *EMED* measurement system of *NOVEL Electronics*. The measurement system consists of a flexible capacitive pressure sensing grid, and a Pliance mobile data conditioning and acquisition system. The sensing grid comprises 16 x 11 (16 rows and 11 columns) pressure sensors encased within a 2 mm thick elastomeric mat, which was applied to the selected handle for measuring the hand-handle interface pressure distributions over the contact region. Each sensor covered an area of 0.766 $cm^2$, including the spacing between the adjacent sensors. The sensing mat was calibrated under a pneumatic bladder in the 0– 30 $N/cm^2$ range. The calibration of the mat was examined after each test against well defined weight. The sensing mat was wrapped around the handle with an adhesive tape, as shown in Fig 2.10. The overlapping of active sensors encountered with smaller handles was eliminated by masking selected rows of sensors. A total of 4 and 2 rows of the

sensing matrix were masked for 30 mm and 40 mm handles, respectively, while no masking was needed for the 48 mm handle.


(a)                                                    (b)
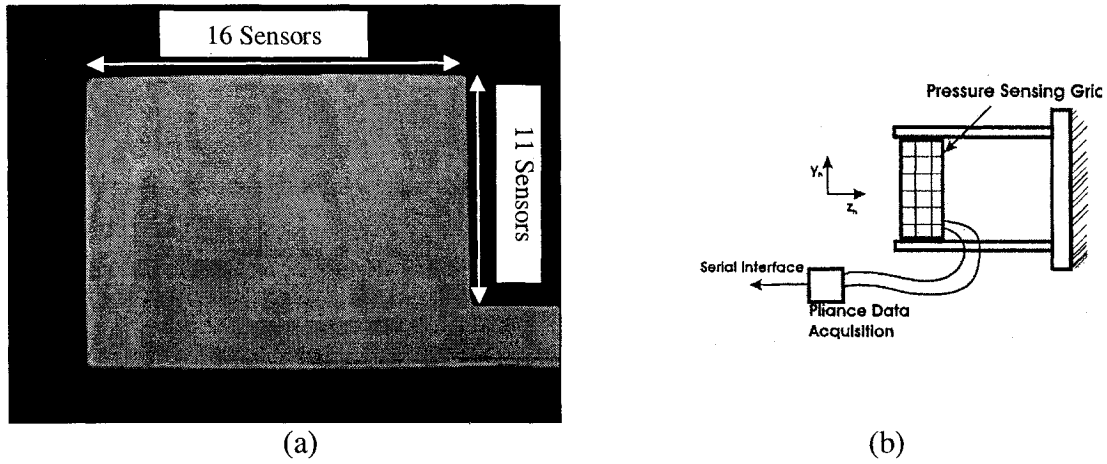
Figure 2.10: (a) Pressure sensing mat; (b) the mat wrapped around a test handle.

The pressure measurements were performed with the bare hand under static grip and push conditions. Each subject was advised to stand on the force platform and grasp the installed instrumented handle with his dominant right hand with a specified arm posture (elbow angle = $90°\pm10°$). The platform height was adjusted to ensure horizontal lower arm and $0°$ shoulder abduction. The subject's hand position with respect to the sensing grid on each handle was marked during the first test and the subject was advised to use the same position in subsequent tests. The subjects were advised to maintain specified grip and push forces using the feedback from the visual displays. The measurements were performed under different magnitudes of grip and push forces in the 0 to 75 N ranges as specified in Table 2.4, to study the effect of their variations on the contact force and on the magnitudes and locations of peak pressures on the three different cylindrical handles.

Figure 2.11 shows the mean of pressure distribution of a participant applied 75 N grip and push forces while gripping 48 mm handle. The experimental design for each subject was a three-factor factorial type. The factors included handle diameter with three

levels (30 mm, 40 mm and 48 mm), grip force ($F_g$) with five levels (0, 15, 30, 50 and 75 N) and push force ($F_p$) with four levels (0, 25, 50 and 75 N). Each subject received brief training on the test procedure and was permitted a number of practice runs prior to the measurements. The measurements with different handles were performed on different days and the order of the specified grip and push forces was randomized for each subject. Each test was performed twice and the data obtained in terms of contact force were examined for the consistency of the measurement.
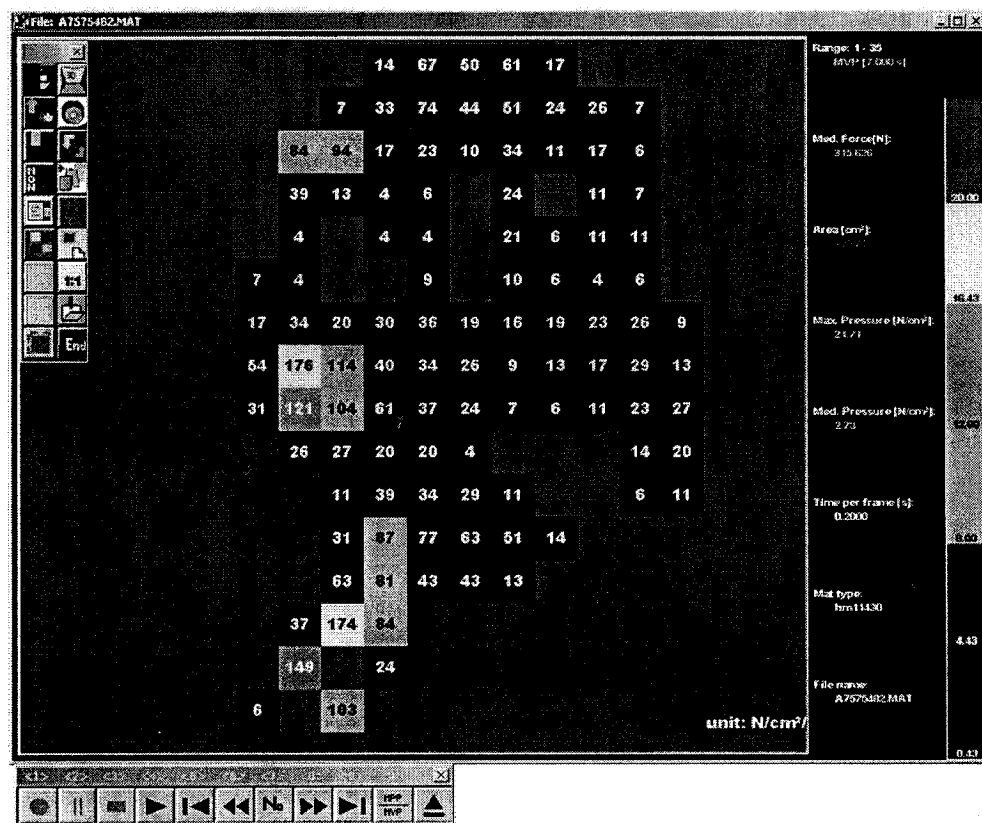


Figure 2.11: The hand/handle interface pressure distributions.

The subjects were instructed to maintain specified grip and push forces to their best ability using the visual displays of both the forces. The contact pressure data were acquired for duration of ten seconds after the subject had assumed steady values of grip

and push forces. The subject was instructed to take a brief rest for approximately one minute between successive measurements.

### 2.3.3 Data analysis

The hand-handle contact pressure distribution was analyzed using the *EMED* software, which computed the total contact force through integration of the local pressure over the effective contact area. The effective contact area was defined as the area covered by sensors with pressure values exceeding a threshold value of 0.143 N/cm$^2$. The threshold value was chosen at this level to minimize electrical background noise in the zero grip and zero push condition. The total contact area can be computed as:

$$A_c = \sum_{i=1}^{n} \Delta A$$

( 2.10)

where $\Delta A$=0.766 cm$^2$ is the sensor area, $i$ and $n$ is the number of active sensors.

Since each sensor area is constant, assuming uniform pressure over the small sensor area the contact force $F_c$ can be estimated from

$$F_c = \Delta A \sum_{i=1}^{n} p_i$$

( 2.11)

where $p_i$ is pressure measured by sensor $i$ and $n$ is the number of active sensors.

The contact condition corresponding to 0 N grip and 0 N push force was realized by lightly grasping the handle covered by the sensing grid, while monitoring the grip and push force displays. The sensing mat, in general, resulted in a contact force in the 1–15 N range under this condition. This was attributed to the subject-related factors, and hysteresis and offset of the sensing mat, and was treated as a bias in the measured signals.

The data acquired for ten subjects and two trials were analyzed to derive the mean and standard deviation values of the contact force corresponding to each grip and push force, and handle size combination. The data attained for two trials revealed very good repeatability in terms of the contact force and contact area.

The *EMED* software could also give and analyze the hand–handle contact pressure distribution and provides the overall peak pressures within specified contact areas. The hand surface was divided into 5 zones, as shown in Figure 2.12, to study the localized peak pressures and contact forces developed within each zone. These zones were identified upon consideration of the hand/handle geometry and the range of hand sizes considered in the study. Zone *1* contains the fingertips of second, third and fourth digits for the range of hand sizes considered, while zone 2 envelops the tip and middle phalange of the first digit and the middle phalanges of digits II, III and IV. Zone *3* consists of the proximal phalanges of the four digits and the adjacent upper extremity of the palm. Zone *4* generally encompasses the upper lateral side of the palm, while the zone 5 in general envelops the upper medial side of the palm. The zone comprising the lower palm and the carpals was excluded, as the contact between this zone and the handles was not observed.

Table 2.6: Sensors numbers in each zone and zonal area ratio to total area for the three different handles.

| Handle Diameter (mm) Zone Number | Zonal Area (cm2) | | | Ratio of Zone Area to Total Area | | |
|---|---|---|---|---|---|---|
| | 30 | 40 | 50 | 30 | 40 | 50 |
| Z1 | 25.278 | 25.278 | 25.278 | 0.25 | 0.214 | 0.188 |
| Z2 | 25.278 | 33.704 | 42.13 | 0.25 | 0.285 | 0.313 |
| Z3 | 25.278 | 25.278 | 25.278 | 0.25 | 0.214 | 0.188 |
| Z4 | 16.086 | 21.448 | 26.81 | 0.159 | 0.182 | 0.199 |
| Z5 | 9.192 | 12.256 | 15.32 | 0.091 | 0.104 | 0.114 |
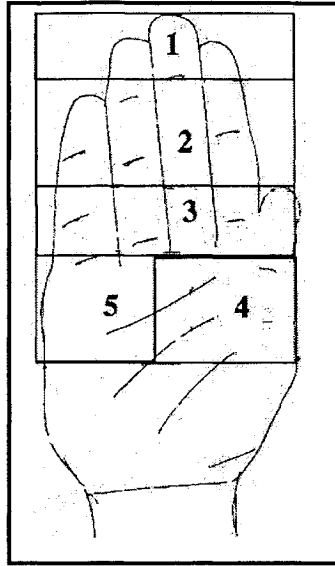
Figure 2.12: The part of hand that in contact with the handle divides to five zones.

## 2.4    Statistical Analyses

In this dissertation, three statistical analysis techniques are employed to derive the linear correlation coefficients, linear multiple regressions and analysis of variance (ANOVA) of the measured data using SPSS 11.5 software. The primary purposes of different statistical analyses include: the study of significance of different contributory factors on the static hand/handle interface peak pressure, contact force and the biodynamic response of human hand-arm exposed to vibration; to build relationships using statistical models for predicting static contact force and peak pressure; and to examine the correlations and associations between the hand-arm biodynamic responses and different definitions of the hand forces in the range of excitation frequencies considered. A brief introductory explanation of the three statistical procedures is given in the following subsections.

## 2.4.1  Linear correlation

Linear correlation provides of measure of, how much the two variables are linearly related, not necessarily how much they are related in general. The most common measure of association between two variables is the correlation coefficient. The correlation coefficient ($r$) is a statistical index of the degree to which two variables are associated. The index was developed by Karl Pearson; it is sometimes called the "Pearson correlation coefficient" (Mendenhall and Sincich, 1984). The correlation coefficient summarizes the relationship between two variables which could be either positive or negative. The Pearson $r$ value ranges from -1.0 to 1.0. A correlation of 1.0 indicates a perfect positive association between the two variables, while a value of -1.0 indicates a perfect negative association. One can think of a correlation as a measure of the degree of overlap, or how much two variables tend to vary together. Their "shared variance" is the amount that the variations of the two variables tend to overlap. The percentage of shared variance is represented by the square of the correlation coefficient, $r^2$. Since the $r^2$ value is interpreted as the percentage of shared variance, it is best to compare two values of $r^2$ rather than those of $r$. For instance, a correlation of 0.8 implies 4 times as much shared variance when compared correlation 0.4, i.e. 0.64 versus 0.16 (Mendenhall and Sincich, 1984).

## 2.4.2  Linear multiple regression

Linear multiple regression assumes that the dependent variable is a linear function of one or more independent variables plus an error introduced to account for all other factors. Multiple linear regressions fit a response variable as a linear combination of a vector of independent variables $\{X\}$ by the method of least squares (Mendenhall and

Sincich, 1984). Multiple regressions establish that a set of independent variables explains a proportion of the variance in a dependent variable at a significant level (significance test of $R^2$), and can establish the relative predictive importance of the independent variables. The multiple regressions generally takes the form

$$Y = c + b_1 X_1 + b_2 X_2 + ... + b_n X_n + e. \qquad (2.12)$$

where the $b_1$, $b_2$, ..., $b_n$ are the regression coefficients for the corresponding $X$ (independent) terms, $c$ is the constant or intercept representing the amount the dependent variable when all the independent variables vanish, and $e$ is the error term reflected in the residuals. Associated with multiple regressions is $R^2$, multiple correlation coefficients, which relate to the percent of variance in the dependent variable due to collectively variation in all of the independent variables.

## 2.4.3 Analysis of variance (ANOVA)

Analysis of variance (ANOVA) is a widely applied statistical technique used to formally compare the effects of different kinds of categorical factors on one or more measured quantitative variable(s). ANOVA is used to uncover the main and interaction effects of categorical independent variables (called "factors") on an interval dependent variable. ANOVA yields the statistical variability of the response variable around the mean, and whether there is separation or overlap suggestive of a notable effect (Turner, and Thayer, 2001). ANOVA is a decomposition of the observed variance into its component parts by different factors level. This involves calculations of the proportion of the total observed variance that is attributable to a given categorical variable or treatment factor. The application of ANOVA requires that the populations are normally distributed,

independent and have equal standard deviations ($\sigma$). However, it has shown that ANOVA is "robust" to violations of its assumptions (Turner and Thayer, 2001; Mendenhall and Sincich, 1984). The probability values computed in an ANOVA are satisfactorily accurate even if the assumptions are violated.

The experimental data acquired with human subjects generally exhibits two types of variabilities; variability due to being part of a group or within the group and variability among or between groups (e.g., on average). A null hypothesis of no difference between categorical independent variables and a quantitative dependent response variable is often tested using ANOVA. The results however deal with two hypotheses: the null and the alternative hypotheses. The null hypothesis states that the means of the different groups are the same (i.e. there are all independent estimates of the same population mean). Consequently, the independent variable has no effect on the dependent variable. Whereas the alternative hypothesis denotes that the sample means are estimates of different population means and hence differ from each other. Accordingly, the independent variable has an effect on the dependent variable.

When three or more population means or more are compared, the null and alternate hypotheses could be written as:

$$H_0 : \mu_1 = \mu_2 = \mu_3 = ..... = \mu_n \; ; \; H1 : not \; all \; means \; are \; equal \qquad (2.13)$$

where H0 and H1 refer to the null and alternate hypotheses outcomes, respectively, $\mu_i$ (i= 1,2,...n) are population means under different levels of independent tested variables. The rejection of a null hypothesis, however does not identify which populations differ significantly. It merely indicates that a difference between at least one pair of means

exists. The analyses are performed by partitioning the variances of each data point taken into different groups. ANOVA compares the within-group variance and the between-group variance, such that:

1. The within-group variance ($MS_w$) is a measure of any variation from one individual to another within each group considered. Generally, the within-group variance should be approximately equal for each group.

2. The between-group variance ($MS_b$) is calculated by taking difference between the total variance (all variances for each data point summed together, regardless of grouping) and the within-group variance.

If the average variance within each of the groups ($MS_w$) is approximately same as the variance among the group means ($MS_b$), the null hypothesis can be considered to be true since all the differences are due only to sampling error. When an independent variable has an effect and the sample means represent different population means resulting in variance among the treatment means ($MS_b$) greater than the average variance within the groups ($MS_w$), the null hypothesis is consider being false and rejected.

The key application of ANOVA is the significance tests involving F-test or the F-ratio test. The *F*-test is an overall test of the null hypothesis that group means on the dependent variable do not differ. It is used to test the significance of each main and interaction effect. For most ANOVA designs, *F-ratio* is between-groups mean square variance divided by within-groups mean square variance (between-groups variance is the variance of the group means from the overall mean of all observations; within-groups variance is a function of the variances of the observations in each group weighted for the group size). The larger the ratio of between-groups variance (a measure of effect) to within-groups variance (a measure of noise), the less likely that the null hypothesis is true. The result is an *F-ratio* statistic (*F-ratio* value) that is compared to probabilities ($p$,

75

based on the F-distribution) given the sample size (N) and number of factors involved (degrees of freedom). This in turn indicates at what probability level observed differences are significant, generally differences being deemed significant if $p<$ .05 (which means there is only a 5% chance of incorrectly concluding that differences are significant when in reality they are not).

The *F-ratio* statistic is the ratio of two variance estimates, given by:

$$F\text{-}ratio = \frac{Variance\ between\ sample\ means}{Variance\ expected\ by\ chance}$$

(2.14)

There are $(k-1)$ degrees of freedom associated with the numerator in the above relation for *F-ratio*, and $(N-k)$ degrees of freedom are associated with the denominator, where $k$ is the number of populations and $N$ is the total number of sample observations. ANOVA are performed to investigate the main and interaction effects of independent variables. The main effects are the unique effects of the categorical independent variables. If the probability of *F-ratio* is less than .05 for any independent, it is concluded that the variable does have an effect on the dependent variable. The interaction effects are the joint effects of pairs, triplets, or higher-order combinations of the independent variables, different from what would be predicted from any of the independents variable acting alone. In the presence of significance interaction, the effect of a single independent variable on a dependent variable varies with the values of another independent variable. The main effects would be less meaningful in a fixed effect model. In this case, the effect of a given factor would be examined at each level of the other factor(s). If the probability of *F-ratio* is less than .05 for any such combination, we conclude that the interaction of

the combination does have an effect on the dependent variable. The interaction between two independent variables, however, does not imply that the two variables are correlated.

Depending on the independent factors employed in the experiment or the study on the dependent measure, ANOVA could be categorized as one-way, two-way and M-way ANOVA. One-way ANOVA analysis tests differences in a single interval dependent variable among two, three, or more groups formed by the categories of a single categorical independent variable. Also known as single classification ANOVA, or one-factor ANOVA, this design deals with one independent variable and one dependent variable. It tests whether the groups formed by the categories of the independent variable seem similar. When the groups seem different, it is concluded that the independent variable has an effect on the dependent.

The two-way ANOVA is used to analyze one interval dependent variable in terms of the categories (groups) formed by two independents variables. Two-way ANOVA tests whether the groups formed by the categories of the independent variables have similar centroids. The M-way ANOVA in similar manner deals with n independents. It should be noted that as the number of independent variable increases, the number of potential interactions proliferates associated with factorial ANOVA. Two independents have a single first-order interaction (AB). Three independents have three first order interactions (AB, AC, BC) and one second-order interaction (ABC). Four independents have six first-order (AB, AC, AD, BC, BC, CD), three second-order (ABC, ACD, BCD), and one third-order (ABCD) interaction, or 10 in all.

Many different ANOVA models have been used, depending on the assumptions related to the sources of error (Turner and Thayer, 2001). The most commonly used

77

models include the fixed, random, and mixed models. A fixed model assumes that the treatments or factors are indeed fixed, and any conclusions drawn about those treatments or factors cannot be extended beyond those levels. A random model assumes that the treatments are random samples of a larger population, and therefore can be used to extrapolate the results beyond the measured values. A mixed model incorporates fixed and random approaches in different parts. Random ANOVA model has been used in this dissertation for analysis of main and interaction effects of various contributory factors.

The different experiment designs could be considered for ANOVA, while the *F-ratio* is influenced by design approach chosen, however the resulting data are interpreted in a similar manner. In this study two ANOVA designs are used to statistically analysis the roles of different factors on: between-groups and within-groups. Between-groups ANOVA design is considered, when a dependent variable is measured for independent groups of samples, where each group is exposed to a different condition. The set of conditions is implied in the experiment called a between-subjects factor. The groups correspond to conditions, which are categories of a categorical independent variable. The variances of the individual groups are analyzed to be examined If the variance of the dependent variable between groups is different from the variance within groups when the variance between groups is sufficiently larger than the variance within groups, as measured by the F ratio, it is concluded that the grouping factor (the independent variables) do have a significant effect. Repeated measures or within-groups ANOVA design is used when a dependent variable is measured repeatedly at different time points (i.e., before and after treatment) for all sample members across a set of conditions (the categories of an independent variable). In the within-groups or repeated measures design,

there is one group of subjects. The conditions are the categories of the independent variable, which is the repeated measures factor, and each subject is exposed to each condition and measured (Turner and Thayer, 2001; Girden, 1992)..

2.5  Summary

Two sets of experimental system, were developed in this dissertation work, have been described in details in this chapter. The experiments work was performed in two phases involving the biodynamic and interface pressure measurements. In first phase, seven adult male subjects participated in the experiments to study the hand-arm biodynamic responses to vibration with six different handles exposed to two levels of broadband random vibration along the $z_h$ and $x_h$- axes, and different grip and push force combinations. The second phase of the experiments work involved measurements of the static hand/handle contact force and contact pressure distributions, and pressure peaks over the hand surface, as functions of the grip and push forces, and handle size. A total of ten adult male subjects participated in this phase. The hand-handle interface contact pressure distributions were acquired at the NIOSH laboratory using the *EMED* measurement system of *NOVEL Electronics*, while those on the biodynamic responses were conducted at the IRSST laboratory. The analyses methods including the statistical analyses have been also described in this chapter.

CHAPTER 3

STATIC CONTACT FORCE AND PRESSURE DISTRIBUTION

AT HAND-HANDLE INTERFACE

3.1    Introduction

Work related musculoskeletal symptoms and injuries, such as carpal tunnel syndrome, tendonitis and vibration induced white finger are common among operators of hand-held power tools (Nathan et al., 1988; Nilsson et al., 1993). Operation of some of these tools demands high grip, push or hand-handle contact force, which is known to be one of the primary factors that increase the risk of cumulative trauma disorders (Radwin et al., 1987; Rempel et al., 1992; Reidel, 1995). Many studies have suggested that the contact force between the hand and a tool handle affect the severity of exposure to the HTV and hand-wrist cumulative trauma disorders (Fransson and Winkel, 1991; Pyykkö et al., 1976; Radwin et al., 1987). The reported studies on biodynamic response of the human hand and arm to HTV suggest that an increase in the hand force yields an increase in the magnitude of the driving-point impedance response (Burström, 1997; Kihlberg, 1995; Gurram et al., 1995). Hartung et al. (1993) has also shown that the magnitude of vibration transmitted from a vibrating handle to the wrist increases considerably with increase in the grip and push forces. The increase also resulted in higher frequency of the peak vibration transmissibility. Other studies have established that the electrical activity of the m.flexor carpi ulnaris and finger-flexor muscles increase with increasing hand-handle coupling intensity, while the peripheral circulation of fingers decreases (Iwata et al., 1972; Pyykkö et al., 1976; Miyashita et al., 1990; Gurram et al., 1995).

Although the above studies have established an association between the magnitude of hand-handle coupling force and various measures of the hand-arm responses, the mechanisms leading to risk of hand-wrist cumulative trauma disorders have not been identified. High contact forces impose high stresses on the anatomical structure of the hand, which may be strongly affected by many factors, such as working posture, weight of the tool, grip and push forces, handle size, individual work habits and hand-handle interface pressure. The hand force in these studies is considered either as the grip force or the push force.

While the majority of the studies on assessment of hand-tool operators have emphasized the consideration of overall contact force (Reidel, 1995; Kaulbars, 1996; ISO-5349-1, 2001; ISO/WD-15230; 2000); the direct measurement of contact force has not yet advanced for application to power tools (Welcome et al., 2004). Moreover, the hand force may have a synergistic effect with vibration exposure on anatomical structures, such as the vascular system, nerves and joints. The assessment of health and safety risk associated with exposure to hand-transmitted vibration, as defined in the current standard (ISO-5349-1, 2001), is solely based upon amplitude, frequency and duration of vibration exposure, while the contribution due to the hand force is ignored. Owing to the strong dependence of the hand–arm responses on the hand force, the need to measure the hand force has been recognized by many investigators, and an international draft standard (ISO/WC 15230, 2004) has been proposed specifically for the hand force measurement. Although ISO-5349-1 (2001) emphasizes the need for measurement of the hand force, the standard provides no guidance regarding the techniques that can be used

for the hand force measurement. This is most likely attributed to lack of a reliable measurement methodology (Welcome et al., 2004).

On the other hands, some studies have suggested that the perception of discomfort, fatigue and loss of productivity is related to concentration of localized forces at the hand-handle interface, as opposed to the total contact force (Gurram et al. 1995). Existence of a high pressure on the surface of the hand, arising from grasping a tool handle, could cause a sense of discomfort or pain under sustained loading, which is often a limiting factor during work and may lead to potential impending tissue damage. Sensitivity of the hand to externally applied pressures has been investigated using an algometer to establish the pressure-discomfort threshold (*PDT*) and pressure-pain threshold (*PPT*) (Muralidhar and Bishu, 2000; Fransson-Hall and Kilbom, 1993; Johansson et al., 1999). These studies concluded that the thenar area, the skin fold between the thumb and index finger, and region around os pisiform have low *PPT* and *PDT* in relation to the rest of the hand surface. The tips of digits IV and V, and the zone near the fourth metacarpal were also found to exhibit low *PDT*.

The grasping and guiding of a tool handle yields highly uneven distribution of forces at the hand surface (Gurram et al. 1995), which could vary considerably with hand and handle sizes, push and grip forces and nature of vibration. Only a few studies have attempted to study the distributed hand forces at the hand-handle interface and its dependence on the handle size, and grip and push forces that could serve as a vital basis for the design of handles. Limited efforts in the area have most likely been attributed to lack of reliable measurement methods. Fellows and Freivalds (1991) applied 14 force-sensing resistors to study the relative distribution of subjects' grip force on wooden (30

mm diameter) and foam covered (38 mm diameter) handles, while performing specified tasks. Gurram et al. (1995) used a total of 20 capacitive sensors to study the hand-handle interface pressure distribution under different magnitudes of grip force and handle vibration. Both studies showed the presence of high magnitude local forces on the tips of the index and middle fingers, and base of the thumb (thenar eminence). It was further shown that the magnitudes of local forces increase considerably with increasing grip force and their concentration shifts considerably under the presence of vibration (Gurram et al., 1995). The dependence of localized pressure peaks on the hand surface, handle size and push force, however, have not been investigated. Moreover, the limited number of sensors used in these studies would affect the accuracy of the reported quantitative data.

In this part of dissertation work, the hand-handle contact force and pressure distributions are acquired for 10 participants using three different diameters of circular cross-section handles, using a 16x11 pressure sensing grid under different combinations of static grip and push forces. The measured data are analyzed to compute the contact area and forces, and to identify the magnitudes and locations of localized pressure peaks occurring at the hand surface as functions of the handle size and static hand forces (grip and push). The relationships between both contact force and peak pressures, and grip and push forces are established for different handle sizes.

3.2    Hand/Handle Interface Contact Force and Effective Contact Area

The hand-handle interface pressure data acquired for the ten subjects are analyzed to derive the total contact force and effective contact area as function of the handle size, and grip and push forces. The total contact force is derived upon integration of the measured

hand-handle interface pressure over the effective contact area, as described in section 2.3.3. The effective area is computed upon considering the number of pressure sensors within the grid that indicate pressure value in excess of the threshold value of 1.43 kPa. It should be noted that each sensor in contact with the hand yields a contact area of 0.766 $cm^2$. The computed contact force and effective area data are further analyzed to derive the mean values and standard deviations of the means for different handle size, and combinations of grip and push forces.

Figure 3.1 illustrates the mean contact forces together with the standard deviation of the means, derived from the data acquired for 10 subjects and for three different cylindrical handle sizes considered (30, 40 and 48 mm diameter). The results show the variations in the contact force as a function of the push force for each handle corresponding to five different magnitudes of static grip force. The results reveal nearly linear dependence of the contact force on both the grip and push forces, as concluded by Welcome et al. (2004). The overall contact force developed at the hand-handle interface is a function of the interface pressures and the effective contact area, which would depend upon the handle size. The results show a linear dependence of the contact force on the push force, irrespective of the grip force magnitude and handle size. The correlation coefficients ($r^2$) of all of the linear fits were greater than 0.99. The measured contact forces show fairly small inter-subject variability as evidenced form the relatively low standard deviations of the mean contact force, which are shown as error bars in the Figure. The results also show that the contact force developed between the hand and the handle increases as the handle diameter decreases, which may be attributed to the higher contact pressure caused by a smaller handle. The contact force developed between the

hand and the smaller 30 mm diameter handle is noticeably larger than that attained with

the larger 48 mm diameter handle.
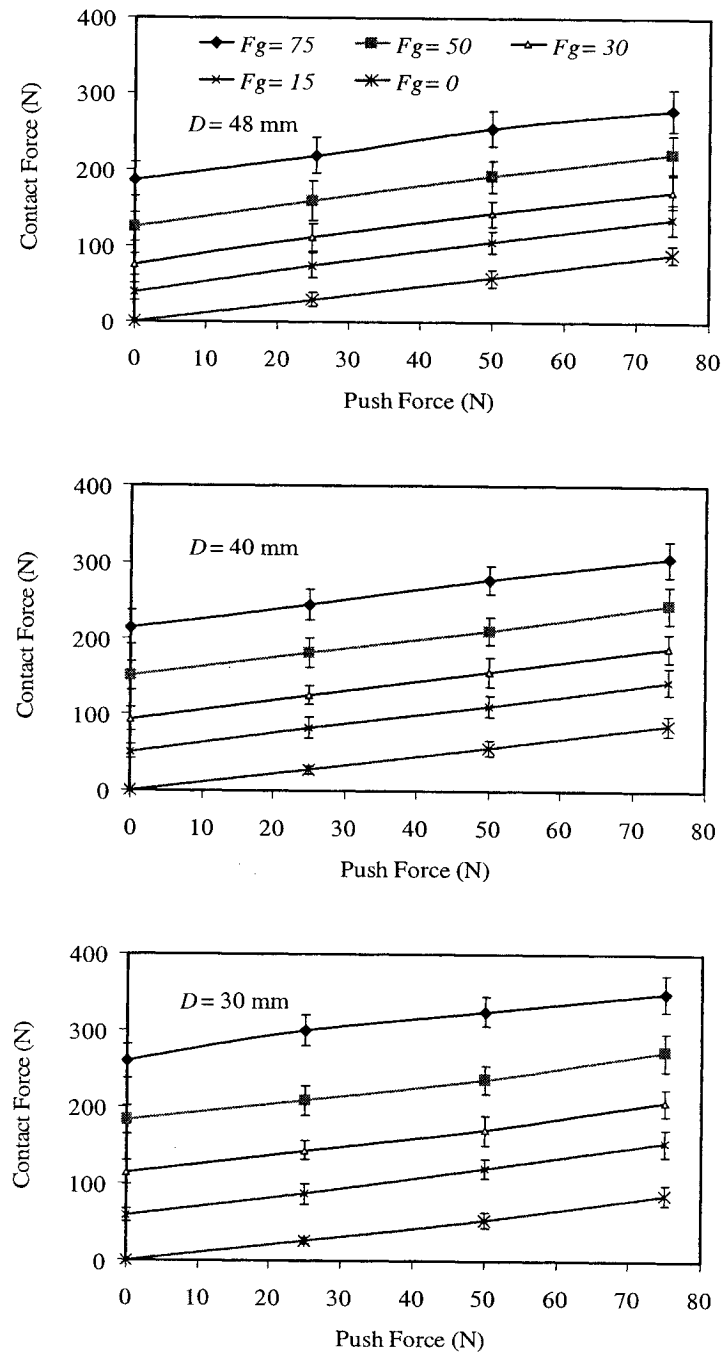


Figure 3.1: Variations in mean contact force as a function of push force under different levels of constant grip force.

Figure 3.2 demonstrates the mean contact force as function of the grip force under different magnitude of constant push force for the three different handles. The results also show a linear dependence of the contact force on the grip force, irrespective of the push force magnitude and the handle size. The correlation coefficients ($r^2$) of all of the linear fits were also greater than 0.99, as obtained for the push force variations in Figure 3.1. The variations in both grip and push forces cause a nearly constant shift in the contact force for different handles. A comparison of Figures 3.1 and 3.2, suggests that the increase in contact force is considerably larger with increasing grip force increases than that with the push forces. The rates of change of contact force with respect to the push force remain similar for all handle sizes, further suggesting approximately direct dependence of the contact force on the push force, irrespective of the handle size and thus the effective contact area.

Owing to the observed linear relationship with respect to the grip $F_g$ and push $F_p$ forces, the contact force $F_c$ can be modeled and expressed as:

$$F_c = \gamma + \alpha( D )F_g + \beta( D )F_p$$

( 3.1)

where $F_g$ and $F_p$ are the constant grip and push forces, respectively. The coefficient $\gamma$ is used to take into account the contact force offset caused by the presence of a preload on the sensing mat around the handle, while $\alpha(D)$ and $\beta(D)$ are the constant coefficients representing the contributions due to grip and push forces respectively, which depend upon the handle diameter. Following the multiple linear regression analysis, the contact force offset is removed by setting $\gamma = 0$. The grip and push force coefficients, derived for each subject, together with their mean values and standard deviations are summarized in

Table 3.1 for different handle sizes. For each subject and handle combination, the linear regressions resulted in correlation coefficients ($r^2$) in excess of 0.99.
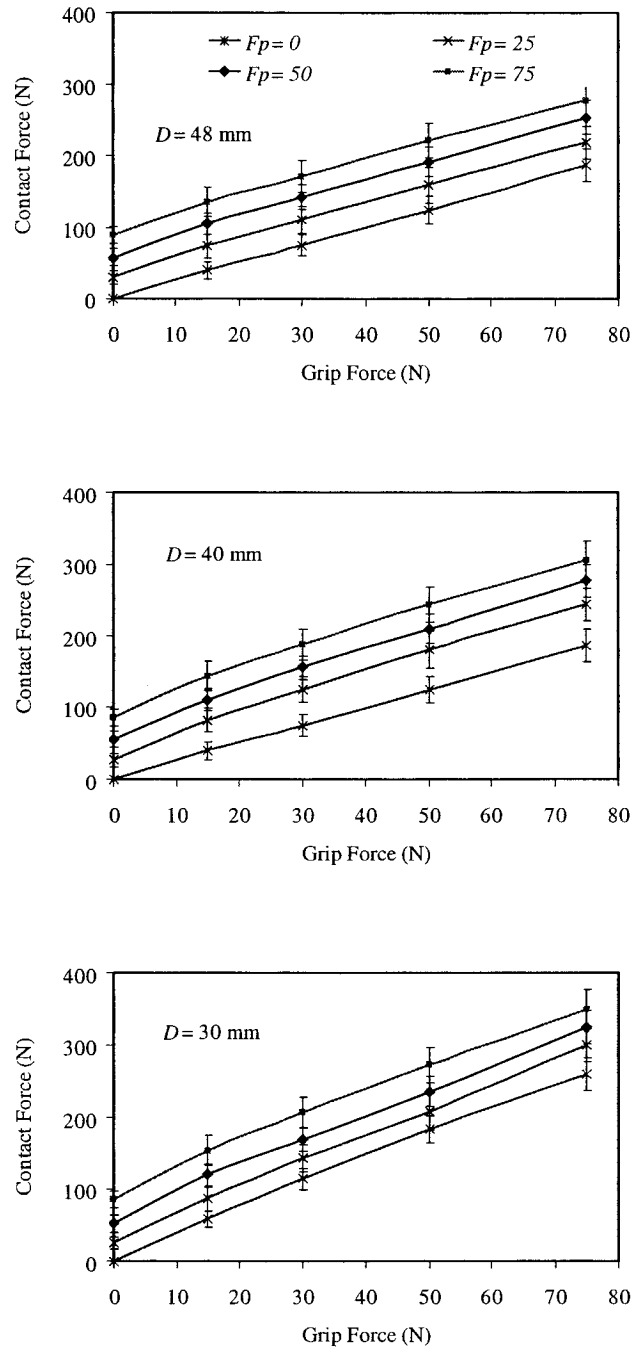


Figure 3.2: Variations in mean contact force as a function of grip force under different levels of constant push force.

Table 3.1: Regression coefficients representing contribution of the grip and push forces to the total contact force.

| Subject | Handle Diameter | | | | | |
|---|---|---|---|---|---|---|
| | 30 mm | | 40 mm | | 48 mm | |
| | α | β | α | β | α | β |
| A | 3.79 | 1.11 | 3.11 | 1.14 | 2.56 | 1.11 |
| B | 3.80 | 1.14 | 3.03 | 1.03 | 2.69 | 1.01 |
| C | 3.50 | 1.12 | 2.77 | 0.90 | 2.24 | 0.99 |
| D | 3.30 | 1.08 | 3.04 | 1.25 | 2.65 | 1.14 |
| E | 3.37 | 1.09 | 2.67 | 1.07 | 2.52 | 1.04 |
| F | 3.02 | 0.98 | 2.63 | 1.02 | 2.34 | 1.36 |
| G | 3.17 | 1.20 | 2.51 | 1.21 | 2.45 | 1.07 |
| I | 3.25 | 1.02 | 3.19 | 1.08 | 2.70 | 1.18 |
| J | 3.32 | 1.04 | 2.76 | 1.20 | 2.74 | 1.21 |
| K | 3.55 | 1.08 | 3.03 | 1.13 | 2.30 | 1.20 |
| Mean ; Std. dev. | 3.40 ; 0.25 | 1.09 ; 0.06 | 2.87 ; 0.23 | 1.10 ; 0.10 | 2.51 ; 0.18 | 1.13 ; 0.11 |

The contact force dependence on the grip force tends to decrease more rapidly with the handle size, while its sensitivity to push force appears to be relatively small when handle diameter is increased from 30 to 48 mm. These variations in dependence of the contact force on the grip and push forces for different handle sizes are attributed to changes in the contact area and hand–handle interface pressure in a complex manner. The variations in the model coefficients $\alpha(D)$ and $\beta(D)$ with respect to the handle size are further illustrated in Figure 3.3. The curve-fittings performed on the data show that the diameter dependence can be described by the following linear functions;

$$\alpha(D) = -0.0496D + 4.878 \qquad (3.2)$$

$$\beta(D) = 0.0022D + 1.021 \qquad (3.3)$$

where $D$ is in mm and the above model considers to be valid for the handle diameter between 30 and 48 mm.
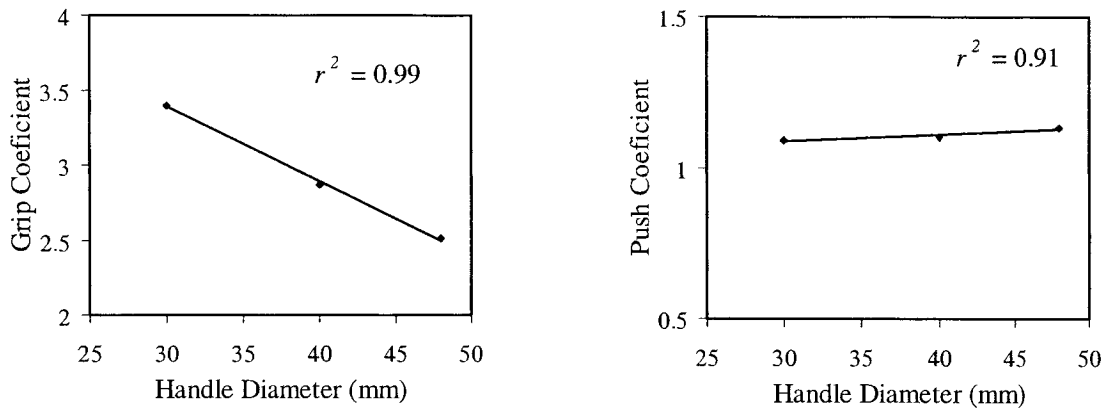
Figure 3.3: Variations in model coefficients with respect to handle diameter.

These results show that despite some variations between individuals, the mean push force coefficient is close to unity for all handles, while the mean grip force coefficient varies from 2.51 to 3.40, decreasing with increase in the handle diameter. The grip force thus contributes on the average three times as much as the push force to the total contact force, while its contribution decreases as the handle diameter increases. The push force can be considered to contribute almost directly to the contact force, since it is applied over a small portion of the hand surface area (upper lateral side of the palm) normal to the applied push force axis. The grip force, on the other hand, causes application of pressure over a larger surface of the handle and thus yields considerably larger contribution to the total contact force, which is derived from summation of grip pressure-induced force components acting normal to the entire contact area. The grip force, as defined in ISO/CD 15230 (2004), involves measurement of axial component alone acting along the $z_h$-axis, while neglecting the non-axial components acting on the handle surface. The consideration of these non-axial components yields considerably larger value of the grip force coefficients. Moreover, as the handle diameter increases, the subjects' hands apply grip pressure over partial handle surface as limited by the hand

size, which results in relatively smaller contribution of the grip component to the contact force. In contrast, the subjects' hands utilize larger proportion of the handle surface while gripping a smaller diameter handle, leading to a larger grip force coefficient.

Figure 3.4 illustrates the effective hand–handle contact area as a function of the grip and push forces for all three handle sizes. The contact areas tend to rapidly approach nearly steady values as the grip force exceeds 30 N, irrespective of the handle size. The 48 mm handle yields the maximum steady value of the contact area, while the 30 mm yields the lowest value. The difference between the contact area between 30 and 40 mm handles is considerably less than that between the 40 and 48 mm handles. Considering that the contact force is a function of the effective contact area and magnitudes of interface pressure, the high contact force developed with the 30 mm diameter would suggest the presence of relatively higher interface pressures. Higher push forces yield slightly larger contact area, irrespective of the handle size and the grip force.

## 3.3    Distribution of Contact Force

The distribution of contact force in the hand/handle interface is analyzed for different handle sizes and combinations of grip/push forces in terms of contact force ratio ($CFR$), defined as the ratio of contact force developed within a zone to the total hand-handle contact force. The five assigned zones of the hand in contact with a handle have been described in details in section 2.3.3. Zones $1$ through $5$ are labeled as $Z1$, $Z2$, $Z3$, $Z4$ and $Z5$, respectively in Figures 3.5 to 3.7, which illustrate the $CFR$ for the five zones under different combinations of grip and push forces for the three handles.
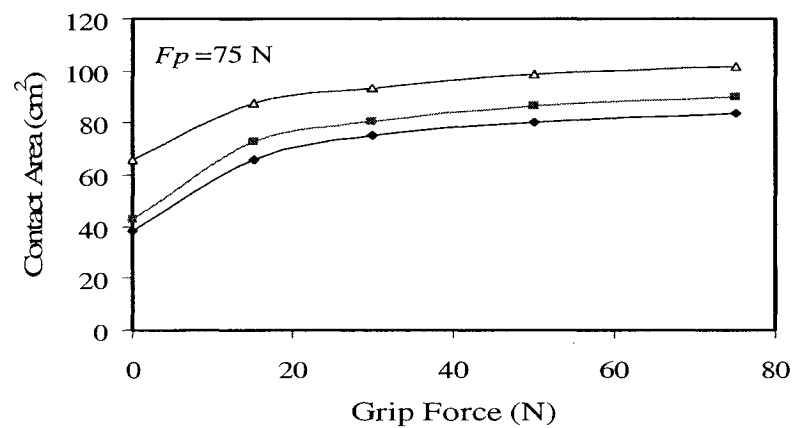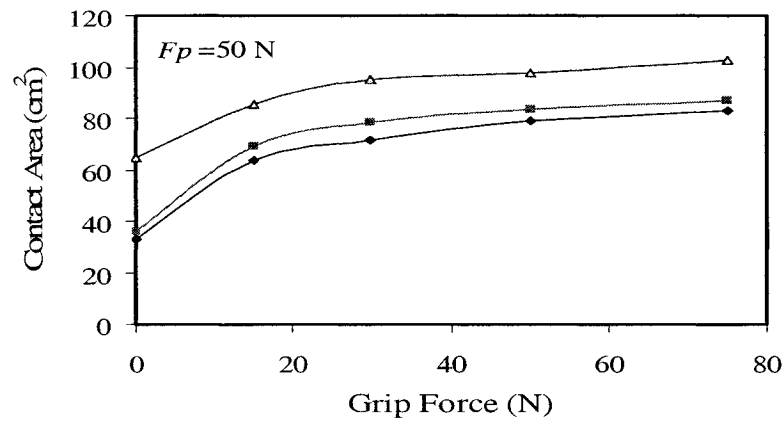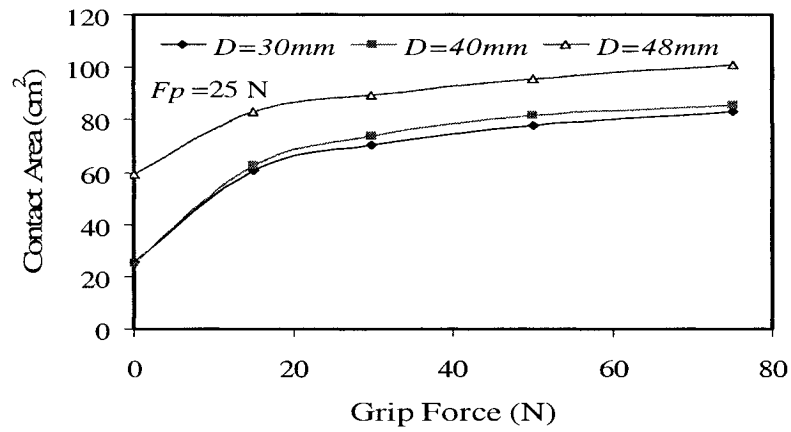
Figure 3.4: Variations in effective contact area as a function of grip force under different levels of constant push force under three different handles

The results clearly show that zone *4* (generally encompasses the upper lateral side of the palm) contributes the most to the total hand-handle interface force for the 48 mm handle, irrespective of the grip and push force combination, as shown in Figure 3.5. The *CFR* of this zone generally increases with increase in push force, and decreases with increase in the hand grip force. The *CFR* values in zones *2-4* seem to asymptotically approach steady values with increase in the push force as the effective contact areas saturate. Under the application of a push force alone, the contribution of zone *3* (proximal phalanges of the digits) to the total contact force is highest after zone *4*, while the contributions of zone *1* (fingertips) is almost negligible. The steady values of *CFR* due to zone *1* increase with increasing grip force, but decrease with increasing push force. For grip force equal to or higher than 15 N, zones *2* and *3* yield comparable values of *CFR*, while the contribution due to zone *5* (the medial side of the palm) is almost negligible for all grip/push combinations.

The distributions of the contact forces for the 40 and 30 mm handles are quite different from the 48 mm handle, as evident in Figs. 3.6 and 3.7, respectively. For the 40 mm handle, the zone *4* yields the highest *CFR* under either zero or light grip force (15 N); while zone *1* shows the largest *CFR* under zero push force and all nonzero grip forces. The contribution of zone *3* comprising the proximal phalanges of the digits is higher than zone *2*. An increase in push force causes an increase in *CFR* of zones *3* and *4*, but decrease in those of zones *1* and *2*. For the 30 mm handle, zone *3* (proximal phalanges of the digits) tends to contribute the most to the total contact force, specifically when the push force is above 15 N, while zone1 yields higher *CFR* for zero push force, suggesting more contact between the fingers tips and proximal phalanges, as shown in Figure 3.7.

The *CFR* of zone *4* is considerably smaller than those observed for the 40 and 48 mm handles.
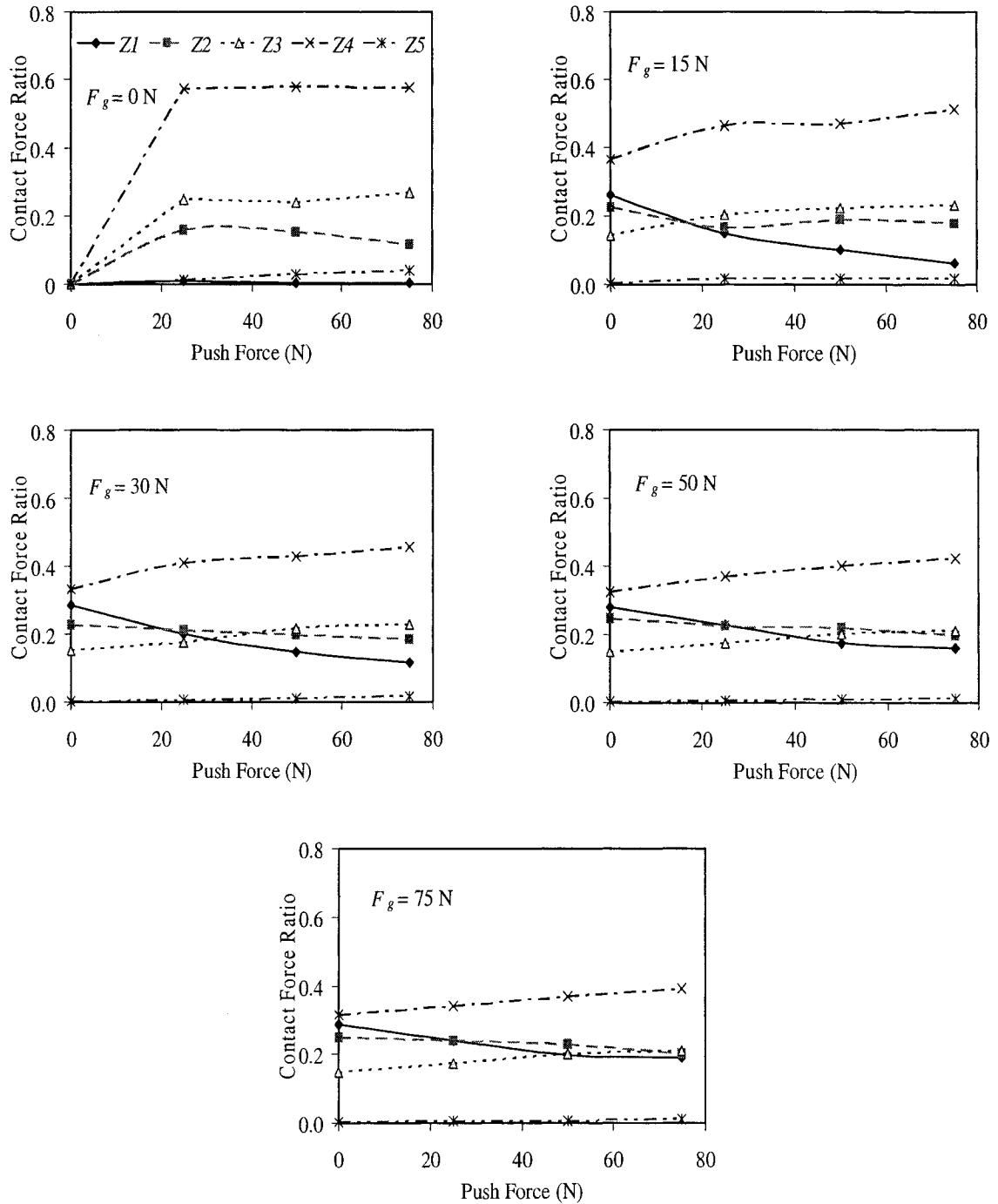


Figure 3.5: Contact force distribution among different zones as functions of the push and grip forces (48 mm handle).
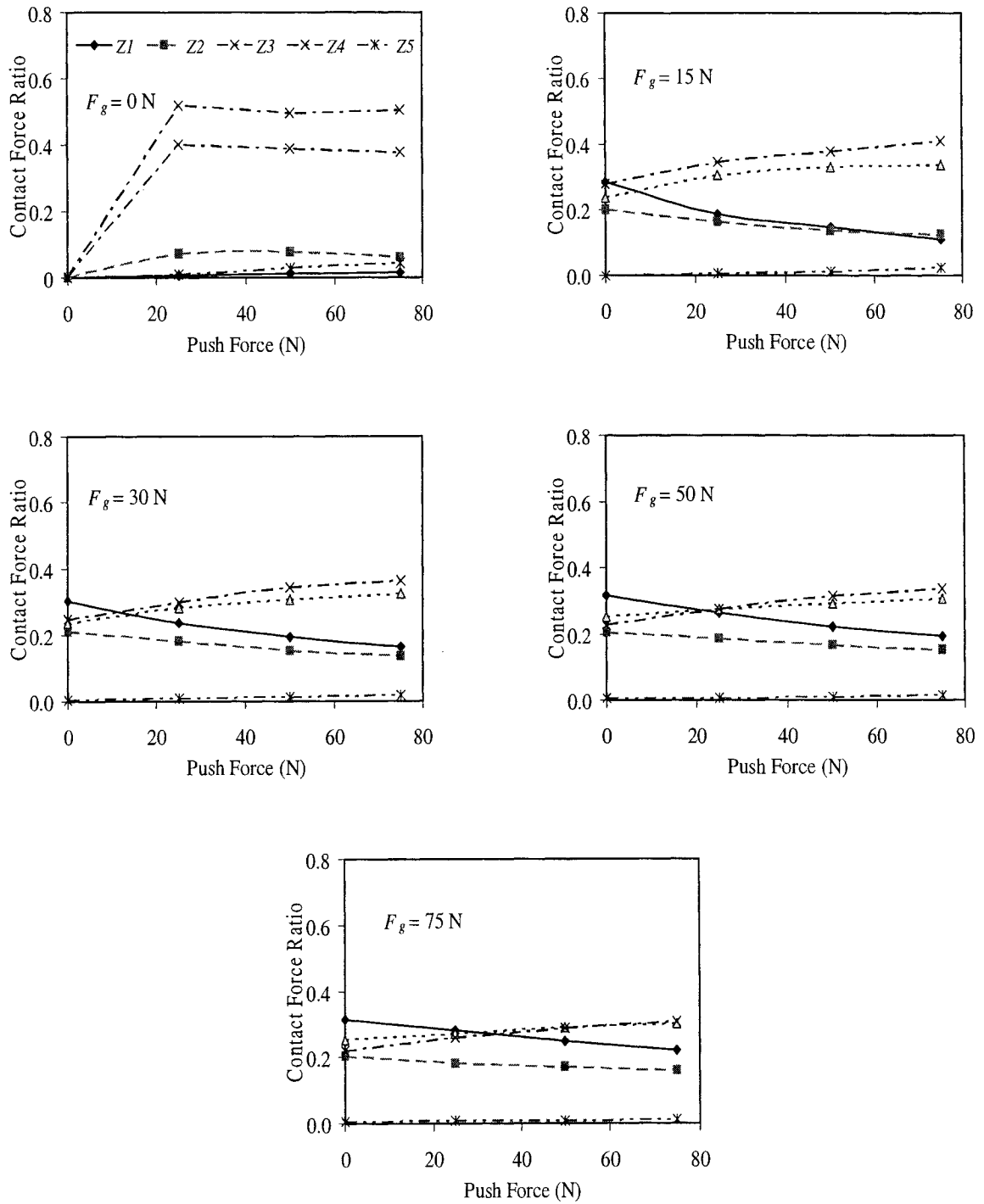
Figure 3.6: Contact force distribution among different zones as functions of the push and grip forces (40 mm handle).
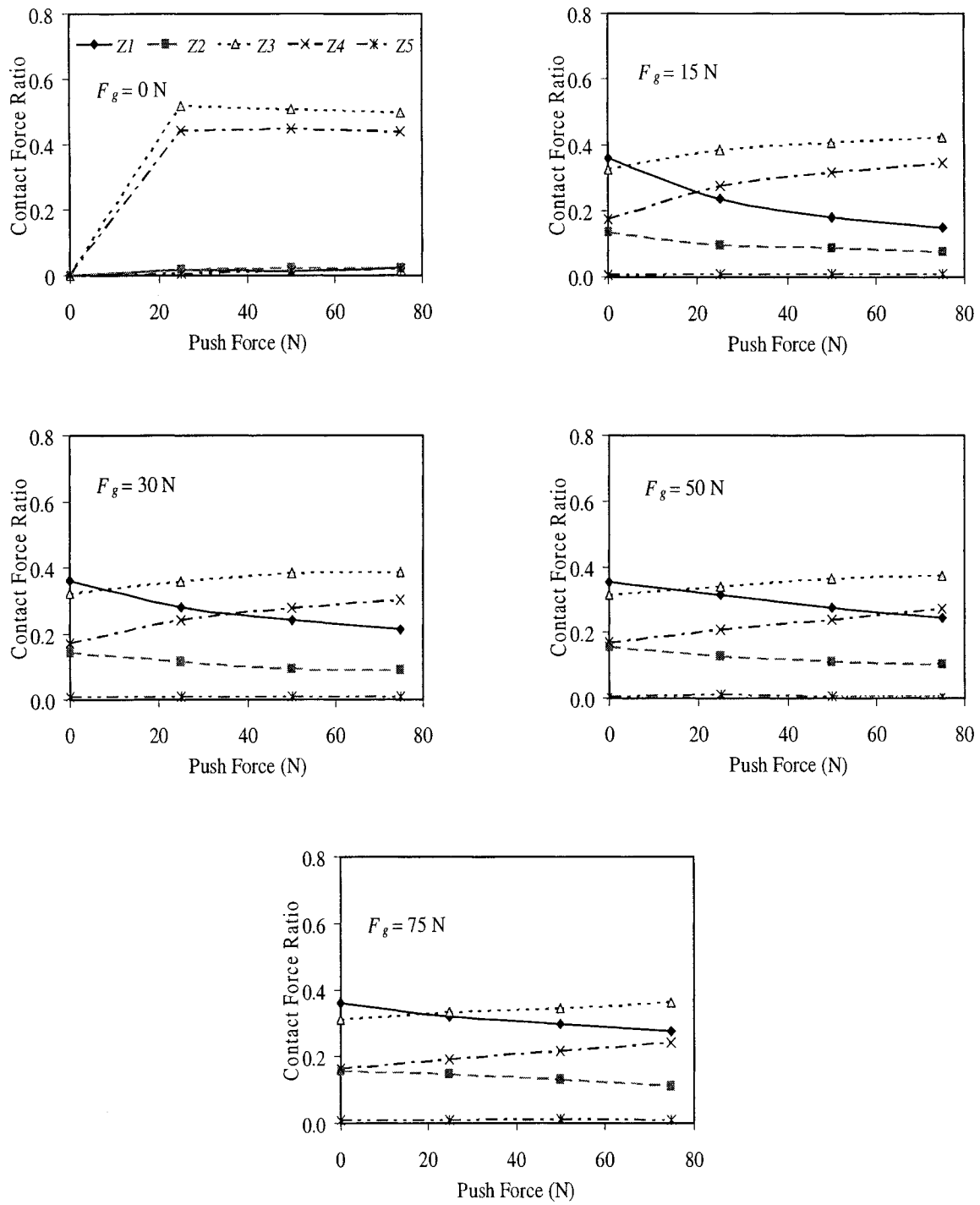
Figure 3.7: Contact force distribution among different zones as functions of the push and grip forces (30 mm handle).

Figures 3.8 to 3.10 demonstrate the *CFR* of each zone as a function of the push force

for different grip forces and handle sizes. The results show similar trends in *CFR* of

different zones for all three handles. The *CFR* of zone *1* decreases as push force

increases, irrespective of the grip force magnitude, and tends to be higher for higher grip

force. The *CFR* of zone *2* comprising the middle phalanges also exhibits similar trends,

while it decays at a relatively slow rate with increase in the push force. The trend,

however, differs under 0 grip condition, where it initially increases from a zero value to a

peak value corresponding to 25 N push force and then either decreases or remains nearly

constant. The *CFR*s of zones *3* and *4* exhibit trends opposite to those observed for zones

*1* and *2*, where *CFR*s generally increase with increasing push force and tend to be lower

under higher grip applied by the subjects. The *CFR* in zone *4* increases considerably with

the increase of push force and decreases with higher levels of grip  force. The *CFR* of

zone *5* comprising upper medial side of palm is negligible for almost all levels of

grip/push forces, and handle sizes.

### 3.3.1   Relationship between the zonal contact force and hand forces

Figures 3.5 to 3.7, show that the distribution of contact force in the hand-handle

interface strongly depends on the grip and push forces, and the handle diameter. Multiple

linear regression analyses showed linear variations in the contact forces measured in each

zone with grip and push forces for all handles, while the correlation coefficients  obtained

were higher than 0.99 in all cases. Owing to extremely small contact force in zone *5*, the

data attained for zone *5* was added to zone *4*. The resulting zone, referred to as zones *45*,

would thus represent the upper palmar surface of the hand.
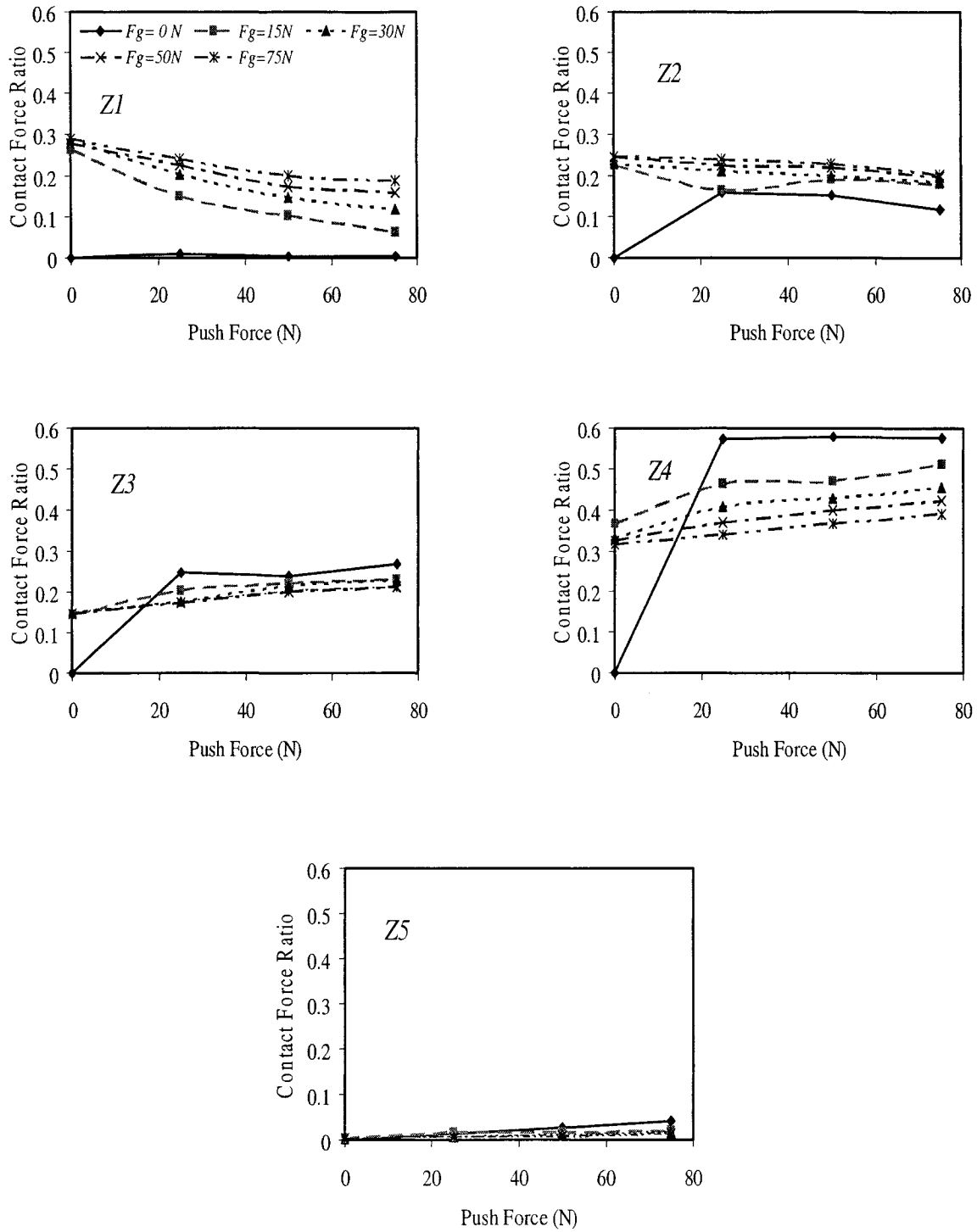
Figure 3.8: Contact force contribution in each zone as function of push force for constant grip force for 48 mm handle.
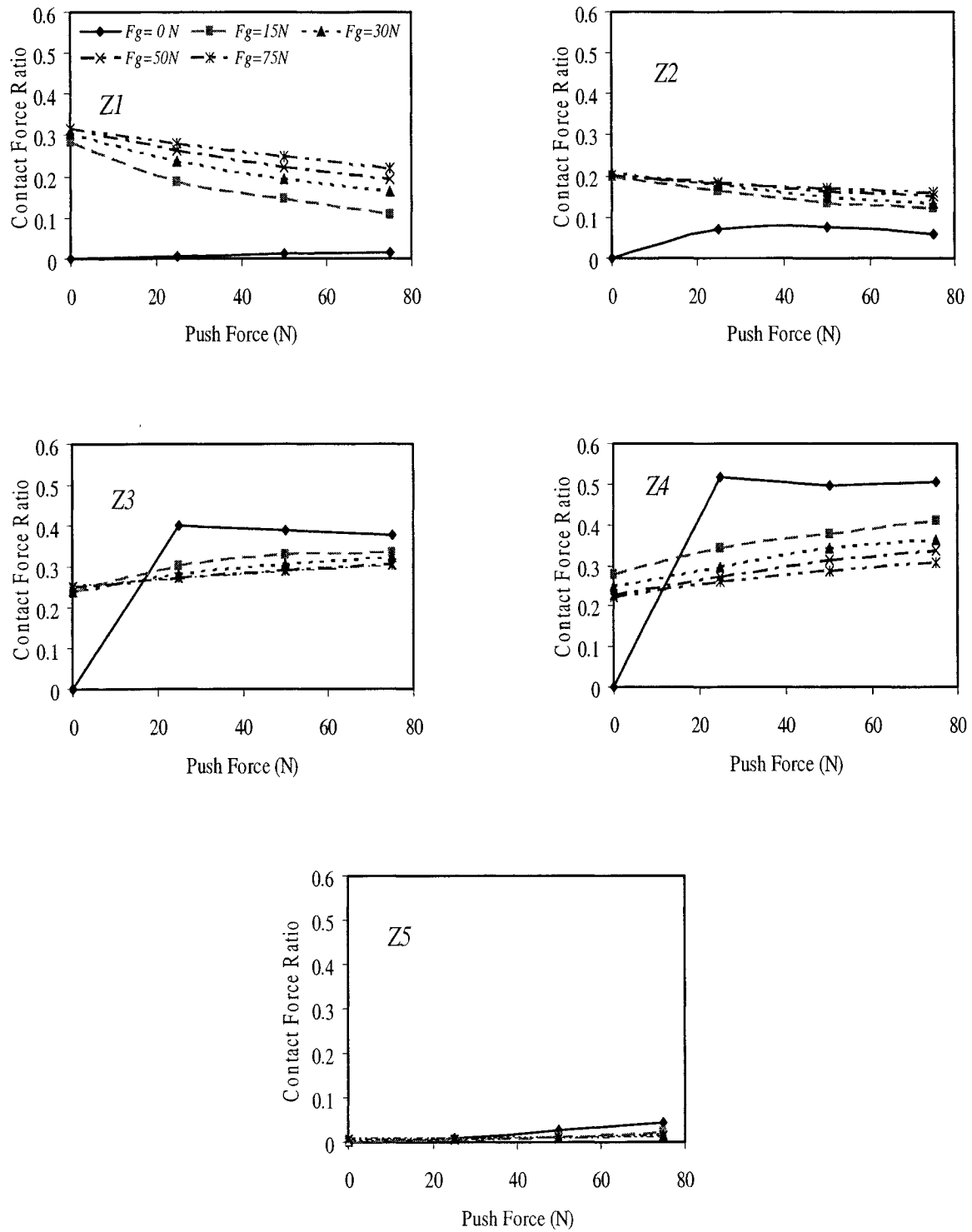
Figure 3.9: Contact force contribution in each zone as function of push force for constant grip force for 40 mm handle.
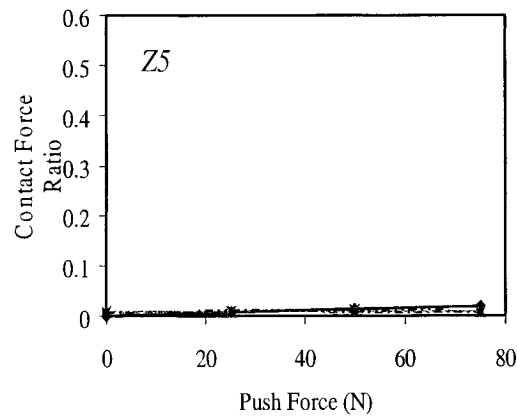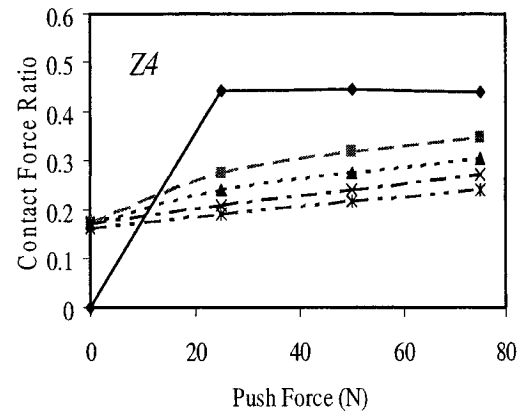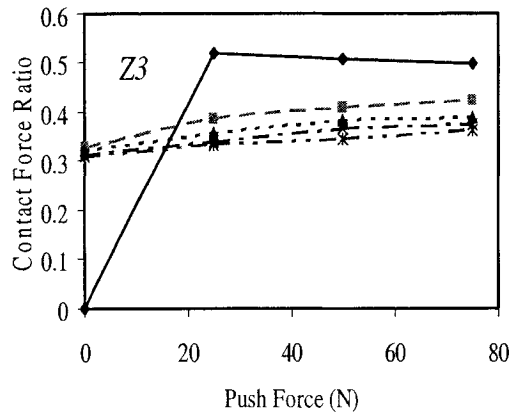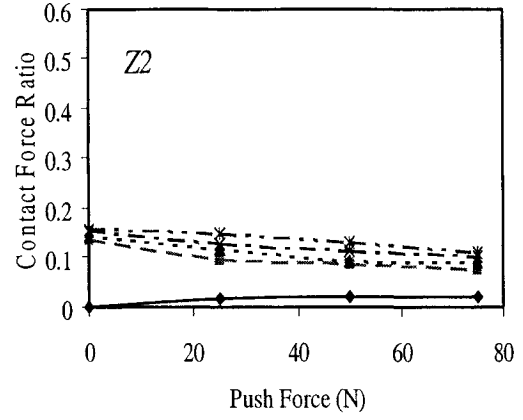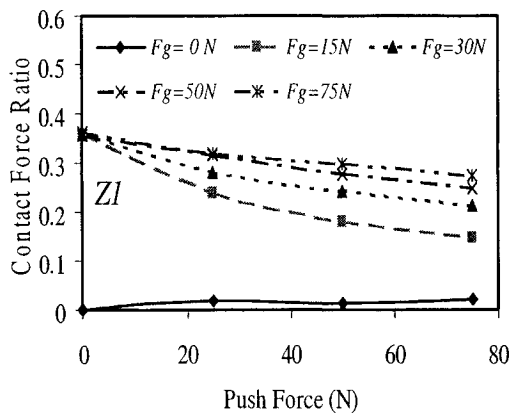
Figure 3.10: Contact force contribution in each zone as function of push force for constant grip force for 30 mm handle.

The contact force developed within each zone can thus be expressed as a linear combination of the grip and push forces, in the following manner:

$$CFZ_j = \alpha_j(D)F_g + \beta_j(D)F_p; \quad j = 1,2,3,45 \tag{3.4}$$

Where $CFZ_j$ is the contact force developed within zone $j$, and $\alpha_j$ and $\beta_j$ are the grip and push force coefficients, which depend upon the handle size.

Table 3.2 summarizes the coefficient values for different zones and handle sizes considered. The results showed that the contact force developed in zones $3$ and $45$, comprising proximal phalanges of the digits and the upper palmar surface, is generally more attributed to the grip and push force, while that in zones $1$ and $2$ it is mostly caused by the gripping action. The small size handle (30 mm) yields higher contact forces attributed to the handle grip at the fingers surface (zones $1,2$ and $3$), while the handle grip contributes more to the forces developed in zones $1$ and $2$ in case of the 48 mm handle.

Table 3.2: Grip ($\alpha j$) and push force ($\beta j$) dependent coefficients describing their contribution to the contact force developed in different zones.

| $D$ (mm) | $\alpha_j$ | $\beta_j$ | $\alpha_j$ | $\beta_j$ |
|---|---|---|---|---|
| | ZONE 1 | | ZONE 2 | |
| 30 | 1.270 | 0.039 | 0.541 | 0.019 |
| 40 | 0.910 | 0.024 | 0.585 | 0.096 |
| 48 | 0.704 | 0.000 | 0.626 | 0.170 |
| | ZONE 3 | | ZONE 45 | |
| 30 | 1.12 | 0.602 | 0.623 | 0.567 |
| 40 | 0.745 | 0.482 | 0.672 | 0.658 |
| 48 | 0.405 | 0.347 | 0.785 | 0.757 |

The variations in the grip dependent coefficient $\alpha_j$ for the three zones ($j=1$ ,$2$, $3$) are observed to be the highest for the 30 mm handle and least for the 40 mm handle. The contact force developed in zones $45$, and attributed to the gripping action, shows less sensitivity to the handle diameter. The contact force developed in this zone shows

100

somewhat comparable contributions due to grip and push forces, for all three handle sizes.

### 3.3.2 Application of regression models

It has been suggested that the severity of the risk posed by exposure to hand-tools vibration is strongly related to contact force. The biodynamic response of the hand and arm exposed to vibration under finger grip condition differs considerably from that under palm grip condition (Dong et al., 2005). A quantitative estimate of the total and localized contact forces may thus be essential for study of biodynamic response of the hand-arm system to vibration rather than applied grip or push forces. Reliable methods, however, do not yet exist for measurement of the contact force, specifically for applications involving tool handles of complex geometry and field trials. The proposed regression model could be a useful tool in contact force estimation from the measured grip and push forces for different handles with diameter within the practical range (30-48 mm).

### 3.4 Location and Magnitude of Hand-Handle Interface Peak Pressure

The hand-handle contact pressure distribution was analyzed using the *EMED* software, which could also provide the overall peak pressures within specified zonal contact areas. For the analysis of localized pressure peaks, the hand surface was divided into 5 zones as described in section 2.3.3. Table 3.3 summarizes mean values and standard deviations (SD) of the hand-handle interface peak pressures observed for the 10 subjects, three handles and different hand force combinations. The Table further presents the location of the peak interface pressure (*PP*) in terms of the contact zone described in Figure 2.12. The results show considerable variations in the peak pressure, as evident

from high values of standard deviations of the mean peak pressures measured for different subjects under different combinations of the hand forces. Such variations would be expected and are mostly attributed to poor repeatability in the pressure imposed by the hand and differences in geometric location of the pressure hot points in relation to the sensor location. The results, however, show consistent location of the high pressure zone, irrespective of the hand force combination. The mean peak pressures for all subjects and handles generally lie in zone *4*, upper lateral side of the palm in the vicinity of the thenar region, although some exceptions are also observed.

Table 3.3: The mean and standard deviation of the peak pressure and its location under various grip/push force levels for different handle sizes.

| $F_g$ (N) | $F_p$ (N) | $PP$(kPa) | SD | Zone | $PP$(kPa) | SD | Zone | $PP$(kPa) | SD | Zone |
|---|---|---|---|---|---|---|---|---|---|---|
| *D* | | 48 mm | | | 40 mm | | | 30 mm | | |
| 0 | 25 | 45.52 | 14.56 | *4* | 33.07 | 11.67 | *4* | 31.34 | 16.15 | *4* |
| | 50 | 68.96 | 27.09 | *4* | 55.36 | 18.84 | *4* | 55.27 | 20.72 | *4* |
| | 75 | 99.35 | 37.11 | *4* | 73.57 | 19.14 | *4* | 76.25 | 28.11 | *4* |
| 15 | 0 | 46.10 | 22.15 | *4* | 36.21 | 11.85 | *4* | 51.25 | 21.75 | *1* |
| | 25 | 79.22 | 30.99 | *4* | 62.21 | 21.15 | *4* | 61.79 | 32.12 | *4* |
| | 50 | 95.84 | 29.91 | *4* | 82.64 | 19.27 | *4* | 90.00 | 37.28 | *4* |
| | 75 | 124.94 | 35.96 | *4* | 104.93 | 26.15 | *4* | 104.37 | 34.23 | *4* |
| 30 | 0 | 62.40 | 19.88 | *4* | 56.00 | 21.23 | *1* | 81.52 | 20.82 | *1* |
| | 25 | 91.10 | 22.11 | *4* | 75.79 | 26.36 | *4* | 79.37 | 40.89 | *4* |
| | 50 | 112.66 | 33.56 | *4* | 102.14 | 28.43 | *4* | 104.64 | 48.77 | *4* |
| | 75 | 144.03 | 48.00 | *4* | 116.93 | 22.07 | *4* | 129.11 | 45.93 | *4* |
| 50 | 0 | 88.38 | 23.81 | *4* | 83.57 | 20.20 | *1* | 110.09 | 24.41 | *1* |
| | 25 | 114.42 | 36.20 | *4* | 102.57 | 31.76 | *4* | 100.45 | 21.37 | *1* |
| | 50 | 144.16 | 38.83 | *4* | 123.43 | 33.24 | *4* | 117.68 | 37.62 | *4* |
| | 75 | 161.62 | 50.58 | *4* | 141.64 | 31.48 | *4* | 146.61 | 42.11 | *4* |
| 75 | 0 | 127.99 | 36.41 | *4* | 111.57 | 21.76 | *1* | 135.62 | 21.33 | *1* |
| | 25 | 154.03 | 39.76 | *4* | 121.71 | 24.98 | *4* | 141.07 | 42.55 | *1* |
| | 50 | 173.31 | 42.43 | *4* | 149.57 | 29.79 | *4* | 145.98 | 24.67 | *3* |
| | 75 | 198.12 | 52.16 | *4* | 156.07 | 28.87 | *4* | 168.30 | 48.94 | *4* |

For the 48 mm handle, the peak pressures invariably occur in this zone, irrespective of the hand force combination. The peak pressures obtained for the 40 mm handle also show the same trend, except in the absence of the push force, a condition requiring lower pressure from the lateral side of the palm (zone *4*). Gripping the handle in this case necessitates application of pressure mostly from the fingers, specifically the finger tips. The location of the peak pressure under such conditions tends to shift to zone 1 comprising the tips of digits 2, 3 and 4, specifically under grip force exceeding 30 N.

Similar trends are also observed for the 30 mm diameter handle, where the peak pressure tends to shift from zone *4* to zone *1* in the absence of the push force. The application of high grip force coupled with light push force, such as push/grip combinations of 25/50 N and 25/75 N, also cause peak pressure to shift from zone *4* to zone *1*. The results further show that application of high grip and push forces could shift the peak pressure towards zone *3* comprising proximal phalanges of the digits. Under such condition, the peak pressures are observed to occur over the surface adjoining zones *3* and *4*. The results suggest that the peak pressure location is also dependent upon the handle size, particularly under low magnitude push forces, which may be attributed to the effective contact area. On a relatively large size handle, the subjects tend to apply grip force using the entire hand surface in contact with the handle including the finger tips, which results in relatively higher pressure in zone *4* for the 48 mm handle even when the push force is absent. Subjects tend to maintain a more stable and controlled grip with smaller size handles leading to more concentration of the contact force and thus the peak pressure near the finger tips for the 30 and 40 mm handles. This is further evident from the comparisons of magnitudes of mean peak pressures obtained for the two handles. The

30 mm diameter handle yields considerably higher values of mean peak pressures in zone *1* under zero push force.

A few studies have established that the high hand-handle interface pressure, arising from grasping a tool handle, could cause discomfort or pain. High pressure peaks could also impair work performance and lead to potential tissue damage. On the basis of the data derived from algometer studies, the pressure-discomfort threshold (*PDT*) limit of 188 kPa has been estimated for the fingers, while the limits of 200 kPa and 100 kPa have been suggested for the palm and the thenar regions, respectively. The corresponding values of the pain pressure threshold (*PPT*) for the finger, palm and thenar were estimated as 560, 576 and 505 kPa, respectively (Johansson et al., 1999). The sustained external applied pressure (*SP*), considered acceptable for a working day on the average, was estimated as 104 kPa (Fransson-Hall and Kilbom, 1993).

Figure 3.11 shows the variations in mean peak pressures as a function of the push force for 5 levels of constant grip forces and three handle sizes, together with the proposed sustained external pressure (*SP*) value (Fransson-Hall and Kilbom, 1993). While the results show some nonlinear variations, specifically for high grip force and 30 mm handle, the increasing trend in the peak pressure with increasing push force could be generally approximated as linear. The augmentation of the grip force level tends to shift the mean peak pressure curves upward also in an approximately linear fashion. Figure 3.12 illustrates a comparison of the mean peak pressures for the three handle sizes and three push force levels (25, 50 and 75 N) as a function of the grip force, together with the *SP* values. It is obvious from the figure that the 48 mm handle tends to develop highest peak pressure for all grip/push combinations, while the 30 and 40 mm handles yield

similar values of mean peak pressures. The 30 mm handle, however, in general causes higher pressure peaks exceeding $SP$ values under application of higher magnitudes of grip and push forces, when compared to those obtained for the 40 mm handle, which could be attributed to the differences in effective contact areas of the two handles.

3.5    Contact Pressure Distribution

Figures 3.13 to 3.15 show variations in the mean peak pressures within the five different contact zones as a function of the push force for three grip force levels and three handles, together with the proposed $PDT$ limit for the thenar (Johansson et al., 1999). For the 48 mm diameter handle, the peak pressures invariably occur within zone *4*, irrespective of the magnitudes of the grip and push forces, as shown in Figure 3.13. Furthermore, the interface peak pressures within this zone are considerably higher than those occurring in the other zones. The mean peak pressure in this zone could approach as high as 200 kPa under high magnitudes of hand forces. The peak pressures and thus the contact force developed within zone 4, upper medial side of the palm, are generally observed to be the highest for all three handles, specifically under high push forces. Lower magnitudes of push forces cause relatively higher pressures within zone *1* (the fingertips of second, third and fourth digits), as discussed earlier, which decrease slightly as the push force is increased.

The contact force and thus the peak pressure tend to shift from zone *1* to zone *2*, comprising the middle phalanges of digits II-IV, as the push force increases further. The results attained for the 40 mm handle also reveal occurrence of peak pressures in zone *4*, except under light push force below 25 N, where the peak pressure occurs within zone *1* (Figure 3.14).

105
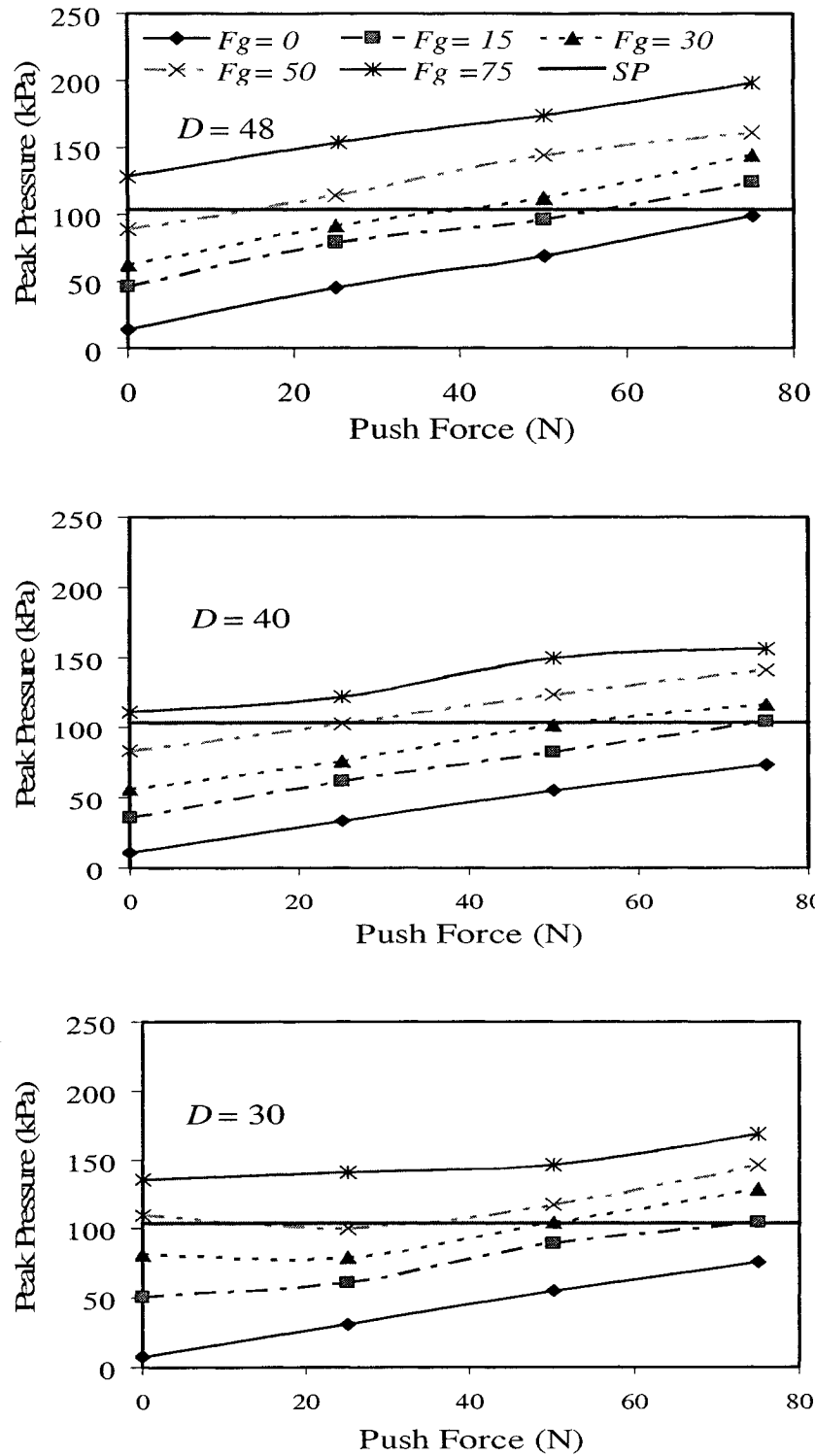
Figure 3.11: Variations of mean peak pressure with push force for different constant grip forces and handle sizes.
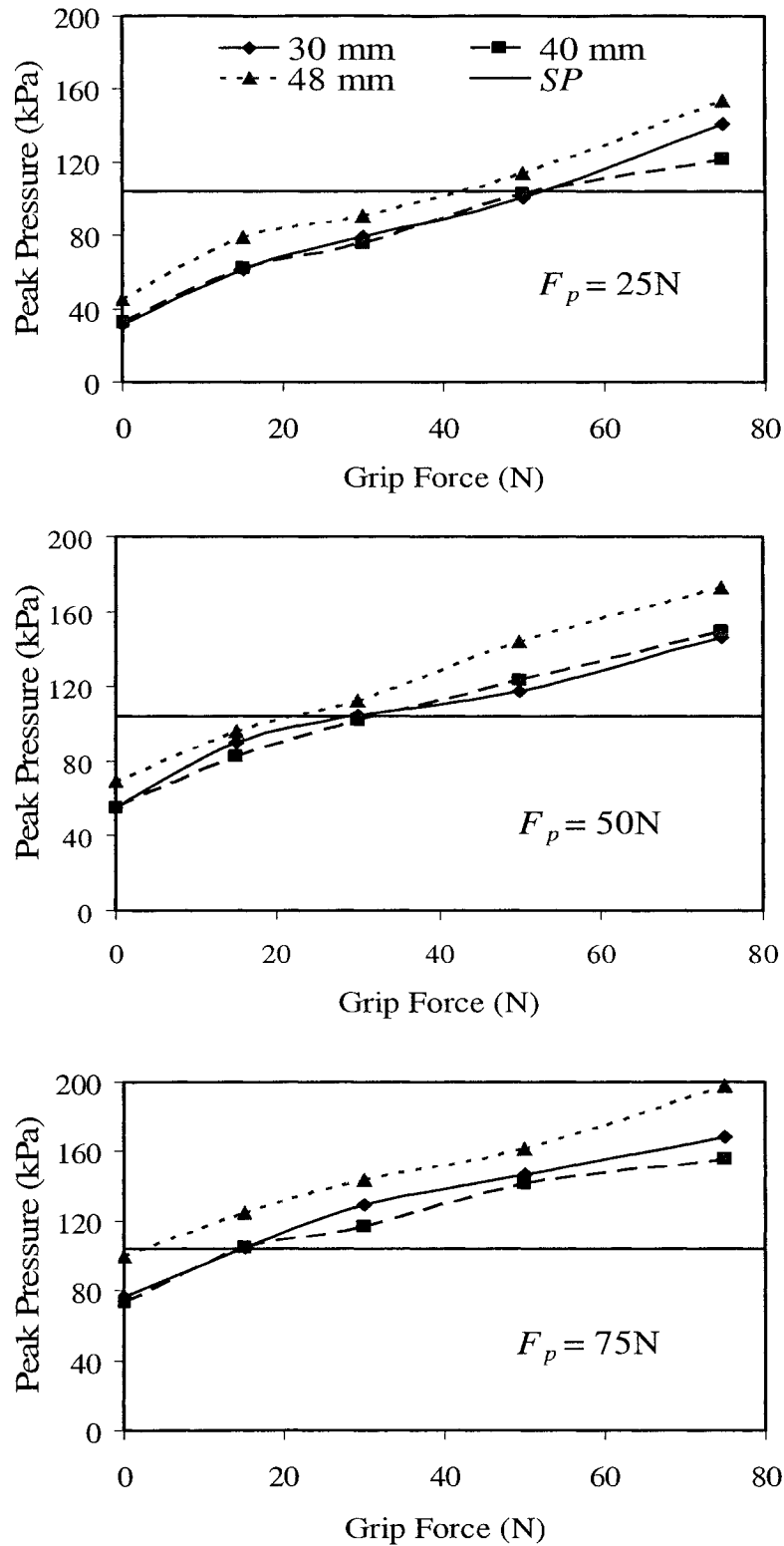
Figure 3.12: Hand-handle interface peak pressures as functions of grip and push forces, and handle sizes.
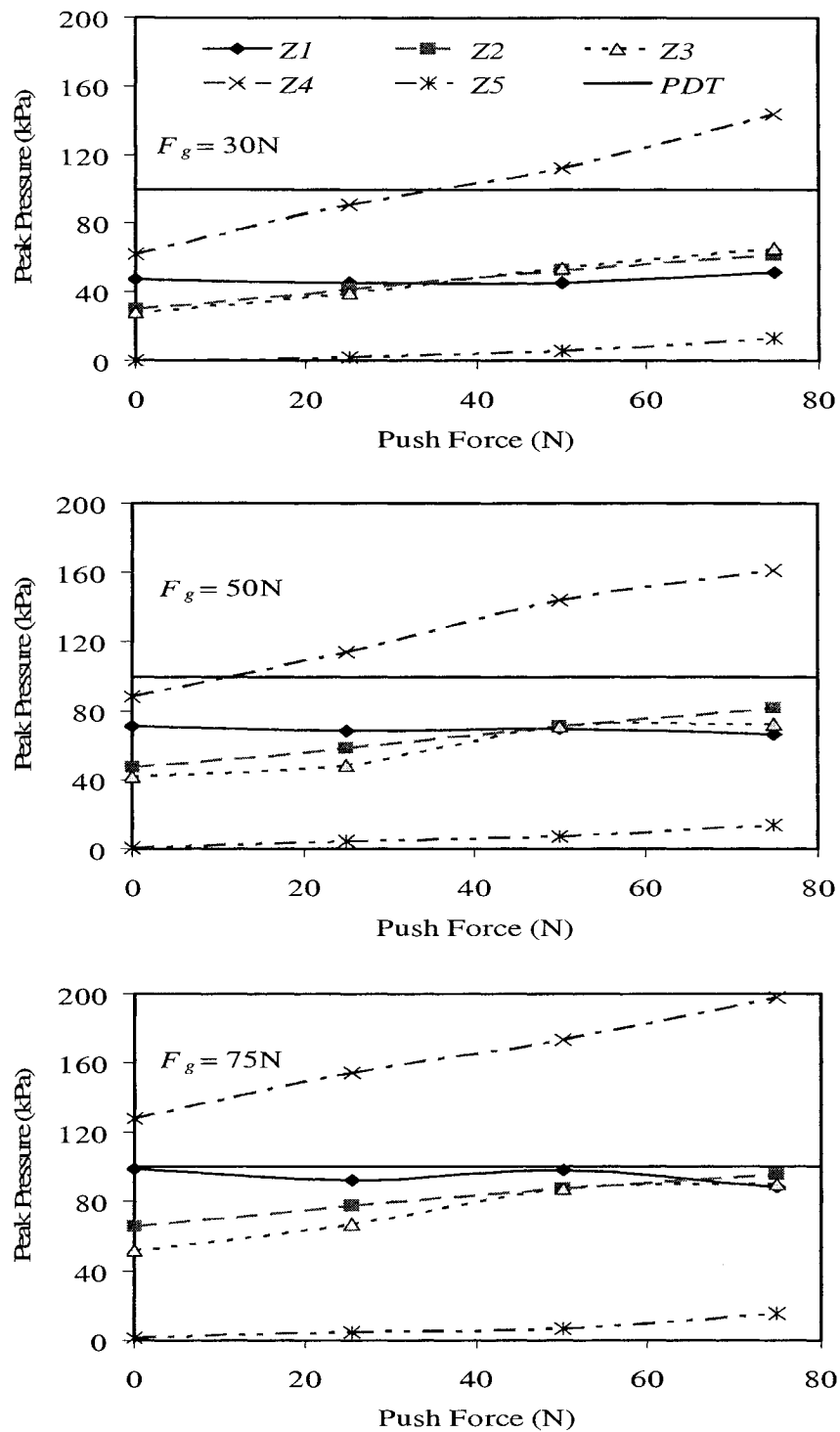
Figure 3.13: Peak pressures in different zones as functions of the push and grip forces (48 mm handle; Zone *1* – 'Z1'; Zone *2* – 'Z2'; Zone *3* – 'Z3'; Zone *4* – 'Z4'; Zone *5* – 'Z5' and *PDT*- *PDT* thenar).
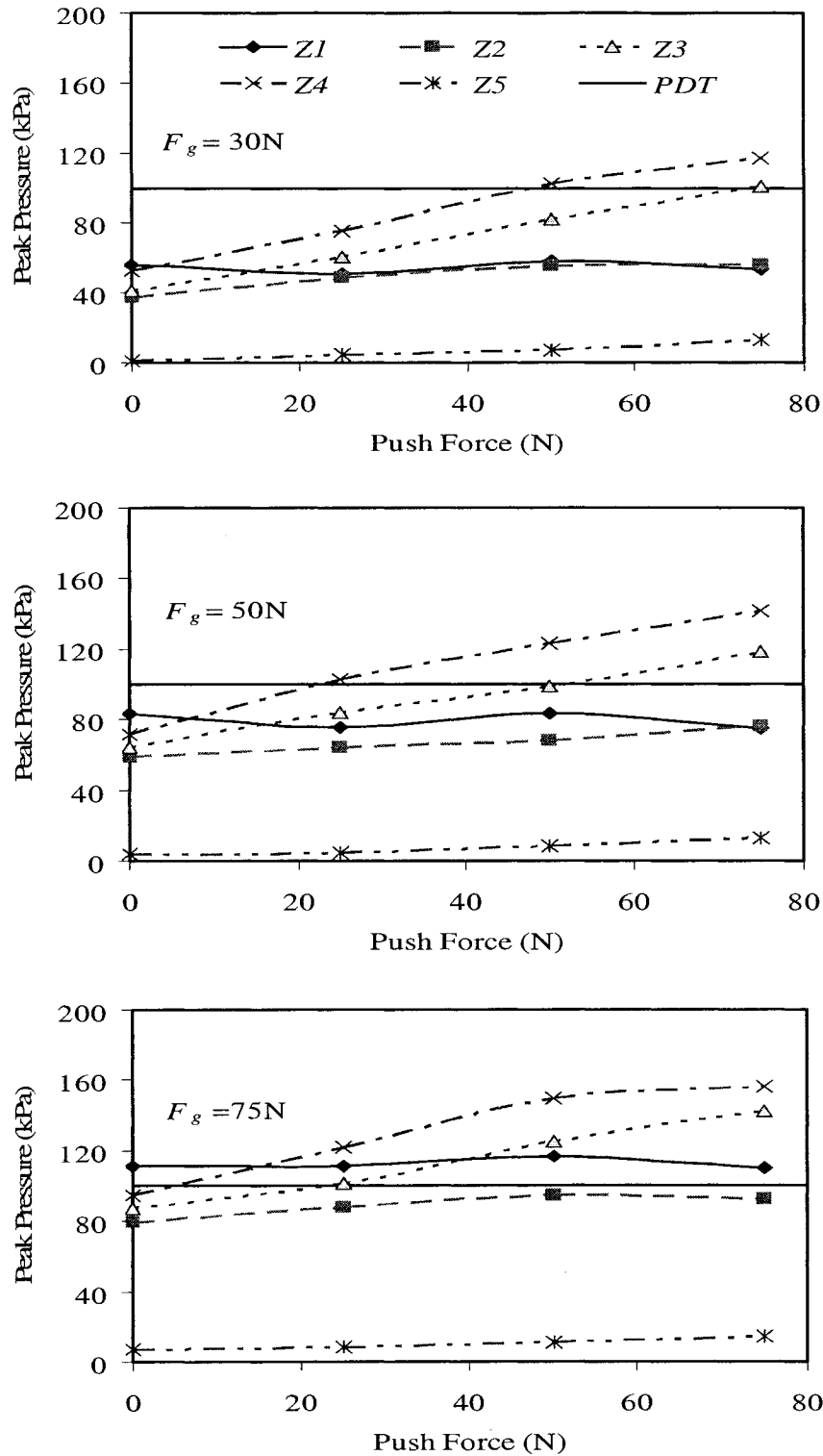
Figure 3.14: Peak pressures in different zones as functions of the push and grip forces (40 mm handle; Zone *1* – 'Z1'; Zone *2* – 'Z2'; Zone *3* – 'Z3'; Zone *4* – 'Z4'; Zone *5* – 'Z5' and *PDT- PDT* thenar).

109
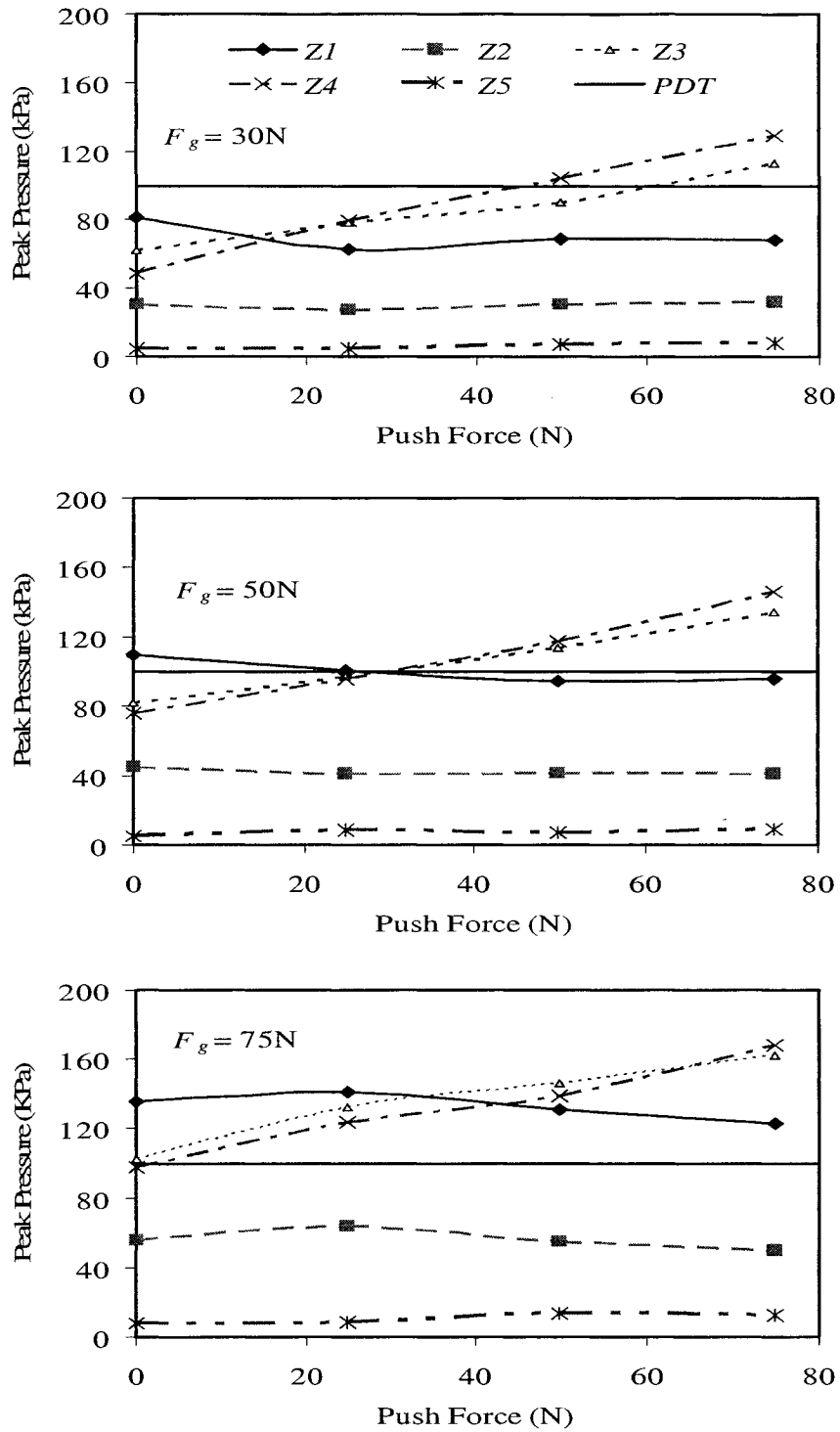
Figure 3.15: Peak pressures in different zones as functions of the push and grip forces (30 mm handle; Zone *1* – 'Z1'; Zone 2 – 'Z2'; Zone *3* – 'Z3'; Zone *4* – 'Z4'; Zone 5 – 'Z5' and *PDT*- *PDT* thenar).

The relative difference in the peak pressures within different zones, however, is considerably smaller when compared to that observed for the 48 mm handle. The results suggest more uniform distribution of peak pressure over zones *1* to *4* for the 40 mm handle. The shifting of peak contact pressure from zone *4* towards zone *1* becomes more apparent for the 30 mm handle, as shown in Figure 3.15. The peak pressures within zones *3* and *4* also approach comparable values, suggesting more uniform distribution of the contact force over the region covering upper medial side of the palm and proximal phalanges of digits III and IV. A comparison of the results presented in Figure 3.13 to Figure 3.15 suggests that a smaller handle (30 mm) yields higher values of peak pressures in zones *1* and *3*, while the larger handle (48 mm) causes high pressures in zone *4*. The 30 mm handle thus yields higher contact force than the 48 mm handle.

An examination of the measured pressure data in view of the reported threshold limits suggests that the peak pressures remain well below the *PPT* values. The measured values, however, exceed the *PDT* limits suggested for the thenar zone (within zone 4) and the sustained pressure *SP* values with the 48 mm handle under applications of 30 N grip force and push force above 25 N. The application of grip force of 50 N or more coupled with push force above 15 N would generate interface peak pressures above the *SP* and *PDT* limits for the thenar area in zone *4*, as shown in Figure 3.13. Under application of high grip and push forces, such as 75/75 N, the peak pressures exceed the *PDT* limits for the thenar and approach that for the palm area.

For the 40 mm handle, the peak hand-handle interface pressures exceed *SP* and *PDT* limits for the thenar area (zone *4*) under application of 30 N grip and push force above 50 N, as evident from Figure 3.14. The application of 50N grip coupled with a 25 N or

higher push force would cause peak pressure exceeding *PDT* of the thenar area. Increasing the grip force to 75 N grip causes higher peak pressures in zone *1* (the fingertips of second, third and fourth digits) and zone *3* (the proximal phalanges of the four digits ) that surpass or approach the *SP* values, irrespective of the push force applied, as shown in Figure 3.15. The use of a 30 mm handle with 30 N grip and push force above 50 N could yield peak pressure values well above the *PDT* limit for the thenar zone (Figure 3.15). Application of a 50 N grip force coupled with minimal push force also causes the peak pressure in zone *1* above the *SP* values, while the addition of a 25 N or more push force would cause pressures to exceed *PDT* limits of the thenar area. Under high grip condition (75 N), the peak pressures developed in zones *1, 3* and *4* exceed the *SP* limit even in the absence of the push force, as illustrated in Figure 3.15. The results suggest that application of high grip and minimal push force on a smaller diameter handle causes high pressures above the *SP* and *PDT* limits in zones *1* and *3* (finger tips, and proximal phalanges of the digits). The magnitudes of these pressure peaks are considerably smaller for the large diameter handle, which tend to cause high pressure peaks in the thenar zone.

3.6    Interface Peak pressure (*PP*) Estimation  from Hand Forces

The results presented in Figure 3.11 and Figure 3.12 suggest that the peak pressure is dependent upon not only the grip and push forces, but also on the handle diameter. The dependence of *PP* on the $F_g$ and $F_p$ alone may thus be described by a linear function of the form:

$$PP = K(D) + A(D)F_g + B(D)F_p$$    ( 3.5)

112

Where $K(D)$, $A(D)$ and $B(D)$ are coefficients dependent on the handle diameter. The constant $K(D)$ is introduced to account for variations in peak pressures imposed by the subjects under 0 grip and 0 push force conditions, and offset in the peak pressure possibly caused by a residual pressure in the sensing mat wrapped around the handle.

Coefficients $A(D)$ and $B(D)$ describe the relative contributions due to grip and push forces to the peak pressure, respectively. Multiple linear regressions were performed to identify the coefficients for each handle, and the resulting handle-size dependent coefficients are summarized in Table 3.4. The correlation coefficients $(r^2)$ of these linear regressions were obtained as 0.942, 0.977 and 0.99, respectively, for 30, 40 and 48 mm handles. A good correlation is obtained between the estimated and measured mean values of the peak pressures, as evident in Figure 3.16.

Table 3.4: Model coefficients characterizing $PP$ dependence on the grip and push forces.

| Handle Diameter | $K(D)$ | $A(D)$ | $B(D)$ |
|---|---|---|---|
| 30 mm | 32.4 | 1.28 | 0.593 |
| 40 mm | 20.1 | 1.16 | 0.809 |
| 48 mm | 24.9 | 1.34 | 0.996 |
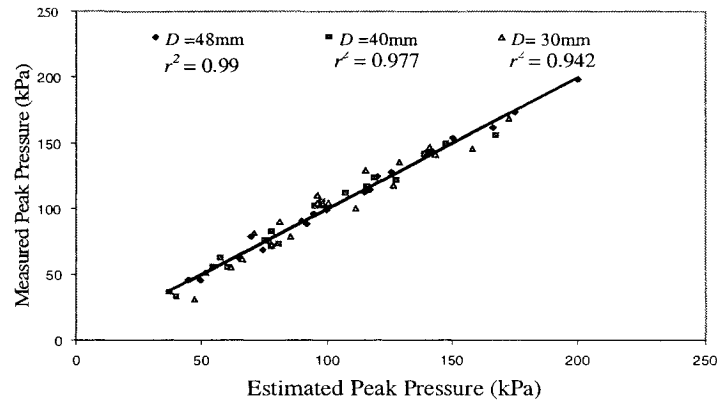


Figure 3.16: Correlation between measured and estimated mean peak pressure for three different handles

113

The coefficient values reveal that the contribution of the grip forces to the peak pressure value is far more significant than that of the push force, which has also been observed for the total contact force in section 3.2. Figure 3.17 illustrates the variations in the regression coefficients with the handle size. The push force coefficient, $B(D)$, varies approximately linearly with the handle size in the range considered in this study, and thus may be expressed as ($r^2 > 0.95$):

$$B(D) = -0.080 + 0.0224D \qquad (3.6)$$

Where D is handle diameter in mm. The grip force dependent and constant coefficients, however, show nonlinear variations with the handle diameter, and both the coefficient values are observed to be smaller for the 40 mm handle. The dependence of both coefficients upon the diameter could be best described by a quadratic function of the form ($r^2 > 0.95$):

$$A(D) = 0.0019D^2 - 0.1462D + 3.94 \qquad (3.7)$$

$$K(D) = 0.102D^2 - 8.3467D + 191.3 \qquad (3.8)$$

The coefficient $K(D)$ may be considered as a bias in the measurement, attributed to few hot pressure points that are observed under zero grip and push condition, when the hand is merely placed on the handle.

Grip Coefficient *A(D)*

2

1.6

1.2

0.8

0.4

0

$r^2 > 0.95$

20    25    30    35    40    45    50

Handle Diameter (mm)

Push Coefficient *B(D)*

2

1.6

1.2

0.8

0.4

0

$r^2 > 0.95$

20    25    30    35    40    45    50

Handle Diameter (mm)

Constant Coefficient *K(D)*

40

30

20

10

0

$r^2 > 0.95$

20    25    30    35    40    45    50
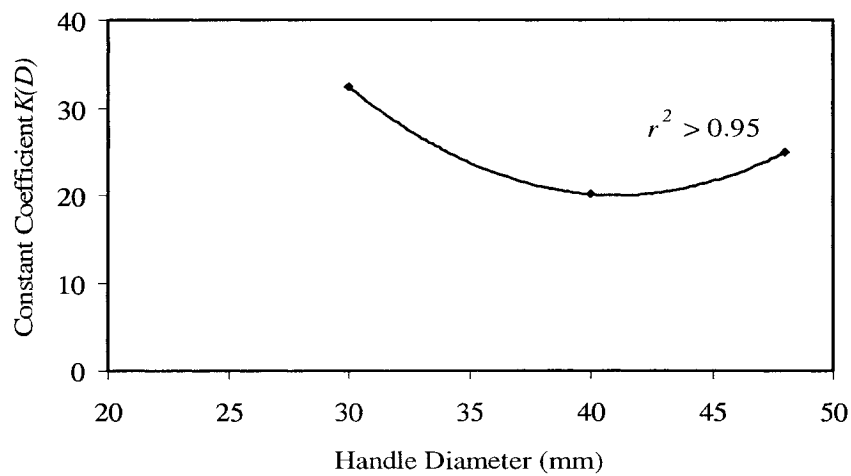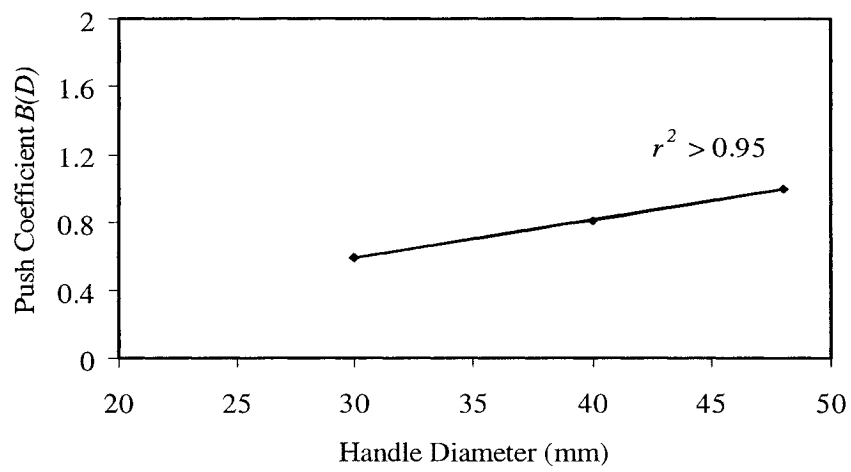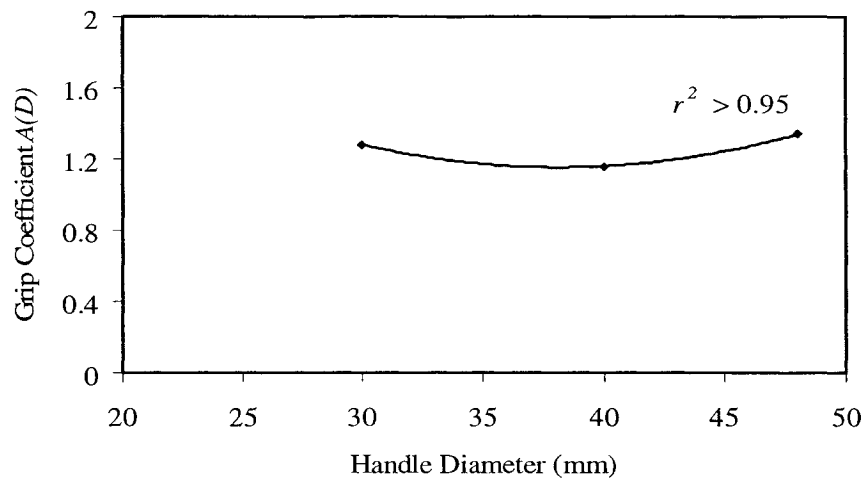
Handle Diameter (mm)

Figure 3.17: Relationships between handle diameter and grip, push and constant coefficients in peak pressure equation.

3.7    Relative Optimal Handle Size

Among the various tool handle design characteristics, handle diameter has been studied extensively since it is an important factor to maximize grip strength, reduce stress on the digit flexor tendons and carpometacarpal ligaments (Meagher, 1987), and it can also influence force exertion in manual work (Blackwell et al., 1999). Thus, many investigators have tried to obtain the optimal handle diameters of a cylindrical handle shape with subjective comfort rating (Hall and Bennett, 1956; Yakou et al., 1997) and finger force measurement using by force gauge or sensors (Amis, 1987; Chen, 1991).

Recent study tested maximum grip force on cylindrical aluminum handles to evaluate the relationships between handle diameter (25–50mm diameter handles), perceived comfort, finger and phalange force distribution, and electromyographic efficiency of finger flexor and extensor muscle activity (Kong and Lowe, 2005). The study found that the mid-sized handles (30, 35 and 40mm) as the most comfortable for maximum grip force exertions. Total finger force capability as inversely related with handle diameter. EMG amplitude of the primary flexor and extensor was unaffected by the handle diameter, so the efficiency of the muscle electrical activity followed the same relationship with handle diameter as total finger force. Individual finger and phalange force distributions were examined to evaluate their relationship with perceived comfort. A non-uniform finger/phalange force distribution, in which finger force was proportional to finger muscle capabilities, exhibited a stronger correlation with subjective ratings of comfort than a uniform finger/phalange force distribution.

The analyses of the data of mean contact force, mean effective area and interface peak pressure of ten subjects concluded that the 40 mm handle could be relatively

considered as the optimum handle among the three investigated handles as far as the contact force and the peak pressure are concern. This handle develops noticeably lower contact force than 30 mm handle and remarkably lower interface peak pressure than 48 mm handle. Although the interface peak pressure and contact area develop from the use of 40 mm handle are less than those developed by 30 mm handle, however their values are comparable.

## 3.8 Statistical Analysis

A three-factor repeated measures analysis of variance (ANOVA) has been carried out on the measured data using SPSS version 11.5. The factors represented the three nominal diameters of the handles ($D$), the four levels of push force ($F_p$) and the five levels of grip force ($F_g$) based on a preliminary analysis using Mauchly's test of sphericity. The three-way ANOVA analyses within subject effect have been performed three times separately to verify the statistical significance of independent variables, i.e., handle size, push and grip forces on the three dependent variables, namely; mean contact force ($F_c$), mean effective contact area ($A_c$) and the hand-handle interface mean peak pressure ($PP$).

The ANOVA of the mean contact force revealed reliably significant results for the grip and push forces ($p<0.001$) and strongly significant for handle diameter ($p<0.001$), which is consistent with Figures 3.1 and 3.2. The analysis also revealed significant handle diameter-by-grip force ($p<0.001$), however no interaction was found between the handle size and the push force and between grip and push forces. The three-factor repeated measures ANOVA of the mean effective area showed very strong significant results for all three main factors ($p<0.001$)—handle diameter, and grip and push forces (which can

117

be observed clearly in Figure 3.4), and significant handle diameter-push force ($p<0.001$) and grip-push forces interactions ($p<0.001$). No interaction was found between the handle size and grip force. ANOVA analysis considering interface peak pressure ($PP$) as dependent variable revealed reliably significant results for both hand forces ($p<0.001$) and barely significant for handle size ( $p \approx 0.05$ ), that could be attributed to considerable variations in the peak pressure measurements (high standard deviation). The only significant interaction between main factors was observed between the handle diameter and grip force, which was also evident for the mean contact force. Table 3.5 summarizes the results obtained from the statistical analyses for the three dependent factors considered.

Table 3.5: Statistical significance levels for the main factors.

| Dependent Variables | Significance Level ($p$) | | | | | |
|---|---|---|---|---|---|---|
| | $D$ | $F_g$ | $F_p$ | $D * F_g$ | $D * F_p$ | $F_g * F_p$ |
| $F_c$ | 0.00 | 0.00 | 0.00 | 0.00 | 0.80 | 0.37 |
| $A_c$ | 0.00 | 0.00 | 0.00 | 0.66 | 0.00 | 0.00 |
| $PP$ | 0.05 | 0.00 | 0.00 | 0.01 | 0.63 | 0.00 |

## 3.9    Conclusions and Summary

It has been established that the severity of the risk posed by exposure to hand–tools vibration increases considerably with increasing hand–tool contact force. Reliable methods, however, do not yet exist for measurement of the contact force. Contact area and force can be effectively measured using the pressure-sensing grid. The results showed that the contact force is linearly dependent upon the grip and push forces and handle diameter. The hand–handle contact force for a given handle size could be derived from a linear combination of the grip and push forces, where the contribution due to grip force is considerably larger. The contact force increases as the handle diameter decreases.

The variations in push force is less sensitive to handle size and tend to cause a constant shift in the contact force over the entire range of grip forces. On the other hand, the effective contact areas for all the handles rapidly approached to nearly steady values as the grip force exceeds 30 N. The effective contact area is inversely proportional with handle diameter.

The magnitudes and distribution of hand-handle interface pressure during a gripping and pushing task vary considerably with the applied grip and push forces, and the handle diameter. The peak pressure for a given handle size could be estimated from a linear combination of the directly measurable grip and push forces, where the weighting of the grip force is considerably higher than the push force. The large size handle (48 mm diameter) yields the highest magnitude of interface peak pressure, while the small handle (30 mm diameter) causes higher contact force, suggesting more uniform pressure distribution over smaller size handles. The locations of localized pressure peaks in the operator's hand vary considerably with handle size and applied grip/push forces. The large size handle (48 mm) considered in this study causes the pressure peaks to occur in the lateral side of the palm (zone *4*) for the entire range of grip and push forces considered. Furthermore, the pressure peaks within this zone are considerably higher than those occurring in the other zones, and exceed the reported threshold limit of the pressure discomfort (*PDT*) and sustained pressure (*SP*) values for preservation of working efficiency over a work day.

Gripping a 40 mm handle in the absence of push force tends to shift the pressure peaks to the finger tips (zone *1*). For a 30 mm handle, the pressure peaks also tend to spread to the proximal phalanges of the digits (zone *3*) depending on the applied grip and

push forces. The relative differences in peak pressures within different zones for the 30 and 40 mm handles are considerably smaller than those observed for the 48 mm handle, suggesting more uniform distribution of pressure for smaller handles. From the results it is concluded that gripping a relatively large size handle encourages the subjects to apply grip force over the entire hand surface in contact with the handle including the finger tips, which results in relatively higher pressure in the lateral side of the palm even when the push force is absent. Subjects tend to maintain a more stable and controlled grip with smaller size handles (30 and 40 mm) considered in the study leading to relatively higher contact force and thus the peak pressure near finger tips.

The application of high grip and push forces, such as 75/75 N, on a 48 mm handle causes peak pressures to exceed the *PDT* limit for the thenar and approach that for the palm area. For the 30 and 40 mm handles, the peak interface pressures exceed *SP* and *PDT* limits for the thenar area under application of 30 N grip and push force above 50 N. Increasing the grip force beyond 50 N causes higher peak pressures in zones *1* and *3* (fingertips and proximal phalanges of the four digits) that surpass or approach the *SP* values, irrespective of the push force applied. The results suggest that application of high grip and minimal push force on a smaller diameter handle causes high pressures above the *SP* and *PDT* limits in zones *1* and *3*. The magnitudes of these pressure peaks are considerably smaller for the large diameter handle, which tends to cause high pressure peaks in the thenar zone. The results suggest that further efforts would be desirable to identify alternate handle sizes and geometry in order to distribute the contact pressure more evenly and to limit the pressure peaks below acceptable *PDT* and *SP* values.

The *CFR*, defined as a ratio of the contact force developed within a zone to the total contact force could also be estimated from a linear combination of the grip and push forces. The relative contributions of grip and push forces to the *CFR* for different zones differ considerably. The results show that the contact force developed at the hand-handle interface of the large size handle is mostly attributed to the force developed in zone *4* (lateral side of palm), irrespective of the magnitudes of grip and push forces applied. The *CFR* of this zone generally increases with increase in push force and decreases only slightly with increase in the hand grip force. A 40 mm handle also yields highest *CFR* due to zone *4* only under zero or light grip condition, while the fingertips zone exhibits highest *CFR* under zero push and all nonzero grip forces. The distribution of the contact forces for a smaller (30 mm) handle is observed to be quite different. The contact force developed within zone *3* (proximal phalanges of digits) contribute most to the total contact force, specifically when the push force is above 15 N, while the *CFR* of zone *1* tends to be higher for zero push force, suggesting more contact between the fingers tips and proximal phalanges.

CHAPTER 4

DRIVING-POINT MECHANICAL IMPEDANCE OF HUMAN HAND-ARM
SYSTEM EXPOSED TO VIBRATION

4.1    Introduction

The severe health consequences posed by the exposure to comprehensive levels of
occupational hand-transmitted vibration have promoted a strong need and desire to
enhance a through understanding of the vibration response characteristics of the human
hand-arm. Although subjective measures could provide substantial information
concerning the minimum threshold and equal sensation, inter-subject variation and poor
repeatability of the subjective data pose difficulties in characterizing the hand-arm
vibration response (Gurram, 1993). On the other hand, the biodynamic response of
human hand-arm to vibration may be characterized using objective methods. However,
the objective measurements of the response of the human tissues pose many difficulties
due to lack of the appropriate sensors and the possibilities of injuries to the subjects
during the tests and other ethical concerns. Alternatively, the force-motion response of
the hand-arm system, expressed in terms of driving-point mechanical impedance ($DPMI$),
apparent mass ($APMS$) or dynamic compliance could be considered as an effective tool to
study hand-arm biodynamic response to vibration. The biodynamic response of the
human hand-arm system to hand transmitted vibration forms an essential and practical
basis to efficiently evaluate vibration exposures, vibration response of the coupled hand-
tool system and to investigate the potential injury mechanisms.

Driving-point mechanical impedance ($DPMI$) at the hand-tool handle interface has
been widely used to characterize the biodynamic response of the hand-arm system

exposed to tool handle vibration (Reynolds and Falkenberg, 1984; Lundström and Burström, 1989; Kihlberg, 1995; Gurram et al., 1995; Burström 1997, Jandák 1998). The primary limitation of the *DPMI* method is that the vibration transmitted to the various parts of the upper extremity and *DPMI* does not directly relate to tissue loading and dynamics of the musculoskeletal structure of the hand-arm system. However, the *DPMI* modulus and phase fully describe the overall mass-spring-damper-like behavior of the hand-arm system. The measured response may be considered to represent the total response of an equivalent mechanical system of the hand-arm system and could be utilized to study the influence of various operating factors, such as hand forces, hand-arm posture, and handle size and shape. The response data thus obtained could be utilized to mechanical-equivalent model of the hand-arm system. On the other hand, the *DPMI* could be effectively applied to estimate the amount of mechanical energy dissipated by the hand-arm structure under a specified hand tool vibration spectrum.

## 4.2    Review of Experimental Studies

Despite the fact that the *DPMI* response of the hand-arm system has been measured in many studies under carefully controlled test conditions, considerable differences are known to exist among the data reported by different investigators. These differences could be partly attributed to differences in experimental and measurement techniques employed, potential dependence of the biodynamic response on various contributory factors and the inherent non-linear dynamic properties of the biological materials (Burström, 1997; Gurram; 1993). The discrepancies could be also in-part attributed to the complex coupling and conjunctions among the different factors. This is partly evident from the relatively broad ranges of free driving-point mechanical impedance of the

human hand-arm system defined in ISO 10068 (1998) on the basis of the synthesis of data reported in different studies under a limited scope of experimental conditions (20-500 Hz frequency range, 25-50 N grip force, push force around 50 N, elbow angle within $90°±15°$ and handle diameter between 19 and 45 mm). The standard, however, does not address the role of various contributing factors, such as grip force, push force and the handle size.

The *DPMI* is well acknowledged to be influenced by many intrinsic and extrinsic variables, such as the frequency, magnitude and direction of vibration, the hand-handle coupling forces, handle size, hand-arm posture and individual characteristics. A number of reported studies have described the dependence of the impedance response on various intrinsic and extrinsic variables, including the frequency and direction of vibration, the grip and push forces, vibration amplitude and individual characteristics (Burström, 1990; Jandák, 1998; Burström, 1997). Although the reported studies have attempted to quantify the influences of one or more of these factors under comparable test conditions, the results could be generally limited to trends only, which are mostly diverse and in part contradictory. The reported studies show considerable differences in the *DPMI* response of the hand-arm system to vibration, particularly in view of the peak magnitude and corresponding frequency, and dependence upon the vibration intensity, hand-handle contact forces and hand-arm posture.

The *DPMI* responses reported by Lundström and Burström (1989) under swept harmonic excitations along the $x_h$-axis revealed peak magnitude near 90 Hz. Studies by Burström (1990, 1997) under same sinusoidal and constant velocity random excitations noted the peak magnitudes near 150 Hz. The data reported by Gurram et al. (1995) did

not reveal a clear magnitude peak under sinusoidal excitation, while a peak magnitude was observed near 160 Hz under random excitations. The *DPMI* response measured under $x_h$-axis random excitation and different magnitudes of grip force (25, 50, 75 and 100 N), by Jandák (1998), revealed peak magnitudes in the 50-63 Hz frequency range. Despite the comparable test conditions employed in these studies, only little agreement exists to quantify the fundamental resonant frequency of the hand-arm system when exposed to vibration along the $x_h$-axis.

The influence of vibration level on the *DPMI* response of the hand-arm system along $z_h$–axis has been reported in a few studies leading to somewhat contradictory conclusions. The measurements performed by Lundström and Burström (1989) showed that lower excitation amplitudes cause higher impedance magnitudes at low frequencies and lower impedance magnitudes at higher frequencies. Burström (1997) found that the *DPMI* amplitude increases slightly with increase in the vibration level, and the increase is more pronounced in the frequency range above 200 Hz. In contrast, another study (Gurram et al., 1995) found that the influence of variations in vibration amplitude on the hand-arm *DPMI* as insignificant. The effect of vibration magnitude on the driving-point mechanical impedance response of the hand-arm system along the $x_h$–axis has been reported in a few studies leading also to rather disagreeing conclusions (Burström, 1990; Gurram et al., 1995; Burström, 1997). These studies observed that an increase in the vibration intensity causes either slightly lower or slightly higher or insignificant change in the *DPMI* magnitude. The *DPMI* magnitude was observed to increase slightly with an increase in intensity of swept harmonic vibration in one study by Burström (1990), while another

study by the same author reported a slight decrease in the *DPMI* magnitude under higher levels of random excitations (1997).

Some differences also exist among the conclusions reported by different studies, concerning the influence of hand forces on *DPMI* response of the human hand-arm exposed to vibration, particularly the influence of push force, although only a few studies have attempted to characterize the effect of push force on the hand-arm biodynamic response. Bernard (1990) showed that push force has little effect on the *DPMI* magnitude at frequencies above 100 Hz and less than 10 % variation in the 20-70 Hz frequency range, while Jandák (1998) found the effect as negligible for push forces up to 100 N. In contrast, Burström (1997) concluded that an increase in push force leads to higher *DPMI* magnitude at higher frequencies and reported that a higher push force causes higher *DPMI* modulus at frequencies below 25 Hz and above 125 Hz of human hand-arm system exposed to vibration along the $x_h$-axis.

With regards to the hand grip force, the reported data generally conclude that a firmer hand grip leads to higher impedance magnitude (Gurram et al., 1995; Burström, 1990; Burström, 1997; Jandák, 1998, Burström and Lundström, 1989; Burström and Lundström, 1994), while considerable disagreements exist with respect to the ranges of frequencies where the effects are more pronounced. A few studies have suggested a strong influence of grip force on the *DPMI* magnitude (Kihlberg, 1995; Gurram et al., 1995; Burström, 1997), while its quantitative effect is not yet clearly established. An increase in the hand grip force yields higher impedance magnitude at frequencies above 50 Hz (ISO-10068, 1998). A study conducted by Riedel (1995) concluded strong effect of hand-handle coupling force on the biodynamic response of the human hand and arm,

where the coupling force was defined as the sum of grip and push forces suggesting equal contribution due to grip and push force on the *DPMI*.

Only a few studies have investigated the influence of hand-arm posture on the dynamic response of the hand-arm system. The biodynamic response in terms of *DPMI* has been reported in only a few studies for hand-arm postures involving elbow flexion angles in the 60° to 180° range (Burström, 1990; Cronjäger and Hesse, 1989; Burström, 1997). These studies have concluded that the variation in the hand-arm posture affects the biodynamic responses, while the response trends do not vary considerably. Burström (1997) has studied the influence of five different elbow flexion angles; 60°, 90°, 120°, 150° and 180°, on the hand-arm system exposed to 13 mm/s constant velocity random excitation along the $x_h$, $y_h$ and $z_h$-axes, while the grip and push forces were held at 25 N and 20 N, respectively. The investigation found that the posture (elbow flexion angle) has an influence on the average impedance magnitude and phase, specifically at frequencies below 50 Hz, while the effect is not evident at frequencies above 100 Hz. The response to swept sinusoidal excitations along the $x_h$-axis in the 2-1000 Hz frequency range and for 25 N grip force was also reported by Burström (1990). The studies concluded that the flexion of the elbow has an influence on both the impedance magnitude and phase.

Cronjäger and Hesse (1989) measured the impedance response along the $z_h$-axis under pseudo-random vibration in the 3-1000 Hz frequency range, for four different postures (elbow angle of 60°, 90°, 150° and 180°) and constant levels of $F_g$ (30 N) and $F_p$ (30 N). The effect of variation in elbow flexion angle was observed at frequencies below 100 Hz, while the influence was negligible beyond 200 Hz. On the basis of measurements performed with 90° and approximately 180° elbow angles, while exposed to random

vibration along the $z_h$-axis, Jandák (1998) concluded that changes in hand-arm posture lead to substantial changes in the biomechanical response. The study also reported higher mechanical impedance magnitude corresponding to the 180° elbow angle.

Considering that the hand-handle contact force depends upon the effective contact area of the hand-handle interface, which further depends on the handle size as evident from the results presented in the previous chapter, the biodynamic response of the hand-arm system would be expected to be influenced by the handle dimensions and geometry. The influence of the handle size on the biodynamic response of human hand-arm system exposed, however, to vibration has been investigated in a single study. The measured mechanical compliance of the hand-arm system exposed to swept sinusoidal excitations, while gripping two different handle sizes (19.1 and 38.1 mm diameter) with a grip force of 25.4 N, showed notable effect of the handle size, while no attempt was made to study and quantify the effect of the handle size (Reynolds and Falkenberg, 1984).

The inconsistent and often contradictory findings of the different studies on the *DPMI* could in-part be attributed to the complex coupling among the different factors. There is thus a need for additional data measured under comparable and representative conditions to help identify definite trends and to gain an insight into the coupling among the different factors. The additional data are also expected to contribute towards enhancement and reliability of the data and their ranges defined in ISO-10068 (1998).

## 4.3    Characterization of *DPMI* under $z_h$- axis

The measured data are analyzed to derive the *DPMI* responses of the hand-arm system exposed to $z_h$-axis vibration in the 8-1000 Hz frequency range for different handle sizes, excitation levels and hand force combinations. The results attained for seven

subjects are initially analyzed to examine the inter-subject variability to identify important trends in view of the various factors and their conjunctions, namely, the handle size and shape, vibration intensity, hand grip and push forces, coupling and contact forces and hand-arm posture.

## 4.3.1   Inter-subject variability

Despite the strong dependence of the biodynamic responses upon individual differences (Burström, 1990; Griffin, 1990; Burström, 1997), the inter-subject variability of the measured *DPMI* data has been reported in a single study (Gurram et al., 1995). The study has reported peak standard errors of 23% and 25% in the *DPMI* magnitude and phase responses, respectively, on the basis of measurements performed on four male subjects.

Figure 4.1 illustrates comparisons of the mean *DPMI* magnitude and phase responses of seven subjects corresponding to 30 N grip and 50 N push force, and three cylindrical handles under the low vibration spectra considered in this study ($a_{h,w}$ = 2.5 m/s$^2$, weighted acceleration according to ISO 5349-1, 2001). Despite considerable variations among the individuals' data, both the magnitude and phase responses exhibit consistent and definite common trends. The mean values of the measured data could thus be used to study and identify the important trends in view of the various factors considered, emphasizing the effects of individual factors.
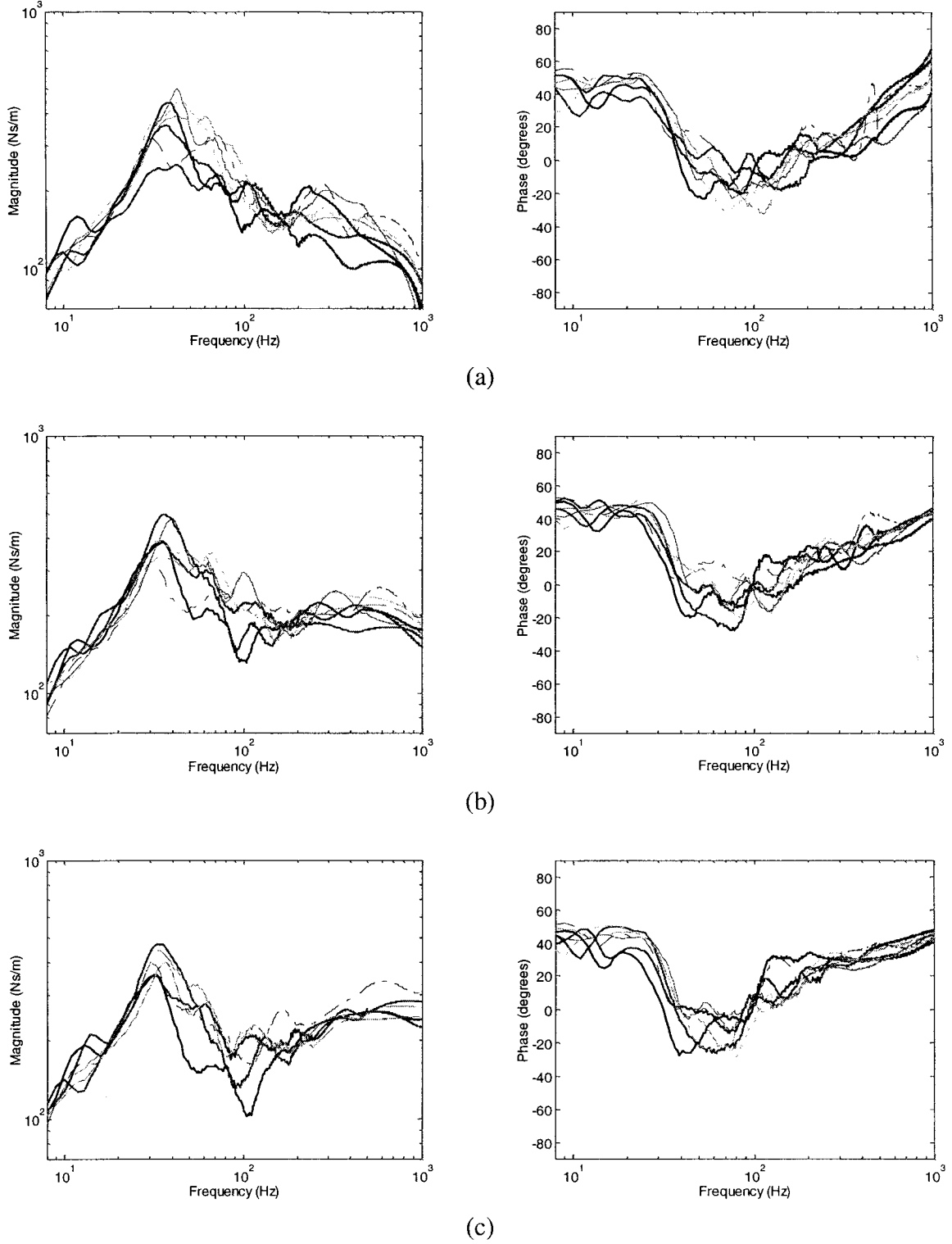
Figure 4.1: Comparisons of mean *DPMI* magnitude and phase responses measured for seven subjects; (a) $D$= 30 mm, (b) $D$= 40 mm, (c) D= 50 mm ($F_g$= 30 N, $F_p$= 50 N and $a_{h,w}$ = 2.5 m/s$^2$).

The *DPMI* magnitude responses of the hand-arm system consistently show peak response occurring in the 30 to 40 Hz frequency range for all subjects and all three handles, which could likely be linked to one of the resonant frequency of the hand-arm system. Such behaviors have been noticed in several studies (Reynolds and Falkenberg, 1984; Hempstock and O'Connor, 1989: Gurram et al., 1995; Burström, 1997; Kihlberg, 1995; Jandák, 1998) which suggest a resonance of the hand-arm system in the 30-50 Hz frequency range. The *DPMI* magnitude response tends to diminish, or at least it does not increase at higher excitation frequencies for all seven subjects. This trend is more pronounced for smaller handle size, when compared to that for the larger handle. While such a trend has been reported in only a few studies (Kihlberg, 1995; Jandák, 1998), number of reported studies has shown opposite trends with magnitude response increasing rapidly with frequency at higher frequencies (Gurram et al., 1995; Burström, 1997; Lundström and Burström, 1989; Cronjäger and Hesse, 1989).

Although no definite explanation can be given to account for such a difference in the *DPMI* magnitude, it is suggested that differences in the handle design, the dynamic characteristics of the experimental setup and the method of mass cancellation (Moustafa and Reynolds, 2004) could lead to the variations in response in the higher frequency range. Such differences in the reported data in earlier studies could be attributed to many factors related to differences in the experimental setup, measurement systems, dynamic characteristics of the handle, etc. The split handle designs used in earlier studies with handle mounted strain gages could be a significant factor due to its relatively less reliability in controlling the grip force and lower natural frequency.

Figure 4.2 shows the coefficient of variation of the *DPMI* magnitude responses attained with all subjects corresponding to the center frequencies of the third octave bands for the three cylindrical handles with $F_g$= 30 N and $F_p$= 50 N, and two different vibration excitation magnitudes .The coefficient of variation of impedance magnitude for other force combinations showed similar trends. The peak variations in the magnitude response among subjects are observed in the 30-100 Hz frequency range for all three handles. The data obtained for the 30 mm handle also shows considerable variations in the magnitude response in the 300-400 Hz frequency range, irrespective of the excitation magnitude. The results show peak standard error of approximately 28 % under higher excitation level, which occurs in the vicinity of the hand-arm system resonance. Moreover, the data acquired with all three handles show similar order of peak standard error.
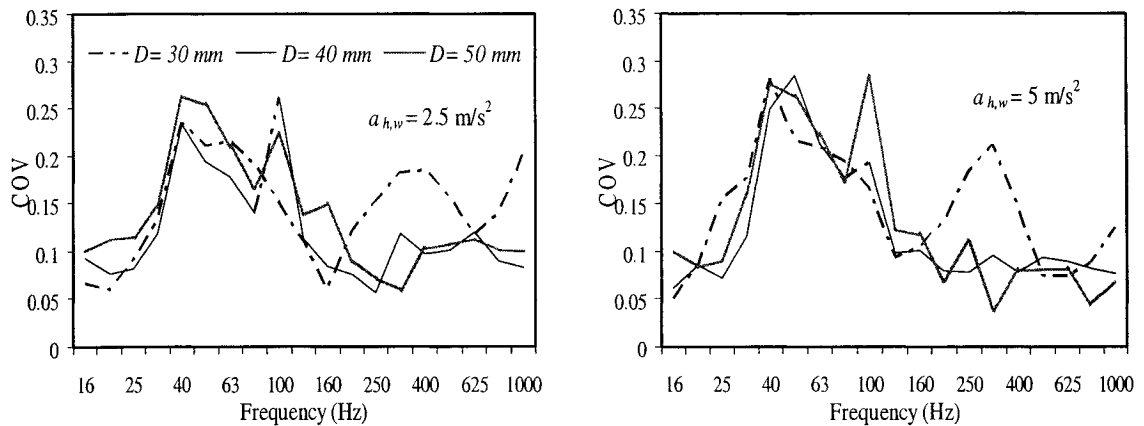


Figure 4.2: Coefficients of variation (COV) of the *DPMI* magnitude response attained for all seven subjects under two levels of excitation (posture *P1*; $F_g$= 30 N and $F_p$= 50 N).

4.3.2  Role of handle size and shape

As mentioned in section 4.1, only one study has presented the measured dynamic compliance of the hand-arm system for two different handle diameters (19 and 38 mm)

for a group of 75 foundry workers (Reynolds and Falkenberg, 1984). From the tabulated values of the compliance, it is shown that both phase and magnitude vary with the handle diameter, while no attempt is made to quantify the effect of the handle size. The influence of the handle size on the hand-arm biodynamic response to $z_h$-axis vibration is demonstrated through comparisons of the mean $DPMI$ magnitude and phase responses attained with three different handle sizes, while the hand-arm system assumed posture $P1$ with bent forearm posture ($90^\circ$ elbow flexion), and exposed to $a_{h,w}= 2.5$ m/s$^2$ weighted rms acceleration and different $F_g/F_p$ force combinations (10/25; 30 /50; 50/75), as shown in Figure 4.3. The figure also shows the mean, lower and upper bounds of idealized values of $DPMI$ magnitude and phase, as defined in ISO 10068 (1998). The idealized values are considered applicable for handle diameter ranging from 19 to 45 mm, grip force between 25 to 50 N, and push force lower or equal to 50 N.

The results show that the $DPMI$ response of the human hand and arm is strongly influenced by the handle diameter, while the effect depends upon the magnitudes of hand forces applied to the handle in a nonlinear manner. The peak $DPMI$ magnitude tends to be higher for smaller diameter handle under lower hand forces, i.e. $F_g= 10$ N and $F_p= 25$ N, when compared to those attained for larger handles. Higher levels of hand forces, however, yield an opposite trend, i.e. the peak $DPMI$ magnitude increases as the handle diameter increases, as evident from the Figure.
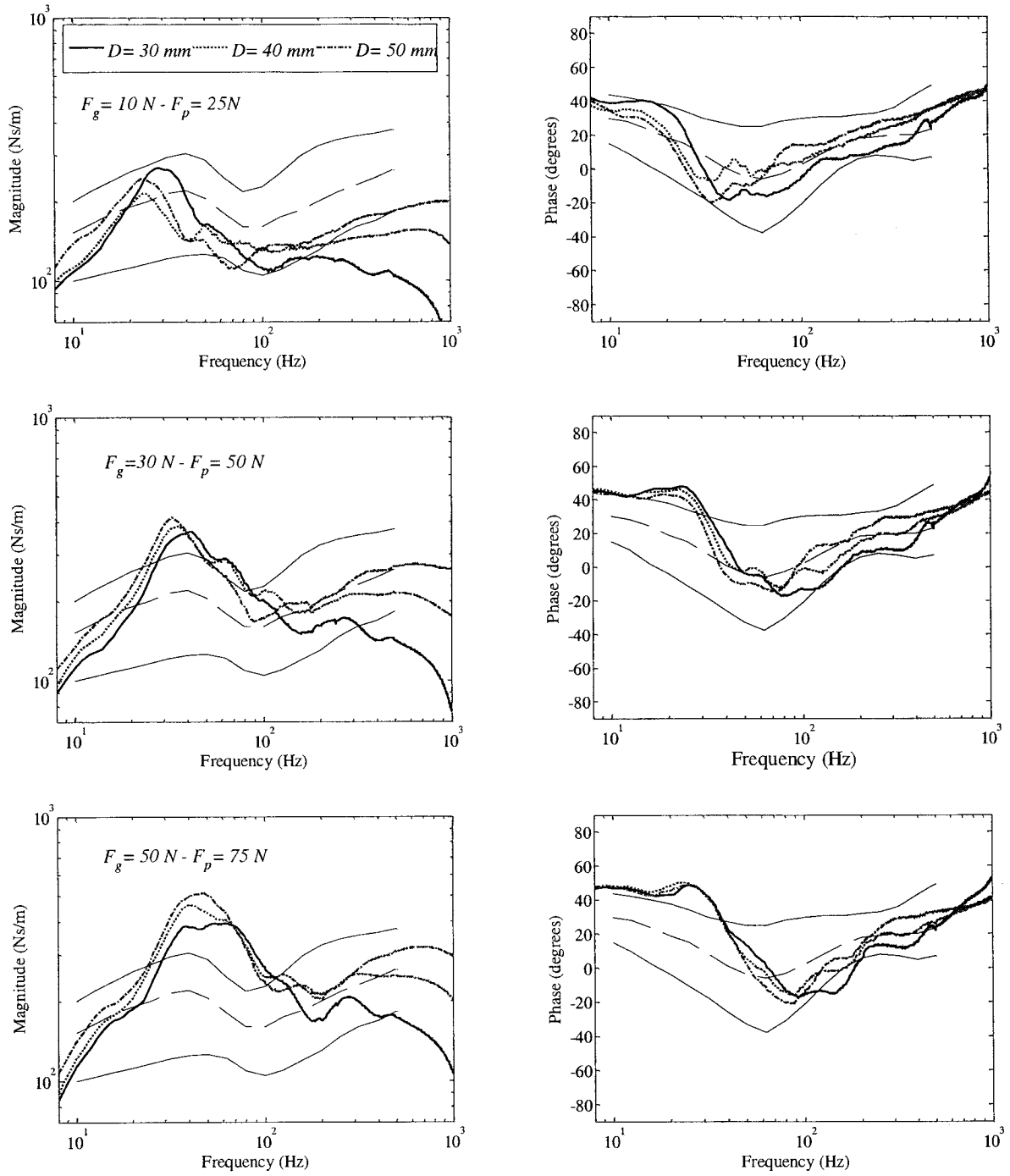
Figure 4.3: Effect of handle size on the mean measured *DPMI* responses and comparisons with the idealized values reported in ISO-10068 (posture *P1*; $F_g$= 30 N; $F_p$= 50 N and; $a_{h,w}$ = 2.5 m/s$^2$).

Moreover, the frequency corresponding to the peak magnitude decreases with increasing handle size. At low frequencies (below 25 Hz), the *DPMI* magnitude increases nearly linearly with frequency and tends to be higher for larger handles, irrespective of the hand force combination chosen in the study. The influence of handle size on the *DPMI* magnitude is most significant at frequencies above 125 Hz for all force combinations, which tends to be considerably higher with larger handle diameter. The handle diameter also has a significant influence on the *DPMI* phase, specifically in the 100 Hz to 600 Hz frequency range, where the phase response is higher with increasing handle diameter.

Comparisons of the measured magnitude and phase responses with the idealized values suggest that the mean magnitude responses under low hand forces ($F_g$= 10 N; and $F_p$= 25 N) lie within the lower and upper bounds defined in ISO 10068 (1998) standard only at frequencies below 200 Hz, while the mean phase responses are within the defined limits in the entire frequency range. Under this test condition, the mean magnitude response with the 30 mm handle is observed to be well below the lower bound of the standardized values at frequencies above 200 Hz. While the idealized values have been defined in the 10 to 500 Hz frequency range, they suggest that the *DPMI* magnitude increases with increasing frequency at frequencies above 100 Hz. This trend is not evident from the mean responses obtained in this study, which generally show decreasing magnitudes at higher frequencies. The mean responses attained under higher levels of hand forces show more important deviations from the bounds of the idealized values, as seen in Figure 4.3. The most notable differences are observed in two frequency ranges: the first being located in the neighborhood of the fundamental frequency corresponding

135

to peak magnitude, where both the magnitude and phase responses lie outside of the standardized bounds; the second being at frequencies above 200 Hz, where the magnitude responses tend to be below the lower bound, specifically for the 30 mm handle.

The phase responses attained with all three handles, however, tend to lie close to the recommended limits in the second frequency range. The discrepancies between the measured and idealized *DPMI* responses could be attributed to many factors associated with the measurement systems and test conditions. The range of idealized values reported in ISO 10068 (1998) have been attained from a synthesis of various datasets reported by different investigators acquired under widely different test conditions using considerably different measurement systems. Furthermore, the synthesis involved many datasets that were acquired many years ago and most likely utilized less reliable systems for measurement of dynamic forces, specifically at higher frequencies where the apparent mass of the hand-arm system is known to be considerably small.

The influence of handle shape on the biodynamic response of the hand-arm system exposed to vibration is further investigated by comparing the data attained for the three semi-elliptical handles with those derived for the cylindrical handles. The semi-elliptical handles were fabricated by placing rectangular inserts (8, 16 and 24 mm) between the two halves of the 30 mm cylindrical handle, which resulted in, 30x38, 30x46 and 30x54 mm elliptical handles, as described in section 2.2.1 and Figure 2.1. The three semi-elliptical handles are designated by *E38*, *E46* and *E54*, respectively. Figure 4.4 shows the mean *DPMI* magnitude and phase responses attained for seven subjects grasping the three elliptical handles with posture *P1* , $F_g$= 30 N and $F_p$= 50 N, and exposed to lower vibration level ($a_{h,w}$ = 2.5 m/s$^2$). The results show relatively small effects on the

impedance magnitude and phase responses, as the major diameter of the elliptic section increases from 38 to 54 mm. It appears that the diameter normal to the $z_h$-axis (vibration axis) and in contact with upper lateral side of the palm and the digits of the subject's plays the major role in view of the biodynamic response of the hand-arm system.
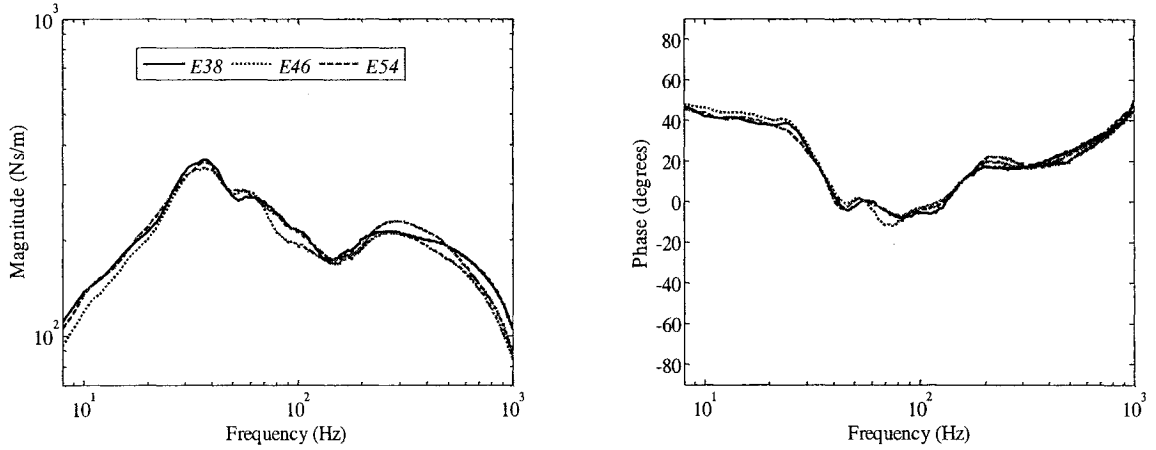


Figure 4.4: Effect of different elliptical handle sizes on the mean measured *DPMI* responses (posture *P1*; $F_g$= 30 N; $F_p$= 50 N and; $a_{h,w}$ = 2.5 m/s$^2$).

Figure 4.5 shows comparisons of the *DPMI* responses of the elliptical handles with the three cylindrical handles ($a_{h,w}$ = 2.5 m/s$^2$, posture *P1*, *Fg*= 30 N and *Fp*= 50 N). At frequencies below 20 Hz, the *DPMI* magnitude response with *E46* handle is very close to that with the 40 mm cylindrical handle, while the magnitude response with *E54* handle is closer to that with the 50 mm cylindrical handle. It could be noted that the circumferences of the *E46* and *E54* handles are comparable to those of the 40 and 50 mm cylindrical handles. The peak magnitude of the *DPMI* response and the corresponding frequency with the *E38* handle are identical to those observed for the 30 mm handle. At frequencies above 100 Hz, notable differences arise between the responses of the 40 and 50 mm cylindrical and elliptical handles.
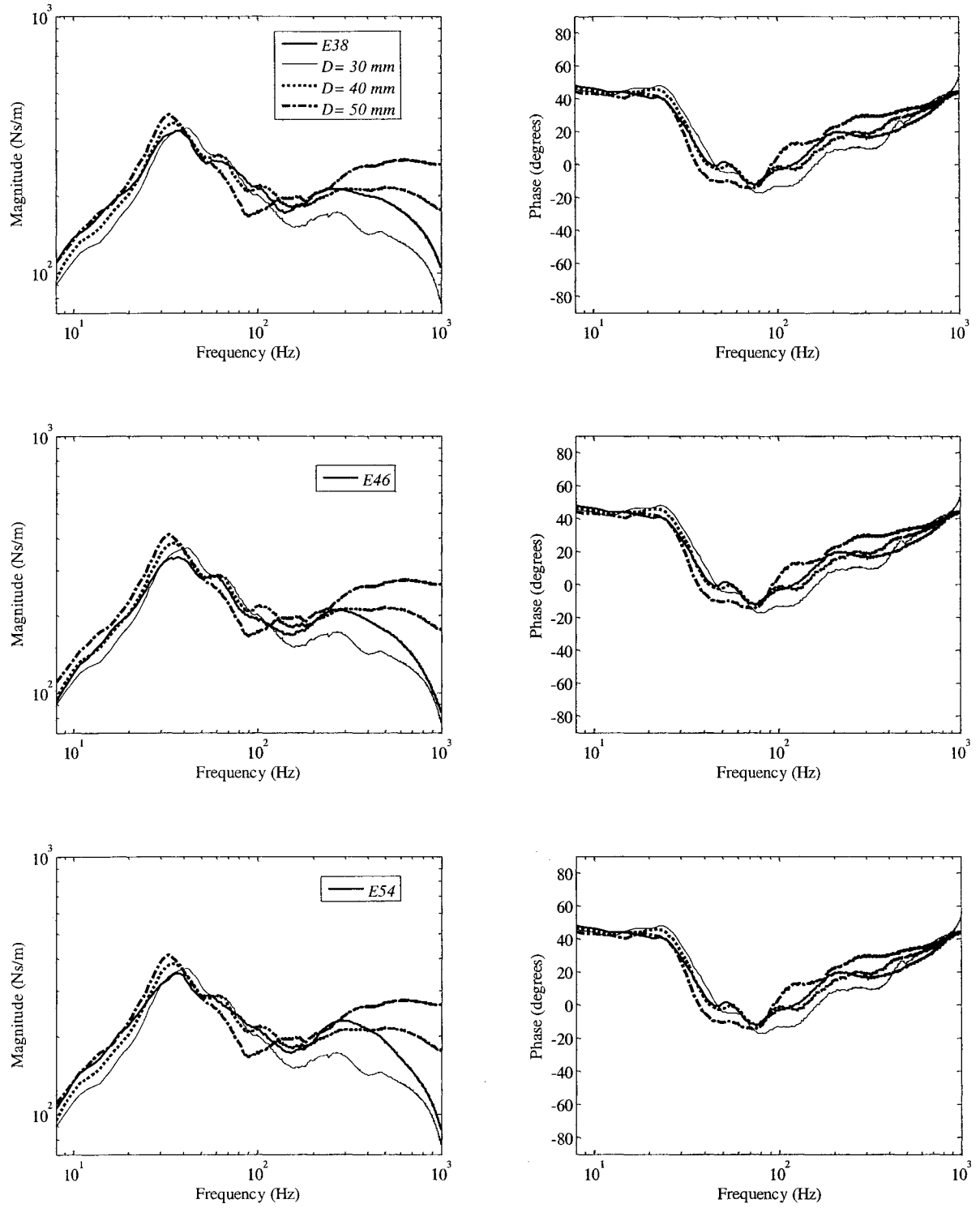
Figure 4.5: The influence of handle shape (elliptical versus cylindrical) on the *DPMI*, ($F_g$= 30 N; $F_p$= 50 N and; $a_{h,w}$ = 2.5 m/s$^2$).

The results attained for all the elliptical handles exhibit increase in the *DPMI* magnitude in the 150 to 300 Hz frequency range, which corresponds more closely to that observed with the largest 50 mm cylindrical handle. However, at frequencies above 300 Hz, the *DPMI* magnitudes with the elliptical handles follow trends comparable to those of the 30 mm cylindrical handle. These results thus suggest that the handle size plays more important role than that of the handle shape on the biodynamic response of human hand-arm system, while the effect of elliptical handle shape is frequency dependent when compared to cylindrical handles.

### 4.3.3 Influence of vibration magnitude

The influence of vibration level on the *DPMI* response of the hand-arm system has been reported in a few studies leading to somewhat contradictory conclusions as summarized in section 4.2. The data acquired in this study under two different magnitudes of vibration ($a_{h,w}$= 2.5 and 5 m/s$^2$ frequency-weighted rms accelerations) is analyzed to study the influence of excitation level on the *DPMI*. The mean *DPMI* magnitude and phase responses attained for seven subjects exposed to two levels of excitations considered in this study for 40 mm handle and *E46* handle are compared in Figure 4.6, for constant levels of $F_g$ (30 N) and $F_p$ (50 N) forces. The results generally show relatively small influence of excitation magnitude on the *DPMI* magnitude and negligible effect on the phase response for both handles. The data attained for other handle sizes also revealed identical trends with regard to the excitation magnitude. An increase in the excitation magnitude yields slightly lower peak magnitude and the corresponding frequency for the cylindrical handle, while the magnitude response at frequencies above 100 Hz is nearly identical for both magnitude of excitations. The

elliptical *E46* handle, however, reveals opposite trend, namely the peak magnitude is higher under higher excitation, while the effect on the corresponding frequency is negligible.



(a)



(b)
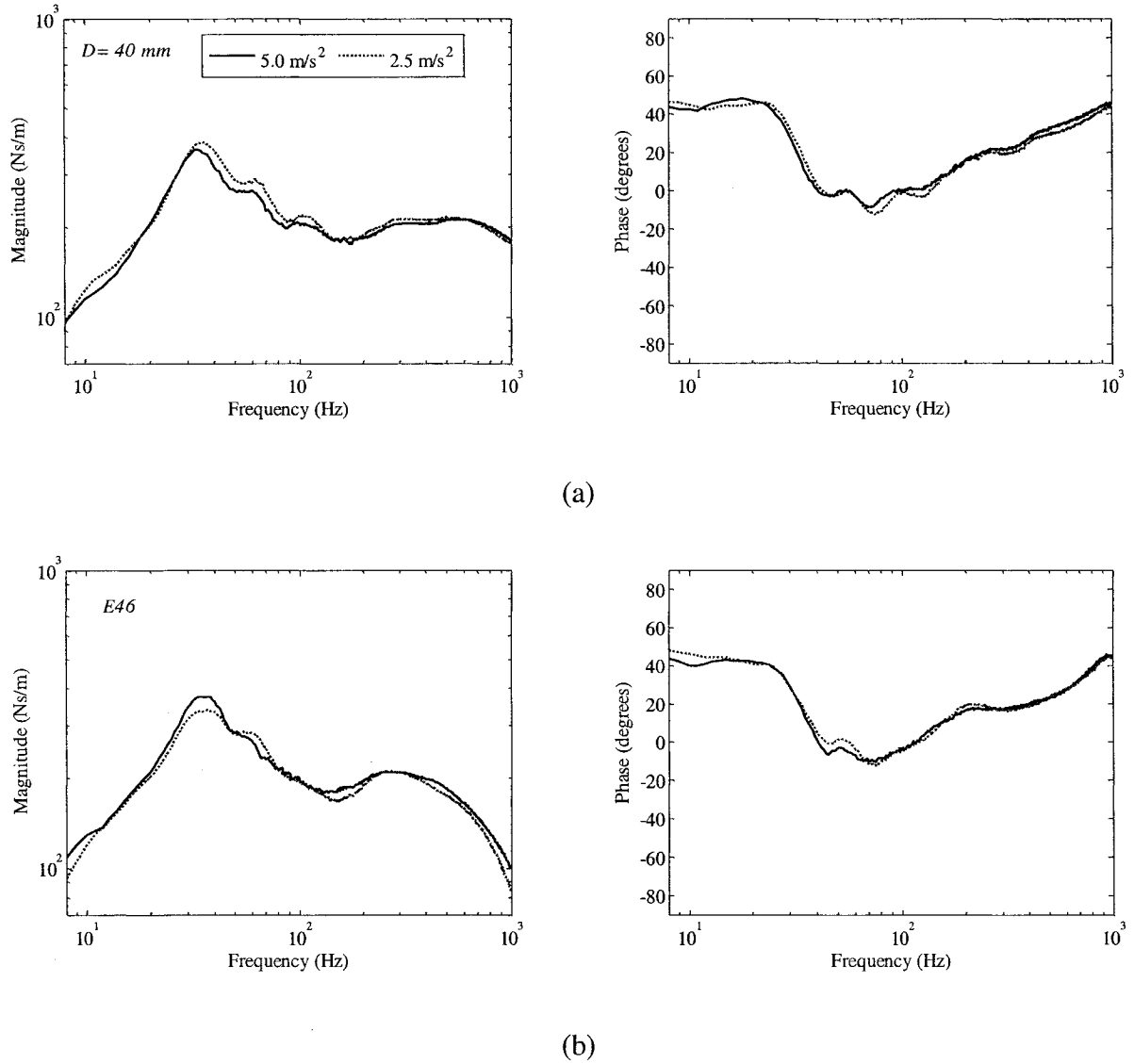
Figure 4.6 Influence of excitation magnitude on the mean *DPMI* magnitude and phase responses measured under 30 N grip and 50 N push forces: (a) *D* = 40 mm; and (b) *E46*.

The results may point to slightly nonlinear behavior of the hand-arm system. The deviations in the magnitude under different excitation levels are well within the range of the inter-subject variability. Owing to the very small deviation in the magnitude response,

it may be concluded that the excitation magnitude has nearly negligible influence on the impedance response of hand-arm system, when compared to the influences in variations in the hand forces and handle sizes. This may further explain the contradictory finding in many published studies on the influence of vibration magnitude on the human hand-arm DPMI response (Burström, 1990; Gurram et al., 1995; Burström, 1997).

## 4.3.4 Influence of hand forces

The mean DPMI magnitude responses attained under vibration level $a_{h,w}$ = 2.5 m/s$^2$, posture P1 and nine different combinations of $F_g$ (10, 30 and 50 N) and $F_p$ (25, 50 and 75 N) forces, are illustrated in Figure 4.7, for the 40 mm cylindrical and E46 elliptical handles. The results, in-general, suggest that at frequencies above 20 Hz, the DPMI magnitude tends to increase with increase in both the grip and push forces; the effect being more emphasized near the frequencies corresponding to peak responses. At frequencies below 20 Hz, the influence of grip and push forces appears to be negligible for both handles, where the DPMI magnitude increases nearly linearly with frequency. The peak magnitudes in general tend to be much higher under combinations of high grip and push forces. The results thus suggest that the combination of push and grip forces, referred to as the coupling force (ISO/CD-15230, 2004), imparted by the hand has a considerable influence on the biodynamic response of the hand-arm system. Similar trends were also observed in the data acquired with other handles and high magnitude acceleration spectrum considered in the study.
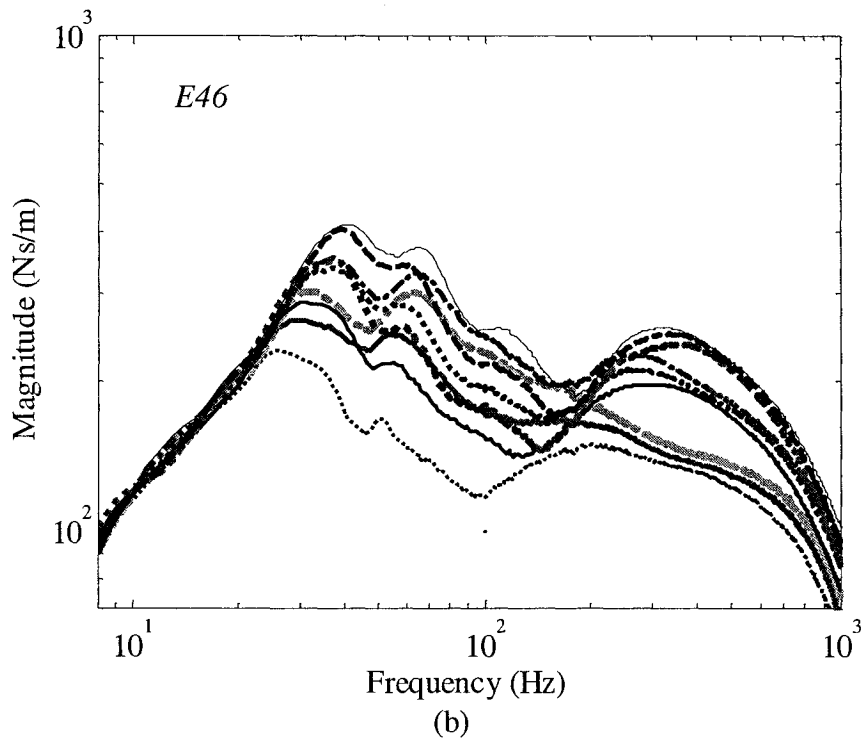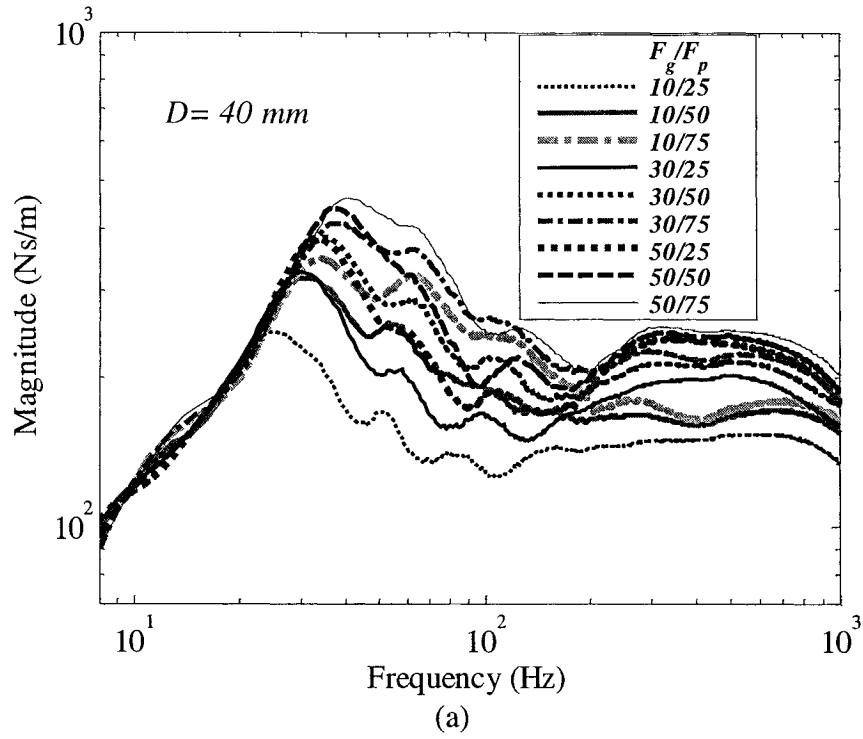
Figure 4.7: Comparisons of *DPMI* magnitude responses attained under different grip-push force combinations on the *DPMI* magnitude (posture *P1*, $a_{h,w} = 2.5$ m/s$^2$): (a) cylindrical 40 mm handle; and (b) elliptical *E46* handle.

The influence of grip force on the mean *DPMI* response under a constant value of push force (50 N) on the *DPMI* magnitude and phase responses attained with the 40 mm and 46E handles is further shown in Figure 4.8. Both handles show comparable trends in *DPMI* magnitude with variations in the grip force, particularly at frequencies below 125 Hz. While the results suggest generally minimal effect of variations in the grip force on the *DPMI* phase response, higher phase angle results under a higher grip force up to approximately 50 Hz while the effect is nearly negligible at higher frequencies.
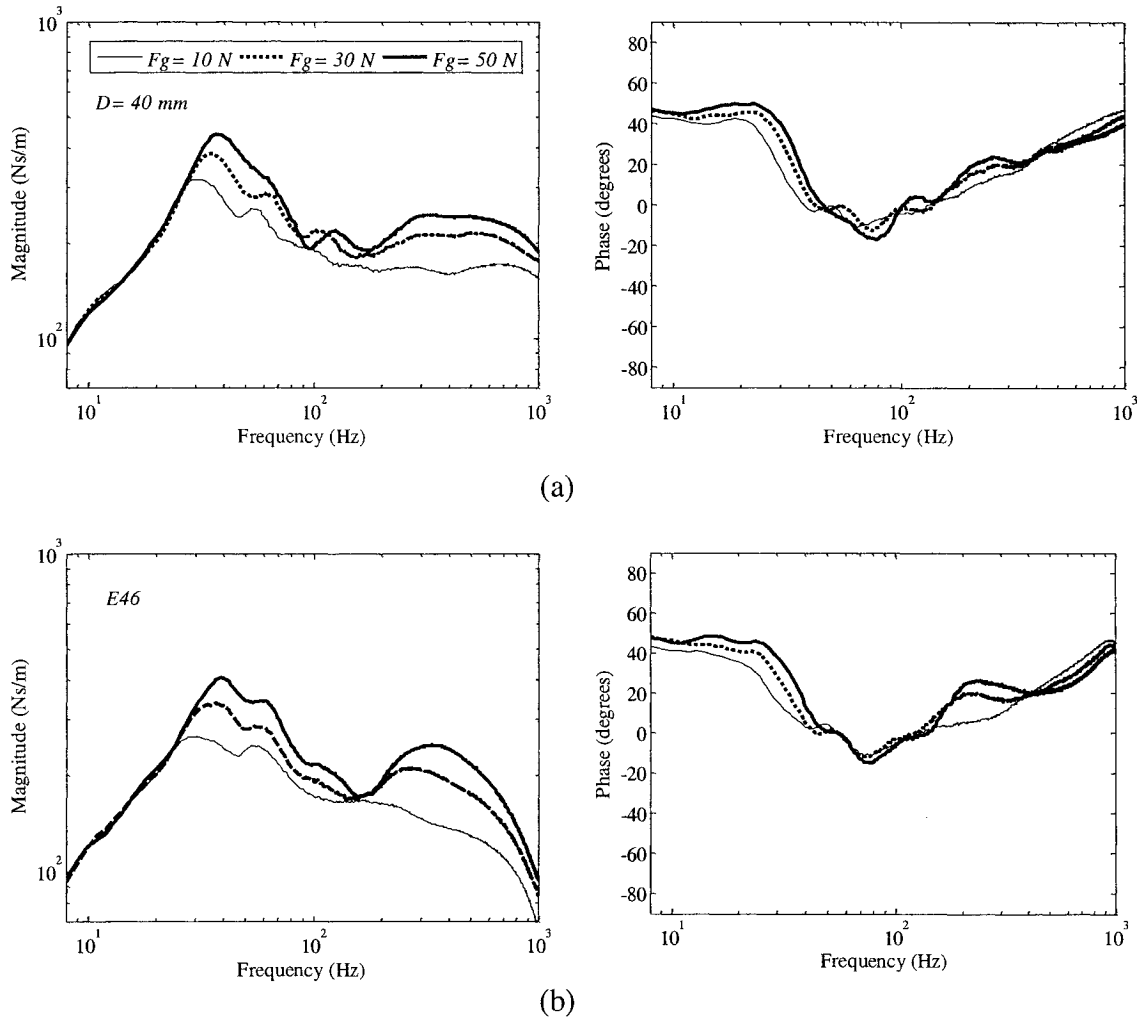


Figure 4.8: Effect of the variations in the grip force on the *DPMI* magnitude and phase responses: (a) cylindrical 40 mm handle; and (b) elliptical *E46* handle ($F_p$= 50 N, posture *P1* and $a_{h,w}$ = 2.5 m/s$^2$).

An important increase in the magnitude with increase in the grip force at frequencies between 25 and 80 Hz and above 200 Hz is clearly evident. Such a trend was also observed with all handles considered in the study. The results further show that the fundamental frequency corresponding to the peak *DPMI* magnitude decreases with decreasing grip force, suggesting softening effect of the hand- arm system, while the peak magnitude and the corresponding frequency increase with increasing grip force.

Increasing the push force yields considerably higher *DPMI* magnitude response in the 30 to 200 Hz frequency range, as shown in Figure 4.9, for a constant level of grip force ($F_g$= 30 N). The increase in the *DPMI* magnitude with increasing push force is much lower at frequencies above 200 Hz, for both handles. A comparison of results shown in Figures 4.8 and 4.9 for varying grip and push forces, respectively, suggests that both the grip and push forces, when taken individually, have almost similar influence on the *DPMI* magnitude response at frequencies near and above the primary resonance, i.e. 20 to 100 Hz. The influence of varying the grip force on the *DPMI* magnitude appears to be more important at frequencies above 200 Hz. The *DPMI* phase response on the other hand appears to be more influenced by variations in the push force.

Owing to complex and nonlinear dependency of the *DPMI* magnitude response on the grip and push forces, the variations in the mean magnitude response are further analyzed to explore correlations with the hand-handle contact or coupling forces. The hand-handle coupling force is defined as a direct and simple summation of the push and grip forces, whereas the contact force is defined as the sum of the distributed normal force at the hand–handle interface surrounding the handle (section 1.3).

144
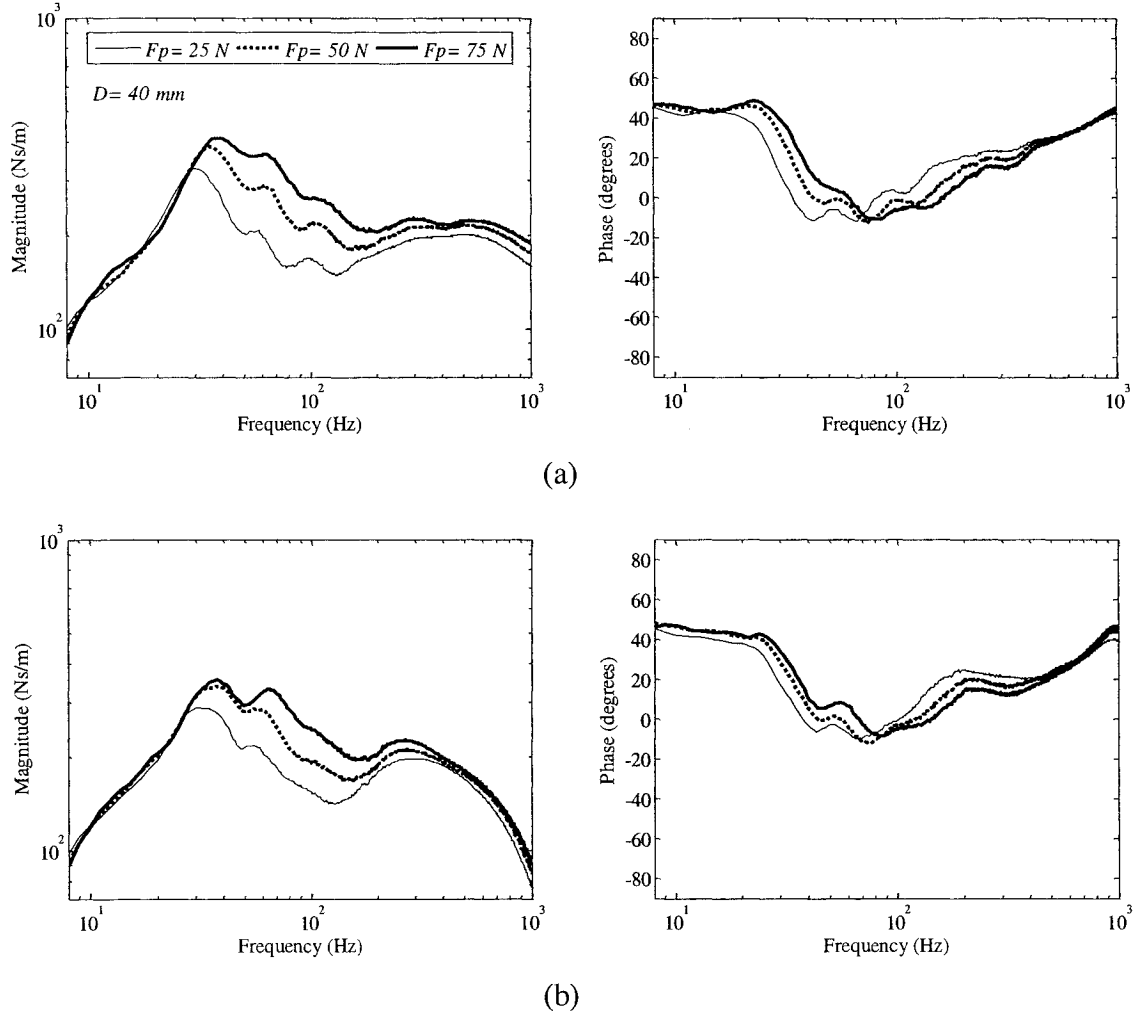
Figure 4.9: Influence of the variations in the push force on the *DPMI* magnitude and phase responses: (a) cylindrical 40 mm handle; and (b) elliptical *E46* handle ($F_g$= 30 N, posture *P1* and $a_{h,w}$ = 2.5 m/s$^2$).

The static contact forces developed within the hand-handle interface under different combinations of handle sizes, and grip and push forces were thus initially evaluated by integrating the measured pressure distribution over the total contact area of the hand with the sensing mat, as described in section 3.2. Owing to nearly linear variation in the contact force with the grip and push forces, a multiple linear regression was performed to account for contributions of grip and push forces to the contact force developed within the hand-handle interface, such that:

$$F_c = \alpha( D )F_g + \beta( D )F_p$$  (4.1)

where $F_c$ is the contact force, and $\alpha$ and $\beta$ are the coefficients represents contributions of grip and push forces, respectively.

The grip and push force coefficients, derived for each subject, together with their mean values and standard deviations are summarized in Table 4.1 for different handle sizes. For each subject and handle combination, the linear regressions lead to correlation coefficients ($r^2$) in excess of 0.95. The regression coefficients of the contact force derived for the cylindrical handles are similar to those derived in section 3.3. For the elliptical handles, the grip coefficients relate to the handle size in a manner similar to that observed for the cylindrical handles; large size handle develops lower grip coefficient, while the push force coefficients of the elliptical handles also suggest same trend, to that obtained for the cylindrical handles, which revealed negligible dependence on the handle size.

Figure 4.10 illustrates variations in the mean values of the contact force acquired for seven subjects for each handle as a function of the grip force ($F_p$= 50 N), and as a function of push force ($F_g$= 50 N). The figure also illustrates the coupling force, defined as the sum of grip and push forces (ISO/CD 15230, 2004; Reidel, 1995). The results conform that the hand-handle contact force varies with variations in the handle size, and grip and push forces, while the variations in the coupling force are independent of the handle size. Furthermore, the contact force is observed to vary with grip and push forces in a linear fashion, irrespective of the handle size.

Table 4.1: Regression coefficients representing the contribution due to grip and push forces to the total contact force.

| Subject | Handle Size | | | | | | | | | | | |
|---|---|---|---|---|---|---|---|---|---|---|---|---|
| | D= 30 mm | | D= 40 mm | | D= 50 mm | | 38E | | 46E | | 54E | |
| | $\alpha$ | $\beta$ | $\alpha$ | $\beta$ | $\alpha$ | $\beta$ | $\alpha$ | $\beta$ | $\alpha$ | $\beta$ | $\alpha$ | $\beta$ |
| A | 3.47 | 0.88 | 2.71 | 1.08 | 2.62 | 1.05 | 3.26 | 1.35 | 2.91 | 1.12 | 2.44 | 0.86 |
| B | 3.88 | 1.2 | 2.98 | 0.9 | 2.8 | 0.96 | 2.86 | 1.15 | 2.43 | 1.14 | 2.30 | 0.93 |
| C | 3.54 | 1.03 | 3.13 | 1.17 | 2.85 | 1.16 | 2.81 | 1.27 | 2.66 | 1.11 | 2.52 | 0.97 |
| D | 3.1 | 0.95 | 2.35 | 1.1 | 2.59 | 1.12 | 2.93 | 1.16 | 2.51 | 1.14 | 2.18 | 0.91 |
| E | 3.38 | 0.92 | 2.74 | 1.02 | 2.55 | 1.05 | 3.31 | 1.17 | 3.32 | 1.12 | 2.64 | 0.88 |
| F | 3.24 | 0.87 | 3.09 | 0.88 | 2.84 | 0.9 | 2.96 | 1.16 | 2.59 | 0.89 | 2.63 | 0.87 |
| G | 3.17 | 0.92 | 2.76 | 0.83 | 2.55 | 0.94 | 2.91 | 1.16 | 2.43 | 1.02 | 2.06 | 0.88 |
| Mean; | 3.40; | 0.97; | 2.82; | 1.00; | 2.69; | 1.03; | 3.01; | 1.20; | 2.69; | 1.08; | 2.40; | 0.90; |
| SD | 0.27 | 0.12 | 0.27 | 0.13 | 0.14 | 0.10 | 0.20 | 0.08 | 0.32 | 0.09 | 0.22 | 0.04 |



(a)



(b)
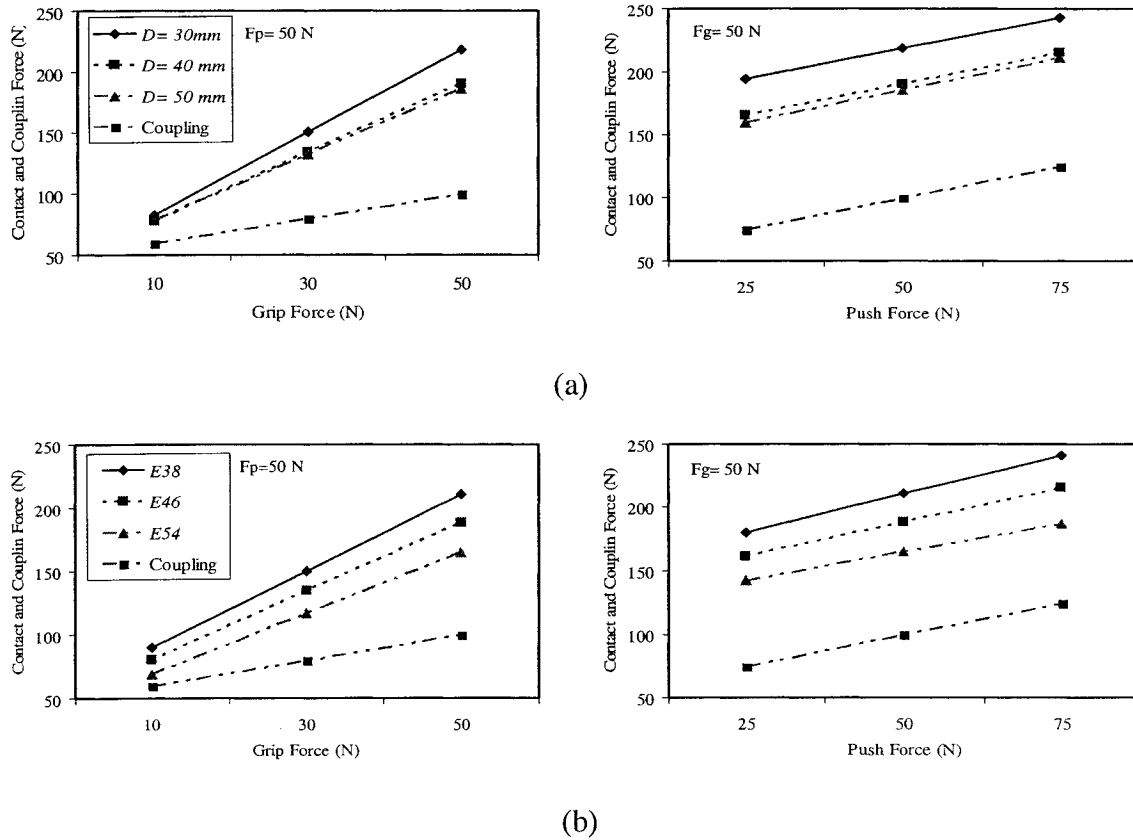
Figure 4.10: Variations in the hand-handle coupling and contact forces as functions of the push and grip forces: (a) cylindrical handles; (b) elliptical handles.

In an attempt to study the dependence of the *DPMI* magnitude on the hand-handle interface forces, linear regression analyses were performed to relate the measured coupling force and total contact force, with the mean *DPMI* magnitude, for all combinations of grip and push forces, and all six handles considered. Figure 4.11 illustrates the variations in the correlation coefficients obtained for the mean *DPMI* magnitude with respect to coupling and contact forces for the all cylindrical and elliptical handles. The correlation coefficients are presented as a function of frequency, and plotted for center frequencies of one-third octave bands. These results, in general, suggest that the mean *DPMI* magnitude is more closely correlated with the coupling force at frequencies below 200 Hz, irrespective of the handle size and shape. A better correlation with the contact force, however, is attained at frequencies above 200 Hz, for all handles.

The strong correlation of the *DPMI* magnitude response with the coupling force at lower frequencies is perhaps attributed to its strong dependence on the push force, as seen in Figure 4.9. This may further be attributed to the mechanical coupling of the entire hand-arm structure with the handle by the coupling force acting between the handle and the palm of the hand at lower frequencies below 200 Hz. The higher correlation with the contact force at higher frequencies is due to strong dependence of the *DPMI* on the grip force, as seen in Figure 4.8. At higher frequencies, the driving-point mechanical impedance is mainly caused by the skin tissues of the hand-arm system, where the grip force contributes far more than the push force, partly due to larger contact area between the handle and the hand skin. The contact force, which increases in proportion to approximately three times the grip force, thus becomes the dominating factor at higher frequencies.
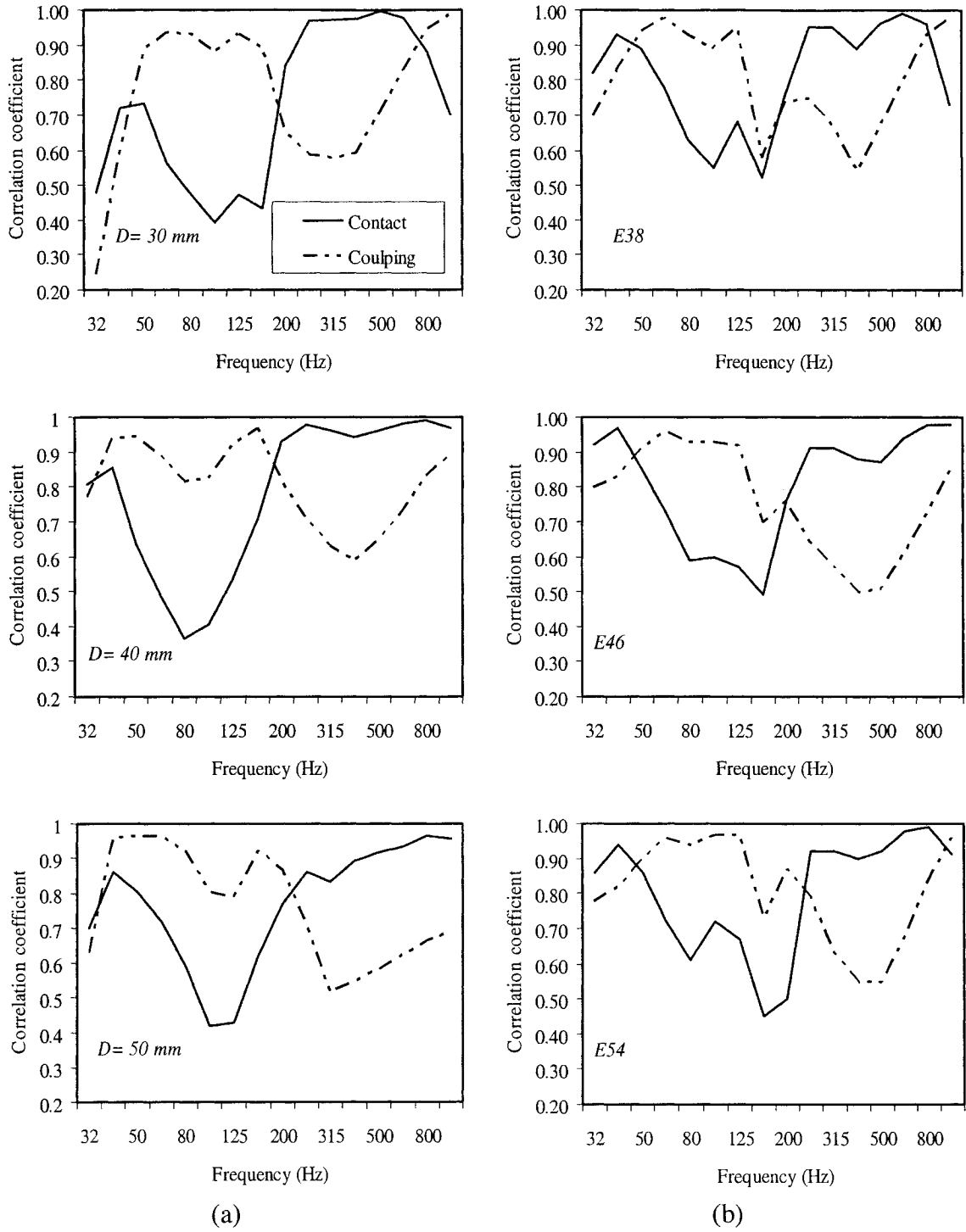
Figure 4.11: Variations in the correlation coefficients describing the relations between the mean *DPMI* magnitude and the contact and coupling forces ($a_{h,w} = 2.5$ m/s$^2$), (a) cylindrical handles; (b) elliptical handles.

149

### 4.3.5 Influence of hand-arm posture

Gripping of tools with elevated arm posture or working with extended arms can cause increasing loading of hand-arm muscles, leading to fatigue, soreness and pain (Freivalds, 2004). Hand-arm posture with 90° elbow angle has been suggested as optimal work posture (Freivalds, 2004). A vast number of studies have established that static forces generated by the human hand are strongly influenced by hand-arm posture (Kattel et al., 1996; Marley et al., 1993; Kuzala and Vargo, 1992). Kattel et al. (1996) concluded that the elbow flexed at 45° allows higher grip strength than that generated at 90° or 180°. Marley et al. (1993) and Kuzala and Vargo (1992), on the other hand, found that maximum grip strength exerted with the elbow in full extension was higher than when it was flexed at 90°.

Despite the contradictions on the effect of elbow angle on the grip strength, the reported studies have clearly shown the effect of posture on the static hand forces, which could be related to variations in the muscle force capacity resulting from muscle length associated with upper limb posture (Danuta, 2003). Donati et al. (1992) observed changes in the activities of the triceps brachii under vibration exposure with variations in the hand-arm posture. The triceps brachii activity of the vibration-exposed hand-arm system with elbow angle closed to 90° was found to be comparable under static as well as dynamic conditions. The presence of vibration, however, resulted in larger increase in the muscle activity for the 180° elbow angle hand-arm posture. Owing to this, considerable influence of hand-arm posture on the hand-arm biodynamic response to vibration is expected.

The influence of hand-arm posture on the biodynamic response to vibration along $z_h$-axis, each test condition was investigated performing the experiments under two different postures. These included the posture *P1*, where the subjects maintained their forearm horizontally aligned with the handle and elbow bent at an angle of 90°; and posture *P2*, with elbow angle extended to 180°. The wrist was maintained in a neutral position for both postures as shown in Figure 4.12. Figure 4.13 illustrates the mean *DPMI* magnitude and phase responses obtained while gripping the 40 mm handle with 30 N grip and 50 N push, and exposed to $a_{h,w}=$ 5 m/s² vibration excitation. The figures compare the responses obtained with two arm postures: *P1*: (90° elbow flexion); and *P2*: (180° elbow flexion). It is evident that the posture *P2* yields significantly higher mechanical impedance magnitude at lower frequencies (below 30 Hz). At very low frequencies, this posture exhibits damper-like behavior, which is also evident from nearly zero phase response. The peak magnitude occurs around 20 Hz, while magnitude response with the posture *P1* yields peak around 33 Hz for this particular handle and hand forces combination.



(a)                              (b)
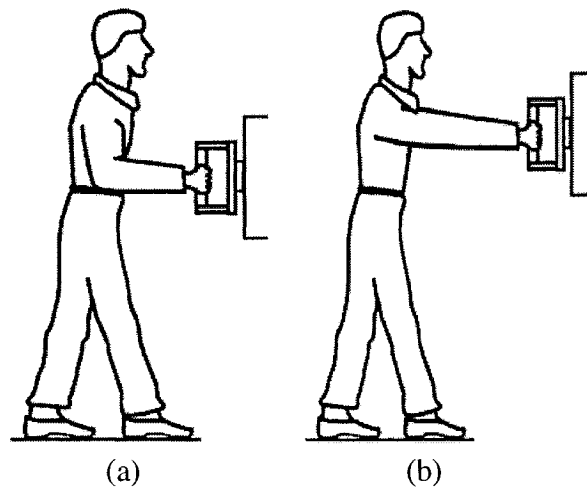
Figure 4.12: Schematic representations of the hand-arm postures employed in this study: (a) posture *P1*; and (b) posture *P2*.

The frequency corresponding to the peak response, often associated with the primary resonant frequency of the hand-arm system, agrees very well with the range of values reported in many studies for *P1* posture (Burström, 1990; Jandák, 1998; Cronjäger and Hesse, 1990; Kohlberg, 1995; Reynolds and Falkenberg, 1984). In the 35-100 Hz frequency range, posture *P1* results in higher impedance magnitude. However, at frequencies above 100 Hz, the posture *P2* causes slightly higher *DPMI* magnitude. The *DPMI* phase response also shows clear influence of the hand-arm posture at frequencies below 80 Hz.
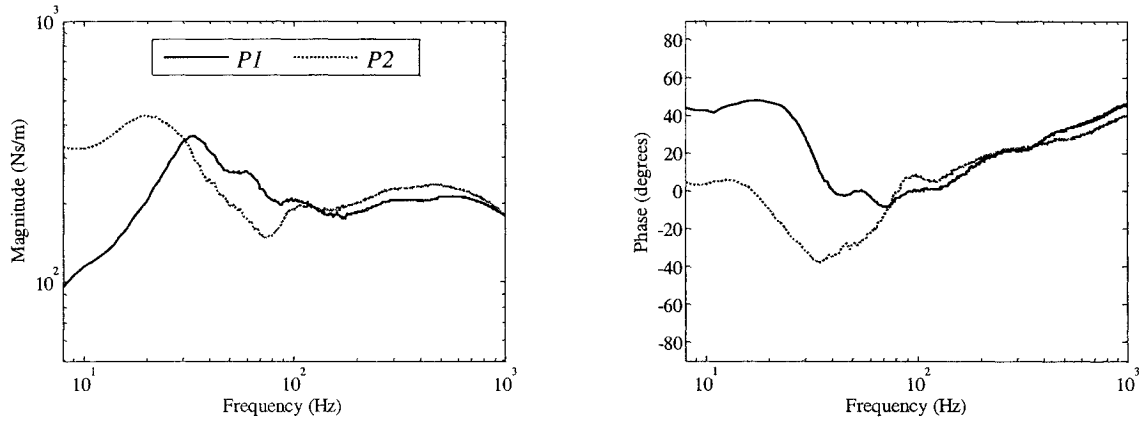


Figure 4.13: Influence of hand-arm posture on mean the *DPMI* magnitude and phase response ($D$= 40 mm; 30 N $F_g$, 50 N $F_p$; and $a_{h,w}$ = 5 m/s$^2$.

Significantly higher impedance magnitude at low frequency for the *P2* posture suggests a relatively higher hand mass coupling with the handle, which permits the flow of low frequency vibration energy through the hand-arm to the whole body. The higher effective mass is further believed to contribute to relatively lower resonant frequency, when compared to that obtained for posture *P1*. The difference in the effective masses associated with the two postures is clearly evident from the mean apparent mass (*APMS*) response of the hand-arm system, shown in Figure 4.14. The figure shows the magnitude

and phase response for the two postures subject to identical conditions ($a_{h,w}$= 5 m/s$^2$ excitation, $F_g$= 30 N, $F_p$= 50 N, and 40 mm handle). The apparent mass magnitude under P2 posture is almost three times higher than that under the P1 posture at the lowest frequency considered in the study (8 Hz). This would represent higher static mass of the hand-arm system coupled with the handle, if the dynamics were considered negligible at such low frequency. The two postures, however, yield comparable magnitudes at frequencies above 32 Hz. The APMS magnitudes approach values below 200 g at frequencies above 200 Hz, suggesting localized coupling between the hand and handle, irrespective of the posture. This phenomenon has also been observed in a few reported studies (Sörensson and Lundström, 1992; Donati et al., 1992; Kihlberg, 1995).
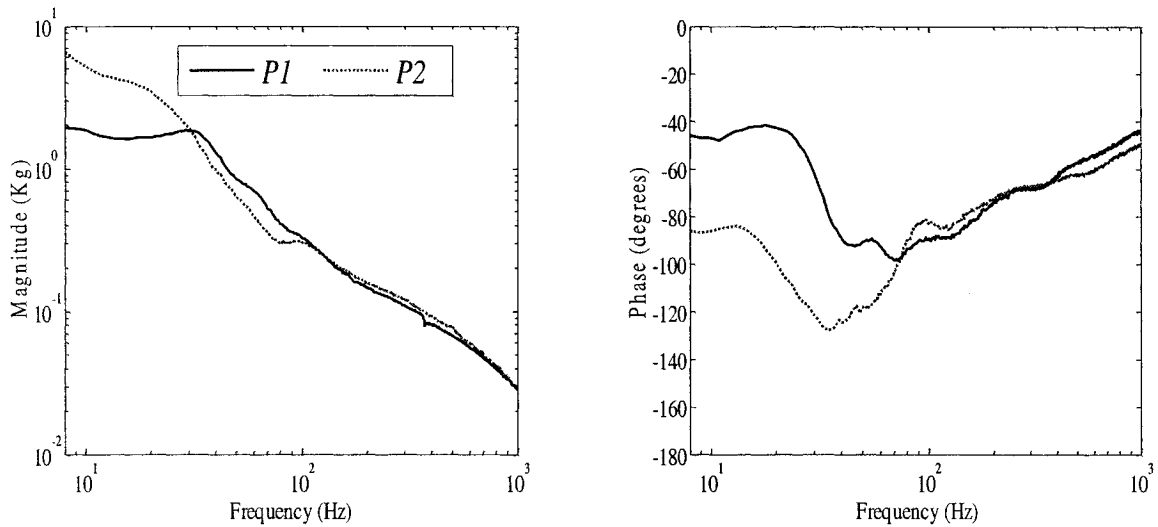


Figure 4.14: Influence of hand-arm posture on the mean APMS magnitude and phase (D= 40 mm; $F_g$= 30 N, $F_p$= 50 N; and $a_{h,w}$ =5 m/s$^2$).

Figure 4.15 illustrates the influence of handle size on the mean DPMI magnitude and phase responses for both postures averaged over seven subjects exposed to high magnitude vibration spectrum ($a_{h,w}$= 5 m/s$^2$), and exerting 30 N grip and 50 N push

forces. Although the variations in the handle size influence the magnitude and phase responses under both postures, the trends are quite different.



(a)



(b)
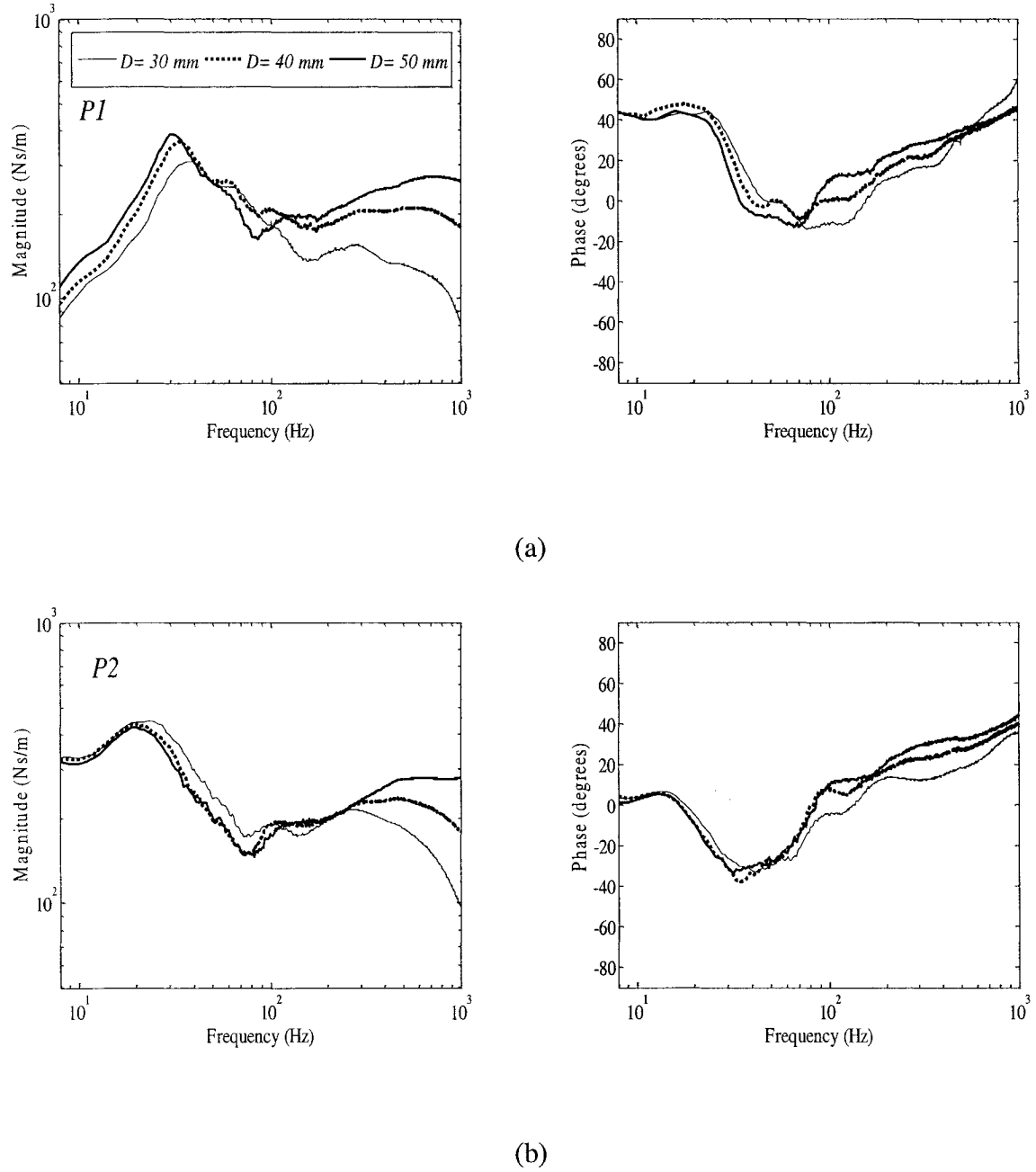
Figure 4.15: Influence of handle size on the mean *DPMI* magnitude and phase response, ($F_g$= 30 N, $F_p$ = 50 N, and $a_{h,w}$ = 5 m/s$^2$): (a) Posture *P1*; and (b) Posture *P2*.

The *P1* posture yields higher low frequency magnitude and lower frequency of peak magnitude as the handle size increases, while the effect of handle size on the magnitude in the 40-100 Hz frequency range is not evident. However, the impedance magnitude increases with the handle size at frequencies above 100 Hz. The *P2* posture exhibits considerably higher *DPMI* magnitude but nearly opposite effect with the handle size on the impedance magnitude at lower frequencies, although the effect is relatively small. The two postures, however, exhibit similar effects of handle size on the impedance magnitude at higher frequencies (above 250 Hz). The variations in the handle size yield only small variations in the phase response for both postures.

The musculoskeletal loads may be even higher when the magnitude of hand forces is increased. The influence of variation in the push and grip forces on the impedance magnitude of the hand and arm system exposed to excitation level of 5 m/s$^2$, while gripping the 40 mm handle with the two postures, is shown in Figure 4.16. An increase in the push as well as grip forces tends to shift the peak impedance towards a higher frequency for both postures. While the influence of push and grip forces in the low frequency region is not evident under the *P1* posture, the *P2* posture clearly shows higher magnitude response at low frequencies, suggesting stronger coupling between the hand-arm and the handle. The stiffening effect of the hand-arm due to higher push or grip forces can be observed at frequencies above the respective primary resonant frequencies up to nearly 100 Hz. The influence of push force in the frequency range above 200 Hz weakens under both postures, while a higher grip force causes higher impedance magnitude at higher frequencies, irrespective of the hand-arm posture.
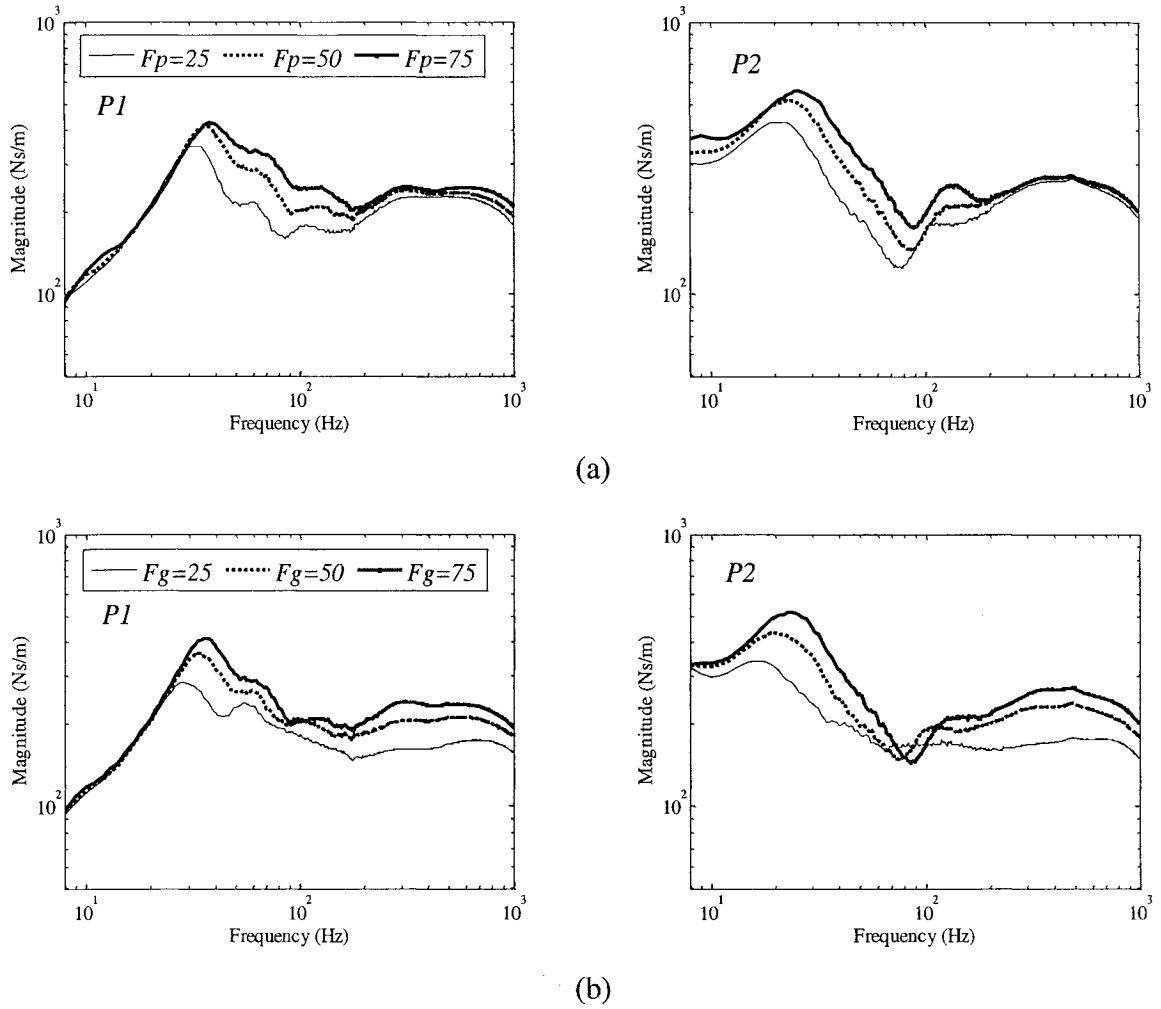
Figure 4.16: Effect of variation in the hand forces on the mean impedance magnitude under two postures ($D$= 40 mm and $a_{h,w}$ = 5 m/s$^2$): (a) variation in push force, $F_g$= 30 N; and (b) variation in grip force, $F_p$= 50 N.

The effect of vibration magnitude on the mean impedance magnitude response for both postures is shown in Figure 4.17, for the subjects exposed to two levels of vibration: 2.5 and 5 m/s², while gripping a 40 mm handle and exerting 30 N grip and 50 N push forces. It is shown that at low frequencies, the effect of vibration magnitude is more slightly pronounced under the P2 posture, while the dependence on vibration magnitude is extremely small, as discussed in 4.3.3.

**P1**

— 2.5 m/s² ------ 5 m/s²

Magnitude (Ns/m)

$10^3$

$10^2$

$10^1$     $10^2$     $10^3$

Frequency (Hz)

(a)

**P2**

Magnitude (Ns/m)

$10^3$

$10^2$

$10^1$     $10^2$     $10^3$

Frequency (Hz)

(b)
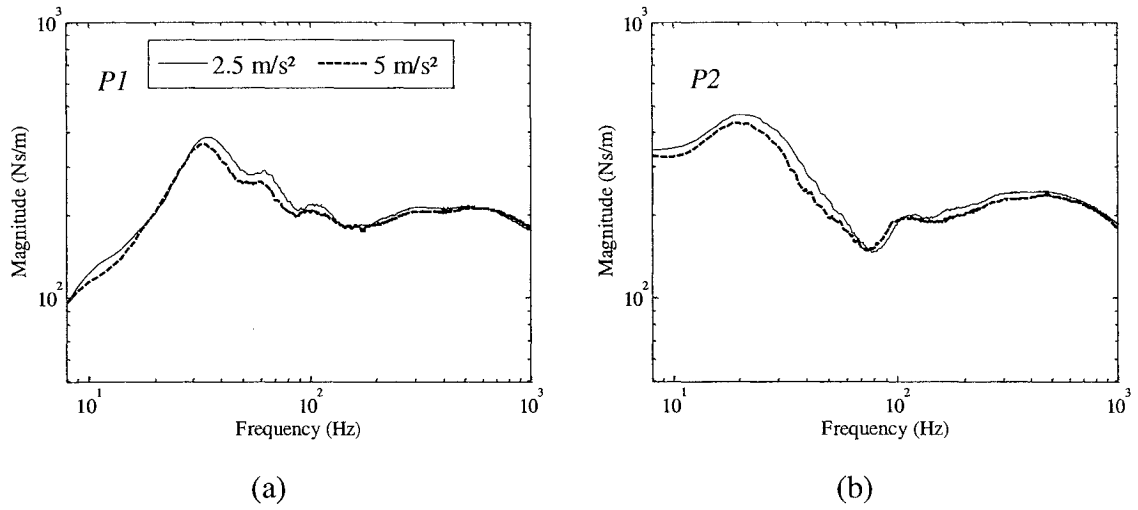
Figure 4.17: Comparison of the influence of vibration magnitude on the mean *DPMI* magnitude under two postures (*D*= 40mm; $F_g$ =30 N and $F_p$=30 N): (a) posture *P1*; and (b) posture *P2*.

### 4.3.6 Statistical analyses

The statistical significance of different parameters on the mean *DPMI* magnitude response of seven subjects corresponding to one-third octave frequency bands was evaluated through multifactor analyses within subject ANOVA using the SPSS software. The statistical analysis design was five-factor factorial type. The factors included vibration levels (*A*) with two levels (2.5 m/s² and 5 m/s²), hand-arm posture (*P*) with two levels (posture *P1* and posture *P2*), handle diameter with three levels (30, 40 and 50 mm), grip force ($F_g$) with three levels (10, 30 and 50 N) and push force ($F_p$) with three levels (25, 50 and 75 N). Repeated measures or within-groups ANOVA design is used since there is one group of subjects exposed randomly to different conditions. The conditions are the categories of the independent variable, which is the repeated measures factor.

Table 4.2 summarizes the results of the statistical analysis of the *DPMI* magnitude measured under $z_h$-axis vibration,, where a factor associated with a $p$ value of less than 0.05 is considered to be statistically significant. The Table summarizes the significance analysis of the main factors as well as the two-way interactions between these factors. The hand-arm posture shows strong significance in view of the *DPMI* magnitude in the low frequency bands (25 Hz and lower), which can also be observed in Figure 4.13. The effect is also significant in the high frequency bands, above 250 Hz. The excitation level appears to be statistically significance only in 25-63 Hz bands, where the magnitude peak occurs, while it is non-significant in the remaining frequency range, which is also seen in Figure 4.6. Handle size reveals insignificance effect on the impedance magnitude in the majority of the frequency bands lower than 125 Hz, however, this trend reverses remarkably in the higher frequency bands. The strong influence of handle size in high frequency bands can be easily seen in Figure 4.3. Both the hand forces (grip and push) show strong significance on the *DPMI* magnitude in the entire frequency range except in the 8 Hz band for the grip force.

The hand-arm posture shows clear interactions with other factors (handle size, grip and push force) at frequency bands lower than that of the peak. The influence of hand-arm posture is most notable in the low frequency bands. The excitation level (*A*), in general, shows weak interactions with other factors (handle size, grip and forces) conforming the low sensitivity of *DPMI* to the vibration magnitude. The interaction between the excitation level and the hand forces, however, could be observed in the 50 to 80 Hz bands. Hand forces show significance interaction between each of them in most of the frequency bands, specifically at low frequency bands.

158

Table 4.2: Statistical significance factor (p) of various contributory factors in view of the *DPMI* magnitude over one-third octave frequency bands under $z_h$-axis vibration.

| Factors | P | A | D | Fg | Fp | P*A | P*D | P*Fg | P*Fp | Fg*Fp | D*Fp | Fg*D | A*Fp | A*Fg | A*D |
|---|---|---|---|---|---|---|---|---|---|---|---|---|---|---|---|
| Frequency (Hz) | | | | | | | Significance Level (p) | | | | | | | | |
| 8 | .00 | .37 | .97 | .23 | .00 | .49 | .01 | .15 | .00 | .06 | .30 | .61 | .04 | .44 | .87 |
| 10 | .00 | .04 | .33 | .00 | .00 | .84 | .00 | .00 | .00 | .04 | .25 | .38 | .22 | .04 | .20 |
| 13 | .00 | .05 | .72 | .00 | .00 | .71 | .00 | .00 | .00 | .00 | .45 | .17 | .56 | .03 | .22 |
| 16 | .00 | .05 | .47 | .00 | .00 | .37 | .00 | .00 | .00 | .00 | .03 | .01 | .14 | .13 | .06 |
| 20 | .00 | .05 | .61 | .00 | .00 | .16 | .00 | .00 | .00 | .00 | .00 | .00 | .05 | .14 | .06 |
| 25 | .00 | .01 | .52 | .00 | .00 | .18 | .00 | .00 | .00 | .00 | .00 | .01 | .00 | .14 | .04 |
| 32 | .62 | .00 | .69 | .00 | .00 | .46 | .00 | .00 | .00 | .00 | .00 | .00 | .00 | .88 | .16 |
| 40 | .18 | .00 | .50 | .00 | .00 | .31 | .06 | .83 | .00 | .01 | .00 | .13 | .06 | .11 | .44 |
| 50 | .12 | .00 | .55 | .00 | .00 | .39 | .17 | .50 | .43 | .18 | .00 | .26 | .04 | .00 | .52 |
| 63 | .02 | .00 | .06 | .00 | .00 | .17 | .33 | .24 | .21 | .32 | .01 | .17 | .03 | .00 | .68 |
| 80 | .01 | .07 | .04 | .00 | .00 | .04 | .40 | .00 | .00 | .41 | .20 | .10 | .01 | .00 | .21 |
| 100 | .18 | .20 | .14 | .03 | .00 | .19 | .12 | .00 | .01 | .00 | .00 | .30 | .48 | .89 | .30 |
| 125 | .60 | .07 | .15 | .00 | .00 | .90 | .01 | .95 | .10 | .00 | .00 | .29 | .58 | .84 | .34 |
| 160 | .02 | .09 | .00 | .00 | .00 | .68 | .00 | .47 | .90 | .52 | .00 | .13 | .14 | .01 | .06 |
| 200 | .03 | .11 | .00 | .00 | .00 | .67 | .00 | .26 | .39 | .00 | .00 | .49 | .49 | .00 | .02 |
| 250 | .01 | .08 | .00 | .00 | .00 | .90 | .00 | .28 | .41 | .00 | .01 | .23 | .91 | .95 | .01 |
| 315 | .00 | .00 | .00 | .00 | .00 | .98 | .00 | .06 | .92 | .04 | .85 | .19 | .86 | .33 | .14 |
| 400 | .00 | .52 | .00 | .00 | .00 | .10 | .00 | .01 | .99 | .71 | .54 | .00 | .54 | .01 | .40 |
| 500 | .00 | .10 | .00 | .00 | .00 | .26 | .02 | .00 | .32 | .01 | .22 | .00 | .47 | .00 | .28 |
| 630 | .02 | .24 | .00 | .00 | .00 | .28 | .00 | .00 | .26 | .00 | .09 | .00 | .31 | .04 | .56 |
| 800 | .05 | .76 | .00 | .00 | .00 | .28 | .04 | .13 | .03 | .00 | .19 | .00 | .41 | .19 | .61 |
| 1000 | .04 | .74 | .00 | .00 | .00 | .12 | .05 | .13 | .00 | .02 | .18 | .00 | .80 | .18 | .70 |

In an attempt to further verify the strong influence of hand-arm posture and its

conjunctions with other contributory factors, independent statistical analyses for the two

considered postures have been performed. The analyses included two levels of excitation

($A$: 2.5 and 5.0 m/s$^2$), three levels of handle diameter ($D$: 30, 40 and 50 mm), three levels

of push force ($F_p$: 25, 50 and 75 N) and three levels of grip force ($F_g$: 10, 30 and 50 N).

The results presented in Table 4.3.clearly show relatively higher significance of the hand

forces for posture $P2$ than those under posture $P1$, which conforms the several trends

observed in the resulted presented in Figure 4.16.

Table 4.3: Results attained from independent statistical analysis for the two postures-significance factor ($p$) of the impedance magnitude in the one-third octave frequency bands for $z_h$-axis under vibration.

| Factors | $A$ | | $D$ | | $F_g$ | | $F_p$ | |
|---|---|---|---|---|---|---|---|---|
| Posture | $P1$ | $P2$ | $P1$ | $P2$ | $P1$ | $P2$ | $P1$ | $P2$ |
| Frequency (Hz) | | | | Significance Level | | | | |
| 8 | .57 | .41 | 00 | .19 | .83 | .19 | .30 | 00 |
| 10 | .06 | .19 | 00 | .05 | .89 | 00 | .69 | 00 |
| 13 | .02 | .14 | .01 | .10 | .14 | 00 | 00 | 00 |
| 16 | .01 | .14 | 00 | .07 | .02 | 00 | .10 | 00 |
| 20 | .05 | .08 | 00 | .12 | .01 | 00 | .18 | 00 |
| 25 | .06 | .08 | 01 | .01 | 00 | 00 | .33 | 00 |
| 32 | 00 | .01 | .06 | 00 | 00 | 00 | 00 | 00 |
| 40 | 00 | .01 | .80 | 00 | 00 | 00 | 00 | 00 |
| 50 | 00 | .02 | .71 | .03 | 00 | 00 | 00 | 00 |
| 63 | .01 | .14 | .45 | .01 | 00 | 00 | 00 | 00 |
| 80 | .01 | .21 | .11 | .07 | 00 | .63 | 00 | 00 |
| 100 | .11 | .87 | .06 | .35 | .01 | .04 | 00 | 00 |
| 125 | .22 | .08 | .01 | .89 | 00 | 00 | 00 | 00 |
| 160 | .05 | .06 | 00 | .05 | 00 | 00 | 00 | 00 |
| 200 | .06 | .07 | 00 | .63 | 00 | 00 | 00 | 00 |
| 250 | .01 | 00 | 00 | .87 | 00 | 00 | 00 | 00 |
| 315 | .01 | .01 | 00 | .08 | 00 | 00 | 00 | 00 |
| 400 | .18 | .11 | 00 | 00 | 00 | 00 | 00 | 00 |
| 500 | .22 | .20 | 00 | 00 | 00 | 00 | 00 | 00 |
| 630 | .79 | .23 | 00 | 00 | 00 | 00 | 00 | 00 |
| 800 | .48 | .20 | 00 | 00 | 00 | 00 | 00 | 00 |
| 1000 | .35 | .83 | 00 | 00 | 00 | 00 | 00 | 00 |

The excitation magnitude is relatively non-significant on the impedance magnitude most of the frequency bands for both postures, except in the bands around the resonance and a few higher frequency bands. The $P1$ posture also suggests higher significance in the lower frequency bands, which also evident in Figure 4.6. For both postures the handle diameter is non-significant in the middle frequency range, under posture $P1$ the handle size shows strong significance in the low frequency bands, this trend is mostly absent for posture $P2$. These results conform the trends observed in Figure 4.15. The Table clearly shows that push force is highly significant in the entire frequency range for posture $P2$, while under posture $P1$ it is not so in the lower frequency bands. Similar trend can also be observed for the grip force. These trends conform the earlier conclusion of stronger coupling between the hand and the handle under posture $P2$ (Figure 4.16).

## 4.4    Characterization of *DPMI* under $x_h$- axis

The measured data are analyzed to derive the mean *DPMI* responses of the hand-arm system exposed to $x_h$-axis vibration, in the 8-1000 Hz frequency range. The results are analyzed to identify important trends in view of the various contributory factors considered and their conjunctions, namely, the handle size (30, 40 and 50 mm), vibration intensity ($a_{h,w}$= 2.5 and $a_{h,w}$= 2.5 m/s$^2$) , hand grip force, ($F_g$; 10, 30 and 50 N) and push force ($F_p$; 0, 25 and 50 N).

## 4.4.1    Inter-subject variability

Figure 4.18 presents comparisons of mean *DPMI* (magnitude and phase) responses of individual subjects attained under $x_h$-axis excitations. The results reveal considerable scatter in the data as it was observed for the $z_h$-axis. The figure shows the responses

corresponding to 30 N grip ($F_g$) and 50 N push ($F_p$) force, and exposed to the $a_{h,w}$= 5 m/s$^2$ excitation level with the three cylindrical handles under $P1$ posture. However, despite the considerable dispersion in the $DPMI$ data obtained for the individuals, both the $DPMI$ magnitude and phase reveal consistent trends in the 8-1000 Hz frequency range. The $x_h$-axis $DPMI$ responses consistently show peak magnitudes in the 125-160 Hz frequency ranges, respectively, for all subjects. This frequency range is in agreement with those reported in a few studies, which have reported the peak $DPMI$ magnitude in the 150-160 Hz range along $x_h$-axis (Burström, 1990; Gurram et al., 1995). A peak in the magnitude response is also observed in vicinity of the 25 Hz band. The range of idealized values of $x_h$-axis $DPMI$ magnitude, reported in ISO-10068 (1998), reveals peak response around 125 Hz.

Figure 4.19 illustrates the coefficients of variations (COV) of the mean $DPMI$ magnitude response, corresponding to center frequencies of the one-third octave bands for the three handles, under posture $P1$, two levels of excitation magnitudes and 30 N grip and 50 N push forces. The variations in the $DPMI$ magnitude are less than 20 % in most of the frequency bands, except at low frequencies, where it increases as the hand forces increases and approaches 27 % in the 8 Hz frequency band. The COV values decline clearly at higher frequencies, irrespective of the handle size and vibration levels. Such variations may be partly attributed to individual's differences in view of the hand-arm structure. The data acquired with the other force combination also revealed similar levels of peak standard errors.
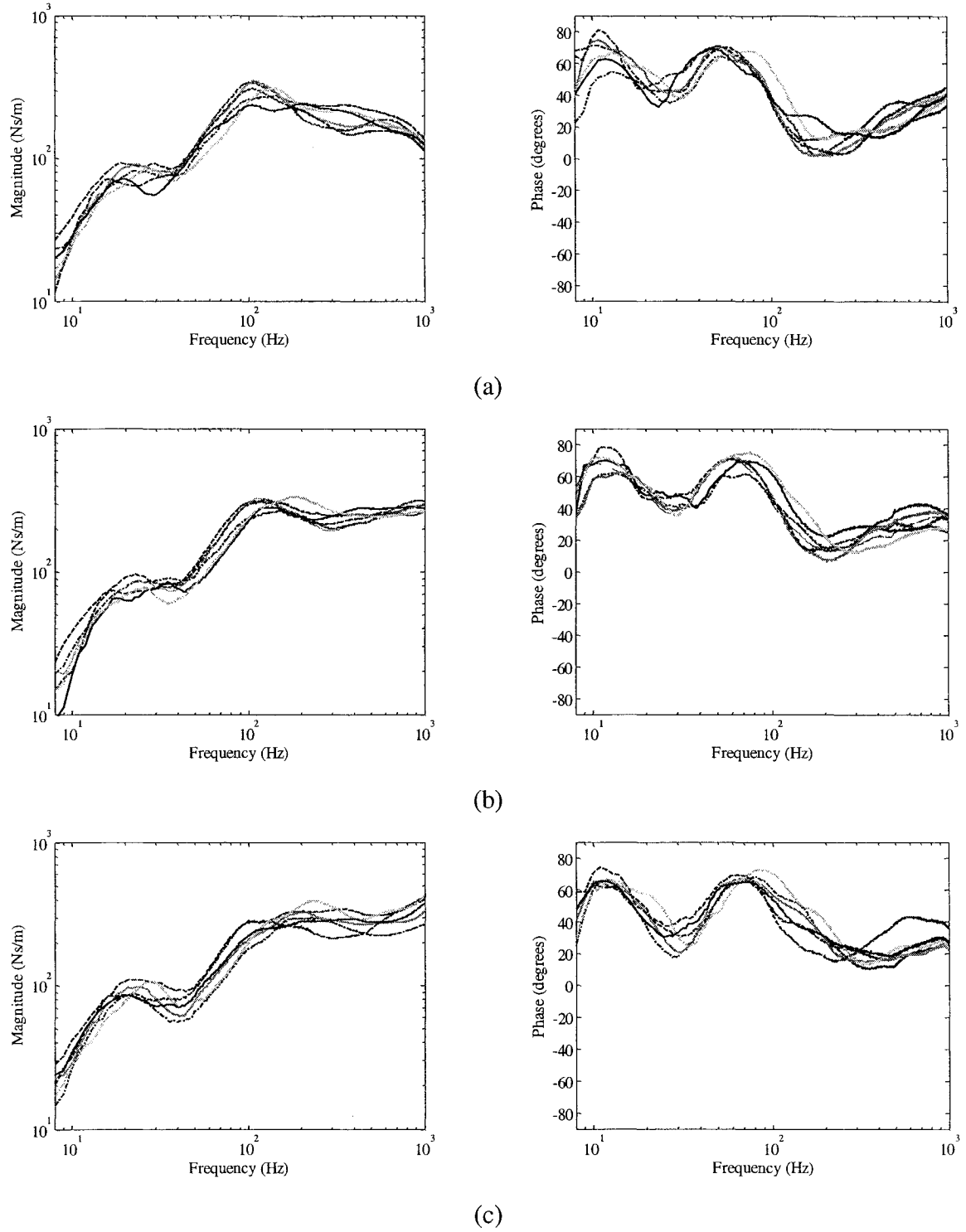
Figure 4.18: Comparisons of mean *DPMI* magnitude and phase responses measured for all subjects under 30 N grip and 50 N push forces, and $a_{h,w} = 5$ m/s² ; (a) *D*= 30 mm, (b) *D*= 40 mm, (c) *D*= 50 mm .

A comparison between the COV values attained for the data under $x_h$-axis vibration (Figure 4.19) with those obtained under $z_h$-axis vibration (Figure 4.2) suggests that the COV values for both vibration axes are comparable. The coefficients of variation of the data under $x_h$-axis vibration, however, are generally slightly lower than those under $z_h$-axis except in the in very low frequency bands while where the COV values of the $x_h$-axis impedance data are higher.
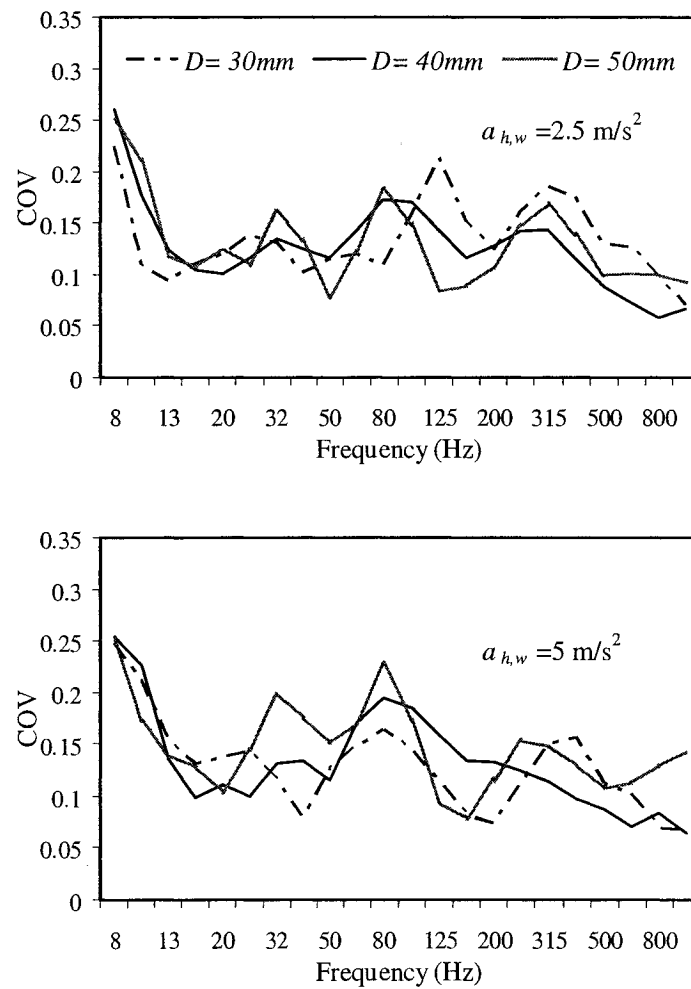


Figure 4.19: Coefficients of variations of the *DPM*1 magnitude responses obtained for over all seven subjects, under two levels of excitation, posture *P1* and 30 N grip and 50 N push forces.

## 4.4.2 Influence of handle size

Variations in the handle size affect the effective hand contact area and thus the contact force, which might influence the biodynamic responses of the hand-arm system, as described in Figure 4.3 for the $z_h$-axis excitation. The effect of handle size on the hand-arm biodynamic response along $x_h$-axis has been reported in a single study, in terms of the mechanical compliance (Reynolds and Falkenberg, 1984). Figure 4.20 illustrates the mean $DPMI$ magnitude and phase responses obtained with three different handles under different $F_g/F_p$ combinations, posture $P1$ and $a_{h,w}$= 2.5 m/s$^2$. The results show that both the $DPMI$ magnitude and phase response of the human hand and arm is strongly influenced by the handle diameter, while the effect on the $DPMI$ magnitude is more pronounced at frequencies above 250 Hz. In general, the larger diameter handles yield higher $DPMI$ magnitude at higher frequencies. An opposite trend, however, is observed in the 63-200 Hz. The 30 mm handle yields slightly higher $DPMI$ magnitude in this frequency range, as evident in Figure 4.20.

The increase in the impedance magnitude in the high frequency range is more remarkable when handle diameter increases from 30 to 40 mm than that when it increases from 40 to 50 mm, suggesting non-linear relationship between impedance response and handle size. In the absence of a push force (Figure 4.20 (a)) the difference between the driving point mechanical impedance magnitudes attained for 40 and 50 mm handles, particularly in the high frequency range, is relatively small. Application of a 25 N push force widens the difference in impedance magnitude between the 40 and 50 mm handles in the high frequency range, while a higher push force level (50 N) does not yield further notable increase in the difference in the magnitude.
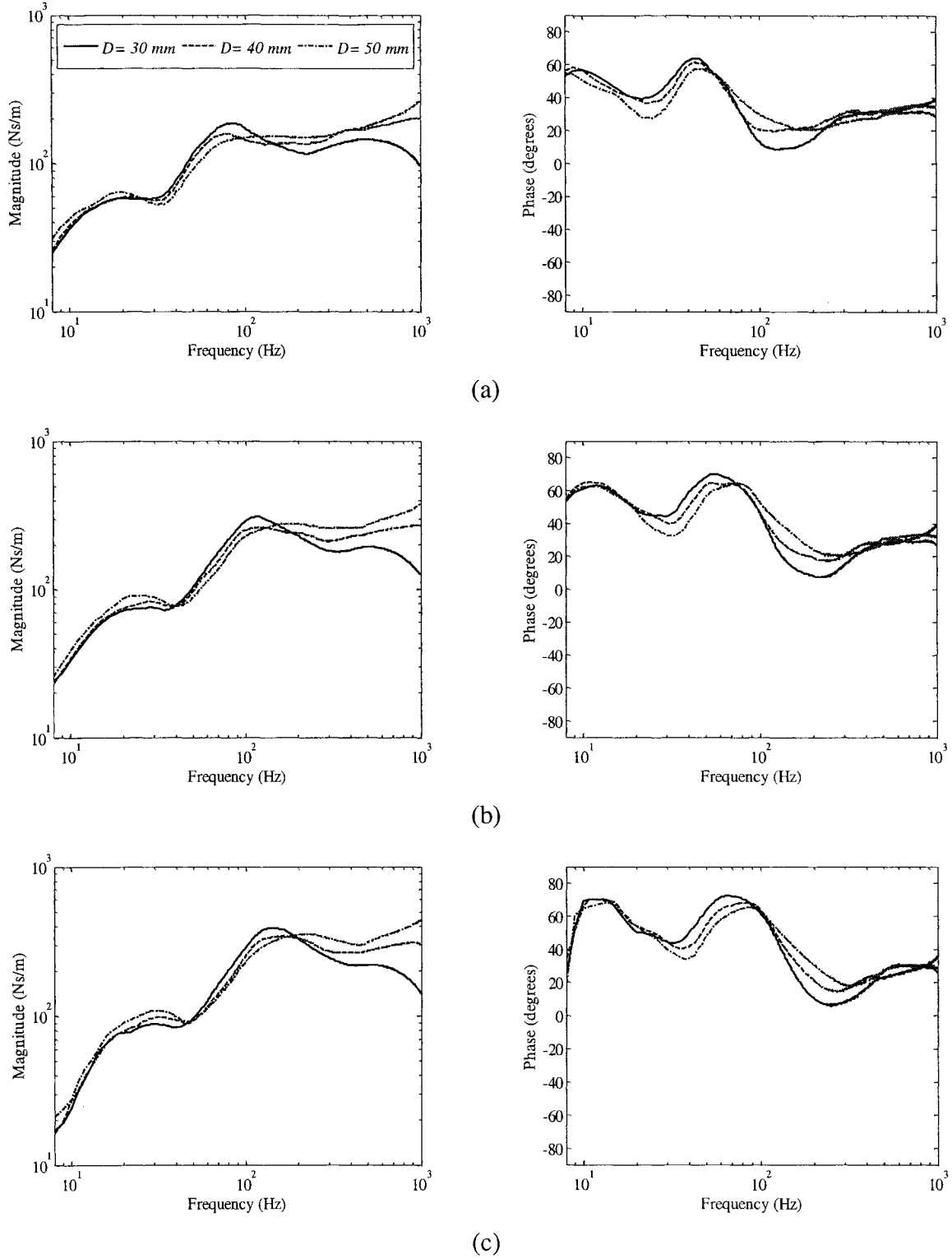
Figure 4.20: Influence of handle size on mean *DPMI* magnitude and phase response under different $F_g/F_p$ combinations ($a_{h,w}$ =2.5 m/s$^2$ and posture *P1*): (a) 10/00; (b) 30/25; and (c) 50/50 N.

### 4.4.3  Influence of vibration magnitude

The effect of vibration magnitude on the driving-point mechanical impedance response of the hand-arm system along the $x_h$–axis has been reported in a few studies leading to somewhat conflicting conclusions as discussed in section 4.2. These studies observed that an increase in the vibration intensity causes either slightly lower or slightly higher or insignificant change in the *DPMI* magnitude. The data acquired under the two different vibration magnitudes ($a_{h,w}$= 2.5 and 5.0 m/s$^2$) are examined to investigate the influence of vibration magnitude on the *DPMI*. Figure 4.21 illustrates the mean *DPMI* magnitude and phase response of seven subjects for the 40 mm handle, posture *P1* with 90° elbow flexion and three different $F_g/F_p$ combinations. The results show relatively small influence of excitation level on the *DPMI* magnitude and phase response, as observed in the reported studies (Burström, 1990; Gurram et al., 1995; Burström, 1997), and for the $z_h$–axis vibration.

An increase in the hand forces further reduced the differences in the *DPMI* magnitudes obtained under different excitation levels. A higher excitation level, however, suggests slightly lower *DPMI* magnitude in the 32-50 Hz and 160-630 Hz frequency ranges, well within the inter-subject variability. The results suggest that the variations in the magnitude of vibration considered in this study yield insignificant effect on the *DPMI* response.
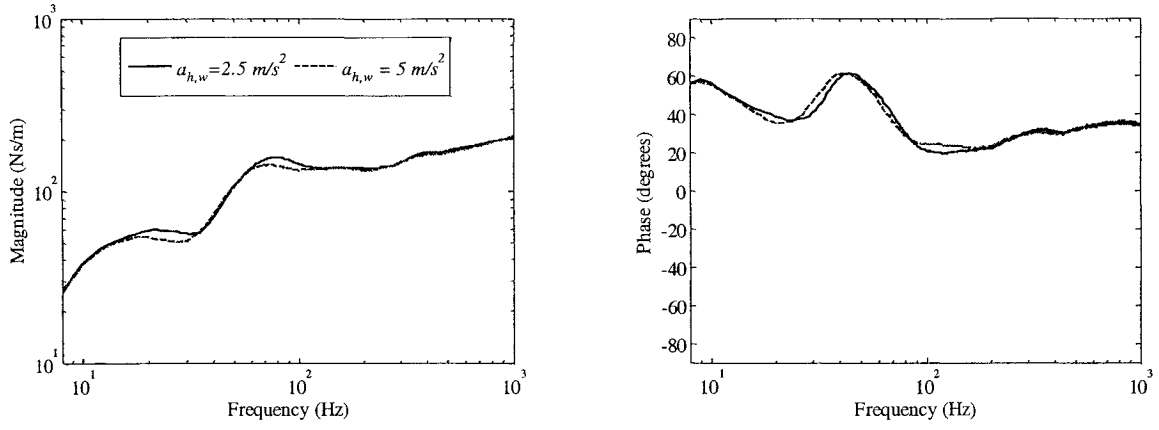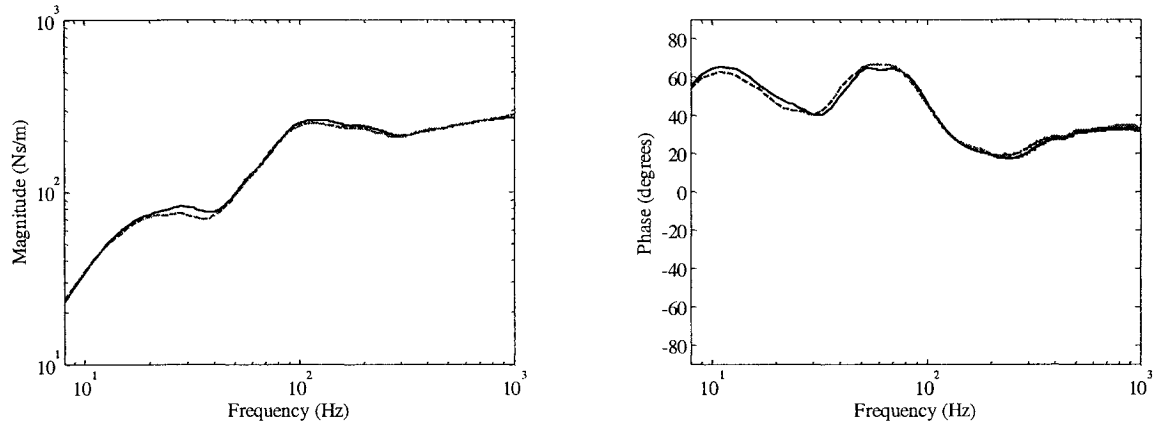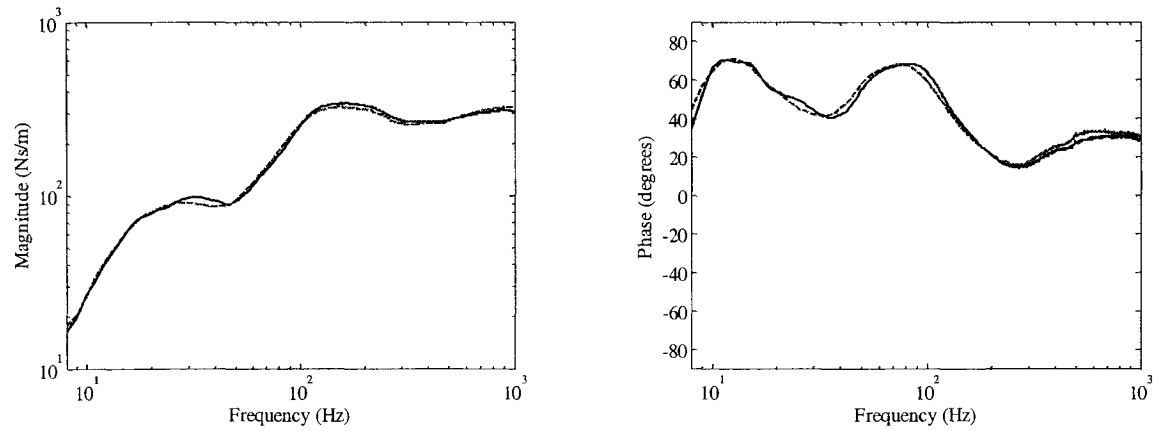
Figure 4.21: Influence of excitation magnitude on the mean *DPMI* magnitude and phase response; under different $F_g/F_p$ combinations: (a) 10/00; (b) 30/25; and (c) 50/50 N. ($D=$ 40 mm and posture *P1*):

4.4.4   Influence of hand-arm posture

Two different hand-arm postures $P1$ and $P2$ involving 90° and 180° elbow flexion, as described in section 2.3.1, were also considered for characterizing the biodynamic responses of the hand-arm system exposed to vibration along the $x_h$–axis. Figure 4.22 shows the mean *DPMI* magnitude and phase responses, while the subjects grasped the 40 mm handle under $a_{h,w}= 5$ m/s² with three different $F_g/F_p$ combinations. The figures compare the responses obtained with the two hand-arm postures, $P1$ and $P2$. Unlike the responses to the $z_h$–axis vibration, the results show negligible effect of the posture on both *DPMI* magnitude and phase response at frequencies above 32 Hz under all hand force combinations presented in the figures. The stretched forearm posture $P2$ yields only slightly higher *DPMI* magnitude in the bands centered below 16 Hz, in a manner similar to that observed in the responses to vibration along the $z_h$–axis. The influence of hand-arm posture on the magnitude response to vibration along the $z_h$-axis, however, was more evident up to 100 Hz.

The posture $P2$ particularly causes enhanced static coupling between the hand and the handle, which could be observed from its high apparent mass response at very low frequencies as shown in Figure 4.23. The apparent mass under posture $P2$ is almost three times of that under posture $P1$ near the 8 Hz band. The higher apparent mass magnitude under the extended arm suggests strong coupling between the hand and the handle. However, it may be concluded that the hand-arm posture has little effect on the $x_h$–axis biodynamic response, except at extremely low frequencies, when compared to that observed for the $z_h$–axis.
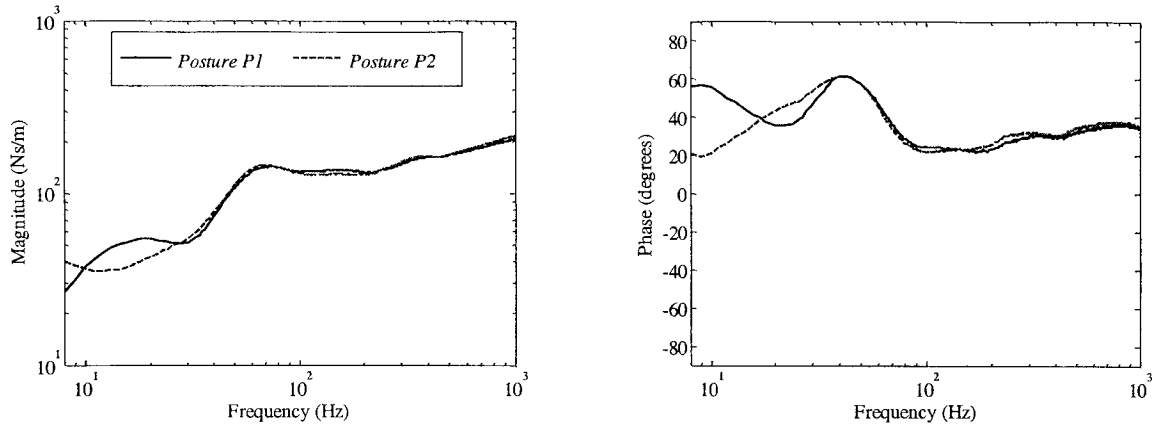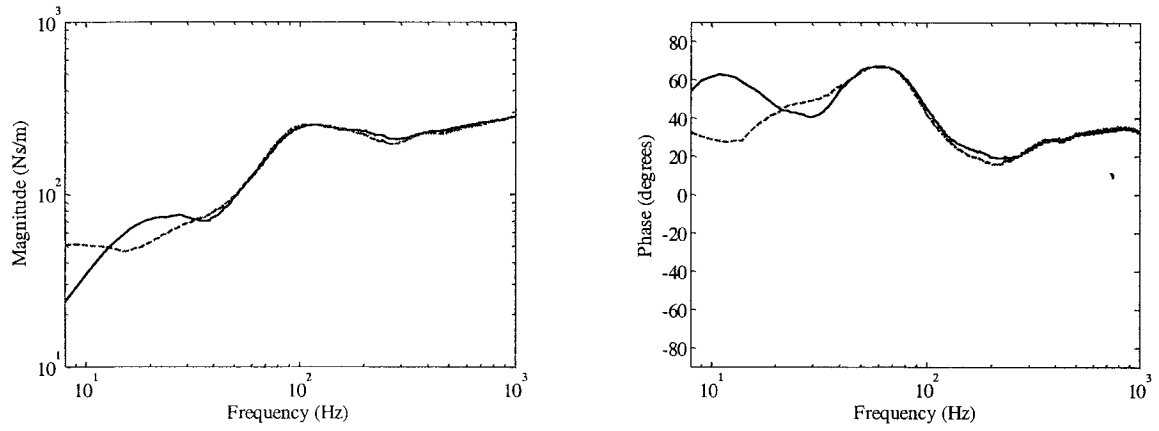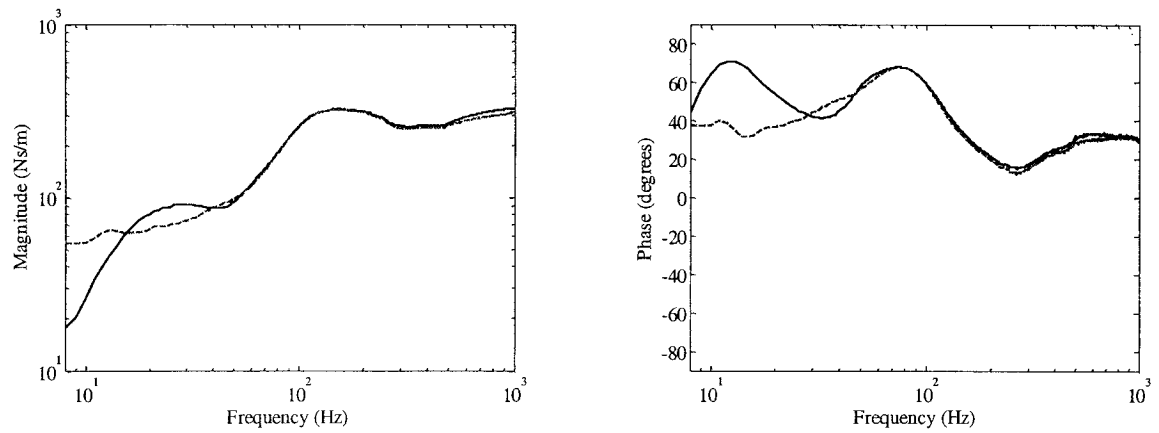
Figure 4.22: Influence of hand-arm posture on the mean *DPMI* magnitude and phase response under different $F_g/F_p$ combinations: (a) 10/00; (b) 30/25; and (c) 50/50 N ($D= 40$ mm and $a_{h,w} = 5$ m/s$^2$).
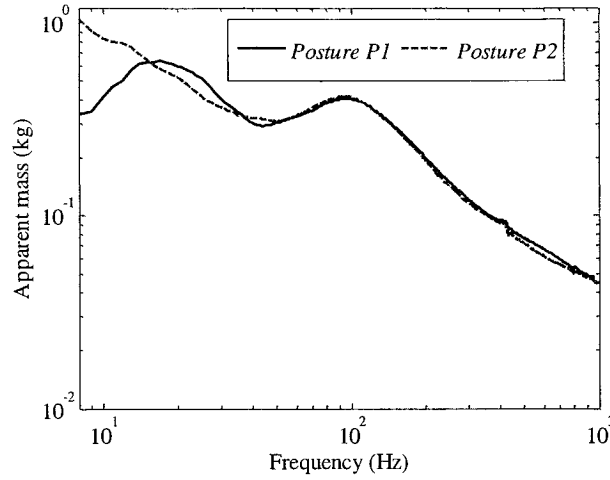
Figure 4.23: Comparison of mean *APMS* magnitude response under the two hand-arm postures, *P1* and *P2* ($D$= 40 mm, $F_g$= 30 N, $F_p$= 50 N and $a_{h,w}$ = 5 m/s$^2$).

The considerable differences observed in the two-axes could be attributed to the direction of the push force applied to the handle. It should be noted that under $z_h$–axis vibration, both the push and grip forces are applied along the same direction of vibration, while under $x_h$–axis vibration, the push force alone is applied along the direction of motion, as shown in Figure 4.24.



(a)                                   (b)
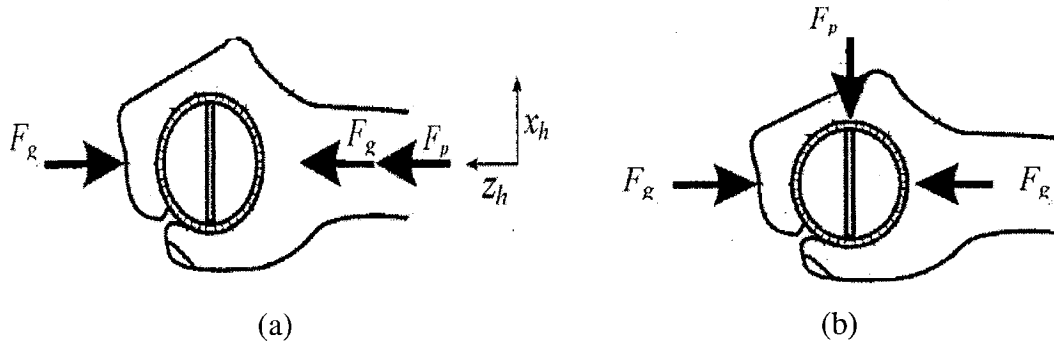
Figure 4.24: Comparisons of the manner of application of grip and push forces: (a) along $z_h$-axis; and (b) along $x_h$-axis.

171

### 4.4.5 Influence of hand forces

Higher magnitudes of hand forces imparted on a tool handle are known to affect the biodynamic responses of the hand-arm system, which may be attributed to higher coupling force response at the driving-point. The mean *DPMI* magnitude responses attained under vibration level ($a_{h,w}$ = 5 m/s$^2$), and nine different combinations of $F_g$ (10, 30 and 50 N) and $F_p$ (0, 50 and 75 N) forces for the two postures *P1* and *P2*, are illustrated in Figure 4.25. The results presented for the 40 mm handle, generally suggest that an increase in the hand forces tends to increase the *DPMI* magnitude. Higher hand forces also cause a shift in the peak magnitude to higher frequencies suggesting stiffer hand-arm system with increasing of either grip and/or push forces.

The influence of variation in the push and grip forces on the impedance magnitude response of the hand-arm system exposed to excitation level $a_{h,w}$ = 5 m/s$^2$ along the $x_h$-axis, while grasping the 40 mm handle and employing both considered postures *P1* and *P2*, are shown in Figure 4.26 and Figure 4.27, respectively. The figures also illustrate the mean, and lower and upper bounds of the idealized values of *DPMI* magnitude and phase, as defined in ISO-10068 (1998). Comparisons suggest that the mean magnitude responses, under moderate hand forces, lie within the lower and upper bounds defined in the standard. Under higher levels of hand forces (e.g., $F_g$= 50 N and $F_p$= 50 N), the *DPMI* magnitude exceeds the upper bound in the 160-250 Hz frequency range, which corresponds to the peak magnitude.
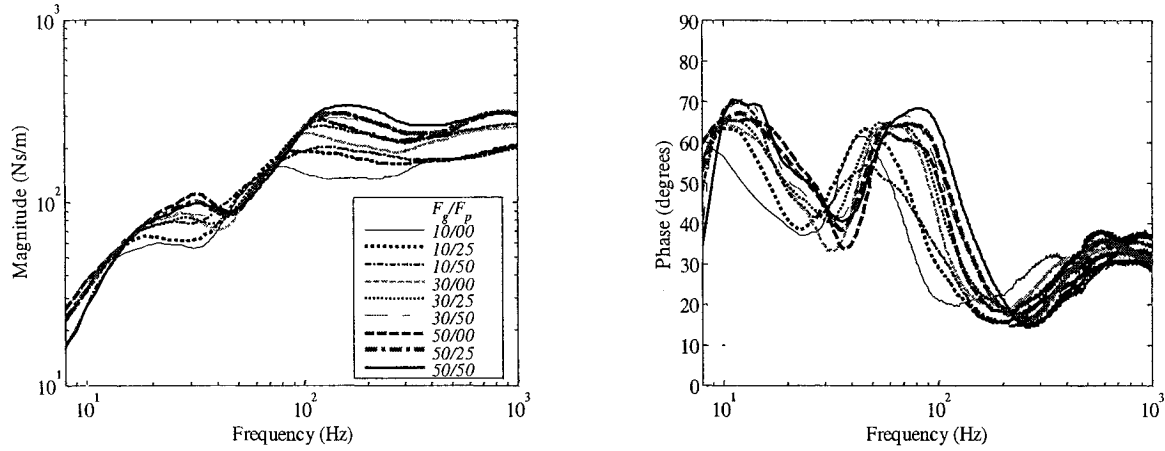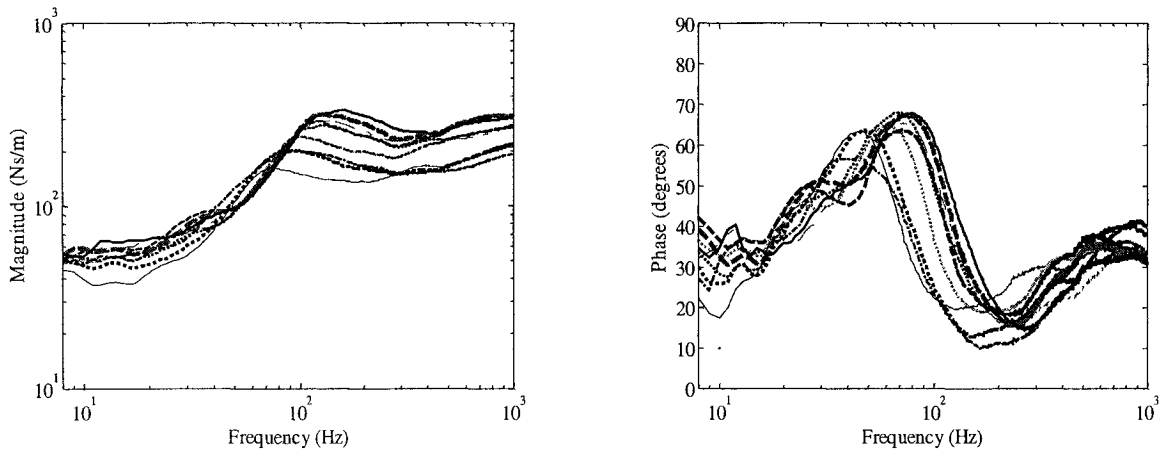
Figure 4.25: Effect of the different grip-push force combinations on the *DPMI* magnitude: (a) posture *P1*; and (b) posture *P2* ($D$= 40 mm, $a_{h,w}$ = 2.5 m/s$^2$).

The mean phase responses generally lie within the recommended bounds, with the exception of the 80-125 Hz frequency range. An increase in the push or the grip force tends to shift the *DPMI* magnitude towards a higher frequency, while the influence of hand forces, particularly the push force, in the low frequency region (lower than 100 Hz), is small. An increase in the push force yields slightly lower *DPMI* magnitude in the low frequency range, which could be partly attributed to high inter subject variability. The

increase in *DPMI* magnitude and phase angle in the 100-500 Hz frequency range with the

increase in push force is evident for both postures as it is shown in Figure 4.26.



(a)



(b)
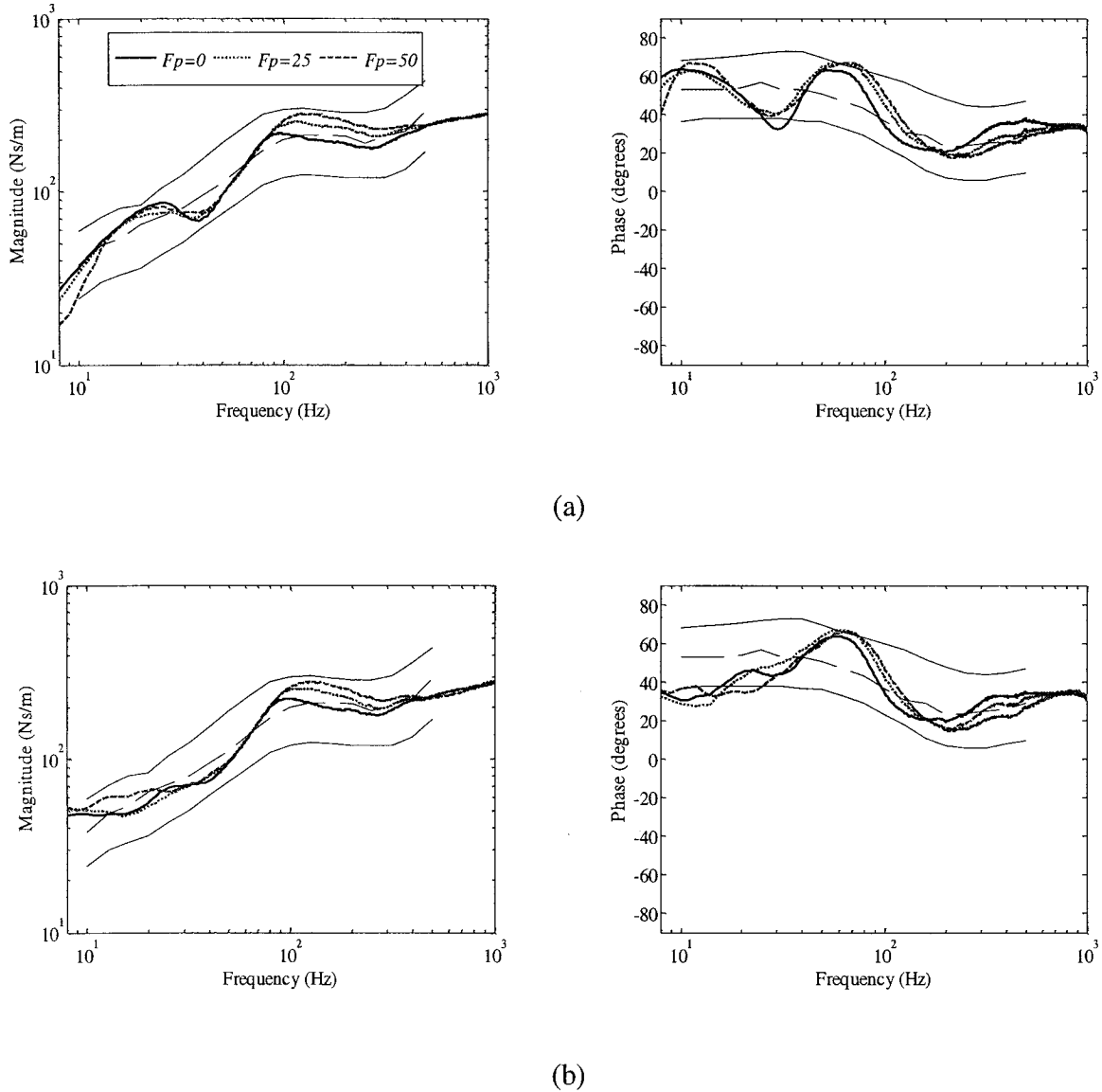
Figure 4.26: Effect of variations in the push force on the mean impedance magnitude and
phase responses ($D$= 40 mm, $F_g$ = 30 N and $a_{h,w}$ = 5 m/s$^2$).; (a) posture *P1*; and (b)
posture *P2*

Higher grip force yields notable increase in the *DPMI* magnitude in the frequency

range above 80 Hz under both hand-arm postures *P1* and *P2*, as shown in Figure 4.27. In

low frequency range, the hand-arm biodynamic responses under two postures reveal

some disparities in trends with regard to grip force variations. While the *DPMI* magnitude is not greatly influenced by varying the grip force levels under posture *P1*, an increase in the *DPMI* magnitude could be observed under posture *P2*.



(a)

(b)
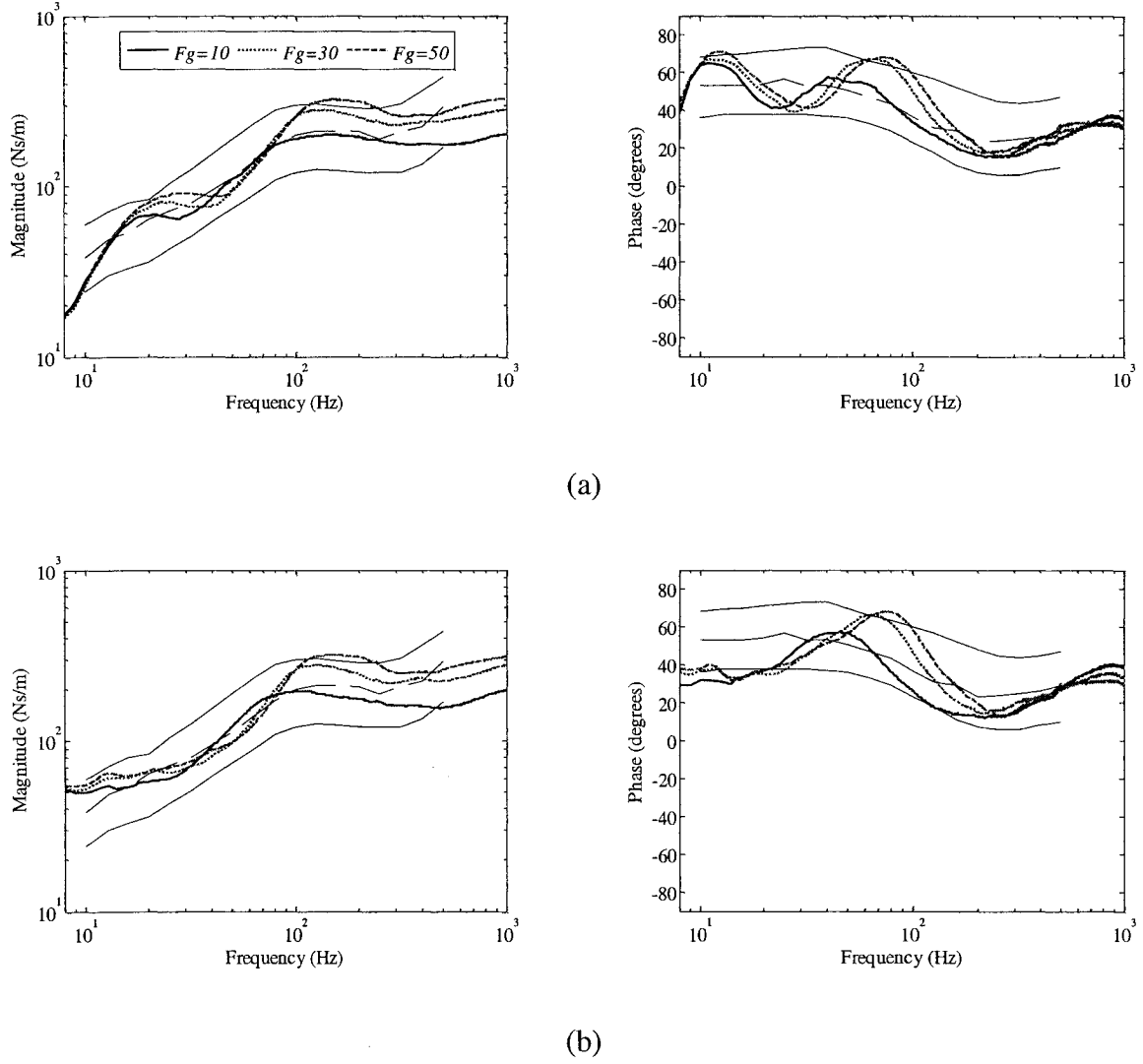
Figure 4.27: Effect of variations in the grip force on the mean impedance magnitude and phase responses ($D$= 40 mm, $F_p$ = 50 N and $a_{h,w}$ = 5 m/s$^2$): (a) posture *P1*; and (b) posture *P2*

175

4.4.6   Statistical analysis ($x_h$-axis *DPMI* magnitude)

The statistical significance of different parameters on the mean *DPMI* magnitude response to $x_h$-axis vibration, of seven subjects was evaluated through multifactor within subject ANOVA. The factors included excitation levels ($A$) with two levels (low and high spectra), hand-arm posture ($P$) with two positions (posture *P1* and posture *P2*), handle diameter with three levels (30, 40 and 50 mm), grip force ($F_g$) with three levels (10, 30 and 50 N) and push force ($F_p$) with also three levels (0, 50 and 50 N). Repeated measures or within-groups ANOVA design is used since there is one group of subjects exposed randomly to different conditions. The conditions are the categories of the independent variables, which is the repeated measures factor.

Table 4.4 presents the results of the statistical analysis on the mean *DPMI* magnitude response along the $x_h$-axis. The Table summarizes the significance analysis of the main factors and the two-way interactions between the factors at the center frequencies of the one-third octave bands. The hand-arm posture shows strong significance in view of the *DPMI* magnitude in the low frequency bands (lower than 25 Hz) as it was observed for the $z_h$-axis response. The influence can also be observed in Figure 4.22. The excitation level demonstrates statistical significance on the *DPMI*, only in the mid-frequency bands (100-250 Hz), where the second magnitude peak occurs. Handle size reveals significant effect on the impedance magnitude in the entire frequency range, except in the 32 Hz band. This result is consistent with the trends observed seen in Figure 4.20. The hand grip force suggests most significant influence in nearly all the frequency bands except for the 80 Hz band. The push force, however shows somewhat different trends, suggesting non-

Table 4.4: Statistical significance factor ($p$) of various contributory factors in view of the *DPMI* magnitude over one-third octave frequency bands under $x_h$-axis vibration.

| Frequency (Hz) | P | A | D | Fg | Fp | P*A | P*D | P*Fg | P*Fp | A*D | A*Fg | Fg*A | D*Fg | D*Fp | Fp*Fg |
|---|---|---|---|---|---|---|---|---|---|---|---|---|---|---|---|
| | Significance Level ($p$) | | | | | | | | | | | | | | |
| 8 | 00 | .42 | 00 | 00 | .44 | .02 | .18 | 00 | 00 | .11 | .92 | .01 | .84 | 00 | .15 |
| 10 | 00 | .56 | 00 | 00 | 00 | .03 | .17 | 00 | 00 | .03 | .14 | .14 | .58 | 00 | 00 |
| 13 | .09 | .51 | 00 | 00 | 00 | .15 | .24 | 00 | 00 | .12 | .02 | .22 | .58 | 00 | 00 |
| 16 | 00 | .07 | 00 | 00 | 00 | .01 | .60 | 00 | .01 | .08 | .28 | .93 | .41 | .04 | 00 |
| 20 | 00 | .17 | 00 | 00 | 00 | .31 | .16 | .01 | 00 | .29 | .01 | .69 | .24 | .01 | 00 |
| 25 | 00 | .09 | .01 | 00 | .01 | .19 | .19 | 00 | .72 | .50 | 00 | .55 | 00 | 00 | 00 |
| 32 | 00 | .02 | .51 | 00 | .01 | .15 | .31 | 00 | .66 | .31 | .05 | .41 | 00 | 00 | 00 |
| 40 | .05 | .44 | .04 | .01 | 00 | .36 | .84 | .46 | .54 | .15 | .01 | .72 | 00 | .83 | 00 |
| 50 | .05 | .11 | 00 | 00 | 00 | .30 | .68 | .44 | .45 | .75 | .36 | .58 | 00 | .37 | .06 |
| 63 | .27 | .25 | 00 | 00 | .27 | .47 | .94 | 00 | .69 | .55 | .06 | .44 | .02 | .24 | .17 |
| 80 | .11 | .56 | 00 | .10 | .03 | .51 | .87 | .01 | .55 | .13 | 00 | .07 | .06 | .80 | 00 |
| 100 | .24 | .03 | 00 | 00 | 00 | .38 | .93 | .55 | .21 | .34 | .07 | 00 | 00 | .56 | 00 |
| 125 | .43 | 00 | 00 | 00 | 00 | .31 | .68 | .29 | .28 | .30 | .57 | .85 | 00 | .18 | 00 |
| 160 | .57 | 00 | .04 | 00 | 00 | .73 | .76 | .01 | .61 | .49 | .03 | .89 | 00 | 00 | .08 |
| 200 | .18 | 00 | 00 | 00 | 00 | .70 | .67 | .02 | .06 | .69 | .02 | .91 | 00 | 00 | 00 |
| 250 | .10 | 00 | 00 | 00 | 00 | .56 | .54 | .03 | .01 | .51 | .09 | .78 | .01 | 00 | 00 |
| 315 | .10 | .10 | 00 | 00 | 00 | .26 | .56 | .07 | 00 | .38 | .97 | .75 | 00 | 00 | 00 |
| 400 | .15 | .35 | 00 | 00 | 00 | .22 | .56 | .03 | 00 | .20 | .45 | .55 | 00 | 00 | 00 |
| 500 | .07 | .34 | 00 | 00 | .04 | .40 | .67 | .22 | 00 | .32 | .54 | .96 | .02 | 00 | 00 |
| 630 | .02 | .44 | 00 | 00 | .43 | .59 | .62 | .52 | 00 | .56 | .87 | .69 | 00 | 00 | .09 |
| 800 | 00 | .59 | 00 | 00 | .21 | .51 | .35 | .15 | .01 | .46 | .97 | .76 | 00 | 00 | .35 |
| 1000 | .23 | .42 | 00 | 00 | .07 | .27 | .45 | .56 | .02 | .14 | .44 | .76 | 00 | 00 | .02 |

177

significant effect in the bands higher than 500 Hz, and in the 8 and 63 Hz bands. That could be attributed to the definition of the push force along $x_h$-axis, as seen in Figure 4.24. As for the $x_h$-axis impedance data, the hand-arm posture shows significant interactions with the hand force in the lower frequency bands. A stronger interaction withthe push force is evident in the frequency bands above 250 Hz. The hand forces further show strong interaction between each other in most of the frequency bands. Handle size shows weak interaction with the hand-arm posture and the vibration magnitude, while it shows strong interaction with hand forces, particularly in the high frequency band.

The multi-factor ANOVA has been repeated for the two different postures $P1$ and $P2$ independently, as described in section 4.3.6 for the $z_h$-axis impedance response. Contrary to the results obtained for the two postures under the $z_h$-axis vibration, the results attained for $x_h$-axis data do not show large differences due to the hand-arm posture, as can be seen in Table 4.5. The similar trends for both vibration axes, is in the association of the hand-arm posture with the hand forces, although only few low frequency bands under posture $P1$ show statistical insignificance on the $DPMI$ magnitude, both hand forces show strong statistical significance at all frequency bands under posture $P2$ reveals, which confirms the stronger hand-handle coupling under this posture comparing to that under posture $P1$. However, the influence of hand-arm posture along the $z_h$-axis is far more evident than that along the $x_h$-axis, as can be observed from results from the ANOVA analysis, and Figure 4.13 and Figure 4.22.

Table 4.5: Results attained from independent statistical analysis for the two postures-significance factor ($p$) of the impedance magnitude in the one-third octave frequency bands for $x_h$-axis under vibration.

| Factors | A | | D | | $F_g$ | | $F_p$ | |
|---|---|---|---|---|---|---|---|---|
| Posture | P1 | P2 | P1 | P2 | P1 | P2 | P1 | P2 |
| Frequency (Hz) | Significance Level | | | | | | | |
| 8 | 00 | .07 | 00 | 00 | .80 | 00 | .06 | 00 |
| 10 | .01 | .22 | 00 | 00 | .03 | 00 | 00 | 00 |
| 13 | .10 | .46 | 00 | 00 | 00 | 00 | 00 | 00 |
| 16 | .80 | .01 | 00 | 00 | 00 | 00 | .09 | 00 |
| 20 | .16 | .90 | 00 | 00 | 00 | 00 | .05 | 00 |
| 25 | .11 | .73 | .02 | .04 | 00 | 00 | .01 | .03 |
| 32 | .06 | .17 | .35 | .94 | 00 | 00 | .04 | .08 |
| 40 | .39 | .72 | .19 | .02 | .01 | .02 | .01 | 00 |
| 50 | .73 | 00 | 00 | 00 | 00 | 00 | 00 | .03 |
| 63 | .86 | .02 | 00 | 00 | .01 | 00 | .05 | .63 |
| 80 | .50 | .76 | 00 | 00 | .05 | .16 | 00 | .14 |
| 100 | .03 | .08 | 00 | 00 | 00 | 00 | 00 | 00 |
| 125 | 00 | .02 | 00 | .02 | 00 | 00 | 00 | 00 |
| 160 | .01 | 00 | .11 | .12 | 00 | 00 | 00 | 00 |
| 200 | .03 | .01 | 00 | 00 | 00 | 00 | 00 | 00 |
| 250 | .06 | .04 | 00 | 00 | 00 | 00 | 00 | 00 |
| 315 | .02 | .26 | 00 | 00 | 00 | 00 | 00 | 00 |
| 400 | .12 | .84 | 00 | 00 | 00 | 00 | 00 | .08 |
| 500 | .26 | .97 | 00 | 00 | 00 | 00 | 00 | .58 |
| 630 | .47 | .70 | 00 | 00 | 00 | 00 | .09 | .29 |
| 800 | .51 | .85 | 00 | 00 | 00 | 00 | .11 | .15 |
| 1000 | .80 | .13 | 00 | 00 | 00 | 00 | 00 | .23 |

## 4.5 Summary and Conclusions

The *DPMI* response of the hand-arm system to $z_h$-axis was found to vary considerably with variations in the grip and push force combinations, handle size and the hand-arm posture. An increase in either the grip or the push force resulted in higher peak magnitude of *DPMI* and the corresponding frequency, suggesting the stiffening of the hand-arm system. The increase in *DPMI* magnitude with increase in grip and push forces

was found to be better correlated with the coupling force, defined as the direct sum of both grip and push forces, at frequencies below 200 Hz. At frequencies above 200 Hz, a better correlation was obtained with the contact force for all three handles. These results suggest nearly equal importance of the grip and push force at frequencies below 200 Hz, and mechanical coupling of the entire hand structure with the handle. At frequencies above 200 Hz, the biodynamic response of the hand-arm system is more strongly influenced by the grip force, which may be attributed to the skin tissue, and the higher contact area of the skin tissue and the handle.

The handle size was found to have a considerable influence on the *DPMI* response along the $z_h$-axis, particularly near the frequency of peak magnitude and at frequencies above 100 Hz, where the effect was observed to be quite considerable. Important influence was also observed on the phase response. The fact that the handle size has a clear effect on the biodynamic response of the hand-arm system suggests that it should be reported among the other extrinsic factors when reporting *DPMI* data.

The biodynamic response of the human hand-arm system exposed to vibration along the $z_h$-axis is strongly influenced by the hand-arm posture. A posture with extended forearm (180° elbow flexion- posture *P2*) yields relatively stronger coupling with the vibrating handle at low frequencies. The low frequency apparent mass magnitude of the hand-arm under this posture is approximately three times than that measured with the bent forearm posture (90° elbow flexion- posture *P1*). The mechanical impedance magnitude of the extended hand-arm (posture *P2*) is significantly higher than that of the bent elbow posture *P1* at lower frequencies (below 30 Hz). At very low frequencies, the posture *P2* exhibits damper-like behavior. The primary resonant frequency, as identified

from the peak *DPMI* magnitude, of the hand-arm system with posture *P2* is considerably lower than that with the posture *P1*, which may be attributed to the higher effective mass under posture *P2*.

The variations in the push and grip forces imparted on the hand reveal remarkable differences in the low frequency impedance magnitude responses under two postures. While the influence of variations in the push and grip forces on the impedance magnitude at low frequencies is not obvious under *P1* posture, the *P2* posture clearly shows higher magnitude response with the increase in either push or grip forces, suggesting stronger coupling between the hand-arm and the handle under this posture. Both the postures, however, resulted in higher peak magnitude of *DPMI* and the corresponding frequency, under higher grip and push forces, suggesting the stiffening of the hand-arm system. The variations in the handle sizes also revealed some differences in the biodynamic responses attained for the two postures. Larger handle size causes higher *DPMI* magnitude at frequencies less than the primary resonant frequency under *P1* posture, but lower magnitude at frequencies below 100 Hz under posture *P2*.

The *DPMI* magnitude response of the hand-arm system to $x_h$-axis vibration revealed peaks in the vicinity of 25 Hz and 150 Hz bands. Increasing the excitation level does not affect the *DPMI* response, suggesting linear response in view of the excitation magnitude. Increasing the hand grip or push forces, generally causes higher frequency corresponding to the peak *DPMI*, suggesting the stiffening of the hand-arm system with the increasing of hand forces. An increase in the hand forces, in general, yields larger *DPMI* magnitude, specifically at frequencies above 100 Hz. The handle size revealed an influence on the *DPMI* magnitude under $x_h$-axis vibration, particularly near the frequencies of peak

181

magnitudes and at frequencies above 250 Hz, where the effect was observed to be quite considerable. The larger handle caused notably higher *DPMI* magnitude at higher frequencies. The variations in the hand-arm posture did not alter the trends in the *DPMI* magnitude, as the observed for $z_h$-axis response.

# CHAPTER 5

## POWER ABSORPTION OF HUMAN HAND-ARM SYSTEM

## EXPOSED TO VIBRATION

### 5.1    Introduction

The most widely reported and serious among the diseases caused by prolonged
vibration exposure could be the vibration white finger (VWF) disease. However, the
pathologic and physiologic mechanisms of VWF are not well understood. The vibration
exposures required to cause VWF are not known precisely, neither with respect to
vibration magnitude and frequency spectrum, nor with respect to daily and cumulative
exposures, as noted in the updated international standard for measurement, evaluation
and assessment of hand-transmitted vibration (ISO-5349-1, 2001). Consequently, it is
unknown precisely which vibration characteristics may be responsible for VWF, and
what the best measure of the vibration is for the exposure assessment (Griffin, 1990). For
many practical reasons, such as technical availability and reliability and convenience of
the measurement, the majority of the studies and all current national and international
standards regarding hand-transmitted vibration use tool handle acceleration spectrum as a
measure to quantify the severity of vibration and to assess the risk of the exposure (Dong
et al., 2004). Measurement and risk assessment of hand-transmitted vibration is mostly
based on the guidelines and dose-response relationship provided in the ISO 5349-1
(2001) standard. However, the standard, which is based on the frequency-weighted rms
acceleration at the tool handle, has been subjected to many criticisms regarding the
frequency-weighting function, daily and lifetime exposures, as well as for the lack of
consideration of other significant factors, such as coupling forces (Burström, 1990; Dong

et al., 2001) While some studies have suggested that the dose-effect relationship overestimates the potential health risks (Louda et al., 1994; Walker et al., 1986) others have shown that it underestimates the risk of the prevalence of HAVS (Pelmear et al., 1990; Nelson and Griffin, 1993).

An epidemiological study has shown that the prevalence of vibration induced white finger could be related to the amount of energy absorbed by the operators (Lidström, 1977). An investigation conducted by Reynolds and Angevine (1977) suggested the existence of a positive correlation between the subjective annoyance and discomfort data with the power absorption in the human hand-arm system exposed to vibration. Within related context, a reasonably good correlation between the power absorbed by the human body exposed to whole-body vibration and the subjective sensation of discomfort has also been reported (Pradko et al., 1965). On the other hand, it has been suggested that the absorbed power by the human hand-arm system could serve as a better measure of the exposure and the associated risk than the frequency-weighted acceleration as recommended in ISO 5349-1 (2001) for the risk assessment of hand-transmitted vibration (Burström, 1990; Cundiff, 1976). From a physical point of view, the power generated in the hand-arm system can be of two forms: reactive and active. The reactive power, attributed to the potential and kinetic energies stored in the elastic tissues of the hand-arm system, do not contribute directly to the net flow of energy between the handle and the hand-arm system and thus there is no energy dissipation. On the other hand, the active component of the power is directly related to the net flow of energy from the handle to the hand. This form of energy is dissipated through the viscous elements of the hand-arm system, where it is converted into work and heat, and may thus be considered as a better

measure of the risk imposed on the hand-arm tissues (Reynolds, 1977; Reynolds and Keith, 1977).

5.2  Review of Experimental Studies

Although the notion of absorbed power for assessing the effects of hand-transmitted has been proposed for more than 30 years, the role of many contributory factors has not been systematically identified. The biodynamic response expressed in terms of absorbed power, is known to depend upon many intrinsic and extrinsic variables, such as the frequency, magnitude and direction of vibration, the hand-handle coupling forces, handle size, hand-arm posture and individual characteristics. Although the reported studies have attempted to quantify the influences of one or more of these factors under comparable test conditions, the results could be generally limited to trends only, which are mostly diverse and in part contradictory, even though the majority of these studies are conducted by the same research group (Burström, 1990; Burström and Lundström, 1988; Burström, 1994; Burström and Lundström, 1994; Burström and Lundström, 1989; Sörensson and Burström, 1996; Sörensson and Burström, 1997; Sörensson, 1998; Bylund and Burström, 2003) . The differences in the reported absorbed power data could be observed not only in the magnitudes, but also in relation to intrinsic and extrinsic factors.

Burström and Lundström (1988) investigated the power absorbed by the human hand-arm system exposed to sinusoidal vibration for three different postures along the $x_h$ and $z_h$ axes. While no significant differences were observed in the absorbed power magnitudes under $x_h$ and $z_h$ axes vibration, an increase in power absorption with respect to frequency could be generally observed up to 1500 Hz. Another study, conducted by the same authors, suggested that vibration along different axes ($x_h$, $y_h$ or $z_h$) yields differences

in power absorbed within the hand and arm, while an increase in the grip force leads to a linear increase in the absorbed power (Burström and Lundström, 1989). On the basis of measurements performed under exposure to vibration spectra of five different tools, it was further concluded that the vibration direction has a great influence on the absorbed power, which also increases rapidly with an increase in vibration magnitude (Burström, 1990). The magnitudes of absorbed power varied from 0.4 to 1.5 W under selected vibration spectra with frequency-weighted rms acceleration ranging from 3.1 to 9.3 m/s$^2$. In another study, laboratory measurements performed under constant velocity spectra of different magnitudes of weighted acceleration in the 3 – 12 m/s$^2$ range, resulted in peak absorbed power in all vibration directions in the order of 0.5 W (Burström, 1994). Sörensson (1998) measured the absorbed power under excitations representing four different tools (chipping hammer, impact drill, breaker and impact wrench), with weighted rms accelerations of 3 and 6 m/s$^2$, and reported that the magnitude of absorbed power lies in the 0.03- 0.2 W range, while the effects of the grip and push forces were observed to be insignificant. Even lower levels of peak absorbed power by the hand and arm, in the order of 0.002 W, have been reported in a recent study (Bylund and Burström, 2003). This study involved measurements with 24 subjects exposed to constant-velocity random vibration spectra of two different magnitudes (3 and 6 m/s$^2$) along the $x_h$ and $z_h$ directions. These magnitudes of absorbed power were found to be considerably lower than those reported in earlier studies under comparable excitations (Burström and Lundström, 1988; Burström, 1994). The results of this study further showed negligible absorbed power under higher frequency vibration, above 630 Hz.

A few studies have concluded that the contact force between the hand and a tool handle affects the severity of exposure to the hand-transmitted vibration and causes hand-wrist cumulative trauma disorders (Pyykkö et al., 1976; Radwin, 1987). This is further supported by the results presented in chapter four, in terms of *DPMI* response of the hand-arm system, since both *DPMI* and absorbed power derive from the driving-point force and velocity. Only a few attempts, however, have been made to quantify the contribution due to hand force on the absorbed power. Considering that the hand-handle contact force depends upon the effective contact area of the hand-handle interface, the amount of absorbed power may be expected to be influenced by the handle size. The influence of handle size in mechanical absorbed power by the hand-arm system exposed to vibration has not yet been investigated.

Unlike the *DPMI*, which is almost independent of the vibration magnitude, significantly higher magnitudes of absorbed power are obtained under higher vibration magnitudes. Owing to the wide variations in conditions of vibration exposure and the contributory factors, the human hand-arm biodynamic response is known to be quite complex. This complexity of the biodynamic response together with the lack of essential data forms the essential motivation for deriving additional data in order to further enhance the understanding of power absorption into the hand-arm system.

5.3    Characterization of Power Absorption under $z_h$- axis

The power absorption characteristics of the human hand-arm system are derived from the measured data and discussed in view of inter-subject variability and various contributory factors. The measured data are analyzed to derive the mean absorbed power characteristics of the hand-arm system exposed to $z_h$-axis vibration, corresponding to

center frequency of each of the one-third octave bands in the 8-1000 Hz frequency range. The total absorbed power was then computed through summation of power values within each of the one-third octave bands. The results are analyzed to identify important trends in view of the various factors considered, namely, the handle size, vibration intensity, hand-arm posture, hand grip and push forces, and contact and coupling forces.

### 5.3.1 Inter-subject variability

Figure 5.1 presents comparisons of absorbed power spectra attained for the three cylindrical handles and all seven participants subject to $a_{h,w}$ = 2.5 m/s$^2$ vibration excitation, under posture $P1$, and grip and push of 30 and 50 N, respectively. The results show considerable dispersion among the data acquired for different subjects, although some definite trends are clearly evident. The results clearly show strong dependence of the absorbed power on the frequency of vibration. Beyond 50 Hz, the absorbed power tends to decline rapidly as the frequency increases, irrespective of the handle size. In addition, the data show the existence of two peaks occurring in the 10-16 Hz and 31.5-50 Hz frequency bands for all three handles. These frequency bands of maximum absorbed power are comparable to those reported in a recent study by Bylun and Burström (2003). Furthermore, the frequency range of the second peak (31.5-50 Hz) corresponds very well with that of the peak $DPMI$ magnitude response of the human hand-arm system exposed to $z_h$-axis vibration presented in the previous chapter and other reported studies (Jandák, 1998; Reynolds and Falkenberg, 1984; Burström, 1990). While the results have been presented for $F_g$= 30 N and $F_p$= 50 N combination only, similar trends were also observed for the other force combinations. The measured data further show that the majority of the absorbed power occurs at frequencies below 200 Hz.
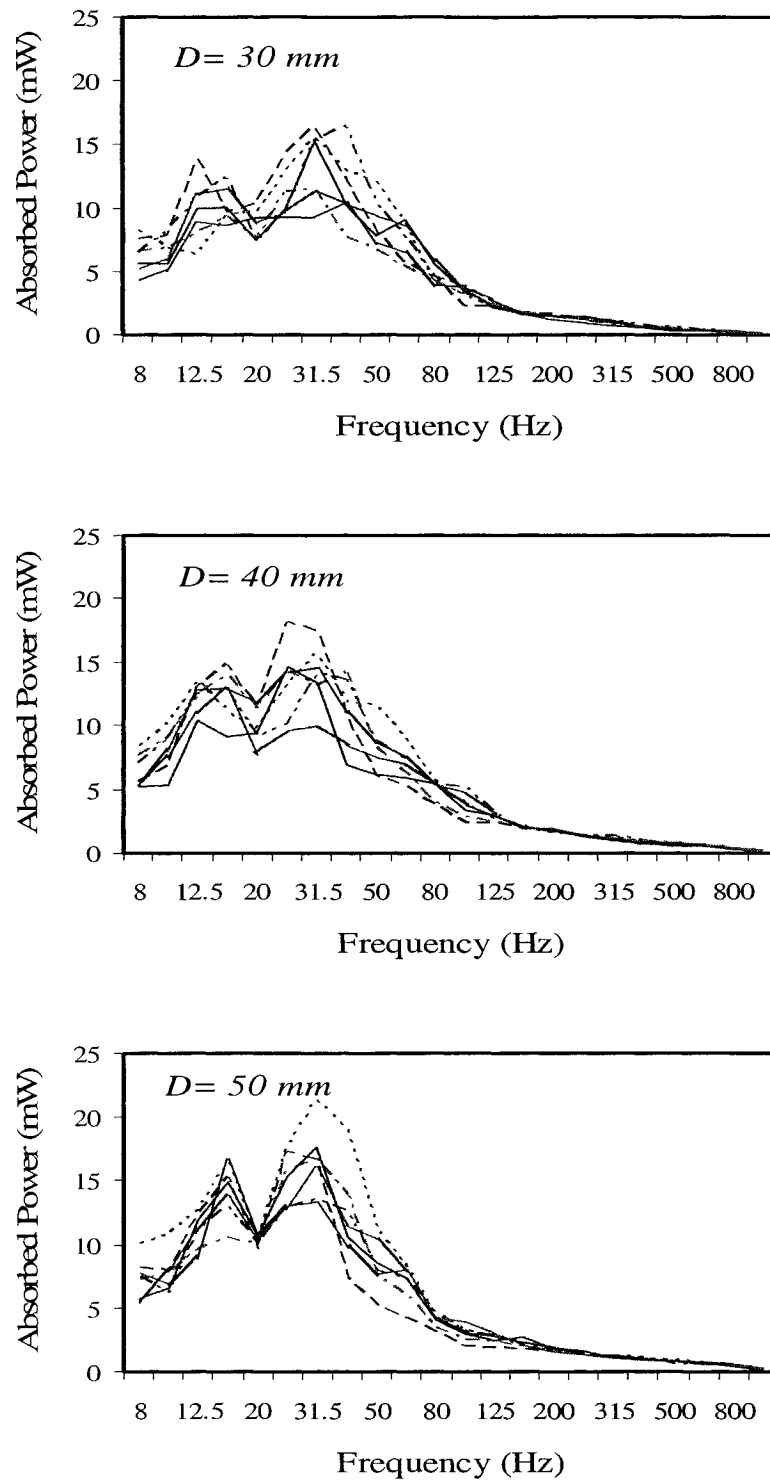
Figure 5.1: Comparisons of absorbed power characteristics of seven participants measured for the three cylindrical handles ($F_g$= 30 N, $F_p$= 50 N and $a_{h,w}$= 2.5 m/s$^2$).

Despite the consistent trends observed in the data attained for all subjects, the results show considerable inter-subject variability in absorbed power in the one-third octave frequency bands. Although the reported studies on power absorbed in the human hand and arm also show significant variations, partly attributed to individual anthropomorphic characteristics (Burström and Lundström, 1988; Burström; 1994), the inter-subject variability of the measured data has not been reported.

Figure 5.2 illustrates the coefficients of variation (COV) of the mean measured absorbed power in one-third octave bands for different combinations of grip and push forces, and all three handles. The results obtained for the lower excitation magnitude ($a_{h,w}$ = 2.5 m/s$^2$) reveal maximum values of COV in the order of 30%, occurring mostly at frequencies below 200 Hz. Such variations may be attributed to individual differences of the hand-arm structure and to some variations in the posture maintained by the subjects. Similar trends were also observed from the data acquired under different grip/push force combinations. While the reported studies on absorbed power did not specify the magnitudes of inter-subject variabilities, comparable variations have been reported for whole body vibration absorbed power (Mansfield and Griffin, 1998). The COV values, however, tend to be lower when the total hand-arm system absorbed power is considered. Figure 5.3 further illustrates the COV of the mean total absorbed power for all three handles and nine combinations of the hand forces under the excitation level of $a_{h,w}$ = 2.5 m/s$^2$. The COV of the mean total absorbed power are observed to be within 9 % for the 40 mm handle, and within 14 % for the 30 and 50 mm handles, which are concededly lower that that observed in the individual frequency bands.
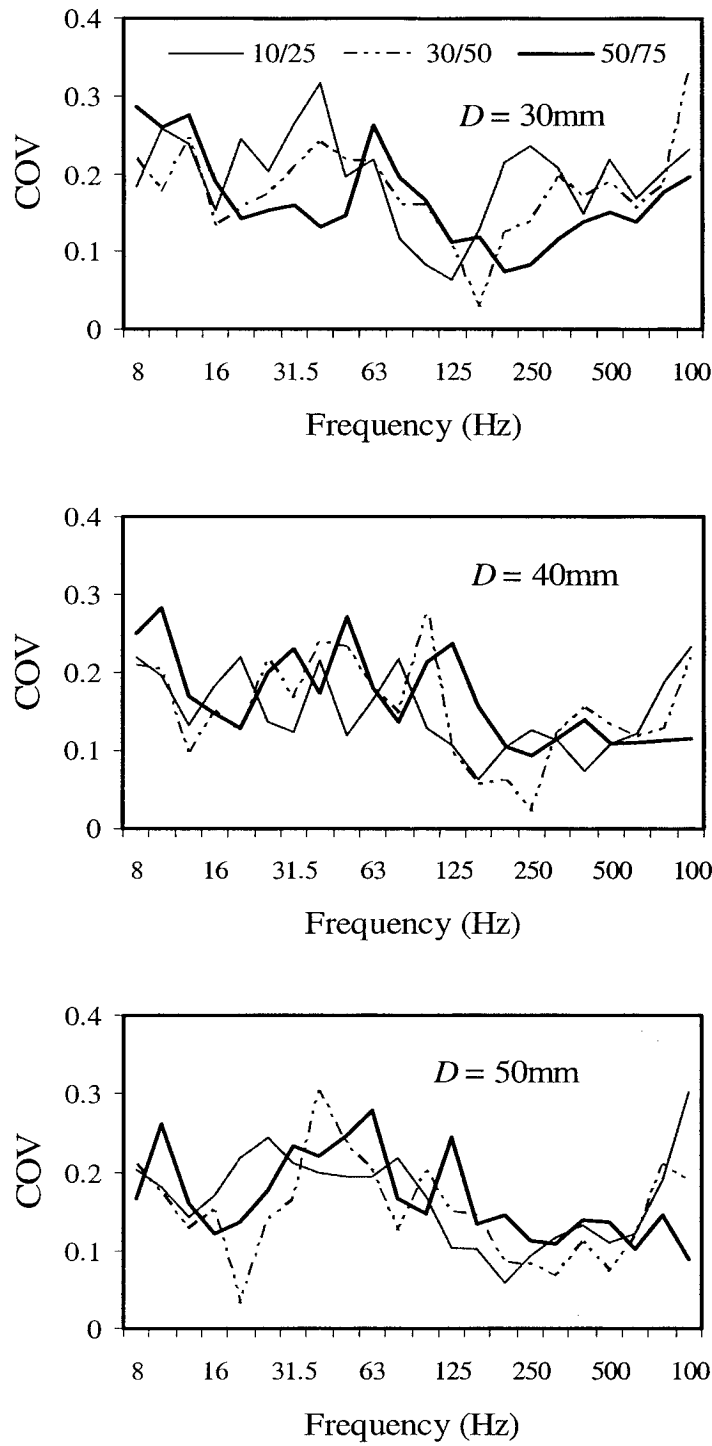
Figure 5.2: Coefficients of variation (COV), of the mean absorbed power data in the one-third octave frequency bands for all seven subjects, under three different $F_g/F_p$ force combinations and three different handle sizes ($a_{h,w}$= 2.5 m/s$^2$).
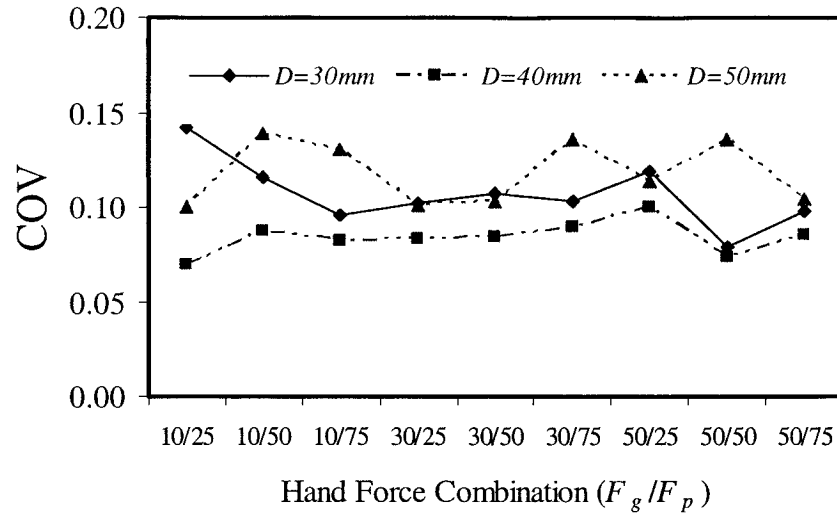
Figure 5.3: Coefficients of variation (COV), of the mean total absorbed power of all seven subjects as a function of the handles size, grip and, push force combinations ($a_{h,w}$= 2.5 m/s$^2$).

### 5.3.2 Influence of vibration magnitude on absorbed power

Unlike the *DPMI* response, the power absorbed into the human hand and arm is strongly dependent upon the magnitude of vibration. The data obtained for the seven subjects are analyzed to derive the mean values of absorbed power corresponding to different handles, hand forces and excitation magnitudes. Figure 5.4 shows the effect of vibration magnitude on the mean absorbed power within different one-third octave bands for the 40 mm handle, *P1* posture, $F_g$= 30 N and $F_p$= 50 N. An increase in weighted vibration magnitude from 2.5 m/s$^2$ to 5.0 m/s$^2$ results insignificant increase in the absorbed power, specifically at frequencies below 200 Hz. The influence of vibration magnitude is further evaluated in terms of mean total absorbed power for all three handles, as presented in Figure 5.5. The results presented for the 30 N grip and 50 N push force combination show that the total absorbed power under the higher excitation level

$(a_{h,w}=5.0$ m/s$^2)$ is approximately four times higher than that obtained under the lower excitation level $(a_{h,w}=2.5$ m/s$^2)$.
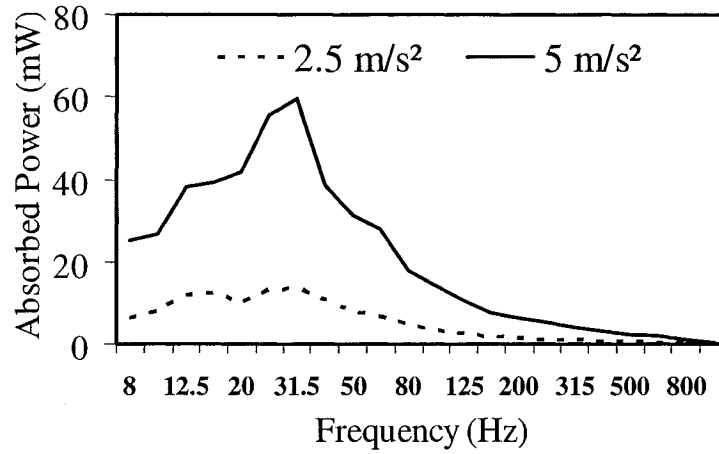


Figure 5.4: Comparison of mean absorbed power attained under two different magnitude of vibration excitations (seven subjects, $D=40$ mm, $F_g=30$ N and $F_p=50$ N)
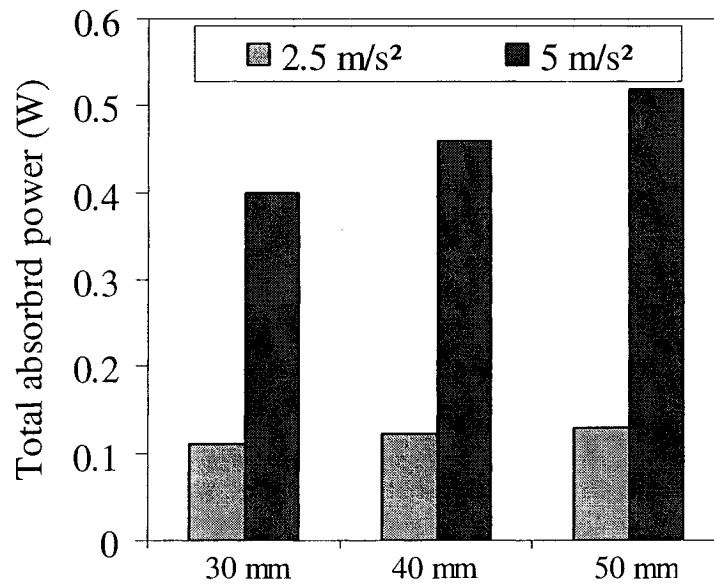


Figure 5.5: Total mean absorbed power response of the hand-arm system exposed to $z_h$-axis vibration and grasping cylindrical handles of different diameter ($F_g=30$N; $F_p=50$N)

## 5.3.3 Influence of handle size on absorbed power

It is obvious from Figure 5.5 that the handle size affects the magnitude of mean total power absorbed into the hand and arm exposed to $z_h$-axis vibration. The influence of handle size on the mean absorbed power is further investigated in the different one-third octave bands for the two excitation magnitudes, under posture $P1$, and 30 N grip and 50 N push force combination, as shown in Figure 5.6. The results clearly show that the magnitude of power absorbed into the hand-arm system increases with increase in the handle diameter under posture $P1$. The increase is more obvious in the low frequency range (below 50 Hz). Similar trends were also observed from the data acquired under different grip/push force combinations.
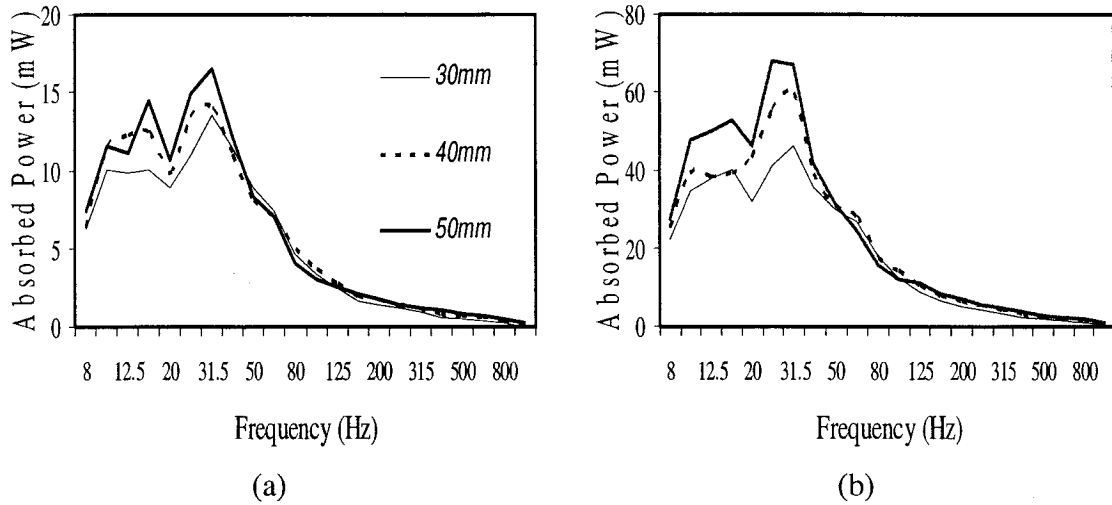


Figure 5.6: Effect of handle size on the mean absorbed power in the one-third octave bands: (a) $a_{h,w} = 2.5$ m/s$^2$ ; (b) $a_{h,w} = 5$ m/s$^2$ (posture $P1$; $F_g = 30$ N; and $F_p = 50$ N).

The influence of handle size on the total mean absorbed power is further investigated by computing the ratio of the total absorbed power under the higher excitation level ($a_{h,w} = 5.0$ m/s$^2$) to that attained under the lower excitation ($a_{h,w} = 2.5$ m/s$^2$) for each handle. The ratios of power attained for different hand force combinations

are analyzed to determine the overall mean ratio and standard deviation of the mean, which are presented in Table 5.1, for each handle size. Depending on the handle size, the ratios vary in a linear manner from 3.6 for the 30 mm handle to 4.0 for the 50 mm handle. The smaller handle tends to diminish the effect of higher vibration magnitude on the absorbed power. The results suggest that a two-fold increase in the weighted magnitude of the excitation would yield nearly four-fold increase in the total absorbed power. This can also be deduced from the absorbed power estimated from the *DPMI* (Z) response and handle velocity $v(j\omega)$, such that:

$$P_{abs}(\omega) = \text{Re}[Z(j\omega)]\,|v(j\omega)|^2 \tag{5.1}$$

Table 5.1: Mean and standard deviation of the ratio of the total absorbed power under high spectra (5.0 m/s$^2$) to that under the lower spectra (2.5 m/s$^2$).

| $D$ (mm) | Ratio | |
|---|---|---|
| | Mean | SD |
| 30 | 3.60 | 0.10 |
| 40 | 3.80 | 0.08 |
| 50 | 4.01 | 0.11 |

The influence of handle shape on power absorption by the human hand-arm exposed to $z_h$-axis vibration, is also analyzed using the measured data acquired with three elliptical cross-section handles (30x38 mm, 30x46 mm and 30x54 mm, denoted as *E38*, *E46* and *E54*, respectively). Figure 5.7 compares the mean absorbed power in the different one-third octave bands for the two excitation magnitudes, posture *P1*, and 30 N grip and 50 N push force combination is presented. The results do not show a particular trend in the mean absorbed power with variations in the size of the elliptical handle. This could be attributed to the fact that the elliptical handle sizes was realized by varying the major diameter of the handles (38, 46 and 54 mm), while the minor diameter was retained as 30

mm of circular handle. The hand palm and fingers were mostly in contact with the handle surface around the minor diameter as shown in Figure 5.8. Moreover, the vibration is applied along a direction normal to the minor diameter surface of the handle; where the majority of vibration energy thus impinges on the palm and fingers.



(a)                                          (b)
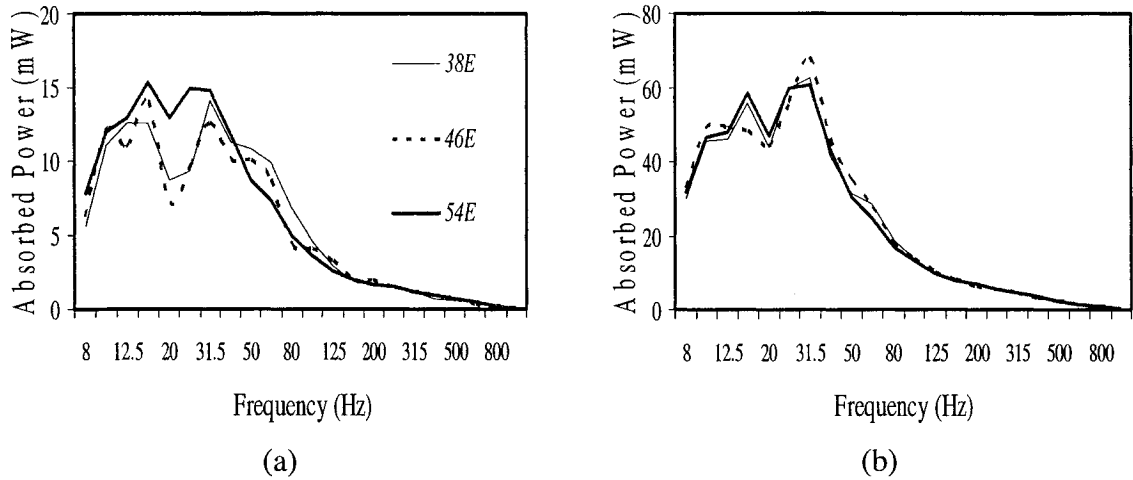
Figure 5.7: Influence of the elliptical handle size on the mean absorbed power response of the hand-arm system exposed to $z_h$-axis vibration: (a) $a_{h,w} = 2.5$ m/s$^2$ ; (b) $a_{h,w} = 5$ m/s$^2$ ($F_g = 30$ N, $F_p = 50$ N and posture $P1$).
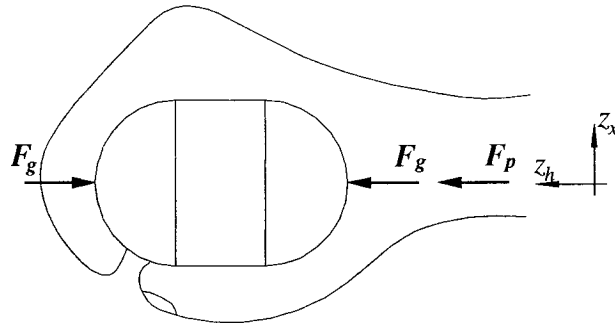


Figure 5.8: Orientation in the subject's hand with an elliptical handle.

Figure 5.9 further compares mean absorbed power characteristics obtained with three elliptical handles with those attained with 40 and 30 mm cylindrical handles under both levels of excitation, posture $P1$, and 30 N grip and 50 N push forces. Unlike the trends observed for the cylindrical handles (Figure 5.6), the elliptical handles do not show

196

a clear trend on the effect of handle size on the mean power response. The elliptical

handles, however, generally cause slightly higher absorbed power than the cylindrical

handles in the lower frequency bands. Further, the mean total absorbed power for the

three elliptical handles under different hand force combinations, have been computed, no

clear trends of the total mean absorbed were observed with the variation of handle sizes

of the elliptical handles.
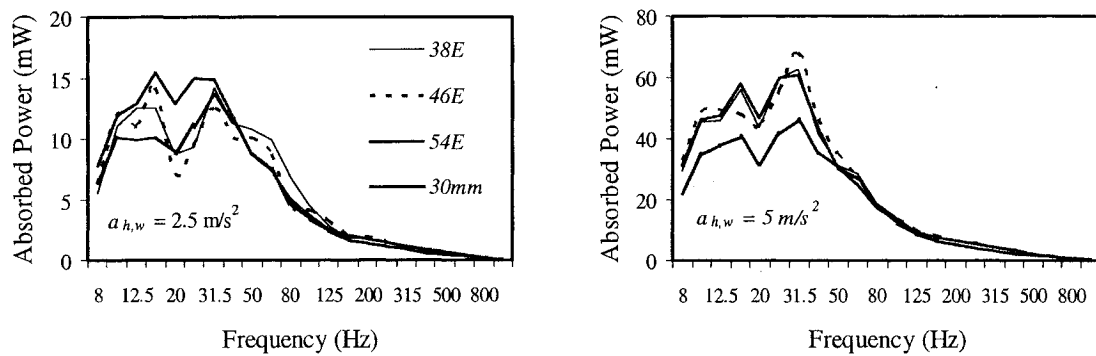


(a)
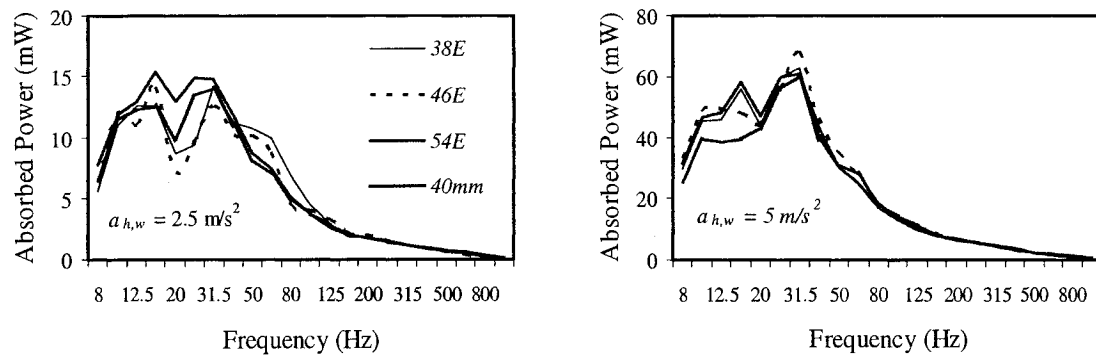
(b)

Figure 5.9: Comparison of mean absorbed power responses measured with elliptical and cylindrical handles: (a) $D$= 30 mm; and (b) $D$= 40 mm ($F_g$= 30 N; $F_p$= 50 N; and posture $P1$).

5.3.4    Influence of hand-arm posture on power absorption

The observed power characteristics of the human hand-arm system were measured under two different hand-arm postures, referred to as the posture *P1-* where the subjects maintained their forearm horizontally aligned with the handle and elbow bent at an angle of 90°; and posture *P2-* with elbow angle extended to 180° (Figure 2.8). The wrist was kept in a neutral position for both postures. The subjects generally experienced higher levels of low frequency vibration of the head and neck, and of the upper body, as well as higher stress in the upper arm, when gripping the handle under posture *P2* particularly when they exerted high grip and/or push forces. The driving-point impedance responses of the hand and arm system presented in the previous chapter, suggested higher hand-handle coupling with the posture *P2* (180° elbow flexion) than that with the *P1* posture. The subjects invariably reported increased transmission of low frequency vibration to the entire hand-arm and the upper body, rapid fatigue when grasping the handle with higher levels of hand forces and posture *P2*. This posture is thus considered to cause relatively higher musculoskeletal loading that could be better understood from the dissipation of the vibration energy into the hand and arm.

Figure 5.10 presents a comparison of the mean spectra of the absorbed power in one-third octave frequency bands, derived from the data acquired for the seven participants, grasping the 40 mm handle, assuming two postures, while applying 30 N grip and 50 N push force, and exposed to 2.5 m/s$^2$ and 5 m/s$^2$ excitation levels. The results clearly show that the magnitude of power absorbed into the hand-arm system with the *P2* posture is significantly higher than the *P1* posture in the low frequency range (below 30 Hz), irrespective of the excitation magnitude. The results show that the peak

absorbed power for posture *P2* occurs in the 16 Hz and 12.5 Hz frequency bands under

2.5 m/s² and 5 m/s² excitation levels, respectively. The corresponding values for the *P1*

posture exhibit two peaks in the 12.5-16 Hz and 40 Hz frequency bands under both

excitations. The results clearly show higher power dissipation at low frequency for the *P2*

posture, which can also be related to the higher damper-like impedance magnitude

response at low frequency associated with this posture (Figure 4.13). The higher power

dissipation further relates to higher coupling between the hand and handle, and

transmission of vibration to the upper arm and to the whole body, as experienced by the

participants.



(a)                                          (b)
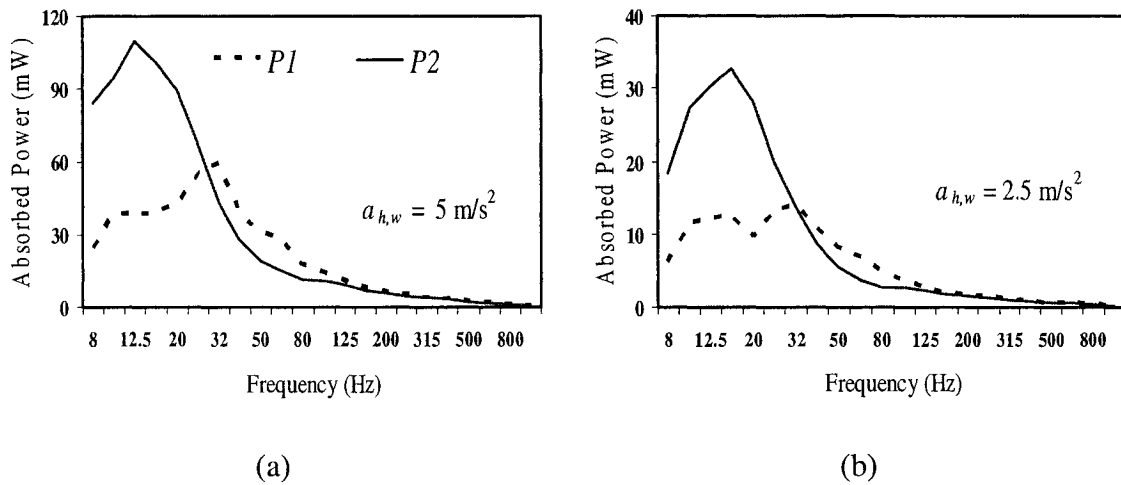
Figure 5.10: Influence of hand-arm posture on the mean absorbed power response under $z_h$-axis vibration: (a) $a_{h,w} = 5$ m/s² ; and (b) $a_{h,w} = 2.5$ m/s² ($F_g = 30$ N; $F_p = 50$ N; $D = 40$ mm).

The effect of the hand-arm posture is further investigated in term of the total

absorbed power. The relative significance of absorbed power under posture *P2* is

analyzed by normalizing the measured power with that measured under posture *P1*,

corresponding to each grip/push force combinations, handle size and magnitude of

vibration. The results attained in terms of power ratios are summarized in Table 5.2. It is

evident that gripping the vibrating handle with posture *P2* generally yields considerably higher power absorbed into the hand-arm system except for light grip and push forces ($F_g$=10 N and $F_p$=25 N) coupled with the larger handle (50 mm). The ratio varies from 0.83 to 1.96, depending on the handle size, excitation level and grip/push force combination. In general, the ratio of absorbed power of posture *P2* to that of posture *P1* increases with increasing hand/handle forces, suggesting that posture *P2* results in stronger coupling between the hand and the handle that increases with the increase in the hand forces. Higher power ratio is observed for higher push force for different grip force levels irrespective of the handle size. The smaller handle yields considerably higher power ratio due to smaller contact area, particularly for the push force. The larger 50 mm handle offers relatively larger contact area for the hand to apply the desired hand forces and thus, it results in a relatively smaller contact pressure between the hand and the handle for a given hand force (Chapter 3). This tends to cause a weaker coupling under light hand forces and thus yields relatively lower absorbed power.

Table 5.2: Ratio of mean total absorbed power of posture *P2* to that of posture *P1* for different grip/push force combination, handle size and excitation level.

| $a_{h,w}$ | 2.5 m/s² | | | 5 m/s² | | |
|---|---|---|---|---|---|---|
| *D* (mm) | 30 | 40 | 50 | 30 | 40 | 50 |
| $F_g/F_p$ (N) | Power ratio | | | | | |
| 10/25 | 1.437 | 1.202 | 0.978 | 1.471 | 1.053 | 0.828 |
| 10/50 | 1.659 | 1.434 | 1.178 | 1.681 | 1.314 | 1.043 |
| 10/75 | 1.856 | 1.689 | 1.372 | 1.746 | 1.504 | 1.201 |
| 30/25 | 1.721 | 1.388 | 1.297 | 1.714 | 1.312 | 1.070 |
| 30/50 | 1.814 | 1.631 | 1.399 | 1.852 | 1.495 | 1.298 |
| 30/75 | 1.896 | 1.701 | 1.470 | 1.869 | 1.572 | 1.308 |
| 50/25 | 1.694 | 1.602 | 1.299 | 1.842 | 1.448 | 1.236 |
| 50/50 | 1.889 | 1.683 | 1.542 | 1.885 | 1.583 | 1.239 |
| 50/75 | 1.963 | 1.761 | 1.522 | 1.826 | 1.665 | 1.405 |

Figure 5.11 shows the influence of hand-arm posture for different handle sizes on the mean absorbed power responses of the hand and arm corresponding to one-third octave bands center frequencies, when exposed to two excitation levels while applying 30 N grip and 50 N push force. For posture *P1*, the results clearly show that the magnitude of absorbed power in the low frequency range (below 50 Hz) increases with increase of the handle diameter, as discussed earlier in section 5.3.3. This particular trend, however, is not evident for the posture *P2*, which reveals peak power absorption for the 30 and 40 mm handles under lower and higher vibration spectra, respectively. The posture *P2* consistently yields considerably higher magnitudes of absorbed power, when compared to those obtained for the *P1* posture, irrespective of the handle size and excitation level. Moreover, the absorbed power response corresponding to posture *P2* appears to be a single-degree-of-freedom- like system behavior.

The influence of handle size on the total mean absorbed power is further investigated by computing the total absorbed power for both postures, all hand/handle force combinations and for two vibration spectra. The total absorbed power quantities computed for the 40 and 50 mm handles were normalized with that obtained for the 30 mm handle, corresponding to each grip and push force, and excitation level combination. The normalized total absorbed power values, presented in Table 5.3, show that the total power for larger handles tends to be higher for posture *P1* and lower for posture *P2*, irrespective of the hand forces and excitation levels. This could be attributed to relatively larger magnitudes of total absorbed power obtained while grasping the smaller handle (30 mm) under posture *P2*. Indeed, this particular posture encourages the use of the upper

body to realize the desired push force, as opposed to posture *P1* that requires exertion of the hand-arm muscles.
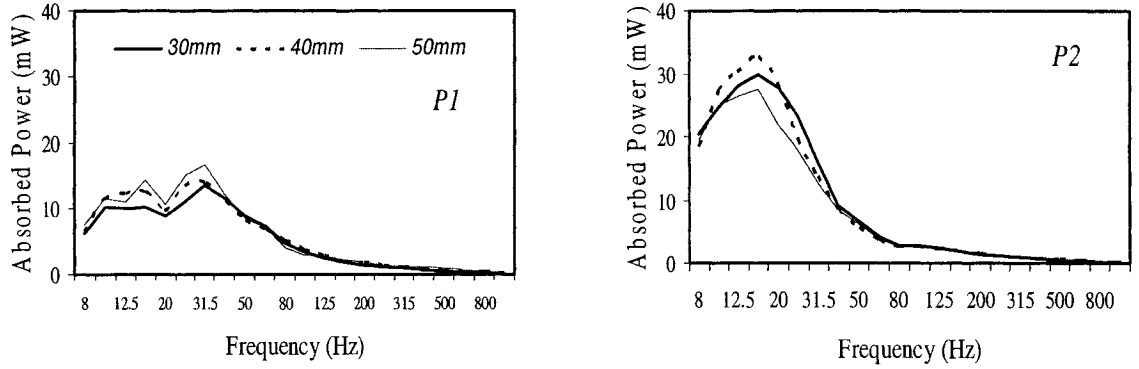
(a)
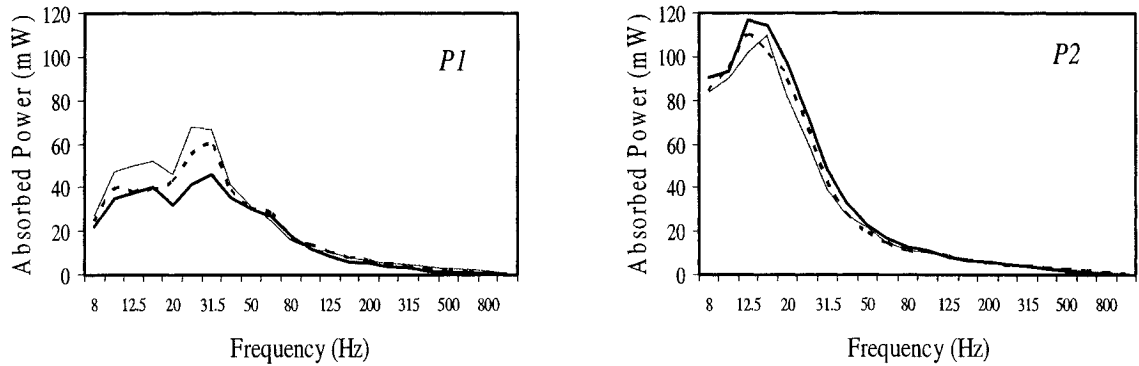
(b)

Figure 5.11: Influence of handle size on the mean absorbed power for two postures measured exposed to, (a) $a_{h,w}$= 2.5 m/s$^2$; and (b) $a_{h,w}$= 5.0 m/s$^2$ ($F_g$= 30 N and $F_p$ =50 N).

The lower contact area and thus the higher contact pressure of the 30 mm handle (Chapter 3), coupled with the tendency to use the upper body could cause relatively higher absorbed power for the *P2* posture. The effect of the handle size on the normalized power becomes more apparent under the higher magnitude of excitation. The posture *P1*

yields higher normalized absorbed power for both handle sizes, while posture *P2* generally reveals lower values of absorbed power with 40 and 50 mm handles, when compared to that attained with the 30 mm handle. Furthermore, the normalized power values under *P2* posture and higher excitations are comparable with those attained under the lower excitation level.

Table 5.3: The total mean absorbed power measured with 40 and 50 mm handles normalized to that measured with the 30 mm handle.

| Posture | *P1* | | | | *P2* | | | |
|---|---|---|---|---|---|---|---|---|
| *D* (mm) | 40 | 50 | 40 | 50 | 40 | 50 | 40 | 50 |
| $a_{h,w}$ | 2.5 m/s² | | 5 m/s² | | 2.5 m/s² | | 5 m/s² | |
| $F_g/F_p$ (N) | Normalized Power | | | | | | | |
| 10/25 | 1.04 | 1.10 | 1.12 | 1.27 | 0.87 | 0.75 | 0.80 | 0.72 |
| 10/50 | 1.08 | 1.13 | 1.15 | 1.31 | 0.93 | 0.81 | 0.90 | 0.81 |
| 10/75 | 1.06 | 1.20 | 1.11 | 1.33 | 0.97 | 0.89 | 0.96 | 0.92 |
| 30/25 | 1.11 | 1.13 | 1.18 | 1.30 | 0.90 | 0.85 | 0.90 | 0.81 |
| 30/50 | 1.11 | 1.16 | 1.15 | 1.30 | 1.00 | 0.90 | 0.93 | 0.91 |
| 30/75 | 1.10 | 1.19 | 1.14 | 1.34 | 0.98 | 0.92 | 0.96 | 0.94 |
| 50/25 | 1.06 | 1.18 | 1.17 | 1.27 | 1.01 | 0.90 | 0.92 | 0.85 |
| 50/50 | 1.10 | 1.16 | 1.17 | 1.32 | 0.98 | 0.94 | 0.98 | 0.87 |
| 50/75 | 1.09 | 1.20 | 1.13 | 1.23 | 0.98 | 0.93 | 1.03 | 0.94 |

## 5.3.5 Influence of hand forces on absorbed power

The influence of variation in the grip and push forces on the mean absorbed power of the hand-arm system exposed to the excitation level of 5 m/s², while gripping the 40 mm handle under the two considered postures, *P1* and *P2*, are shown in Figures 5.11 and 5.12. The Figures also show the influence of grip and push forces on the absorbed power measured using the 30x46 mm elliptical handle (*E46*) under posture *P1*. The push force is held constant at 50 N while the $F_g$ is held constant at 30 N for the results presented in

203

the Figures 5.11 and 5.12, respectively. Under posture *P1* and at frequencies below 40 Hz, the results do not show a definite trend with regard to the influence of push as well as grip forces on the mean absorbed power with both cylindrical and elliptical handles. The same trend was also observed in the *DPMI* magnitude response, where the *DPMI* magnitude response appears to be more influenced by variations in the hand forces at frequencies above the primary resonance (Figures 4.8 and 4.9).

The influence of variation in hand forces is more noticeable in the higher frequency bands; an increase in hand forces cause slightly higher absorbed power in the 40-100 Hz frequency bands for both handles. Grasping the handle with posture *P2*, however, reveals strong effects of both the grip and push forces on the mean absorbed power at frequencies below 160 Hz and 80 Hz, respectively. The effect of grip force is not evident at low frequencies, in the 8-12.5 Hz frequency bands for the *P2* posture. An increase in either the grip or push force for this posture yields higher absorbed power values and higher frequencies of peak absorbed power. The effects of both hand forces under this posture are more evident those observed under posture *P1*. Identical trends were also observed with regards to the *DPMI* responses (Figure 4.16). The contribution due to a higher grip force appears to be more important than that caused by a higher push force in the 12.5-40 Hz frequency bands. However, for both hand-arm postures and all handles, the influence of grip and push forces diminishes at frequencies above 100 Hz. For elliptical handle (*E46*), the influence of the hand force on absorbed power is almost identical of that of cylindrical handle (40 mm) as can be seen in Figures 5.11 and 5.12.
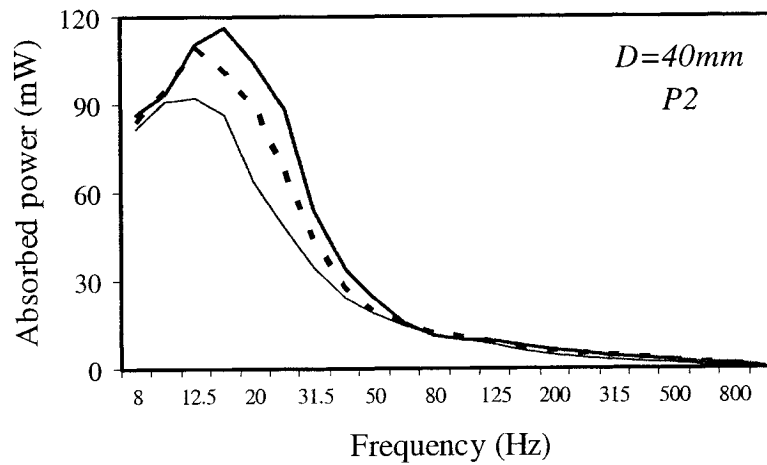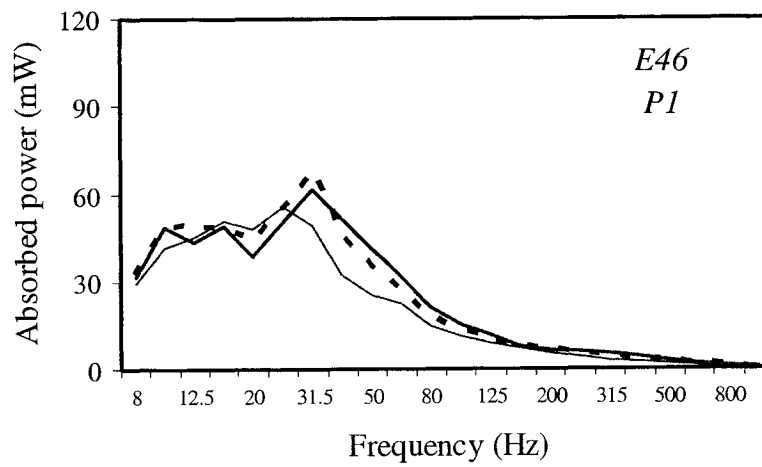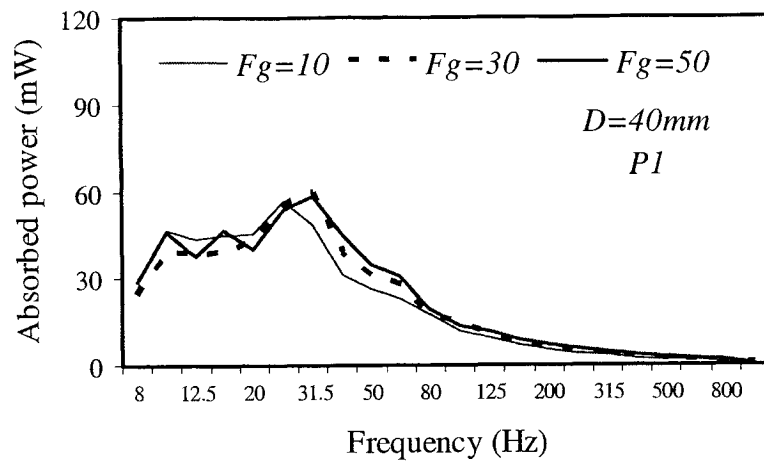
Figure 5.12: Influence of variations in grip force on the mean absorbed power at center frequencies of one-third octave bands for the two postures ($F_p$= 50 N and $a_{w,h}$ = 5 m/s$^2$).
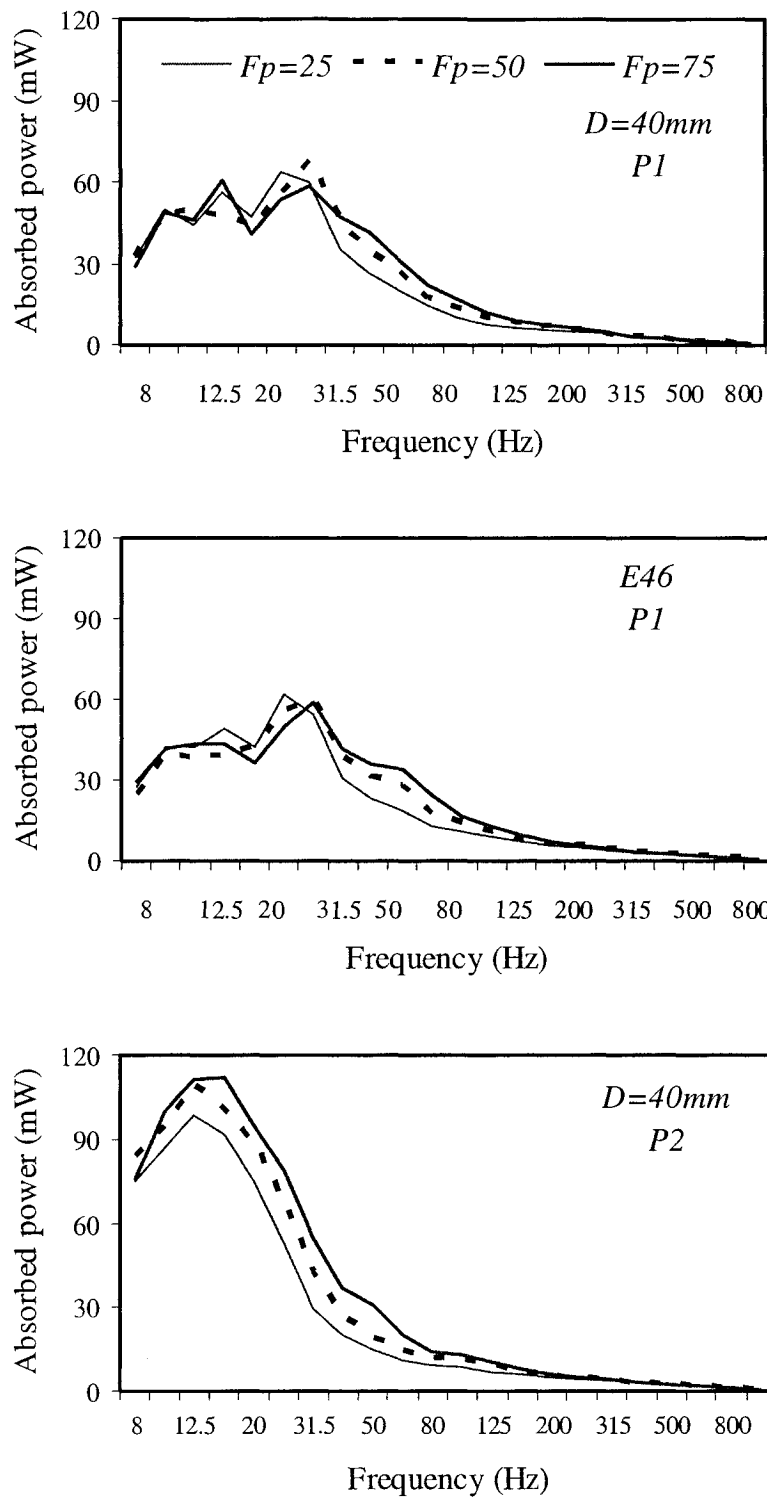
Figure 5.13: Influence of variations in push force on the mean absorbed power at center frequencies of one-third octave frequency bands for the two postures ($F_g$= 30 N and $a_{w,h}$ = 5 m/s$^2$)

An increase in the grip force, in general, causes a shift of the second absorbed power peak (around 31.5 Hz- under posture *P1*) slightly to the right in the frequency domain. This is in agreement with results present by Jandák (1989), which showed that an increase in the grip force does not yield higher energy dissipation but rather causes a shift in the frequency of the peak absorbed energy. Burström and Lundström (1988), on the other hand, concluded that a higher grip force causes higher amounts of dissipated energy over the entire frequency range, except at low frequencies where the effect is negligible. Similar effects of the grip force have also been observed on the driving-point mechanical impedance characteristics of the hand-arm system (chapter 4).

For the push force, the observed trends tend to contradict some of the reported findings. Burström and Lundström (1992) reported that the energy absorption increases, in general, with increasing push force, while opposite trends were observed at frequencies below 16 Hz. Another study by Burström (1994) has reported that higher push forces result in higher power absorption at frequencies below 100 Hz. The lack of a definite trend in the dependence of low frequency absorbed power on the push force (particularly under posture *P1*) together with the contradictory findings of the reported study may suggest relatively small influence of the push force, well within the range of inter-subject variability.

The influence of hand forces is further examined in term of the total mean absorbed power, as illustrated in Figures 5.13 and 5.14. The figures show the effect of grip and push forces, respectively, on the total mean absorbed power for the 40 mm handle exposed to the higher excitation level ($a_{h,w}$= 5.0 m/s$^2$). The results, in general show, irrespective of the posture, that an increase in either of the hand forces leads to an

increase in the total absorbed power. The increase in the total absorbed power with increasing grip and/or push forces is, however, far more evident under posture $P2$. Similar trends were also observed from the data acquired for handle sizes and excitation levels. The higher influence of hand forces on absorbed power under posture $P2$ over that of posture $P1$, further confirms the strong coupling between the hand and handle under that posture, specifically at low frequency vibration as it was observed in section 4.3.5 and in Figure 4.13.
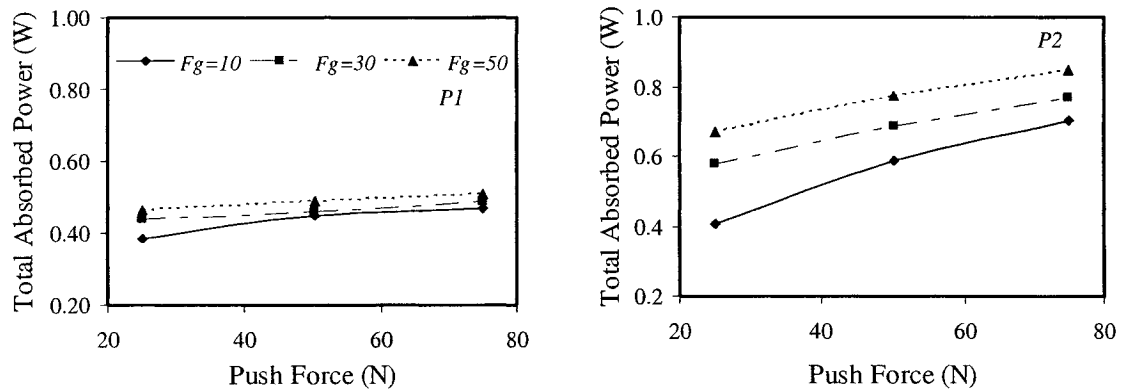
Figure 5.14: The influence of variations in grip force on the total mean absorbed power under two postures ($D$= 40mm and $a_{h,w}$= 5.0 m/s$^2$).
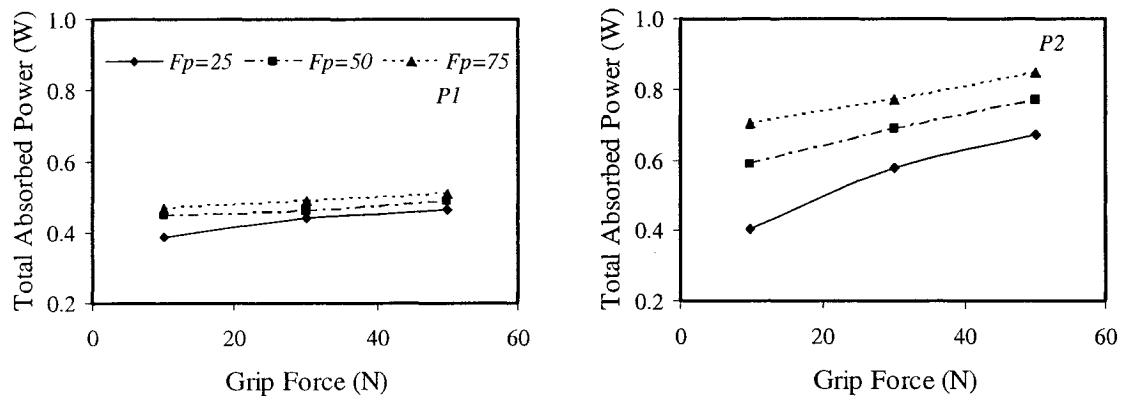
Figure 5.15: The influence of variations in the push forces on the total mean absorbed power under two postures (40mm handle and $a_{h,w}$= 5.0 m/s$^2$).

The influence of grip and push forces on the total mean absorbed power are further investigated in terms of percent increase with reference to the values obtained under 10 N grip or 25 N push forces. The percent increase in the total absorbed power due to push force alone is computed for each level of grip force in relation to the absorbed power corresponding to constant 25 N push force. The effect of grip force is obtained in a similar manner for each push force level, while the nominal grip level is chosen as 10 N. The results obtained thus reflect the magnification in the total absorbed power with increasing grip or push force for the two different postures, three handle sizes and two excitation levels considered. The results, summarized in Table 5.4, show that an increase in the push force alone leads to considerably higher percentage increase in absorbed power for posture *P2* than for posture *P1*, specifically under lower levels of grip force. The highest increase in the total absorbed power approaches 88 % under posture *P2* with 50 mm handle at 10 N grip force and $a_{h,w}= 5$ m/s$^2$ excitation level, when the push force increases from 25 to 75 N. The maximum increase under *P1* posture is only 29 %, and it also occurs at 10 N grip force and $a_{h,w}= 5$ m/s$^2$ excitation level, when the push force is increased from 25 to 75 N.

The maximum percentage increase in absorbed power due to increase in the grip force under *P1* posture is observed to be 21 %, which occurs with the 40 mm handle at 25 N push force when the grip force increases from 10 to 50 N under $a_{h,w}= 5$ m/s$^2$ excitation level. The maximum percentage increase for the *P2* posture approaches 72 % under same conditions with the 50 mm handle. The results suggest that the percent increase in absorbed power is more influenced by the push force than the grip force, irrespective of the posture, while the effect is more pronounced for posture *P2*. This may be attributed to

the fact that a considerable portion of vibration energy enters the hand-arm system through the upper lateral side of the palm, which mostly contributes to the application of the push force.

Table 5.4: The percent increase in total absorbed power due to increase in the push force alone under constant levels of $F_g$, and due to grip force alone under constant levels of $F_p$.

| Posture | | | P1 | | | | | | P2 | | | | | |
|---|---|---|---|---|---|---|---|---|---|---|---|---|---|---|
| $a_{h,w}$ | | | 2.5 m/s² | | | 5 m/s² | | | 2.5 m/s² | | | 5 m/s² | | |
| D (mm) | | | 30 | 40 | 50 | 30 | 40 | 50 | 30 | 40 | 50 | 30 | 40 | 50 |
| Reference | $F_g$ (N) | $F_p$ (N) | Percent increase in total power | | | | | | | | | | | |
| | 10 | 50 | 13 | 17 | 17 | 14 | 16 | 18 | 30 | 39 | 40 | 30 | 45 | 48 |
| | 10 | 75 | 14 | 17 | 25 | 24 | 22 | 29 | 47 | 64 | 75 | 47 | 74 | 88 |
| | 30 | 50 | 4 | 4 | 7 | 7 | 4 | 6 | 10 | 22 | 16 | 15 | 19 | 29 |
| $F_p$=25 N | 30 | 75 | 11 | 9 | 17 | 14 | 11 | 18 | 22 | 34 | 33 | 25 | 33 | 44 |
| | 50 | 50 | 4 | 7 | 2 | 5 | 5 | 9 | 15 | 23 | 21 | 8 | 15 | 10 |
| | 50 | 75 | 8 | 10 | 10 | 14 | 10 | 10 | 25 | 22 | 29 | 13 | 26 | 26 |
| | 30 | 25 | 7 | 14 | 10 | 10 | 15 | 12 | 28 | 32 | 46 | 28 | 43 | 45 |
| | 50 | 25 | 12 | 15 | 20 | 16 | 21 | 16 | 32 | 52 | 60 | 15 | 66 | 72 |
| | 30 | 50 | 0 | 2 | 1 | 2 | 3 | 2 | 8 | 16 | 20 | 13 | 17 | 26 |
| $F_g$=10 N | 50 | 50 | 3 | 5 | 5 | 7 | 9 | 8 | 17 | 23 | 37 | 20 | 31 | 28 |
| | 30 | 75 | 4 | 7 | 3 | 1 | 4 | 2 | 6 | 8 | 10 | 8 | 9 | 11 |
| | 50 | 75 | 6 | 9 | 6 | 7 | 9 | 0 | 12 | 13 | 18 | 12 | 20 | 15 |

Relationship with coupling and contact forces

A few studies have concluded that the hand-handle coupling and contact forces strongly affect the biodynamic response, the severity of exposure to the hand-transmitted vibration and hand-wrist cumulative trauma disorders (Fransson and Winkel, 1991; Pyykkö et al., 1976; Radwin et al., 1987; Riedel, 1995). The measured data are thus analyzed to study the effects of both the coupling and the contact forces on the absorbed power under two considered postures; P1 and P2.

Figure 5.16 shows the variation in the total mean absorbed power with the hand-handle coupling and contact forces. The results suggest nearly linear variations in the total mean absorbed power with the coupling force for all three handles under two

postures, with correlation factors varying from 0.78 to 0.95 under high magnitude spectra

($a_{h,w}$ = 5.0 m/s$^2$). While similar trends are also evident with variations in the contact

force, relatively poor correlations are obtained, with correlation coefficients varying from

0.45 to 0.79 for the high excitation spectra. The results further show that the larger handle

leads to more power absorption under posture *P1*, while the reverse trend prevails under

posture *P2*. In almost all cases, higher correlations between absorbed power and both

forces under posture *P2* over that of posture *P1*, suggesting higher hand-handle coupling

under that posture. Similar trends were also observed for the low excitation spectra.
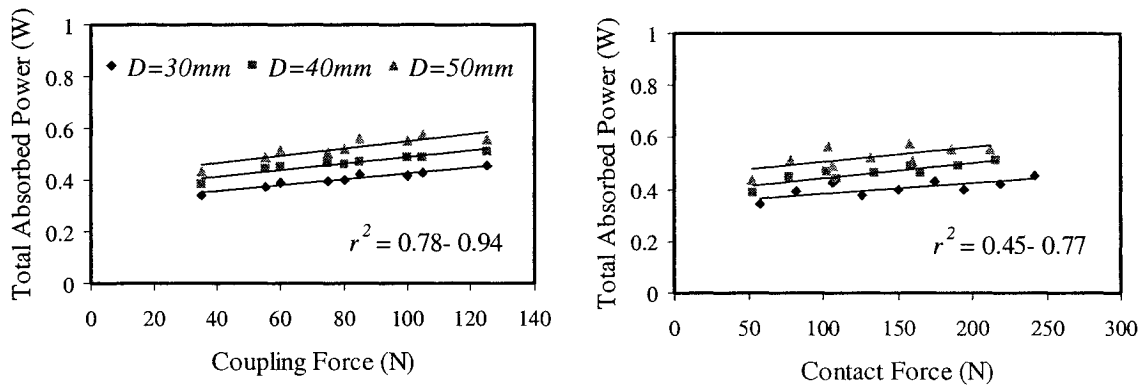


(a)
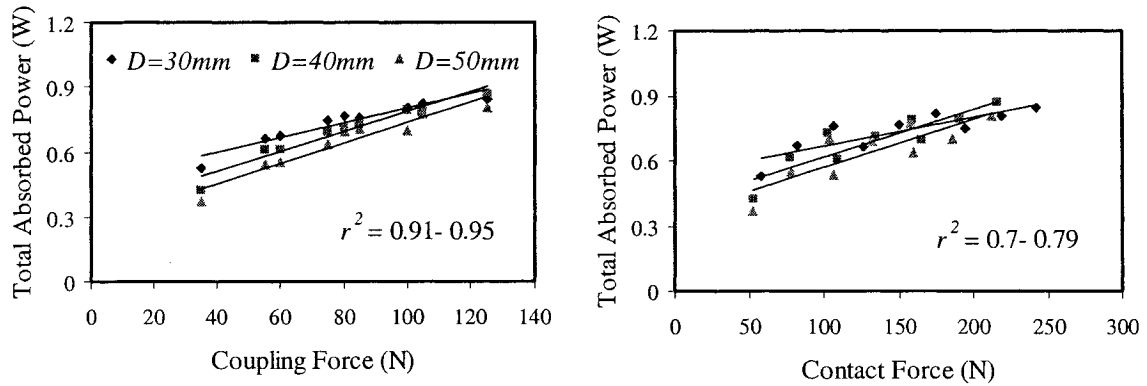
(b)

Figure 5.16: Variations in the of mean total absorbed power in the 8-1000 frequency
range, as a function of the coupling and contact forces ($a_{h,w}$= 5.0 m/s$^2$): (a) posture *P1*;
and (b) posture *P2*.

5.3.6   Role of excitation frequency in power absorption

The role of vibration frequency is investigated by analyzing the proportion of power absorbed within a frequency band to the total absorbed power for the three cylindrical handles with two postures considered in this study. For this purpose, the measured data are analyzed to derive the mean values of total absorbed power for each handle and hand force combination under both excitation levels. Considering that the total absorbed power in the frequency range above 200 Hz represents only 5% or less of the total absorbed power for both postures, the analyses are limited to frequencies up to 200 Hz. The total absorbed power is thus computed within three frequency bands (8-50 Hz, 8-100 Hz and 8-200 Hz) and normalized with respect to the total absorbed power over the entire frequency range for each handle size, excitation spectrum and hand-force combination, in order to study the relative proportions of absorbed power in these low frequency bands. The mean values of the proportions of the absorbed power within the selected frequency bands together with the standard deviations are summarized in Table 5.5, as a function of the hand force combination, for both magnitude spectra and all three handle sizes. The proportion of the total absorbed power in the selected frequency bands does not vary considerably with either the handle diameter or the vibration magnitude, as evident from the relatively low standard deviation values.

The proportions, however, show significant variations with the grip and push force combinations for posture *P1*, while a clear trend could not be observed. The absorbed power proportions are not influence by the hand force combination under posture *P2*, as evident from the table. These proportions for the same frequency range are higher under posture *P2* than those evaluated for posture *P1*. Table 5.5 shows that 75 to 84% and 88 to

212

90 % of the total power is dissipated in the 8-50 Hz frequency range, irrespective of the excitation magnitude, handle size and hand forces for postures $P1$ and $P2$, respectively. This would represent the most significant frequency range in view of the injury potential, since a large number of hand power tools transmit predominant vibration in this frequency range (Griffin, 1998). The proportions of the absorbed power increase only slightly with increase in the frequency range. It is evident that the proportion of the absorbed power in the 8-100 Hz and 8-200 Hz frequency ranges vary from 91 to 95 % and 96 to 98 % for both postures, respectively. For the 8-200 Hz range, the ratio of absorbed power to the total absorbed power is around 96 % for all force combinations, suggesting insignificant effect of hand-handle applied forces.

Table 5.5: Mean and standard deviation of the proportions of total absorbed power in the three frequency ranges, as a function of the hand force combination.

| Frequency range | 8-50 Hz | | | | 8-100 Hz | | | | 8-200 Hz | | | |
|---|---|---|---|---|---|---|---|---|---|---|---|---|
| Posture | $P1$ | | $P2$ | | $P1$ | | $P2$ | | $P1$ | | $P2$ | |
| $F_g/F_p$ (N) | Mean | SD | Mean | SD | Mean | SD | Mean | SD | Mean | SD | Mean | SD |
| 10/25 | .84 | .01 | .88 | .02 | .93 | .01 | .94 | .01 | .97 | 00 | .97 | .01 |
| 10/50 | .81 | .01 | .89 | .01 | .92 | .01 | .95 | .01 | .97 | 00 | .98 | 00 |
| 10/75 | .78 | .02 | .89 | .01 | .92 | .01 | .95 | .00 | .97 | 00 | .98 | 00 |
| 30/25 | .82 | .01 | .90 | .01 | .92 | .01 | .94 | .01 | .96 | 00 | .97 | 00 |
| 30/50 | .79 | .01 | .90 | .01 | .91 | .01 | .95 | .00 | .96 | 00 | .98 | 00 |
| 30/75 | .79 | .02 | .89 | .01 | .91 | .01 | .95 | .00 | .96 | 00 | .98 | 00 |
| 50/25 | .80 | .01 | .90 | .01 | .91 | .01 | .94 | .00 | .96 | 00 | .97 | 00 |
| 50/50 | .77 | .01 | .90 | .01 | .91 | .01 | .95 | .00 | .96 | 00 | .97 | 00 |
| 50/75 | .75 | .01 | .89 | .01 | .90 | .01 | .95 | .00 | .96 | 00 | .98 | 00 |

Assessing the effect of varying either the grip or push force on the total absorbed power particularly under posture $P1$ was, however, difficult due to the lack of definite trends in the low frequency range, as it was discussed in section 5.3.5. The effect of variations in these forces on the total absorbed power would thus rely on the relative contribution of the absorbed power in the low frequency range under this posture. To

investigate the influence of hand forces in two different frequency bands, the measured data are thus further analyzed to derive the mean total power in two different frequency ranges: 8-31.5 Hz and 31.5-1000 Hz. Figure 5.17 illustrates the total mean power measured in the two frequency ranges, as a function of the push and grip forces, for the 40 mm handle, exposed to high excitation level and under two considered postures. The results clearly show an increase in the total absorbed power in the 31.5-1000 Hz range with an increase in either of the hand forces for both postures.

Furthermore, in general, the increase in the absorbed power in this frequency range is nearly linear with the push force. No clear trends, however, could be observed on the effects of hand grip and push forces on the mean total absorbed power in the low frequency range (8-31.5 Hz) under posture $P1$, while same linear trend of the total absorbed power in the 31.5-1000 Hz could be observed under posture $P1$, which confirms the strong coupling between hand and handle under this posture. The results, however, show that the total absorbed power in this low frequency range is considerably larger than that in the high frequency range, irrespective of the hand-arm posture. The results may suggest relatively small influence of the hand forces on the absorbed power in the low frequency range under posture $P1$, which is consistent with the observations made from the measured driving-point mechanical impedance data (chapter 4). Similar trends were observed for other handles and low spectra for both hand-arm postures. This coupled with relatively higher inter-subject variability in the lower frequency range (Figure 5.1) could contribute to the contradictory conclusions reported in different studies concerning the role of hand forces on the absorbed power response of the human hand-arm system

(Burström, 1990; Burström and Lundström, 1988; Burström and Lundström, 1989; Sörensson, 1998).
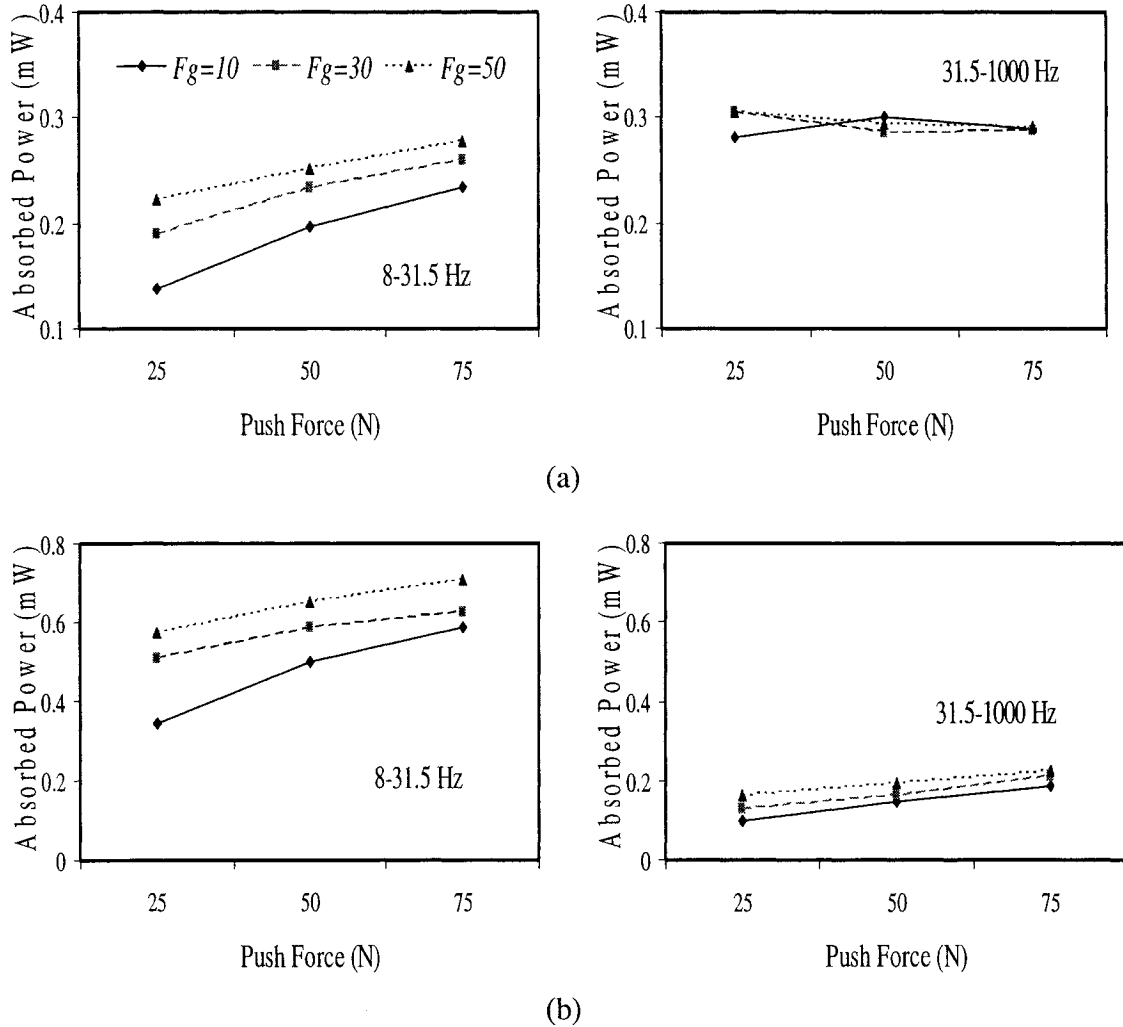


Figure 5.17: Variations in the total mean absorbed power in the 8-31.5 Hz and 31.5-1000 Hz ranges , as a function of push force ($D$= 40 mm and $a_{h,w}$= 5.0 m/s$^2$): (a) posture $P1$; and (b) posture $P2$.

Further analysis on the role of vibration frequency is performed by evaluating the absorbed power in various frequency bands and the results are analyzed to study correlations between the total absorbed power within different frequency bands and different measures of the hand forces. The results reveal somewhat different relationships

between the total mean absorbed power, and the coupling and contact forces. For posture $P1$, the mean absorbed power, in general, shows weak correlation with the coupling force in the 8-50 Hz frequency range, as seen in Figure 5.18, for the high excitation spectra ($r^2$ values ranging .55 to .80 for the different handles) and even weaker correlation with the contact force ($r^2$ values ranging from .26 to .74), as evident in Figure 5.18(a). While under posture $P2$, the mean absorbed power shows strong correlation with the coupling force in the same frequency range ($r^2$ values ranging .85 to .92 for the different handles) since most of the absorbed power under this posture occurs in this frequency range (Figure 5.19). On the other hand, high correlation coefficients are also observed with the coupling force in the 50-200 Hz frequency range under both postures ($r^2 = .92$ to .94 and .86 to .91 for posture $P1$ and $P2$, respectively), while relatively poor correlations between the mean absorbed power and the contact force ($r^2 = .45$ to .62) are observed for both postures in the same frequency range, as illustrated in Figure 5.18(b) and Figure 5.19(b).

On the contrary, the absorbed power shows excellent correlation ($r^2 \geq .96$) with the contact force in the 200-1000 Hz frequency range, irrespective of the handle size or hand-arm posture, and lower correlation factors with the coupling force (.73 to .84) for different handles, as seen in Figure 5.18(c) and Figure 5.19(c), although the amount of absorbed power in this frequency range is very small (less than 5%). Similar correlations between the driving-point mechanical impedance and the hand-handle coupling and contact forces have also been observed (chapter 4). Considering that the majority of the power absorption by the hand-arm system occurs in the frequency range up to 200 Hz, the absorbed power is, in general, expected to be more related to the hand-handle coupling force than to the contact force.

216
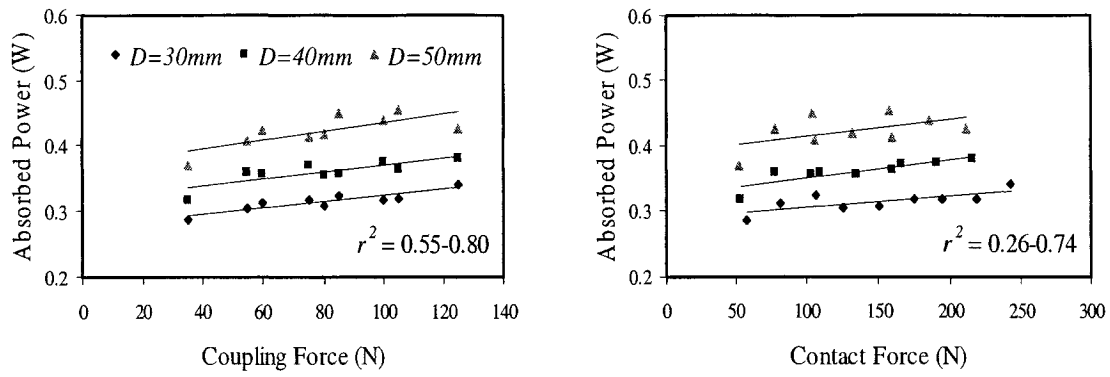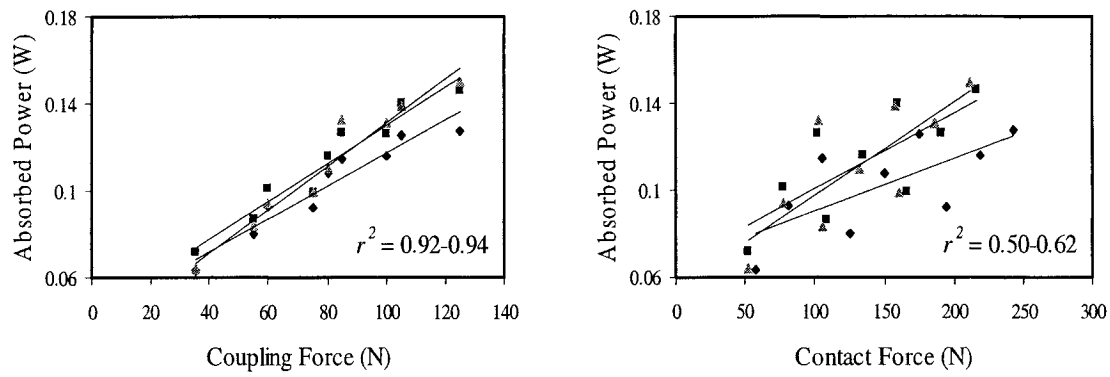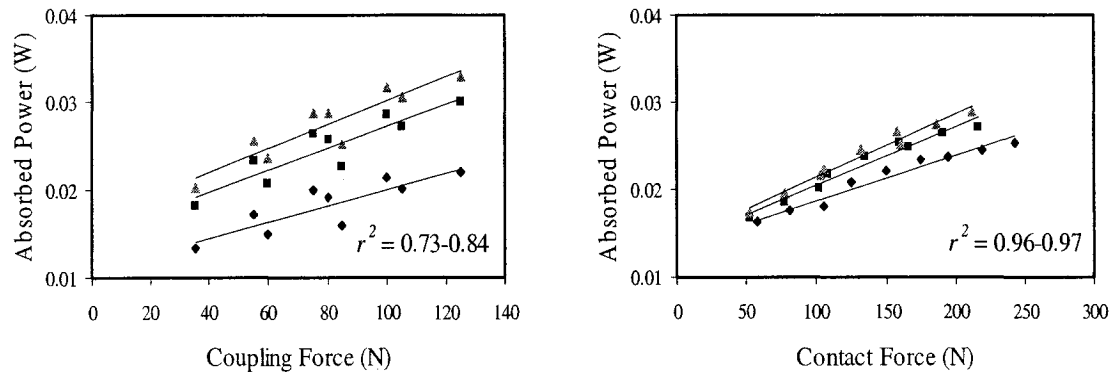
Figure 5.18: Variations in the mean total absorbed power in different frequency ranges as a function of coupling and contact forces: a) 8-50 Hz; b) 50-200 Hz; and c) 200-1000 Hz. (Posture *P1* and $a_{h,w}$= 5.0 m/s$^2$).
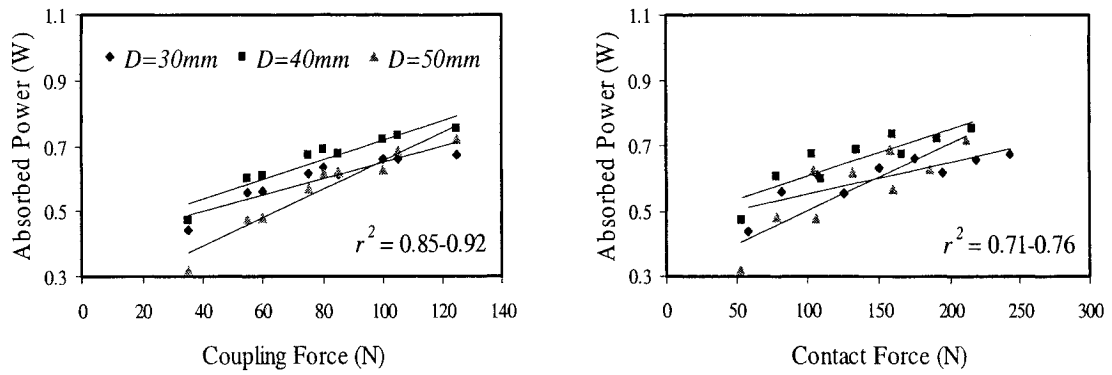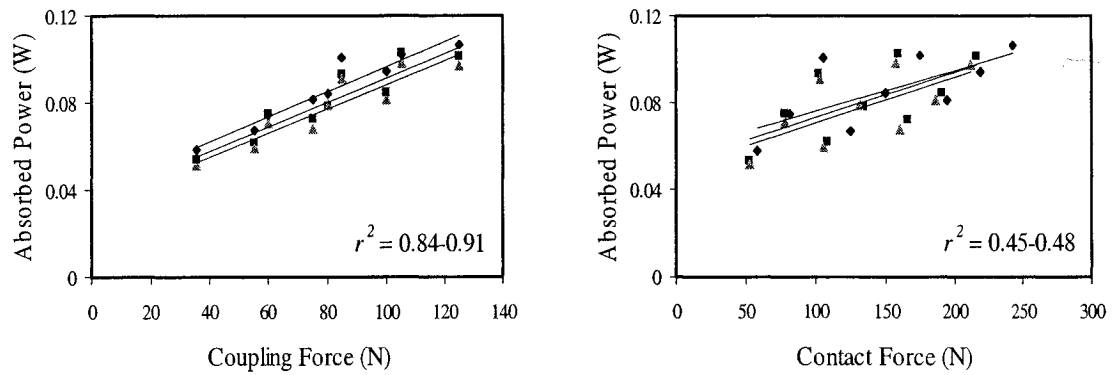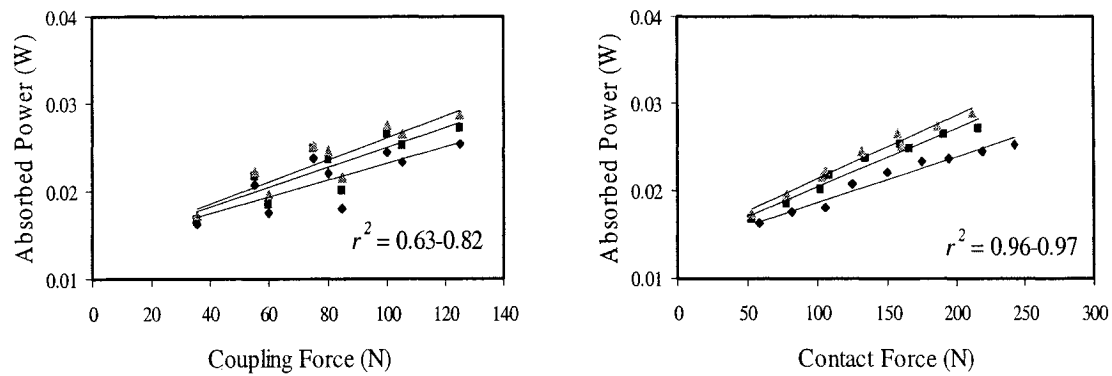
Figure 5.19: Variations in the mean total absorbed power in different frequency range as a function of coupling and contact forces; a) 8-50 Hz; b) 50-200 Hz; and c) 200-1000 Hz . (Posture $P2$ and $a_{h,w}$= 5.0 m/s$^2$).

## 5.3.7 Statistical analysis ($z_h$-axis)

Multi-factor analysis of variance (ANOVA) has been performed on the total absorbed power using SPSS version 11.5. The factors represented the three nominal diameters of the handles ($D$), three levels of push force ($F_p$), three levels of grip force ($F_g$), two excitation magnitude ($A$) and two hand-arm postures ($P$) based on a preliminary analysis using Mauchly's test of sphericity. The ANOVA results of the mean total absorbed revealed statistical significance for all considered factors, except for the handle diameter. The statistical non-significance of the handle size on the mean total absorbed power could be related to the opposing effects of the handle size in conjunction with the hand-arm posture. Increasing the handle size yields higher absorbed power under posture *P1* and lower absorbed power under posture *P2*. The analysis of the mean total absorbed power also revealed significant two-way interactions between all the main factors, except with the handle diameter. The handle diameter shows non-significant interactions with the excitation magnitude, grip and push forces. The only significant interaction of the handle size is observed with the hand-arm posture. This is consistent with the trends observed in the mean data presented in previous sections. Moreover, the influence of handle size depends on the hand arm posture, suggesting coupling between two factors.

The ANOVA analysis has also been repeated for each posture separately. The results obtained for both analyses, however, were observed to be comparable. The results for both postures suggest strong statistical significance for all main factors, including the handle size. The results also show strong two-way interactions between all the main factors with the exception of the handle size and hand forces for both postures. Table 5.6

219

summarizes the multi-factor ANOVA results of the total mean absorbed power for each

posture and both hand-arm postures.

Table 5.6: Statistical significance factor ($p$) of various contributory factors of the mean total absorbed power under $z_h$-axis vibration.

| Factors | Both postures | P1 | P2 |
|---------|---------------|-----|-----|
| $F_g$ | 00 | 00 | 00 |
| $F_p$ | 00 | 00 | 00 |
| $D$ | .74 | 00 | 00 |
| $A$ | 00 | 00 | 00 |
| $P$ | 00 | - | - |
| $F_g * F_p$ | .03 | 00 | 00 |
| $F_g * D$ | .80 | .49 | .28 |
| $F_g * A$ | 00 | 00 | 00 |
| $F_g * P$ | 00 | - | - |
| $F_p * D$ | .52 | .07 | .08 |
| $F_p * A$ | 00 | 00 | 00 |
| $F_g * P$ | 00 | - | - |
| $D * A$ | .52 | 00 | 00 |
| $D * P$ | 00 | - | - |
| $P * A$ | 00 | - | - |

Multifactor ANOVA was further performed on the mean absorbed power response of

seven subjects corresponding to one-third octave frequency bands to examine the

statistical significance of the considered parameters in different frequency bands. Table

5.7 summarizes the results of the statistical analysis of the mean absorbed power

measured under $z_h$-axis vibration, where a factor associated with a $p$ value of less than

0.05 is considered to be statistically significant. The Table summarizes the significance

analysis of the main factors as well as the two-way interactions between these factors.

The excitation level shows strong significance in view of the mean absorbed power in all

the frequency bands, which can also be observed clearly in Figure 5.4 and 5.5. Handle

size reveals non-significant effect on the mean absorbed power in the frequency bands

lower than 80 Hz, where most of the absorbed power occurs (Table 5.5). This is

Table 5.7: Statistical significance factor ($p$) of various contributory factors in view of the mean absorbed power over one-third octave frequency bands under $z_h$-axis vibration.

Significance Level ($p$)

| Factors / Frequency (Hz) | Fg | Fp | D | A | P | Fg*Fp | Fg*D | Fg*A | Fg*P | Fp*D | Fp*A | Fp*P | D*A | D*P | A*P |
|---|---|---|---|---|---|---|---|---|---|---|---|---|---|---|---|
| 8 | .95 | .21 | .97 | .00 | .00 | .28 | .30 | .61 | .16 | .71 | .01 | .00 | .88 | .00 | .00 |
| 10 | .82 | .05 | .88 | .00 | .00 | .79 | .91 | .54 | .00 | .92 | .00 | .00 | .57 | .00 | .00 |
| 12.5 | .33 | .04 | .96 | .00 | .00 | .28 | .72 | .08 | .00 | .37 | .00 | .00 | .53 | .00 | .00 |
| 16 | .10 | .03 | .89 | .00 | .00 | .41 | .59 | .02 | .00 | .92 | .01 | .00 | .68 | .00 | .00 |
| 20 | .01 | .09 | .90 | .00 | .00 | .28 | .59 | .00 | .00 | .96 | .08 | .00 | .91 | .00 | .00 |
| 25 | .00 | .02 | .72 | .00 | .00 | .03 | .91 | .00 | .00 | .94 | .02 | .00 | .19 | .00 | .01 |
| 31.5 | .00 | .00 | .65 | .00 | .00 | .00 | .67 | .00 | .00 | .49 | .00 | .00 | .09 | .00 | .00 |
| 40 | .00 | .00 | .55 | .00 | .00 | .04 | .27 | .00 | .19 | .02 | .00 | .00 | .07 | .00 | .00 |
| 50 | .00 | .00 | .60 | .00 | .00 | .29 | .35 | .00 | .03 | .01 | .00 | .04 | .23 | .00 | .00 |
| 63 | .00 | .00 | .66 | .00 | .00 | .03 | .77 | .00 | .00 | .01 | .00 | .00 | .43 | .00 | .00 |
| 80 | .12 | .00 | .12 | .00 | .00 | .27 | .69 | .09 | .00 | .73 | .00 | .00 | .00 | .01 | .00 |
| 100 | .04 | .00 | .04 | .00 | .00 | .00 | .04 | .00 | .00 | .09 | .00 | .00 | .00 | .00 | .00 |
| 125 | .00 | .00 | .02 | .00 | .00 | .00 | .05 | .00 | .33 | .36 | .00 | .00 | .00 | .00 | .00 |
| 160 | .00 | .00 | .00 | .00 | .01 | .93 | .94 | .00 | .54 | .03 | .00 | .05 | .00 | .00 | .00 |
| 200 | .00 | .00 | .00 | .00 | .00 | .98 | .73 | .00 | .34 | .00 | .00 | .27 | .00 | .00 | .00 |
| 250 | .00 | .00 | .00 | .00 | .05 | .67 | .25 | .00 | .89 | .06 | .00 | .23 | .00 | .00 | .01 |
| 315 | .00 | .00 | .00 | .00 | .09 | .95 | .09 | .00 | .72 | .40 | .00 | .42 | .00 | .00 | .01 |
| 400 | .00 | .01 | .00 | .00 | .90 | .77 | .22 | .00 | .58 | .65 | .00 | .89 | .00 | .00 | .51 |
| 500 | .00 | .03 | .00 | .00 | .39 | .67 | .00 | .00 | .09 | .11 | .00 | .66 | .00 | .00 | .02 |
| 630 | .00 | .11 | .00 | .00 | .23 | .74 | .00 | .00 | 1.00 | .30 | .00 | .58 | .00 | .00 | .01 |
| 800 | .00 | .43 | .00 | .00 | .64 | .76 | .00 | .00 | .59 | .55 | .02 | .56 | .00 | .00 | .25 |
| 1000 | .00 | .91 | .00 | .00 | .07 | .91 | .00 | .00 | .14 | .57 | .84 | .75 | .00 | .11 | .00 |

221

consistent with the ANOVA results of the mean total absorbed power, since the influence of handle size yields an opposing effect to that of the hand-arm posture (Figure 5.10). Hand forces show strong significance on the mean absorbed power in the majority of the frequency bands with the exception of lower frequency bands for both the grip and push forces and in the higher bands (630 Hz and above) for the push force. The hand-arm posture shows strong significance in view of the mean absorbed power in the relatively low frequency bands (200 Hz and lower), which can also be observed in Figure 5.9.

The excitation level ($A$) shows statistically significant interactions with hand forces in most of the frequency bands considered, with the exception of very low frequency bands (12.5 Hz or lower), and in the 20 and 1000 Hz bands with push and grip forces, respectively. The excitation level also reveals significant interaction with the hand-arm posture in nearly all the frequency bands, and non-significant interactions with the handle size in the frequency bands lower than 40 Hz. The hand-arm posture shows clear interactions with the grip and push forces, particularly in the low frequency bands, which confirms with the trends observed in Figures 5.11 and 5.12. The hand-arm posture also shows strong interactions with handle size, which is consistent with the conclusions derived from Figure 5.10 and Table 5.3, where the influence of handle size is affected by the hand-arm posture.

In an attempt to verify the influence of hand-arm posture and its conjunctions with other contributory factors, independent statistical analyses are performed for the two postures. The analyses included two levels of excitation ($A$: 2.5 and 5.0 m/s$^2$), three levels of handle diameter ($D$: 30, 40 and 50 mm), three levels of push force ($F_p$: 25, 50 and 75 N) and three levels of grip force ($F_g$: 10, 30 and 50 N). The results presented in Table

5.10 clearly show relatively higher significance of the hand forces for posture $P2$ than those observed under posture $P1$. This is specifically observed in the low frequency bands, where most of the power is absorbed by the hand arm system, which confirms the trends observed in Figures 5.12 to 5.15. The influence of handle size appears to be stronger under $P1$ posture than that under $P2$ posture, which is also observed in Figure 5.10 and Table 5.3.

Table 5.8: Results attained from independent statistical analysis for the two postures-significance factor ($p$) of the mean absorbed power in the one-third octave frequency bands for $z_h$-axis under vibration.

| Factors | A | | D | | $F_g$ | | $F_p$ | |
|---|---|---|---|---|---|---|---|---|
| Posture | P1 | P2 | P1 | P2 | P1 | P2 | P1 | P2 |
| Frequency (Hz) | | | | Significance Level | | | | |
| 8 | 00 | 00 | 00 | .14 | .22 | .38 | .07 | 00 |
| 10 | 00 | 00 | 00 | 00 | .01 | .01 | .74 | 00 |
| 13 | 00 | 00 | 00 | .02 | .02 | 00 | .05 | 00 |
| 16 | 00 | 00 | 00 | .01 | .06 | 00 | .18 | 00 |
| 20 | 00 | 00 | 00 | .01 | .14 | 00 | .27 | 00 |
| 25 | 00 | 00 | 00 | .01 | .42 | 00 | .16 | 00 |
| 32 | 00 | 00 | 00 | 00 | 00 | 00 | .22 | 00 |
| 40 | 00 | 00 | .04 | .03 | 00 | 00 | 00 | 00 |
| 50 | 00 | 00 | .08 | .06 | 00 | 00 | 00 | 00 |
| 63 | 00 | 00 | .73 | .03 | 00 | 00 | 00 | 00 |
| 80 | 00 | 00 | .11 | .06 | .01 | .95 | 00 | 00 |
| 100 | 00 | 00 | .03 | .10 | .02 | .14 | 00 | 00 |
| 125 | 00 | 00 | 00 | .31 | 00 | 00 | 00 | 00 |
| 160 | 00 | 00 | 00 | .92 | 00 | 00 | 00 | 00 |
| 200 | 00 | 00 | 00 | .44 | 00 | 00 | 00 | 00 |
| 250 | 00 | 00 | 00 | .23 | 00 | 00 | 00 | 00 |
| 315 | 00 | 00 | 00 | .03 | 00 | 00 | .02 | .03 |
| 400 | 00 | 00 | 00 | .03 | 00 | 00 | .15 | .03 |
| 500 | 00 | 00 | 00 | 00 | 00 | 00 | .17 | .16 |
| 630 | 00 | 00 | 00 | 00 | 00 | 00 | .32 | .25 |
| 800 | 00 | 00 | 00 | 00 | 00 | 00 | .60 | .74 |
| 1000 | 00 | 00 | 00 | 00 | .01 | 00 | .99 | .83 |

## 5.4 Characterization of Power Absorption under $x_h$- axis

The data acquired under $x_h$-axis vibration are also analyzed to derive the biodynamic response of the hand-arm system exposed to $x_h$-axis vibration in terms of absorbed power. The absorbed power responses are evaluated in the 8-1000 Hz frequency range, under different combinations of experimental conditions involving variations in hand forces, hand-arm posture and excitations magnitude. Mean responses within the one-third octave frequency bands together with the total power are analyzed to identify important trends in view of the various factors considered.

### 5.4.1 Inter-subject variability

Despite the strong dependence of the biodynamic response in terms of absorbed power upon individual differences (Burström and Lundström, 1989; 1994), the inter-subject variability of the measured absorbed power data has not been reported in the literature. The comparisons of absorbed power responses of individual subjects exposed to vibration along $x_h$-axis, obtained in this study and illustrated in Figure 5.20, suggest significant scatter in the data, as it was observed in the data acquired under $z_h$-axis vibration. The figure shows the responses corresponding to 30N grip ($F_g$) and 50N push ($F_p$) force, and 2.5 and 5 m/s$^2$ excitation levels, while grasping the 40 mm handle with $P1$ posture. Despite the considerable scatter in the $DPMI$ and absorbed power data obtained for the individuals, the measured data reveal consistent trends in the 8-1000 Hz frequency range. The absorbed power data obtained for all subjects show peaks in the 20-32 Hz and 100-160 Hz bands, which are comparable to those reported by Bylun and Burström (2003). Both the $DPMI$ (chapter 4) and absorbed power responses thus reveal comparable trends in view of the frequency ranges of the dominant responses.

(a)                                                                 (b)
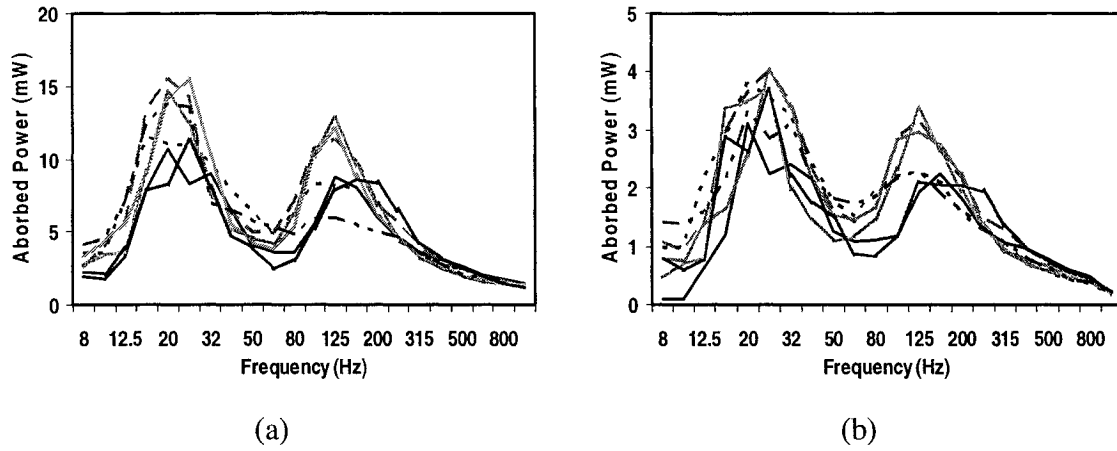
Figure 5.20: Comparisons of absorbed power responses of the hand-arm system exposed to $x_h$-axis vibration obtained for seven subjects: (a) $a_{h,w}=5$ m/s$^2$ ; and (b) $a_{h,w}=2.5$ m/s$^2$ ($D=40$ mm , $F_g=30$ N, $F_p=50$ N and posture $P1$).

Figure 5.21 illustrates the coefficients of variations (COV) of the mean absorbed power response, corresponding to center frequencies of the one-third octave bands for the 40 mm handle, under posture $P1$, two levels of excitation magnitude and three different combinations of the grip/push forces; (10/25, 30/50 and 50/50). The variations in the absorbed power are less than 20 % in the frequency bands above 125 Hz and tend to be higher in lower bands. The magnitude of COV increases as the hand forces increase and approaches 35 % in the 8 Hz frequency band under $F_g=10$ N and $F_p=25$ N. The absorbed power responses reveal relatively higher variability, around 30% in the 50-125 Hz frequency range. The COV values approach as high as 55% at low frequencies under relatively high hand forces, $F_g=30$ N and $F_p=50$ N under 2.5 m/s$^2$ excitation level, as shown in Figure 5.21.
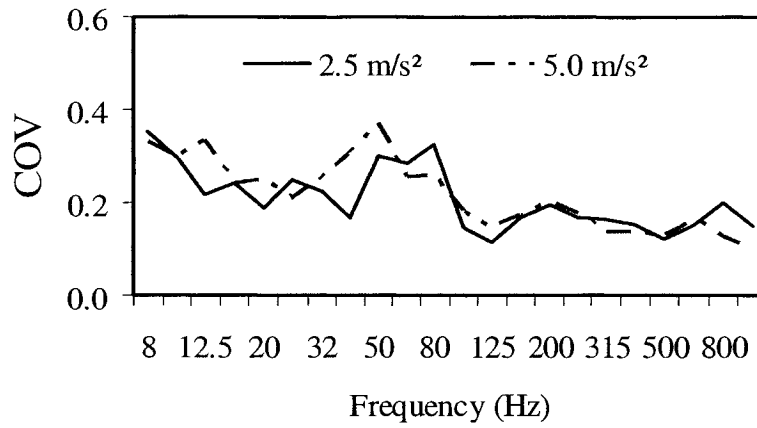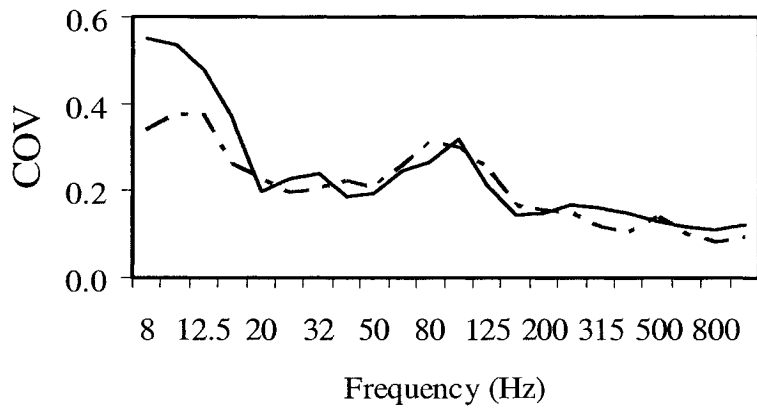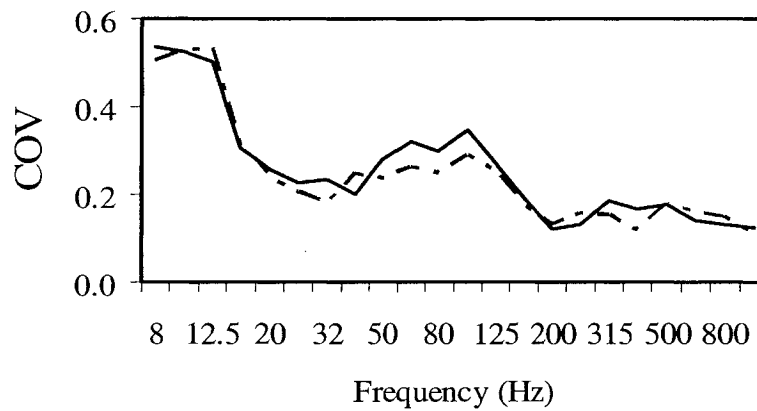
Figure 5.21: Coefficients of variations of the absorbed power attained under two levels of excitations and three levels of $F_g/F_p$ combinations, ($D$= 40 mm): (a) 10/25 N; (b) 30/50 N; and (c) 50/50 N.

226

The COV values for both the measures decline to around 10% at higher frequencies, irrespective of hand forces and vibration levels. Such variations may be partly attributed to individual's differences in view of the hand-arm structure. The data acquired with the other handles (30 and 50 mm) also revealed similar levels of peak standard errors. The COV values tend to be considerably smaller, when the total absorbed power of the hand-arm system is considered, as shown in Figure 5.22, as it was observed from the $z_h$-axis response. The figure illustrates the COV of the mean total absorbed power for all combinations of hand forces, two vibration levels, $P1$ posture and 40 mm handle.
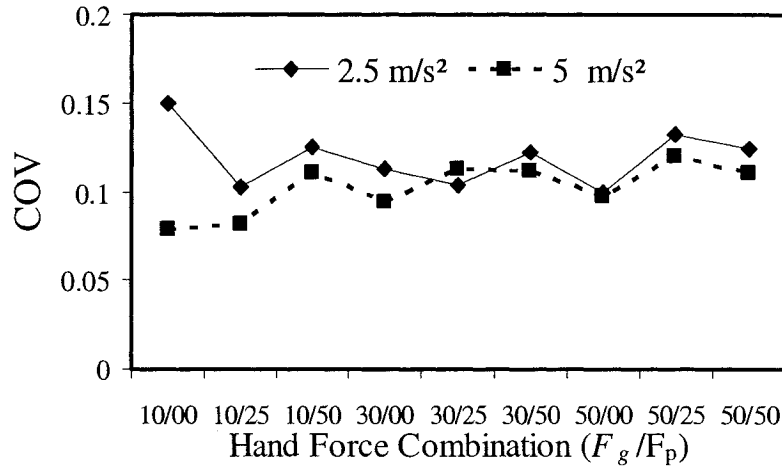


Figure 5.22: Coefficients of variation (COV) of the total absorbed power evaluated for nine different hand forces combinations, $P1$ posture and two excitation levels ($D$= 40 mm).

5.4.2   Influence of vibration magnitude on absorbed power under $x_h$-axis

The data acquired under $x_h$-axis vibration with two different vibration magnitudes ($a_{h,w}$= 2.5 and 5 m/s$^2$) are examined to investigate the influence of vibration magnitude on the absorbed power responses. Figure 5.23 illustrates the mean absorbed power responses of seven subjects, under different grip/push force combinations for the 40 mm handle and posture $P1$ with 90° elbow flexion. An increase in the weighted vibration magnitude from

2.5 m/s² to 5 m/s², results in nearly four-fold increase in the absorbed power as it was observed in the absorbed power response to $z_h$-axis vibration. The response show two peaks in the absorbed power response in the 16-25 and 63-160 Hz bands. The magnitudes of both and the corresponding frequencies increase with increasing grip/push forces.
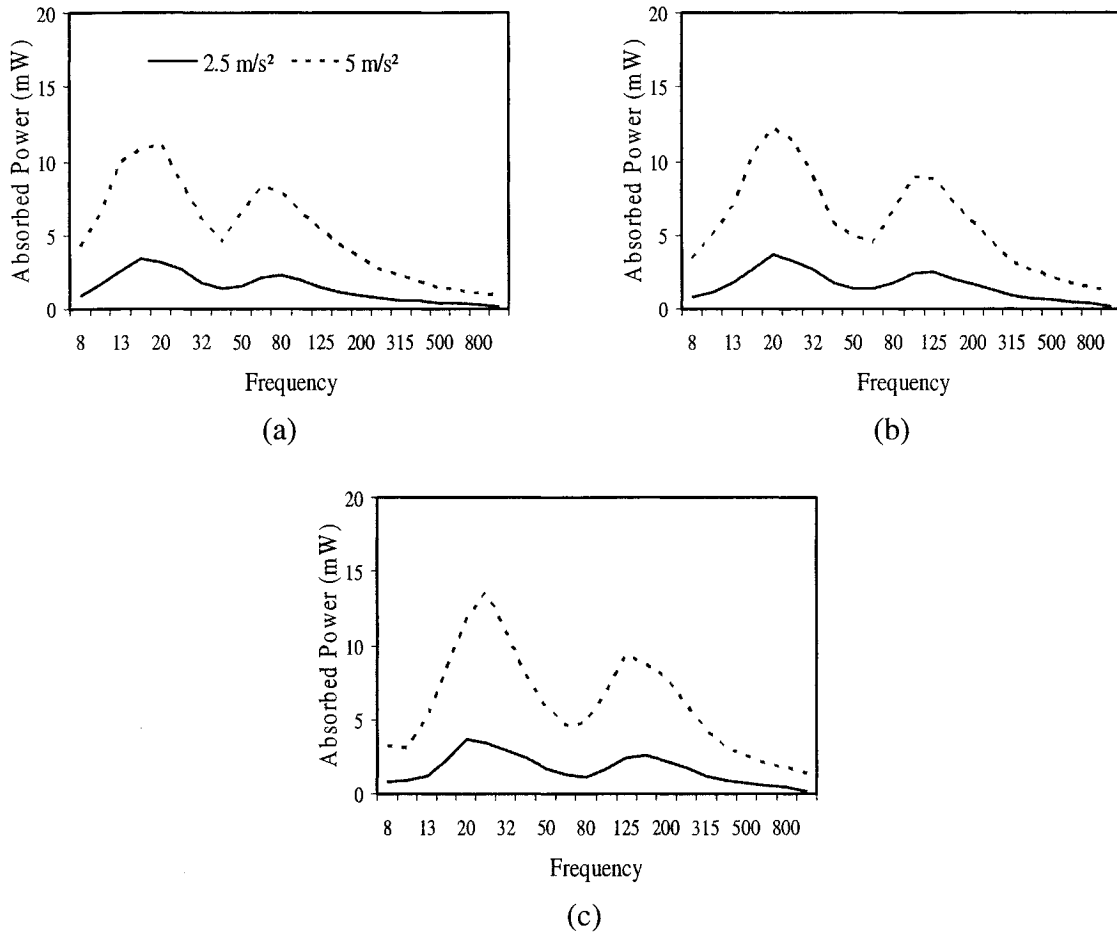


Figure 5.23: Influence of excitation magnitude on absorbed power response to $x_h$-axis vibration under different $F_g/F_p$ combinations: (a) 10/00; (b) 30/25: and (c) 50/50 ($D$= 40 mm, $P1$ posture).

Similar trends were observed with $z_h$-axis vibration. Both vibration axes under posture $P1$ exhibit two absorbed power peaks, while the peaks under $x_h$-axis occur at 16-25 and 63-160 Hz bands, the peaks under $z_h$-axis vibration happen at 10-16 and 31.5-50 Hz. Both absorbed peaks under $x_h$-axis vibration are related to the frequencies of $DPMI$

magnitude peaks, whereas the second power peaks under $z_h$-axis vibration related to the frequency of *DPMI* magnitude peak. On the other hand, the absorbed power under $z_h$-axis vibration is approximately four times or even higher for the same test conditions than that under $x_h$-axis vibration.

### 5.4.3 Influence of handle size on absorbed power under $x_h$-axis

Figure 5.24 illustrates the mean absorbed power response spectra to $x_h$-axis vibration obtained with three different handle sizes under two levels of vibration; $a_{h,w}$=2.5 and 5 m/s$^2$, and under 30 N grip and 50 N push forces, and posture *P1*. The handle size effect on the absorbed power at frequencies above 250 Hz is very small due to low velocity at the driving–point in this frequency range. In general, the larger diameter handles yield higher *DPMI* magnitude and slightly larger absorbed power at higher frequencies. A larger handle diameter also yields higher observed power peak in the 20-25 Hz bands. An opposite trend, however, is observed in the 63-200 Hz frequency range, where the effect on the magnitude is relatively small. The smaller handle (30 mm diameter) yields slightly higher *DPMI* magnitude and the absorbed power in this frequency range, as evident in the Figure. Unlike the *DPMI* magnitude response (chapter 4), a larger handle causes higher power absorption at low frequencies, in the vicinity of the fundamental peak response, but yields lower magnitude of the second peak occurring in the 125-160 Hz bands. The same trends were also observed from the data acquired under different grip/push force combinations.
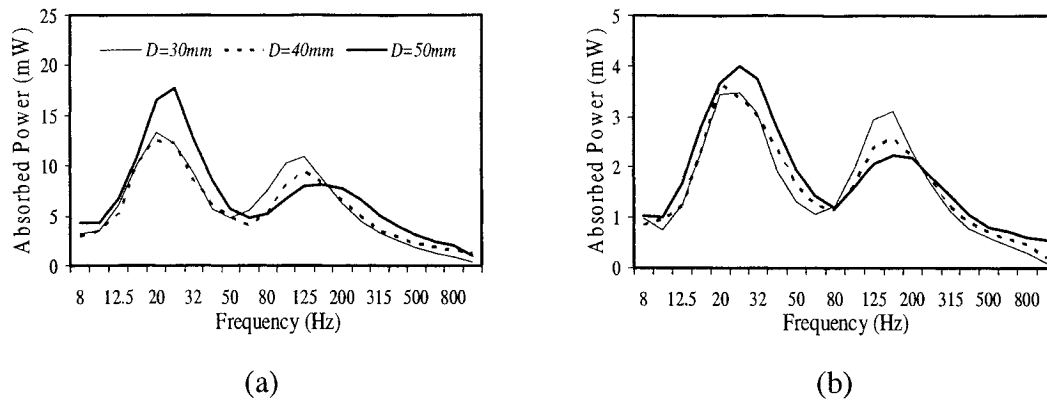
Figure 5.24: Influence of handle size on the mean absorbed power response spectra: (a) $a_{h,w} = 2.5$ m/s$^2$; and (b) $a_{h,w} = 5$ m/s$^2$, ($F_g$=30 N, $F_p$=50 N and posture $P1$).

The influence of handle size on the absorbed power is further investigated in terms of the mean total power. The magnitudes of total power absorbed into the hand-arm system obtained for the 40 mm and 50 mm handles, corresponding to each excitation level and hand force combination, are normalized with respect to that measured for the 30 mm handle under the same excitation and hand force combination. The values obtained for all hand force combinations are applied to derive the mean total power and thus the overall normalized total absorbed power and its standard deviation (SD). The relatively low SD could indicate the negligible effect of the hand force combination on the ratios of the absorbed power for different handle sizes, as evident in Table 5.9. Increasing the handle size from 30 to 40 mm yields little or no effect on the mean total absorbed power, while a further increase in the handle size to 50 mm yields 10 % to 15 % higher values.

Table 5.9: Mean and standard deviation of the total absorbed power measured with 40 and 50 mm handles normalized to that measured with the 30 mm handle ($P1$ posture).

| $D$ (mm) | Normalized total power (Mean; Standard deviation) | |
|---|---|---|
| | $a_{h,w} = 5$ m/s$^2$ | $a_{h,w} = 2.5$ m/s$^2$ |
| 40 | .969; .024 | .977; .015 |
| 50 | 1.155; .026 | 1.101; .026 |

230

## 5.4.4 Influence of hand-arm posture on power absorption under $x_h$-axis

Two different hand-arm postures $P1$ and $P2$, involving 90° and 180° elbow flexion, respectively, were considered in order to investigate the influence of hand-arm posture on the absorbed power by the hand-arm system exposed to vibration along the $x_h$-axis. Figure 5.25 shows the mean absorbed power responses obtained, while the subjects grasped the 40 mm handle under 5 m/s² rms acceleration excitation, and two different $F_g/F_p$ combinations; 10/25 and 30/5. The figures compare the responses obtained with the two hand-arm postures, $P1$ and $P2$. The results show negligible effect of the posture on the absorbed power response at frequencies above 32 Hz. The stretched forearm posture ($P2$) yields considerably higher absorbed power at bands centered below 40 Hz. Relatively higher effect on the absorbed power over $DPMI$ response (section 4.3.5) is attributed to higher excitation velocity at low frequencies coupled with slightly higher $DPMI$ magnitude. This particular posture causes enhanced static coupling between the hand and the handle, which could be observed from its high apparent mass response at very low frequencies (Figure 4.14).



(a)                                      (b)
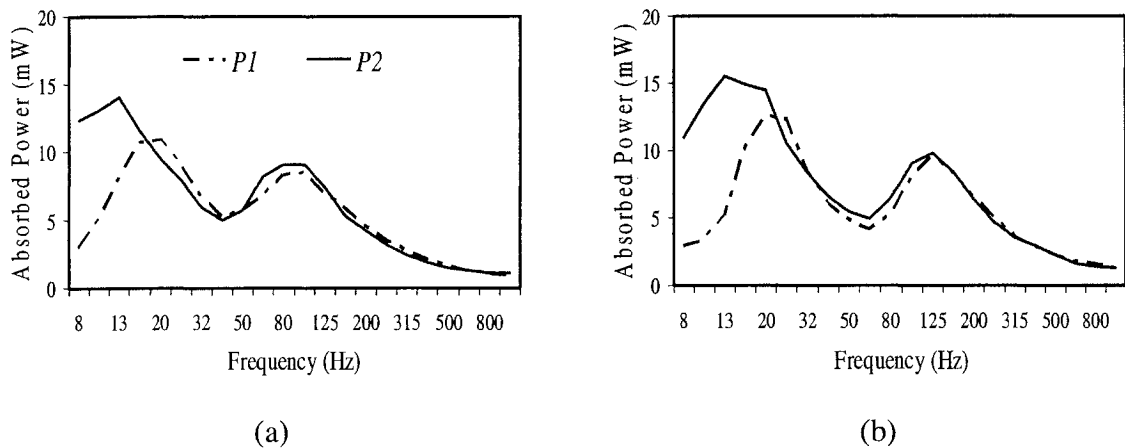
Figure 5.25: Influence of hand-arm posture on mean absorbed power under two different $F_g/F_p$ combinations: (a) 10/25; and (b) 30/50 ($D$= 40 mm, $a_{h,w}$ = 5 m/s²).

The influence of the hand-arm posture is further evaluated by comparing the mean total absorbed power values obtained for each posture, excitation level, handle size and $F_g/F_p$ force combination. The values computed for the posture *P2* are normalized with respect to those attained for posture *P1*, corresponding to particular excitation, handle size and the grip/push force combination. The resulting ratios, summarized in Table 5.10, describe the amplification of total power for posture *P2* with reference to the power associated with posture *P1*.

Table 5.10: Ratio of total mean absorbed power under *P2* posture to that under *P1* posture for the three handles, nine $F_g$ / $F_p$ combinations and the two vibration levels.

| $a_{h,w}$ (m/s²) | 2.5 | | | 5 | | |
|---|---|---|---|---|---|---|
| *D* (mm) | 30 | 40 | 50 | 30 | 40 | 50 |
| $F_g/F_p$ (N) | Absorbed Power Ratio | | | | | |
| 10/00 | 1.00 | .98 | .93 | 1.00 | .98 | .99 |
| 10/25 | 1.15 | 1.15 | 1.09 | 1.09 | 1.17 | 1.13 |
| 10/50 | 1.17 | 1.20 | 1.22 | 1.21 | 1.26 | 1.25 |
| 30/00 | 1.06 | 1.11 | 1.04 | 1.06 | 1.09 | 1.04 |
| 30/25 | 1.14 | 1.11 | 1.10 | 1.10 | 1.12 | 1.14 |
| 30/50 | 1.21 | 1.20 | 1.23 | 1.21 | 1.29 | 1.23 |
| 50/00 | 1.12 | 1.17 | 1.07 | 1.11 | 1.13 | 1.17 |
| 50/25 | 1.15 | 1.14 | 1.16 | 1.17 | 1.12 | 1.18 |
| 50/50 | 1.21 | 1.22 | 1.22 | 1.22 | 1.23 | 1.30 |

The results show that grasping the vibrating handle with posture *P2*, in general, yields higher power absorbed into the hand-arm system except in the absence of the push force and light grip force ($F_g$=10 N and $F_p$=0 N), where the ratios are close to unity, irrespective of the handle size and the excitation level. The amplification ratio tends to increase with increasing grip/push forces, suggesting stronger contribution due to increasing push force. Linear regression analyses performed between the absorbed power ratio and the coupling force (summation of push and grip forces) revealed relatively

strong correlation ($r^2$ values of .79 and .81 under $a_{h,w}$=2.5 m/s$^2$, and .86 and .84 under

$a_{h,w}$=5 m/s$^2$, for the 30 and 50 mm diameter handles, respectively), while weaker

correlations were found for the 40 mm handle ($r^2$ values of .67 and .57 under 2.5 and 5

m/s$^2$ excitations), as can be seen in Figure 5.26.
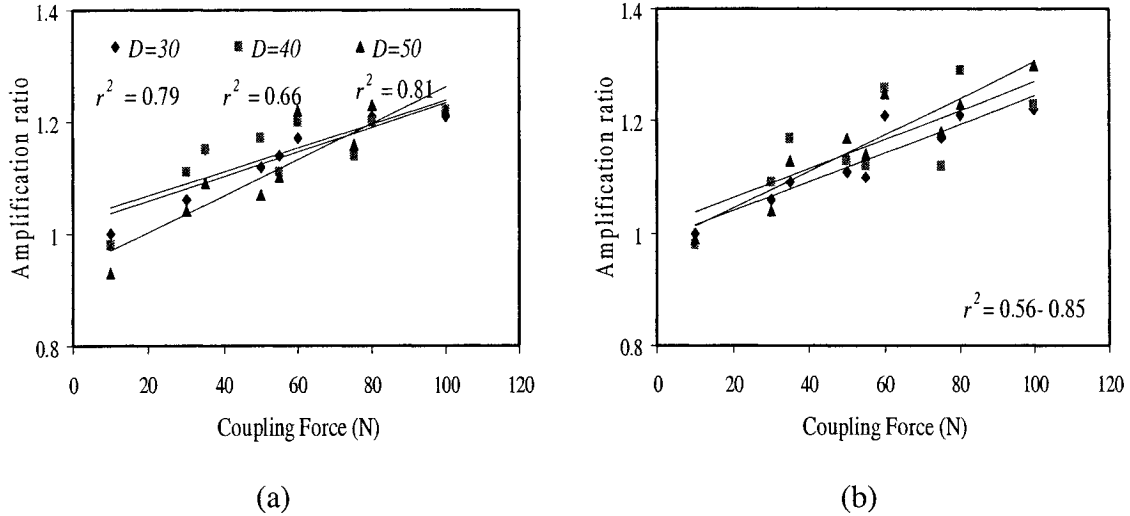


Figure 5.26: Correlation between amplification ratio ($P2/P1$) of total absorbed power and coupling force for three different handles: (a) $a_{h,w}$= 2.5 m/s$^2$; and (b) $a_{h,w}$= 5 m/s$^2$.

## 5.4.5 Influence of hand forces on absorbed power under $x_h$-axis

The influence of variations in the push and grip forces on the mean measured

absorbed power response of the hand-arm system in one-third octave frequency bands

under exposure to excitation level of 5 m/s$^2$ along the $x_h$-axis, while grasping the 40 mm

handle, is shown in Figures 5.27 and 5.28, respectively. An increase in the push or the

grip force tends to shift the absorbed power peaks towards a higher frequency, while the

influence of hand forces, particularly the push force, in the low frequency region (lower

than 100 Hz), is very small (Figure 5.27). The influence of push and grip force is more

evident on the magnitude of first peak occurring in the 12.5 Hz band under posture P2 than that observed for the posture P1 as it is evident from the figures.

For P1 posture, an increase in the push force (grip force held constant, i.e., $F_g = 30$ N) yields higher absorbed power, specifically at frequencies above 100 Hz, as evident in the figures. A lower push relents to only slight variations in power in the 16-40 Hz bands with no definite trend. Similar trends in the absorbed power above 100 Hz are also observed for posture P2. Higher hand forces (50 N) coupled with posture P2, however, cause higher energy dissipation at frequencies below 32 Hz. An increase in the grip force (constant push force, $F_p = 50$N) yields only a slight increase in the absorbed powers. A clear tendency in the absorbed power at low frequency could not be observed as in the case of push force. The data attained for the other handles (30 and 50 mm) also revealed similar tendencies in view of the hand force variations.



(a)                                              (b)
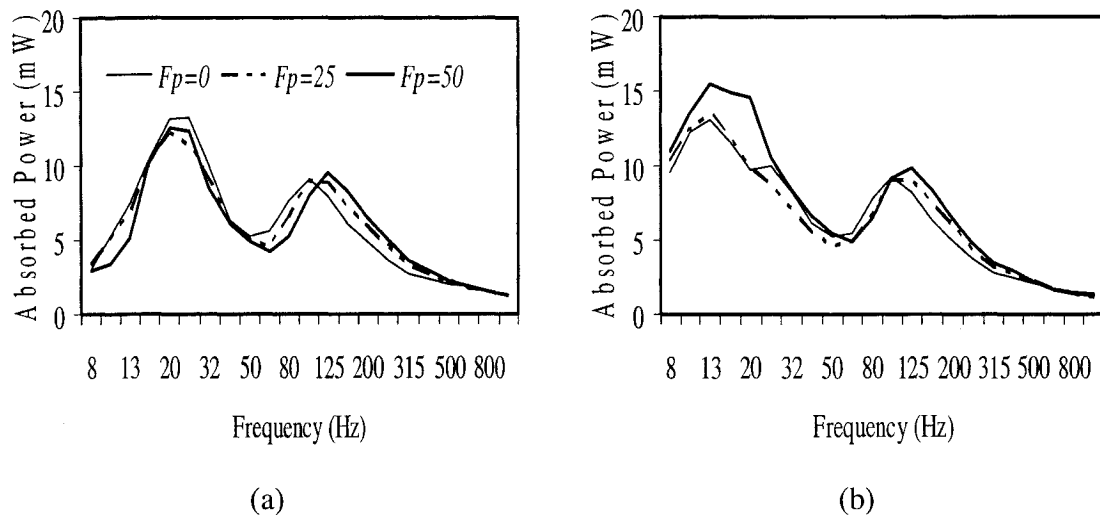
Figure 5.27: Effect of variations in push force ($F_p$) on the mean absorbed power under two postures: (a) Posture P1 force; and (b) Posture P2 force ($D= 40$ mm, $F_g=30$ N and $a_{h,w} =5$ m/s$^2$).
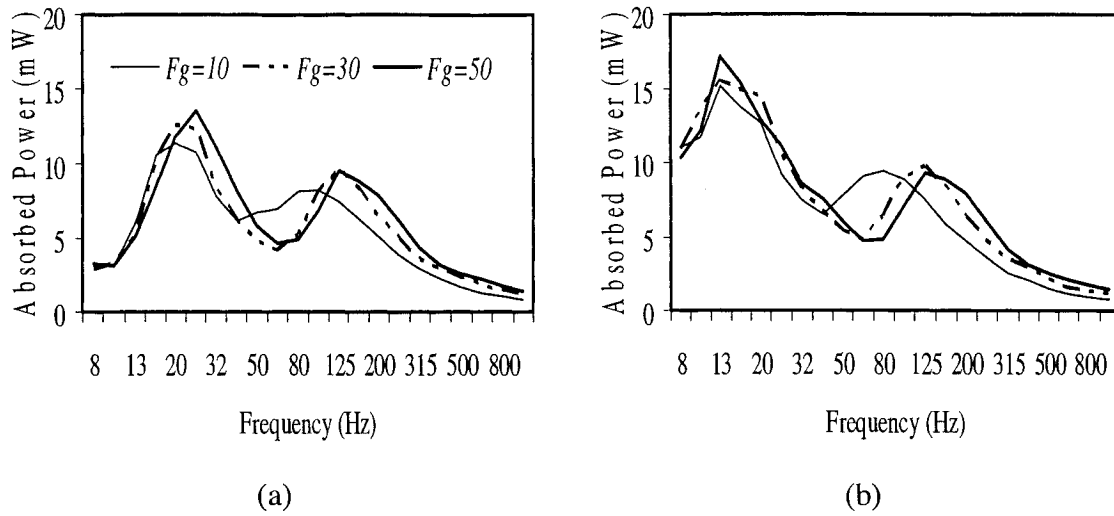
Figure 5.28: Effect of variations in grip force ($F_g$) on the mean absorbed power under two postures: (a) Posture *P1* force; and (b) Posture *P2* force ($D$= 40 mm, $F_p$=50 N and $a_{h,w}$ =5 m/s$^2$).

Owing to the lack of definite trends caused by variations in the hand forces in the spectra of the absorbed power, the influence of variations of hand forces is further attempted in term of the mean total absorbed power, computed through summation of power values within each one-third octave band. Figure 5.29 and Figure 5.30 illustrate the influence of push and grip forces on the mean total absorbed power for the 50 mm handle and the two hand-arm postures, respectively, under high vibration spectra ($a_{h,w}$ = 5 m/s$^2$). As it is evident from the figures, the influence of hand forces on the mean total absorbed power depends upon the hand-arm posture. Under posture *P1*, the variations in the push force cause only small variations in the total absorbed power, while a higher grip force causes slightly higher energy absorption. The response under *P2* posture with 180° elbow flexion, on the other hand, causes considerable increase in the absorbed power with increase in either hand force suggesting a higher coupling between the handle and the hand-arm system exposed to vibration along $x_h$-axis. Similar variations in the total absorbed power were also observed under vibration along $z_h$-axis.
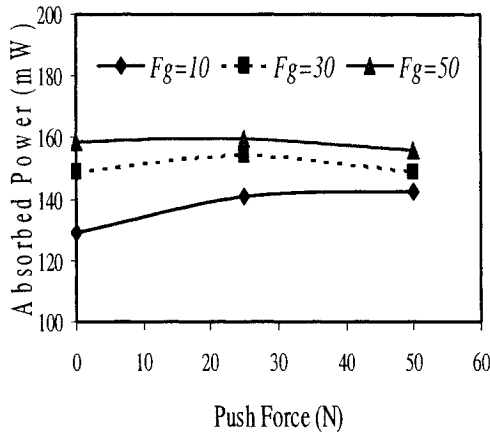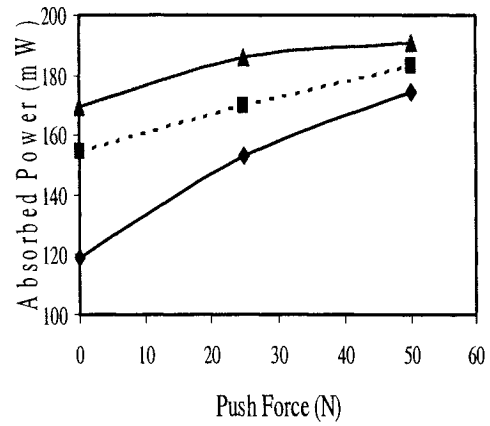
Figure 5.29: The influence of variations in the push force ($F_p$) on the mean total absorbed power: (a) posture $P1$; and (b) posture $P2$ ($D$= 50 mm, $a_{h,w}$=5.0 m/s$^2$).
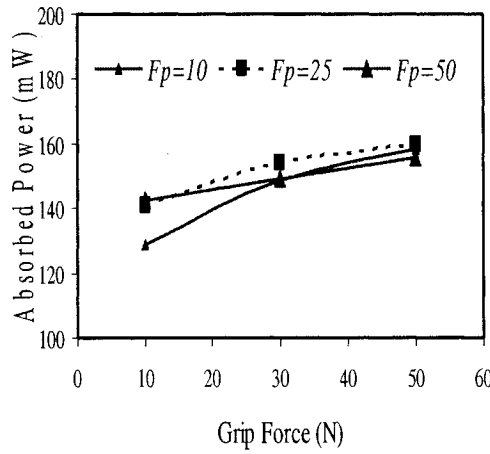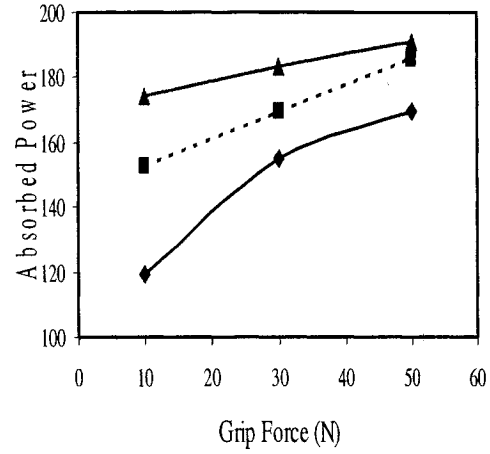


Figure 5.30: The influence of variations in the grip force ($F_g$) on the mean total absorbed power: (a) posture $P1$; and (b) posture $P2$ ($D$= 50 mm, $a_{h,w}$= 5.0 m/s$^2$).

To further clarify the association between the hand forces and the absorbed power under two different postures ($P1$ and $P2$) considered in this study, linear regressions were performed between the coupling force ($F_p$ + $F_g$) and the absorbed power for the three handles and two vibration levels. Higher linear correlation factors were found between

236

the coupling force and the absorbed power under the *P2* posture (.77 to .89) than under the *P1* posture (.27 to .47). Figure 5.31 shows this relationship for the 50 mm handle corresponding to the two vibration levels and two postures.
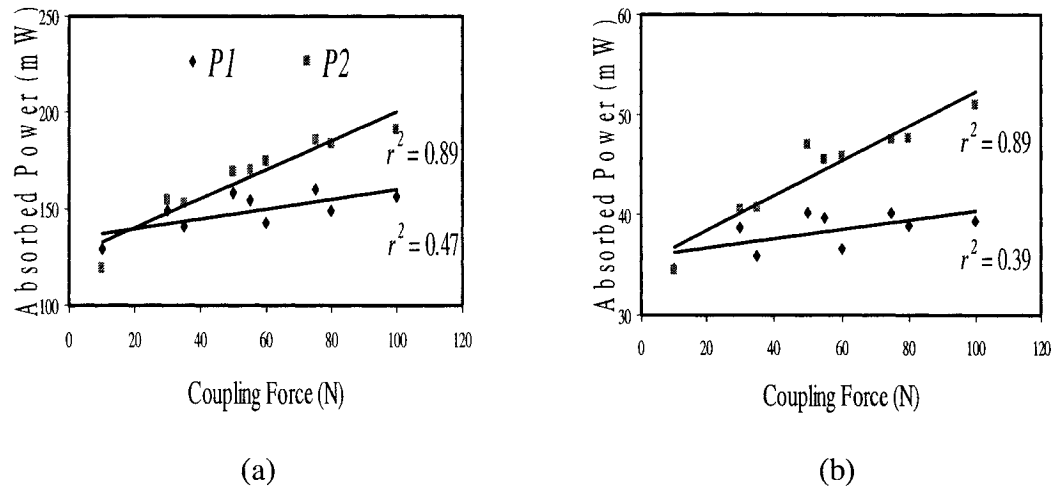


Figure 5.31: Variations in the total absorbed power with the coupling force for 50 mm handles and two postures: (a) $a_{h,w}$=2.5 m/s$^2$ ; and (b) $a_{h,w}$=5 m/s$^2$.

### 5.4.6 Role of excitation frequency in power absorption

The role of vibration frequency in power absorption is explored by analyzing the percentage of power absorbed within different frequency bands to that of the total absorbed power for the three cylindrical handles and different grip/push force combinations under two postures considered in this study, as described earlier in section 5.3.6 for the $z_h$-axis vibration. These portions could demonstrate the most important frequency range of vibration in view of the absorbed power. The absorbed power portions could further help in identifying an alternate and more effective frequency weighting function than that proposed in ISO-5349-1 (2001). The measured data are thus analyzed to derive the mean values of total absorbed power for each handle and hand force

combination under both excitation levels. Considering that the most of absorbed power occurs in the frequency range below 200 Hz, the analyses are limited to frequencies up to 200 Hz. The total absorbed power is further computed within three frequency bands (8-50 Hz, 8-100 Hz and 8-200 Hz) and normalized with respect to the total absorbed power over the entire frequency range for each handle size, excitation spectrum and grip/force combination, in order to study the relative proportions of absorbed power in these low frequency bands.

The mean values of the proportions of the absorbed power within the selected frequency bands together with the standard deviations are summarized in Table 5.11, as a function of the hand force combination, for both excitation spectra and all three handle sizes. The proportions of the total absorbed power in the selected frequency bands do not vary considerably with either the handle diameter or the vibration magnitude, as evident from the relatively low standard deviation values. The proportions, however, show some variations with the grip and push force combinations, while a clear trend is not evident. The results show that 54 to 60% and 60 to 63%, of the total power is dissipated in the 8-50 Hz frequency range for postures *P1* and *P2*, respectively, irrespective of the excitation magnitude, handle size and hand forces. The proportions of the absorbed power increase with increase in the frequency range and reach 65 to 79% and 72-80% of total power dissipated in the 8-100 Hz frequency range under postures *P1* and *P2*, respectively. For the 8-200 Hz range, the ratio of absorbed power to the total absorbed power varies from 84 to 91%, while the relative difference between the absorbed power proportions for the two considered postures becomes smaller.

Table 5.11: Mean and standard deviation of the proportion of absorbed power in three frequency ranges, as a function of the hand force combination.

| Frequency range | 8-50 Hz | | | | 8-100 Hz | | | | 8-200 Hz | | | |
|---|---|---|---|---|---|---|---|---|---|---|---|---|
| Posture | *P1* | | *P2* | | *P1* | | *P2* | | *P1* | | *P2* | |
| *Fg/Fp* (N) | Mean | SD | Mean | SD | Mean | SD | Mean | SD | Mean | SD | Mean | SD |
| 10/00 | .60 | .02 | .60 | .01 | .79 | .01 | .79 | .02 | .91 | .01 | .91 | .01 |
| 10/25 | .56 | .02 | .62 | .02 | .75 | .02 | .80 | .02 | .90 | .02 | .92 | .01 |
| 10/50 | .55 | .01 | .63 | .02 | .74 | .03 | .81 | .01 | .89 | .02 | .92 | .01 |
| 30/00 | .58 | .03 | .61 | .02 | .73 | .01 | .75 | .01 | .89 | .01 | .90 | .01 |
| 30/25 | .55 | .03 | .61 | .03 | .70 | .01 | .74 | .01 | .87 | .02 | .89 | .01 |
| 30/50 | .54 | .03 | .63 | .02 | .68 | .01 | .74 | .01 | .86 | .02 | .90 | .02 |
| 50/00 | .56 | .03 | .62 | .02 | .70 | .01 | .73 | .01 | .87 | .01 | .89 | .01 |
| 50/25 | .55 | .03 | .62 | .03 | .68 | .01 | .72 | .01 | .86 | .01 | .88 | .01 |
| 50/50 | .54 | .02 | .63 | .02 | .65 | .02 | .72 | .01 | .84 | .02 | .88 | .01 |

## 5.4.7 Statistical analysis ($x_h$-axis)

Multi-factor analysis of variance (ANOVA) has been carried out on the total absorbed power under $x_h$-axis vibration using the SPSS software. The main factors included the three nominal diameters of the handles ($D$: 30, 40 and 50 mm), three levels of push force ($F_p$: 0, 25 and 50), three levels of grip force ($F_g$: 10, 30 and 50 N), two excitation magnitudes ($A$: 2.5 and 5.0 m/s$^2$) and two hand-arm postures ($P$: *P1* and *P2*), based on the results of the preliminary analysis using Mauchly's test of sphericity. The ANOVA results of the mean total absorbed power revealed statical significance for all the considered factors. The analysis of the mean total absorbed power along $x_h$-axis also revealed significant two-way interactions between the considered factors with exception of the handle size, which shows non-significance with the hand forces and hand-arm posture. The ANOVA has been performed for the two postures independently; the results for the total mean absorbed power along $x_h$-axis reveal strong statistical significance for all factors under posture *P2*, while the push force shows non-significant influence under posture *P1*. This is consistent with the trends seen in Figure 5.29. The results also show

two-way interactions between all considered factors except between the handle size and

the grip force for the two postures and between push force and excitation level and

handle size under posture *P1*. Table 5.12 summarizes the multi-factor ANOVA results for

the total mean absorbed power, while considering each individual hand-arm posture, and

both postures.

Table 5.12: Statistical significance factor ($p$) of various contributory factors of the mean total absorbed power under $x_h$-axis vibration.

| Factors | Both postures | *P1* | *P2* |
|---------|---------------|------|------|
| $F_g$ | 00 | 00 | 00 |
| $F_p$ | 00 | .12 | 00 |
| $D$ | 00 | 00 | 00 |
| $A$ | 00 | 00 | 00 |
| $P$ | 00 | - | - |
| $F_g * F_p$ | 00 | 00 | 00 |
| $F_g * D$ | .17 | .05 | .28 |
| $F_g * A$ | 00 | 00 | 00 |
| $F_g * P$ | .01 | - | - |
| $F_p * D$ | .06 | .38 | .02 |
| $F_p * A$ | 00 | .14 | 00 |
| $F_g * P$ | 00 | - | - |
| $D * A$ | 00 | 00 | 00 |
| $D * P$ | .12 | - | - |
| $P * A$ | 00 | - | - |

Multifactor ANOVA was further performed on the mean absorbed power response of

seven subjects corresponding to one-third octave frequency bands to examine the

statistical significance of the considered parameters in different frequency bands. Table

5.13 summarizes the results of the statistical analysis of the mean absorbed power

measured under $x_h$-axis vibration. The Table summarizes the significance analysis of the

main factors as well as the two-way interactions between these factors. The excitation

level certainly shows strong significance in view of the mean absorbed power in all

frequency bands, which can also be seen in Figure 5.22. The hand-arm posture is

statically significant on the mean absorbed power in the low frequency bands (40 Hz and lower). This result also conforms the trend shown in Figure 5.24. Handle size reveals significance on absorbed power in all the frequency bands, except in the 50, 63 and 160 Hz bands. Both the hand forces show non-significance on the mean absorbed power in the lower frequency band (16 Hz and lower). While the grip force shows strong significance in the remaining frequency bands, the push force shows non-significance in the 32, 63-100 and 630-1000 Hz bands.

The excitation level shows strong interaction with grip force in frequency bands higher than 20 Hz, while it reveals interactions with push force in the 20, 25 and 125-500 Hz bands. The excitation magnitude interacts statically with the hand-arm posture in frequency bands lower than 40 Hz, while it shows strong interactions with the handle size in nearly all the frequency bands. The grip force shows significant interaction with the handle size in the 40 Hz and higher bands, and with the hand-arm posture mostly in the low frequency bands (10-40 Hz). The hand forces show interactions between each other mostly in the mid frequency bands (25-125 Hz). Push force shows significant interactions with the handle size in the 200-800 Hz bands, while hand-arm posture shows weak interactions with handle size in most of the frequency bands. The ANOVA results generally conform with the trends observed in the mean data in previous Figures.

Table 5.13: Statistical significance factor ($p$) of various contributory factors in view of the mean absorbed power in different one-third octave frequency bands under $x_h$-axis vibration.

| Factors Frequency (Hz) | Fg | Fp | D | A | P | Fg*Fp | Fg*D | Fg*A | Fg*P | Fp*D | Fp*A | Fp*P | D*A | D*P | A*P |
|---|---|---|---|---|---|---|---|---|---|---|---|---|---|---|---|
| | | | | | | | Significance Level ($p$) | | | | | | | | |
| 8 | .95 | .73 | .02 | .00 | .00 | .43 | .87 | .73 | .83 | .22 | .27 | .00 | .00 | .00 | .00 |
| 10 | .94 | .10 | .02 | .00 | .00 | .42 | .62 | .98 | .01 | .84 | .05 | .00 | .01 | .03 | .00 |
| 12.5 | .84 | .53 | .00 | .00 | .00 | .96 | .92 | .83 | .00 | .55 | .29 | .00 | .00 | .14 | .00 |
| 16 | .56 | .05 | .00 | .00 | .00 | .95 | .54 | .45 | .00 | .73 | .08 | .00 | .00 | .85 | .00 |
| 20 | .00 | .00 | .00 | .00 | .00 | .49 | .90 | .00 | .00 | .01 | .00 | .00 | .00 | .05 | .00 |
| 25 | .00 | .01 | .00 | .00 | .00 | .00 | .06 | .00 | .01 | .43 | .00 | .00 | .00 | .07 | .00 |
| 31.5 | .00 | .16 | .00 | .00 | .00 | .00 | .00 | .00 | .00 | .10 | .07 | .38 | .00 | .04 | .00 |
| 40 | .00 | .01 | .00 | .00 | .02 | .00 | .00 | .00 | .01 | .76 | .01 | .69 | .00 | .10 | .10 |
| 50 | .00 | .00 | .30 | .00 | .67 | .00 | .00 | .00 | .74 | .71 | .01 | .16 | .09 | .87 | .30 |
| 63 | .00 | .58 | .05 | .00 | .45 | .07 | .00 | .00 | .06 | .30 | .50 | .10 | .00 | .52 | .08 |
| 80 | .00 | .20 | .00 | .00 | .36 | .00 | .00 | .00 | .00 | .50 | .13 | .08 | .00 | .39 | .12 |
| 100 | .00 | .42 | .00 | .00 | .59 | .00 | .00 | .00 | .16 | .61 | .47 | .12 | .00 | .71 | .40 |
| 125 | .00 | .01 | .00 | .00 | .68 | .00 | .00 | .00 | .90 | .76 | .00 | .68 | .00 | .69 | .48 |
| 160 | .00 | .00 | .07 | .00 | 1.00 | .03 | .00 | .00 | .22 | .57 | .00 | .87 | .00 | .70 | 1.00 |
| 200 | .00 | .00 | .00 | .00 | .50 | .34 | .00 | .00 | .10 | .00 | .00 | .92 | .00 | 1.00 | .15 |
| 250 | .00 | .00 | .00 | .00 | .22 | .11 | .00 | .00 | .07 | .00 | .00 | .12 | .00 | .72 | .01 |
| 315 | .00 | .00 | .00 | .00 | .22 | .05 | .00 | .00 | .03 | .00 | .00 | .02 | .00 | .47 | .08 |
| 400 | .00 | .00 | .00 | .00 | .32 | .03 | .00 | .00 | .01 | .00 | .00 | .01 | .00 | .08 | .11 |
| 500 | .00 | .03 | .00 | .00 | .19 | .01 | .00 | .00 | .05 | .00 | .00 | .03 | .00 | .03 | .01 |
| 630 | .00 | .73 | .00 | .00 | .22 | .02 | .00 | .00 | .18 | .00 | .07 | .00 | .00 | .06 | .01 |
| 800 | .00 | .96 | .00 | .00 | .23 | .76 | .00 | .00 | .29 | .02 | .84 | .10 | .00 | .02 | .00 |
| 1000 | .00 | .90 | .00 | .00 | .97 | .52 | .00 | .00 | .49 | .19 | .39 | .18 | .00 | .12 | .09 |

242

Multifactor ANOVA was also performed on the mean absorbed power response corresponding to one-third octave frequency bands under two postures independently to examine the influence of hand-arm posture and its conjunctions with other contributory factors. The results presented in Table 5.14 clearly show relatively higher significance of the hand forces for posture P2 than those obtained under posture P1. This conforms the earlier conclusion that an extend arm posture yields a stronger handle-hand coupling.

Table 5.14: Results attained from independent statistical analysis for the two postures-significance factor ($p$) of the mean absorbed power in the one-third octave frequency bands under $x_h$-axis under vibration.

| Factors | $F_g$ | | $F_p$ | | $D$ | | $A$ | |
|---|---|---|---|---|---|---|---|---|
| Posture | P1 | P2 | P1 | P2 | P1 | P2 | P1 | P2 |
| Frequency (Hz) | Significance Level | | | | | | | |
| 8 | .91 | .78 | .03 | .02 | 00 | 00 | 00 | 00 |
| 10 | .05 | .17 | 00 | 00 | .01 | 00 | 00 | 00 |
| 13 | 00 | 00 | 00 | 00 | 00 | 00 | 00 | 00 |
| 16 | 00 | 00 | .05 | 00 | 00 | 00 | 00 | 00 |
| 20 | .02 | 00 | .27 | 00 | 00 | 00 | 00 | 00 |
| 25 | 00 | 00 | .47 | 00 | 00 | 00 | 00 | 00 |
| 32 | 00 | 00 | .57 | .02 | 00 | 00 | 00 | 00 |
| 40 | .03 | 00 | .22 | .03 | 00 | .02 | 00 | 00 |
| 50 | 00 | 00 | .33 | .01 | .46 | .68 | 00 | 00 |
| 63 | 00 | 00 | .54 | .03 | .11 | .39 | 00 | 00 |
| 80 | 00 | 00 | .11 | .09 | 00 | .02 | 00 | 00 |
| 100 | 00 | 00 | .17 | 00 | 00 | 00 | 00 | 00 |
| 125 | 00 | 00 | .08 | .10 | 00 | .02 | 00 | 00 |
| 160 | 00 | 00 | 00 | 00 | .27 | .28 | 00 | 00 |
| 200 | .01 | 00 | 00 | 00 | 00 | .03 | 00 | 00 |
| 250 | 00 | 00 | 00 | 00 | 00 | 00 | 00 | 00 |
| 315 | 00 | 00 | 00 | .02 | 00 | 00 | 00 | 00 |
| 400 | 00 | 00 | .01 | .11 | 00 | 00 | 00 | 00 |
| 500 | .03 | 00 | .07 | .41 | 00 | 00 | 00 | 00 |
| 630 | 00 | 00 | .58 | .94 | 00 | 00 | 00 | 00 |
| 800 | 00 | 00 | .95 | .85 | 00 | 00 | 00 | 00 |
| 1000 | 00 | 00 | .98 | .82 | 00 | 00 | 00 | 00 |

The significance of handle size is comparable under both postures; it shows statical significance in all the frequency bands except in the 50, 63 and 160 Hz bands. Grip force also shows similar significance for both postures, where it shows stronger significance in all the frequency bands except in the 8 and 10 Hz bands. The influence of push force shows remarkable difference under two postures. Under posture $P2$, it shows high significance in most of the frequency bands lower than 400 Hz, where most of the power is absorbed by the hand-arm system. For posture $P1$, the push force reveals non-significance in the 16-100 Hz bands. This is consistence with the ANOVA results obtained for the total absorbed power which shows non-significance of the push force on the total mean power under posture $P1$.

## 5.5 Summary and Conclusions

Despite the considerable variations observed in the power absorption response among the individuals, definite trends in the responses could be observed with regards to the variations considered in the study. The total power absorbed by hand-arm system exposed to vibration along $z_h$-axis is almost five times more than that derived for vibration along the $x_h$-axis under the same test conditions. An increase in the weighted vibration magnitude from 2.5 to 5 m/s$^2$ results in nearly four-fold increase in the absorbed power, for both axes of vibration, which is attributed to its definition. More than 90% and 80% of the total absorbed power occurred within the 8-200 Hz frequency range under the $z_h$- and $x_h$-axis vibration, respectively. The handle diameter was found to have an obvious effect on the absorbed power along $z_h$-axis; the amount of power absorbed into the hand increased with the handle diameter under posture $P1$, while an opposite trend was

observed under the posture $P2$. For the $x_h$-axis vibration, the influence of handle size is less notable that that along the $z_h$-axis.

A hand-arm posture with extended forearm (180° elbow flexion- posture $P2$) yields relatively stronger coupling with the vibrating handle at low frequencies and consequently higher power absorption in both; $x_h$ and $z_h$-axes. However, the absorbed power characteristics of the hand-arm system exposed to $z_h$- and $x_h$-axes vibration show considerable differences accordingly to hand-arm posture adopted. For the $z_h$-axis vibration exposure,, the one-third octave band absorbed power spectra revealed two distinct peaks in the vicinity of 12.5 and 40 Hz bands for posture $P1$, and a single peak in the 16 Hz band for posture $P2$. The total power absorbed by the hand-arm under posture $P2$ is remarkably higher than that under posture $P1$, under the same test conditions. Whereas, the peak absorbed power under $x_h$-axis vibration occur in the vicinity of 25 Hz and 150 Hz bands. The magnitude of absorbed power is more emphasized near the 25 Hz band due to relatively higher velocity at lower frequencies. Depending on the handle size, vibration level, and grip and push forces, the total power absorbed by the extended hand-arm (posture $P2$) could be up to 88% and 30% higher than that of the hand-arm posture with bent elbow (posture $P1$) along the $z_h$- and $x_h$-axes, respectively. The results of the study clearly show strong influence of the hand-arm posture on the biodynamic measures of the hand-arm system exposed to vibration along the $z_h$-axes and somehow relatively weaker effect along the $x_h$-axes. It is thus imperative that the biodynamic responses be reported for the specific posture considered together with the many other factors, while additional studies would be desirable to further explore the effects of postural variations

and the means to account for the effects within the idealized values provided in the current standard

Increasing the hand grip or push force generally causes higher power responses, suggesting stronger coupling between the hand and the handle which strengthens with increasing hand forces. While the absorbed power does not reveal a definite trend with respect to the hand forces for the bent elbow posture ($P1$), particularly at low frequencies, higher absorbed power was associated with the extended forearm posture ($P2$) with increase in either of the hand forces for both vibration axes. This observation was conformed by a stronger linear correlation between the coupling force (summation of grip and push forces) and absorbed power under the $P2$ posture for vibration along the $x_h$-axis.

The total absorbed power was found to be more correlated with the coupling force rather than with the contact force. This result is consistent with other observations, i.e. namely a larger handle leads to lower contact force and higher absorbed energy, when compared to that of the smaller handles. Considering that the coupling force represents equal contribution of the grip and push forces, and that the contact force emphasizes a considerable larger weighting on the grip force, the results suggest that the total amount of absorbed power of the hand-arm system would likely be most dependent on the push force. This could mean that the majority of the absorbed power enters the hand-arm system at the upper lateral side of the palm, which mostly contributes to the realization of the push force. The power absorbed in the frequency range above 200 Hz showed strong correlation with the contact force.

The results suggest that 75 to 84 % and 54 to 63 % of the total power is dissipated in the 8-50 Hz frequency range in response of vibration along $z_h$- and $x_h$-axes, respectively,

246

irrespective of the excitation magnitude, handle size and hand forces. Considering that a large number of percussion and rotary hand power tools transmit predominant vibration at frequencies below 50 Hz, relatively high injury risk may be associated with exposure to hand-transmitted vibration in this frequency range. Although the frequency-weighting defined in the current standard (ISO-5349-1) emphasizes the importance of transmitted vibration up to 16 Hz, it suppresses the vibration at frequencies above 16 Hz at a rate of 6 dB/decade. The results obtained in this study suggest that the weighting function may provide an underestimate of the injury potential. The cut-off frequency of the recommended weighting function in the order of 50 Hz may better represent the power dissipation properties of the human hand and arm exposed to hand-transmitted vibration, meanwhile different weighting functions correspondent to different axes of vibration would be recommended.

# CHAPTER 6

## DEVELOPMENT OF ANALYTICAL HAND-ARM

## VIBRATION MODEL

### 6.1 Introduction

Considerable efforts have been made to derive biomechanical and mechanical equivalent models of the human hand and arm exposed to vibration. The mechanical model development tasks have been mostly motivated by the desire to develop effective vibration mechanisms for the tools through analyses of coupled hand-tool models (Cherian et al., 1996; Daikoku and Ishikawa, 1989; Reynolds and Falkenberg, 1984; Byström et al., 1982) and to assess the vibration attenuation potentials of anti-vibration glove materials (Gurram, 1993). The applications of mechanical equivalent or biodynamic models of the human hand and arm offer considerable potential to carry out assessments through both analytical and experimental analyses, where the involvement of human subjects could be considerably reduced (Kinne and Melzig, 1996; Bullinger et al., 1989). The hand-arm vibration (HAV) models, when integrated with the analytical model of a power tool, could permit efficient evaluations of the tool design factors and vibration attenuation devices.

A number of biodynamic models of the human hand and arm have been proposed to study the vibration amplitude and power flow in the coupled hand, tool and work piece system; the potential performance benefit of vibration attenuation mechanisms; and to develop test rigs and hand-arm simulators for the assessment of vibration transmission performance of different tools (Daikoku and Ishikawa, 1989; Mishoe and Suggs, 1977; Reynolds and Falkenberg, 1984; Gurram et al., 1995; ISO-10068, 1998). Although the

proposed models provide little insight on the pathological changes caused by HTV, they serve as useful tools to study vibration amplitudes and power flow in the coupled hand, power tool and work piece system.

The driving point mechanical impedance of the hand-arm system has been characterized by mass excited, lumped parameter biodynamic models, where the model parameters are derived from the measured impedance data. Lumped parameter models, ranging from simple single-degree-of-freedom (DOF) to many-DOF, have been proposed by different investigators (Daikoku and Ishikawa, 1989; Mishoe and Suggs, 1977; Gurram et al., 1995; ISO-10068, 1998). In view of the wide frequency range of power tool vibration and the non-linear viscoelastic properties of human biological materials, the accuracy of the model could be related to its number of degrees of freedom (DOF). A baseline model, its DOF and parameters are often identified from the measured impedance data using the impedance relationships of pure mechanical elements. The model is then refined to fit the measured impedance data, using trial and error curve fitting methods. Alternatively, optimization algorithms have also been employed to derive the model parameters (Gurram et al., 1995). However, the methodologies employed to identify the models and their parameters raise additional concerns regarding their suitability and applicability. The identifications based upon curve-fitting a target dataset do not represent a unique solution, and it is possible to realize a vast number of model parameter sets that would equally satisfy the target curve and a specified error criterion (Rakheja et al., 1993).

A number of reported biodynamic models have been reviewed for their potential application in realizing a hand-arm simulator and assessment of vibration behavior of

249

hand-held power tools (Rakheja et al., 2002). The evaluations were performed using three different criteria: (a) the ability of the model to characterize the driving-point mechanical impedance of the human hand-arm within the range of idealized values presented in ISO-10068 (1998); (b) the magnitude of model deflection under a static push force; and (c) the vibration properties of the human hand and arm evaluated in terms of natural frequencies and damping ratios. From the relative evaluations of 12 different models, it was concluded that a vast majority of these models cannot be applied for development of a hand-arm simulator or the assessment of dynamic behavior of the coupled hand-tool system. The higher-order models, three- and four-degrees-of-freedom, in general yield impedance characteristics within the range of idealized values, but exhibit excessive static deflections. Moreover, these models involve very light masses (in the 1.2- 4.8 grams range), and exhibit either one or two vibration modes at frequencies below 10 Hz. The majority of the lower-order models yield reasonable magnitudes of static deflections but relatively poor agreement with idealized values of driving-point mechanical impedance (Rakheja et al., 2002).

The biodynamic response characteristics of hand-arm system exposed to vibration have been shown to be influenced by several factors, among which hand-arm posture, vibration excitation frequency, individual differences, grip and push forces probably represent the most significant parameters. The wide range of variations observed among the data reported by different investigators for *DPMI* and absorbed power could be an indicative of the influence these different parameters can have on these response functions. The strong dependency of the *DPMI* response on different factors, as evidenced from the data reported in the literature (Dong et al., 2001), would limit the

applications of the proposed models. While most of the investigations on biodynamic response of human hand-arm to vibration recognize the influence of hand forces on the biodynamic response, only one reported model has attempted to identify grip force dependent parameters (Gurram et al., 1995). The development of a hand-arm biodynamic model with considerations of both grip and push forces variations has not been yet attempted.

## 6.2    Interpretation of Biodynamic Measures

The biodynamic response of the human hand-arm system exposed to vibration can be characterized using different biodynamic response functions, which have often been used interchangeably to describe the force-motion relationship at the hand handle interface, as a function of the vibration frequency. These include the driving-point mechanical impedance (*DPMI*), the apparent mass (*APMS*) and the mechanical compliance. The *DPMI* relates the driving force and the resulting velocity response at the driving point, while the apparent mass (*APMS*), in a similar manner, relates the driving force and the resulting acceleration response, as described earlier in section 2.2.3.

The *APMS* can be related to *DPMI*, such as

$$APMS(\ j\omega\ )=\frac{DPMI(\ j\omega\ )}{j\omega} \tag{6.1}$$

The apparent mass magnitude at a very low frequency is equal to static mass of the hand-arm system in coupled with the handle. It is obvious from the above equations that at high frequency the *APMS* tends to vanish (approached a few grams), while the *DPMI* tends to emphasize the magnitude response at higher excitation frequencies. It is evident

251

from equation (6.1), that the *DPMI* response leads the *AMPI* response by 90° in phase angle.

The reported models have been developed on the basis of the measured data under different conditions and types of excitations. The available data were acquired under vibration applied along a single axis. The models are thus considered valid along that individual axis of vibration in an uncoupled manner (Daikoku and Ishikawa, 1989; Mishoe and Suggs, 1977; Reynolds and Falkenberg, 1984; ISO-10068, 1998; Gurram et al., 1995). Apart from the shortcomings of different reported model discussed in section 6.1, conceptual misrepresentation of the number of degrees of freedom (DOF) is also obvious. The reported models assume that the (DOF) of the hand-arm model is identical of the number of lumped masses in the model. The resonant frequencies of different models are not consistence with the *DPMI* or *APMS* magnitude peaks or transfer functions of different masses. The reported models and formulations generally consider the dynamic force at the driving point as input and the velocity (displacement or acceleration) as the response to characterize the *DPMI*. The experimental conditions however involve motion excitation at the driving-point, which effectively reduces the DOF by one.

Figure 6.1 shows, as an example, the structure of the model proposed by Daikoku and Ishikawa (1989) to characterize the $z_h$-axis impedance. The model is referred to as three-DOF, while it is clearly a two-DOF model when the mass motion $z_1(t)$ is known. The model parameter, the natural ($\omega_n$) and damped ($\omega_d$) frequencies, and damped ratios ($\xi$) computed considering three- and two- DOF model are summarized in Table 6.1.

Table 6.1: Model parameters of the hand-arm system ($z_h$-axis) model proposed by Daikoku and Ishikawa (1989) and corresponding frequencies and damping ratios.

| mode | $m$ (kg) | $k$ (N/m) | $c$ (Ns/m) | Three-DOF | | | Two-DOF | | |
|------|----------|-----------|------------|-----------|-----------|--------|-----------|-----------|--------|
| | | | | $f_n$ (Hz) | $f_d$ (Hz) | $\xi$ (-) | $f_n$ (Hz) | $f_d$ (Hz) | $\xi$ (-) |
| $z_1$ | 0.00452 | 230000 | 124 | 3.87 | 3.6 | 0.28 | - | - | - |
| $z_2$ | 0.211 | 32700 | 65.1 | 75 | 66 | 0.48 | 39.58 | 38 | 0.26 |
| $z_3$ | 0.466 | 404 | 9.26 | 1147 | - | 1.94 | 178.2 | 156.4 | 0.41 |
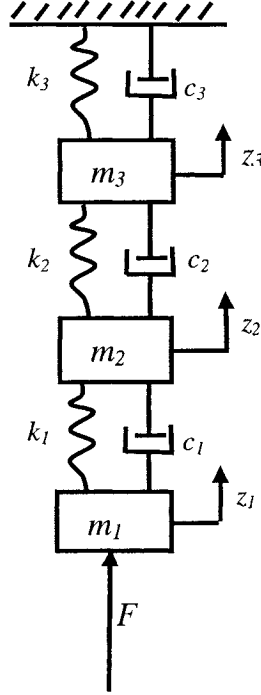


Figure 6.1: Three-DOF hand-arm model structure proposed by Daikoku and Ishikawa (1989).

The equations of motion for the hand-arm system model are solved using the model parameters (Table 6.1) to obtain the biodynamic response of hand-arm system in terms of *DPMI* and *APMS*, and the transfer functions between the driving point ($z_1$) and other axes ($z_2$ and $z_3$).

Figure 6.2 shows the *DPMI* and *APMS* magnitude and phase responses as well as the transfer functions. The frequency corresponding to peak magnitude of transfer function ($Z_2/Z_1$) is corresponding with the primary resonant frequency near 38 Hz. The *APMS*

253

magnitude peak response also reveals close to the primary resonant frequency (38 Hz) of

the model, while the *DPMI* magnitude peak near 40 Hz, as evident in Figure 6.2. From

the results, it is clear that the response peaks do not correspond with the eigenvalues of

the three-DOF system. The model structure, showed thus to be considered as two-DOF.
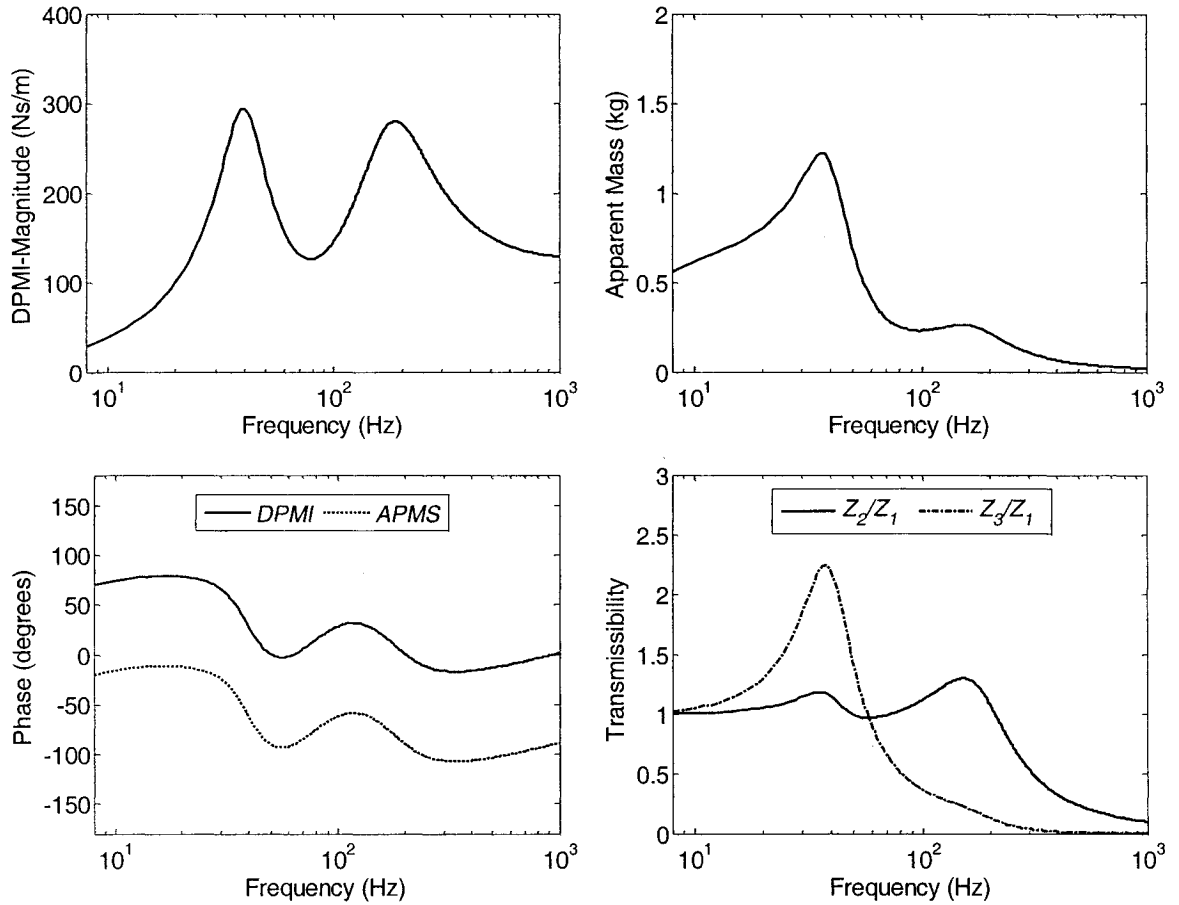


Figure 6.2: The responses of hand-arm model along $z_h$-axis proposed by Daikoku and
Ishikawa (1989).

## 6.3   Development of the Human Hand-Arm Model

In this section, mechanical-equivalent hand-arm models are formulated to

characterize the biodynamic measures, namely the *DPMI* magnitude and phase, and the

absorbed power under vibration along axes, $x_h$ and $z_h$. The models along the axes are

considered to be uncoupled. Owing to the strong influence of the hand-handle coupling

254

forces, and handle size, the models are initially attempted for fixed values of these variables. The model parameters are thus identified for the commonly used handle size of 40 mm, and widely suggested levels of hand forces, $F_g$= 30 N and $F_p$= 50 N (ISO-10068, 1998). Two different model structures, three-DOF comprising 4 masses and two-DOF comprising 3 masses, as shown in Figure 6.3 (b) and (d) are considered. Two additional model structures are also consider by letting, $m_1 = 0$ as shown in Figure 6.3 (a) and (c).



(a) : model (A)        (b): model (B)        (c) : model (C)        (d ): model (D)
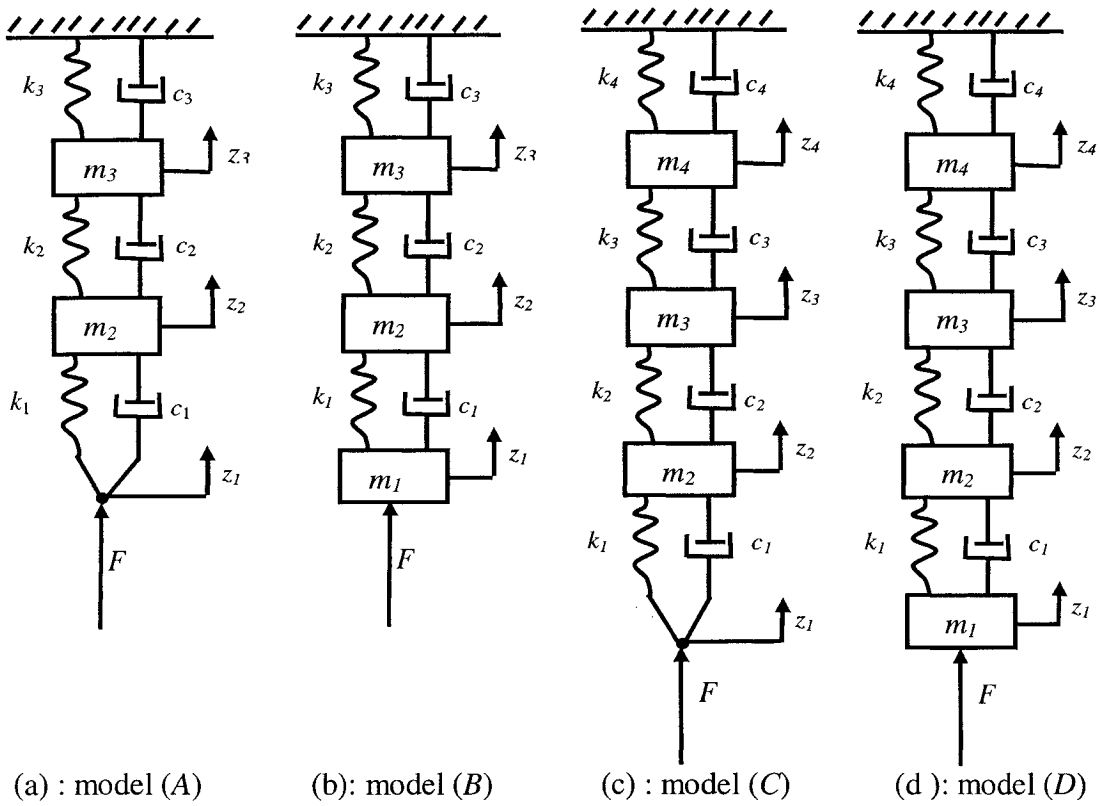
Figure 6.3: Different hand-arm model structures.

The equations of motions for the two- and three-DOF models including mass $m_1$ and driving-point can be generally expressed as:

$$m_4 \ddot{z}_4 + k_4 z_4 + c_4 \dot{z}_4 + k_3 ( z_4 - z_3 ) + c_3 ( \dot{z}_4 - \dot{z}_3 ) = 0 \qquad (6.2)$$

$$m_3\ddot{z}_3 + k_3(z_3 - z_4) + c_3(\dot{z}_3 - \dot{z}_4) + k_2(z_3 - z_2) + c_2(\dot{z}_3 - \dot{z}_2) = 0 \qquad (6.3)$$

$$m_2\ddot{z}_2 + k_2(z_2 - z_3) + c_2(\dot{z}_2 - \dot{z}_3) + k_1(z_2 - z_1) + c_1(\dot{z}_2 - \dot{z}_1) = 0 \qquad (6.4)$$

The resultant driving-point force due to excitation $z_1(t)$ of $m_1$ is derived as:

$$F = m_1\ddot{z}_1 + k_1(z_1 - z_2) + c_1(\dot{z}_1 - \dot{z}_2) \qquad (6.5)$$

Manipulations of the above equations by substitution of equation (6.5) into (6.2) to (6.4) yields:

$$F = m_1\ddot{z}_1 + m_2\ddot{z}_2 + m_3\ddot{z}_3 + m_4\ddot{z}_4 + k_4 z_4 + c_4 z_4 \qquad (6.6)$$

The above equation yields following expression for the *APMS*:

$$M(s) = \frac{F}{\ddot{Z}_1} = m_1 + m_2\left(\frac{\ddot{Z}_2}{\ddot{Z}_1}\right) + m_3\left(\frac{\ddot{Z}_3}{\ddot{Z}_1}\right) + m_4\left(\frac{\ddot{Z}_4}{\ddot{Z}_1}\right) + \left(\frac{k_4}{s^2} + \frac{c_4}{s}\right)\left(\frac{\ddot{Z}_4}{\ddot{Z}_1}\right) \qquad (6.7)$$

where $s = j\omega$. Equations (6.2- 6.4) are rearranged to calculate the transfer functions in equation (6.7) such that:

$$
\begin{bmatrix}
(m_2 + \dfrac{k_2+k_1}{s^2} + \dfrac{c_2+c_1}{s}) & (-\dfrac{k_2}{s^2} - \dfrac{c_2}{s}) & 0 \\[2mm]
(-\dfrac{k_2}{s^2} - \dfrac{c_2}{s}) & (m_3 + \dfrac{k_3+k_2}{s^2} + \dfrac{c_3+c_2}{s}) & (-\dfrac{k_3}{s^2} - \dfrac{c_3}{s}) \\[2mm]
0 & (-\dfrac{k_3}{s^2} - \dfrac{c_3}{s}) & (m_4 + \dfrac{k_3+k_4}{s^2} + \dfrac{c_3+c_4}{s})
\end{bmatrix}
\begin{bmatrix}
\dfrac{\ddot{Z}_2}{\ddot{Z}_1} \\[2mm]
\dfrac{\ddot{Z}_3}{\ddot{Z}_1} \\[2mm]
\dfrac{\ddot{Z}_4}{\ddot{Z}_1}
\end{bmatrix}
=
\begin{bmatrix}
(\dfrac{k_1}{s^2} + \dfrac{c_1}{s}) \\[2mm]
0 \\[2mm]
0
\end{bmatrix}
\qquad (6.8)
$$

Equation (6.8) is solved to compute the transfer functions, which are applied in equation (6.7) to calculate *APMS* response of the model. The *DPMI* response of the model, Z(s), is then derived from:

$$Z(s) = sM(s) \tag{6.9}$$

The absorbed power response of the model can also be calculated based upon the indirect method, which considers the real component of the *DPMI* multiplied by the corresponding square of the rms velocities, such that:

$$P_{abs}(\omega) = Re[\, DPMI(\, j\omega\,)]\, |v(\, j\omega\,)|^2 \tag{6.10}$$

### 6.3.1 Identification of model parameters

The parameters of the hand-arm model are identified through a curve-fitting algorithm in order to achieve a close match with the mean measured *DPMI* magnitude and phase, and the absorbed power responses corresponding to the selected conditions ($D$= 40mm, $F_g$= 30 N, $F_p$= 50 N and $a_{h,w}$= 5 m/s² rms). The requirement for matching both these functions could improve the uniqueness of the model parameters or at least to narrow the range of parameters values. A parametric optimization technique is used to determine the base model parameters whereby an objective function is defined to minimize an error function of computed and mean values of the *DPMI* magnitude and phase and absorbed power responses measured in the 8-1000 Hz frequency range. The objective function is defined by a weighted sum of squared magnitude and phase errors associated with *DPMI* at selective frequency values (more than 200 discrete frequencies) and power absorption functions at center frequencies of the one-third octave bands as:

$$E(\lambda) = minimize\left(\left|\sum_{i=1}^{Nd}\alpha\{|Z(\omega_i) - Z_m(\omega_i)| \}^2 + \sum_{i=1}^{Nd}\beta\{|\phi(\omega_i) - \phi_m(\omega_i)| \}^2 + \right|\right.$$

$$\left. \sum_{i=1}^{th}\gamma\{|P_{ab}(\omega_i) - P_{abm}(\omega_i)| \}^2 \right) \tag{6.11}$$

257

Where $Z_m$ and $\phi_m$ are the measured *DPMI* magnitude and phase response corresponding to excitation frequency $\omega_i$, respectively, $Z$ and $\phi$ are the corresponding model responses, *Nd* is the number of discrete frequencies selected in the 8-1000 Hz frequency range. $P_{abm}$ and $P_{ab}$ are the measured and calculated absorbed power responses, respectively and *th* is the number of one-third octave bands in the considered frequency range. $\alpha$, $\beta$ and $\gamma$ are the weighting factors that are applied to ensure somewhat comparable contributions of modulus and phase errors and the absorbed power in the objective functions.

The weighting factors assume different values in different frequency ranges in order to ensure comparable contributions due to low- and high-frequency response characteristics. Theses weighting factors are also chosen to emphasize the contributions due to either *DPMI* or absorbed power functions to the total error function. For applications in HAV, the *DPMI* response is much higher than the absorbed power. A considerably larger value of weighting factor $\gamma$ may thus be selected to emphasize the power absorption response error in the minimization function. Finally, $\lambda$ is a vector of modal parameters to be identified. For the three-DOF model, the parameter vector is expressed as:

$$\lambda = \{m_1, m_2, m_3, m_4, k_1, k_2, k_3, k_4, c_1, c_2, c_3, c_4\}^T \tag{6.12}$$

where $T$ designates the transpose.

The minimization problem, expressed in equation (6.11), is solved subject to following inequality parametric constraints:

$$m_1 > 0; m_2 > 0; m_3 > 0; m_4 > 0;$$

$$c_1 > 0; c_2 > 0; c_3 > 0; c_4 > 0;$$

$$k_1 > 0; k_2 > 0; k_3 > 0; k_4 > 0; \ and \sum_{i=1}^{4} m_i \leq 6 \qquad (6.13)$$

The total model mass is constrained to realize the model mass in the order of average values of the male hand-arm system, which is approximately 8% of the total body mass (Chaffin and Anderson, 1984), Moreover the minimum value of the total mass would depend on the vibration axis and the hand-arm posture. From the *APMS* data acquired with a total of seven subjects, it is evident that the total mass of the hand-arm system coupled with handle is larger along the $z_h$-axis than that along the $x_h$-axis. Furthermore, the *APMS* magnitude of the extended arm posture (*P2*) at low frequency was observed to be approximately three times higher than that for the posture *P1*. The parameter constraints are thus varied in accordance with the axis of vibration and the hand-arm posture. The constrained minimization problem, defined in equation (6.11), was solved using MATLAB routine. The solutions were obtained for different starting values of the parameter vector, and the resulting model parameters were examined to obtain optimal values and minimum error of the objective function. The different optimization runs corresponding to different starting values generally converged to similar values of the model parameters and the error functions.

The model parameters are identified for the four model structures, described in Figure 6.3. These include a two-mass two-DOF model (referred to as model *A*), a three-mass two-DOF model (referred to as model *B*), a three-mass three-DOF model (referred to as model *C*), and a four-mass three-DOF model (referred to as model *D*). The model parameters identified for the four models of the hand arm-system exposed to vibration

along the $z_h$-axis, (40 mm handle, $F_g$= 30 N, $F_p$= 50 N and posture *P1*) are summarized in

Table 6.2. The results show that the different model structures converge to significantly

different model parameters. The two- and three-mass and three-DOF mode structures

with visco-elastic driving-point ($m_1$= 0), however, show somewhat comparable values of

the model parameters. Comparable parameters values are also obtained for the two model

structures with the driving-point mass ($m_1 \neq 0$).

Table 6.2: Parameters identified for the different hand-arm model structures ($z_h$-axis, *D*=
40 mm, $F_g$= 30 N, $F_p$ = 50 N and posture *P1*)

| Model | $m_1$ | $m_2$ | $m_3$ | $m_4$ | $k_1$ | $k_2$ | $k_3$ | $k_4$ | $c_1$ | $c_2$ | $c_3$ | $c_4$ |
|-------|-------|-------|-------|-------|-------|-------|-------|-------|-------|-------|-------|-------|
| A | - | .043 | 1.239 | - | 292647 | 73257 | 1000 | - | 750 | 200 | 80 | - |
| B | .025 | 1.367 | 1.608 | - | 53862 | 5684 | 2812 | - | 174 | 51 | 62 | - |
| C | - | .029 | 1.281 | 1.57 | 254969 | 64334 | 100 | 73849 | 750 | 211 | 75 | 73 |
| D | .023 | 1.4 | 1.5 | .53 | 53157 | 6000 | 8000 | 2335 | 182 | 41 | 5 | 101 |

Parameters of the mechanical-equivalent models of the hand-arm system exposed to

$x_h$-axis vibration ale also identified in a similar manner. Table 6.3 summarizes the

parameters for the four model structures under vibration along $x_h$-axis, on the basis of

data acquired with the 40 mm handle, and 30 N grip and 50 N push force, and posture *P1*.

The results also show that the different model structures yield considerably different

model parameters. However, both the two-DOF models (models *A* and *B*) parameters are

comparable, while parameters of the three-mass three-DOF (model *C*) differ significantly

from parameters of the two-DOF models and model *D*. All the model structures converge

towards high values of $k_1$ and $c_1$ when compared with other stiffness and damping

coefficients. The hand-arm model mass closest to the vibrated handle (either $m_1$ or $m_2$

depending on model structure), tends to be the lowest.

Table 6.3: Parameters for different hand-arm model structures ($x_h$-axis, $D$= 40 mm, $F_g$= 30 N, $F_p$= 50 N and posture $P1$)

| Model | $m_1$ | $m_2$ | $m_3$ | $m_4$ | $k_1$ | $k_2$ | $k_3$ | $k_4$ | $c_1$ | $c_2$ | $c_3$ | $c_4$ |
|-------|-------|-------|-------|-------|-------|-------|-------|-------|-------|-------|-------|-------|
| A | - | .309 | .347 | - | 148734 | 6342 | 1111 | - | 251 | 28 | 12 | - |
| B | .026 | .3 | .325 | - | 153258 | 7119 | 945 | - | 220 | 26 | 15 | - |
| C | - | .06 | .25 | .3 | 411394 | 207718 | 6480 | 1004 | 500 | 290 | 21 | 12 |
| D | .027 | .298 | .2 | .645 | 146700 | 8618 | 500 | 3980 | 218 | 16 | 23 | 15 |

## 6.3.2 Validity of the identified models

The equality of the identified models is examined by comparing the biodynamic responses of the models with the mean measured data corresponding to selected conditions. Equations (6.7) to (6.10) are solved to compute both the *DPMI* and absorbed power responses of the four models. Figures 6.4 to 6.7 compare the model responses in terms of impedance magnitude and phase, and absorbed power with the respective mean measured data, for the four models under $z_h$-axis vibration. The figures show that all the model structures considered can predict both the biodynamic responses reasonably well in the 8-1000 Hz frequency range, when variations in the hand forces and handle size are neglected.

In similar manner, the validity of the identified models along $x_h$-axis vibration is examined by comparing the biodynamic responses of the models with the mean measured data corresponding to selected conditions ($F_g$= 30 N, $F_p$= 50 N, 40 mm handle and posture $P1$). Equations (6.7) to (6.10) are solved to compute both the *DPMI* and absorbed power responses of the four model structures (*A, B, C,* and *D*).
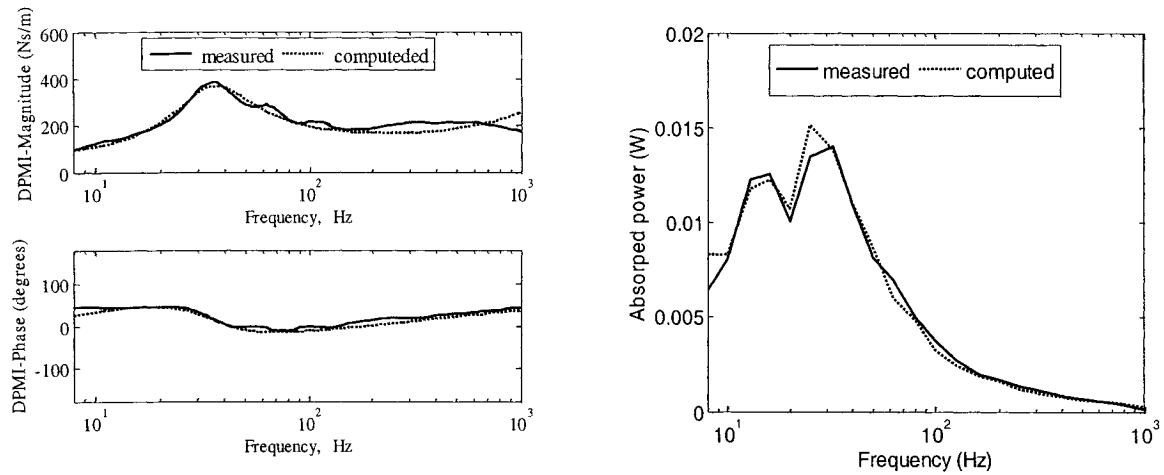
Figure 6.4: Comparison of hand-arm model $A$ biodynamic responses with the mean measured data ($z_h$-axis).
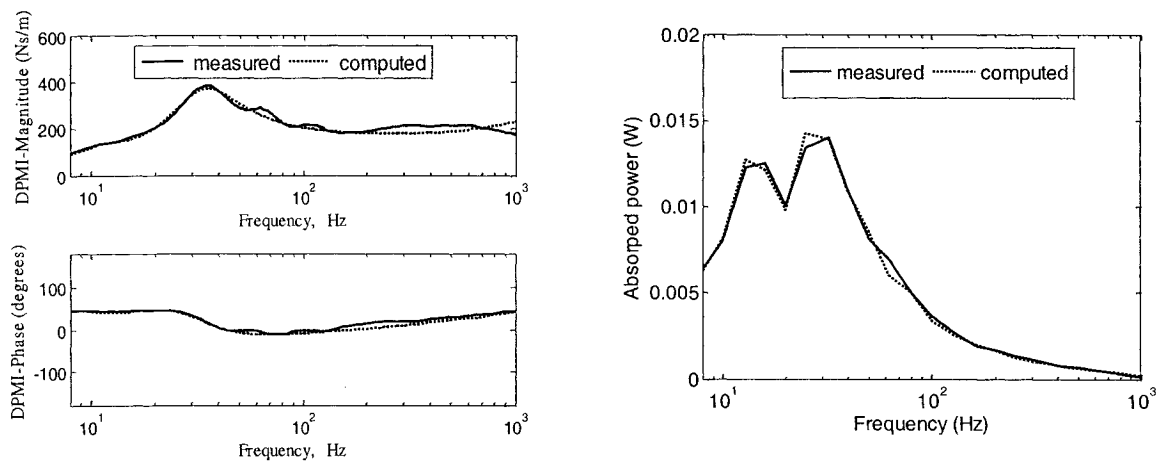


Figure 6.5: Comparison of hand-arm model $B$ biodynamic responses with the mean measured data ($z_h$-axis).
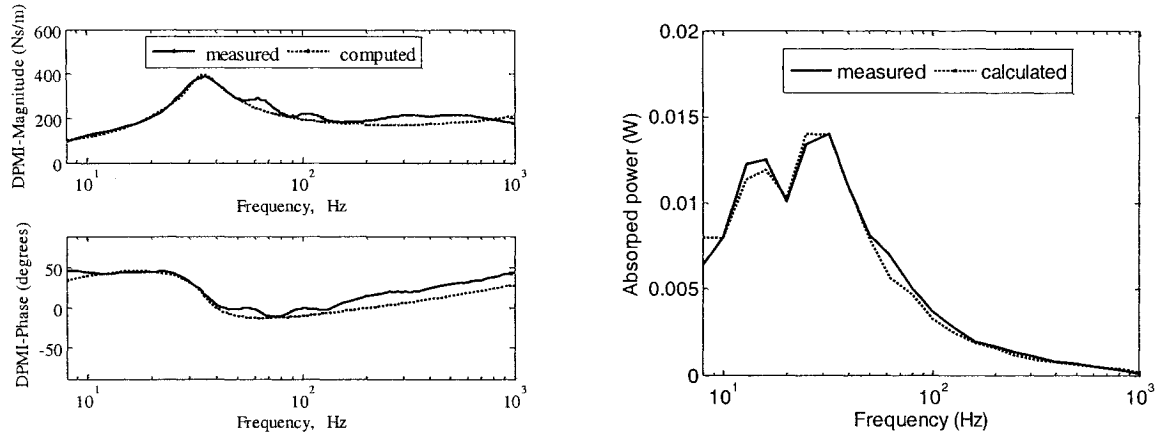
Figure 6.6: Comparison of hand-arm model $C$ biodynamic responses with the mean measured data ($z_h$-axis).
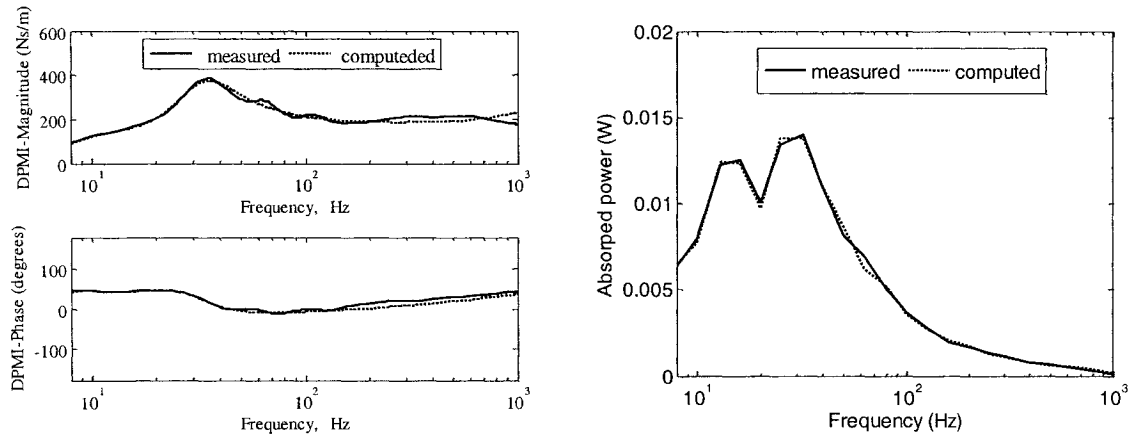


Figure 6.7: Comparison of hand-arm model $D$ biodynamic responses with the mean measured data ($z_h$-axis).

Figures 6.8 to 6.11 compare the model responses in terms of impedance magnitude and phase, and absorbed power with the respective mean measured data, for the four models under $x_h$-axis vibration. The figures show that all the model structures considered can predict both the biodynamic responses reasonably well in the 8-1000 Hz frequency range. The model $A$, however, can be considered as an exception; it yields poorest prediction of the $DPMI$ magnitude and phase responses, when variations in the hand

263

forces and handle size are neglected. Model $D$ yields the best prediction of absorbed power among the other models.
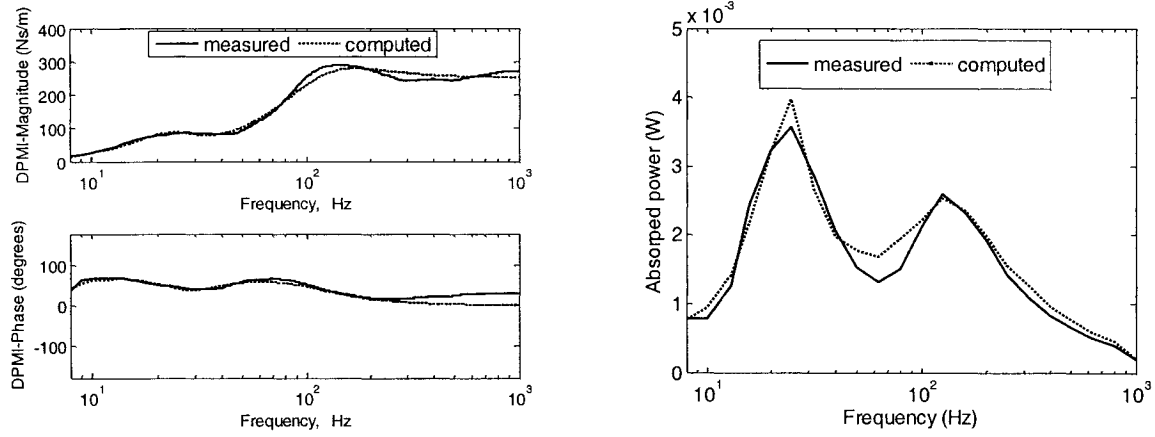


Figure 6.8: Comparison of hand-arm model $A$ biodynamic responses with the mean measured data ($x_h$-axis).
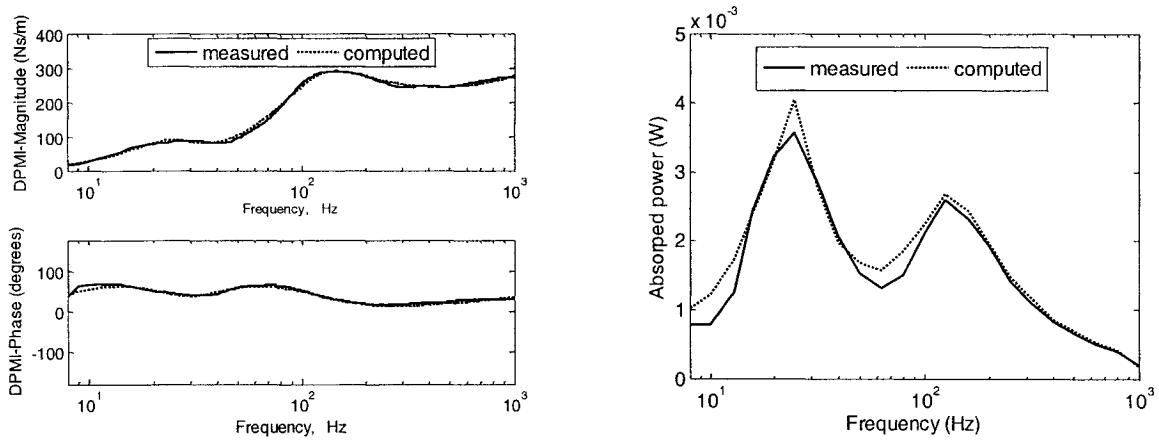


Figure 6.9: Comparison of hand-arm model $B$ biodynamic responses with the mean measured data ($x_h$-axis).
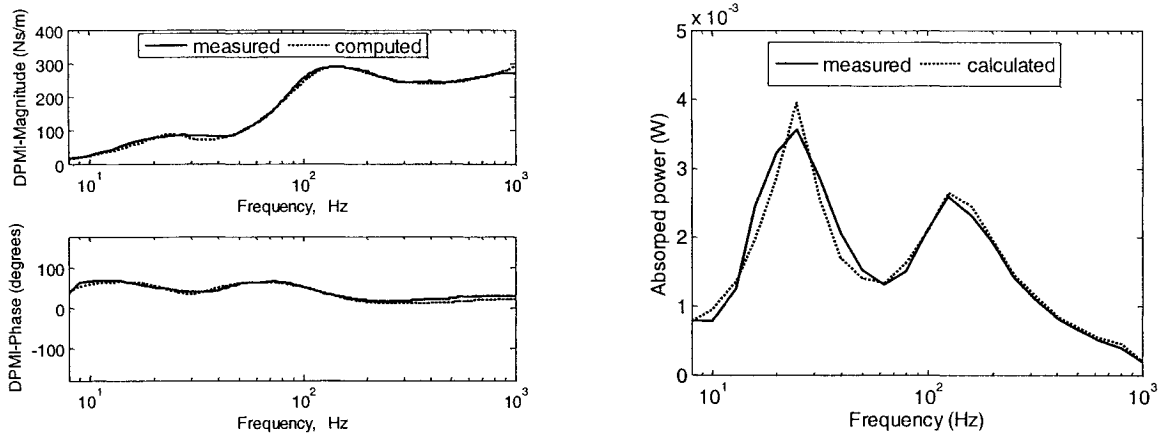
Figure 6.10: Comparison of hand-arm model $C$ biodynamic responses with the mean measured data ($x_h$-axis).
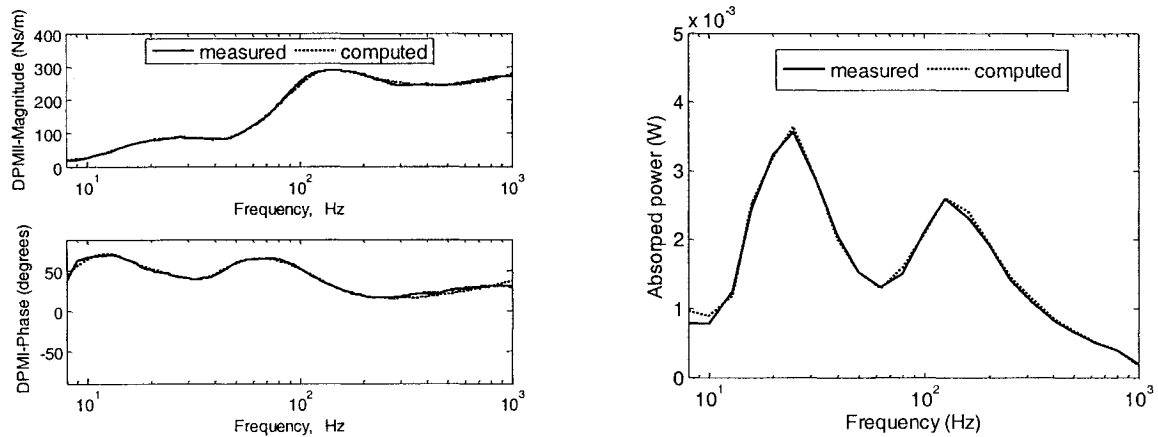


Figure 6.11: Comparison of hand-arm model $D$ biodynamic responses with the mean measured data ($x_h$-axis).

## 6.4 Model Parameters as Function of Hand Forces

The measured data clearly revealed significant influences of the hand-handle interface forces on the biodynamic responses. These primarily include the directly measurable grip and push forces imparted on the vibrating handle, and may also be expressed in terms of coupling and/or contact forces. A number of studies have speculated higher injury risks due to higher magnitude of hand forces (Fransson and

Winkel, 1991; Pyykkö et al., 1976; Radwin et al., 1987). It is thus desirable to derive the mechanical-equivalent models and their parameters that could be applied over a wide range of hand forces. In this study, different model structures are further explored to identify the model parameters as functions of the hand forces, while exposed to $z_h$- and $x_h$-axes vibration. The parameters identification is based upon the data acquired for nine-different combinations of grip and push ($F_g/F_p$) forces. The structure of the model $C$ along $z_h$-axis vibration was excluded due its relatively poor performance, as judged by the criteria defined in (Rakheja et al., 2002). The biodynamic responses of model $C$ were observed to be relatively less accurate than those predicted by models $B$ and $D$ (Figures 6.3 to 6.7). Moreover, the model $C$ resulted in high magnitude deflection under a static push force, exceeding 50 cm under a static push force of 50 N. On the other hand, for the hand-arm mechanical model along $x_h$-axis, the three model structures ($A$, $B$, and $C$) develop similar static deflection in the order of 5 cm, while model $D$ leads to highest deflection (12 cm) when the models is subject to $F_p$= 50 N. The models $A$ and $D$ along the $x_h$-axis vibration are thus excluded due to relatively poor prediction of the $DPMI$ responses as can be observed in Figure 6.8 (model $A$), and high magnitude deflection under a static push force of 50 N (model $D$).

### 6.4.1 Two-mass and two-DOF mode (structure $A$ -$z_h$-axis)

The optimization problem defined in equation (6.11) is solved for each combination of hand forces ($F_g/F_p$). The resulting model parameters, considered valid for a particular hand forces combination, are then examined to identify trends with variations in hand forces. The results revealed that a number of model parameters remain relatively less sensitive to variations in the hand forces. For the model structure $A$, (two mass, two-

266

DOF) these particularly included $m_3$, $k_3$, $c_1$ and $c_3$. This approach resulted in a simpler model for practical applications and realization of the hand-arm vibration simulator. These model parameters were thus considered fixed for the entire range of $F_g/F_p$, such that: $m_3=$ 1.26 kg; $k_3=$ 1000 N/m; $c_1=$ 750 Ns/m; and $c_3=$ 77 Ns/m. The remaining parameters of the model $A$ identified for different hand forces combinations under $z_h$-axis vibration are summarized in Table 6.4.

Table 6.4: Variations in the hand-arm model (structure $A$) parameters with hand forces under $z_h$-axis vibration ($m_3=$ 1.26 kg; $k_3=$ 1000 N/m; $c_1=$ 750 Ns/m; and $c_3=$ 77 Ns/m).

| $F_g$ (N) | $F_p$ (N) | Coupling Force (N) | $k_1$ (N/m) | $k_2$ (N/m) | $c_2$ (Ns/m) | $m_2$ (kg) |
|---|---|---|---|---|---|---|
| 10 | 25 | 35 | 215414 | 33468 | 124 | .031 |
| 10 | 50 | 60 | 260001 | 57825 | 160 | .042 |
| 10 | 75 | 85 | 300788 | 72810 | 193 | .048 |
| 30 | 25 | 55 | 256802 | 48098 | 152 | .039 |
| 30 | 50 | 80 | 292648 | 73258 | 200 | .043 |
| 30 | 75 | 105 | 343618 | 93845 | 222 | .05 |
| 50 | 25 | 75 | 284724 | 63041 | 181 | .046 |
| 50 | 50 | 100 | 336025 | 88082 | 216 | .048 |
| 50 | 75 | 125 | 371448 | 104059 | 250 | .061 |

In attempt to relate the identified model parameters with the hand forces, linear correlations between the parameters and the coupling force ($CF$) were performed. The analyses revealed positive correlations between the parameters ($k_1$, $k_2$, $c_2$, $m_2$) and the $CF$, while the linear correlation factors varied in the 0.92 to 0.99 range, as shown in Figure 6.12.

400000

350000

$k_1$ (Ns/m)

300000

250000

$r^2 = 0.99$

200000

0          50          100          150

Coupling Force (N)

120000

90000

$k_2$ (Ns/m)

60000

$r^2 = 0.98$

30000

0          50          100          150

Coupling Force (N)

300

250

$c_2$ (Ns/m)

200

150

100

$r^2 = 0.98$

0          50          100          150

Coupling Force (N)

0.08

0.06

$m_2$ (kg)

0.04

0.02

0

$r^2 = 0.92$

0          50          100          150
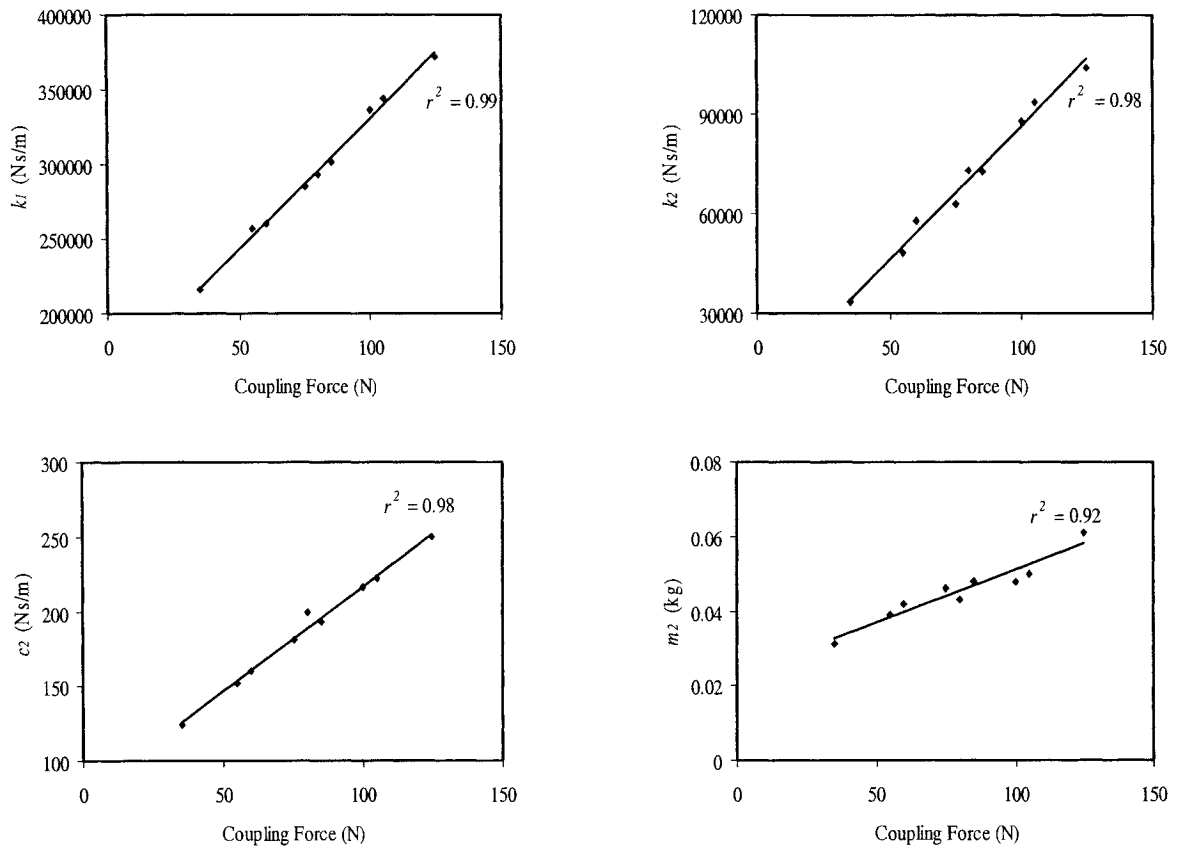
Coupling Force (N)

Figure 6.12: Linear correlations between the parameters of model $A$ and the coupling force ($z_h$-axis; posture $P1$).

From the results presented in Figures 6.4 to 6.7, it is evident that model structures $B$ and $D$ yield more accurate predictions of the biodynamic responses than model $A$. This is particularly observed in the $DPMI$ magnitude response near the primary resonance, and $DPMI$ phase response in the high frequency range. The model $A$ structure, however, could be considered more feasible in view of the hand forces variations, as it yields nearly linear dependence on the coupling force. The regression analysis resulted in following relationship between the model parameters and the coupling force ($CF$):

$k_1 = 1755 * CF + 155325; \ r^2 = 0.99$

$k_2 = 809 * CF + 5792; \ r^2 = 0.98$

$m_2 = .0003 * CF + .0226; \ r^2 = 0.92$

$c_2 = 1.40 * CF + 76.8; \ r^2 = 0.98$ 

(6.14)

The above relations suggest that higher coupling force between the hand and handle yields higher values for $k_1$ and $k_2$. Although the mechanical equivalent models are not intended to yield any bio-mechanical behavior of the hand-arm system, the variations in these parameters could be interpreted in view of the biological properties. An increase in coupling force would yield higher stiffness of the hand tissues directly in contact of the hand, and higher muscles contractions and thus the higher stiffness of the overall structure. A higher coupling force also yields stronger coupling between the hand and handle, and thereby an increase in the hand mass $m_2$ coupled with the handle. The support and the corresponding visco-elastic properties ($m_3$, $k_3$, $c_3$) do not vary considerably with the coupling force. The damping property of the skin tissue ($c_1$) in contact with the handle does not show the effect of the coupling force. The increase in energy dissipation of the hand-arm system with increasing $CF$ is most likely reflected by the increasing value of damping coefficient $c_2$.

### 6.4.2 Three-mass and two-DOF model (structure $B$, $z_h$-axis))

The parameters of the three-mass and two-DOF model structure $B$ (Figure 6.3(b)) are identified corresponding to all $F_g/F_p$ combinations. Similar to the model structure $A$, some of the model parameters revealed low sensitivity to variations in the hand forces, particularly the coupling force. These include all masses $m_1$, $m_2$, and $m_3$. The variations in the remaining identified parameters with the hand forces are summarized in Table 6.5.

269

Table 6.5: Variations in the hand-arm model (structure $B$) parameters with hand forces under $z_h$-axis vibration. ($m_1$= .025 kg; $m_2$= 1.367 kg; and $m_3$= 1.086 kg)

| $F_g$ (N) | $F_p$ (N) | Coupling Force (N) | $k_1$ (N/m) | $k_2$ (N/m) | $k_3$ (N/m) | $c_1$ (Ns/m) | $c_2$ (Ns/m) | $c_3$ (Ns/m) |
|---|---|---|---|---|---|---|---|---|
| 10 | 25 | 35 | 26504 | 4274 | 2098 | 118 | 46 | 53 |
| 10 | 50 | 60 | 41774 | 5250 | 2507 | 156 | 50 | 59 |
| 10 | 75 | 85 | 51778 | 6378 | 3059 | 186 | 55 | 63 |
| 30 | 25 | 55 | 38209 | 4537 | 2146 | 138 | 47 | 54 |
| 30 | 50 | 80 | 53862 | 5684 | 2812 | 174 | 51 | 61 |
| 30 | 75 | 105 | 68013 | 6444 | 3080 | 208 | 59 | 62 |
| 50 | 25 | 75 | 49233 | 4583 | 2054 | 160 | 47 | 56 |
| 50 | 50 | 100 | 66732 | 5368 | 2624 | 187 | 55 | 63 |
| 50 | 75 | 125 | 81322 | 6812 | 3292 | 215 | 64 | 64 |

Figure 6.13 shows the linear correlations ($r^2$) between the $CF$ and different hand-arm model parameters. The $r^2$ values vary from 0.67 to 0.99. Similar to model $A$, the highest correlation factor is observed for $k_1$, which shows linear increase as $CF$ increases. All other parameters also suggest positive correlations with $CF$, as obvious from Figure 6.13. The model parameters could be estimated for different coupling forces ($CF$) from these linear relationships;

$k_1$= 605.5* $CF$+ 4608, $r^2$= 0.99;

$k_2$= 28.17*$CF$+3228, $r^2$ =0.72;

$k_3$= 13.73*$CF$+1532, $r^2$= 0.67;

$c_1$= 1.12*$CF$+82.3, $r^2$= 0.95;

$c_2$= .198*$CF$+37.5, $r^2$=083;

$c_3$= .134*$CF$+49.2, $r^2$= 0.73

(6.15)
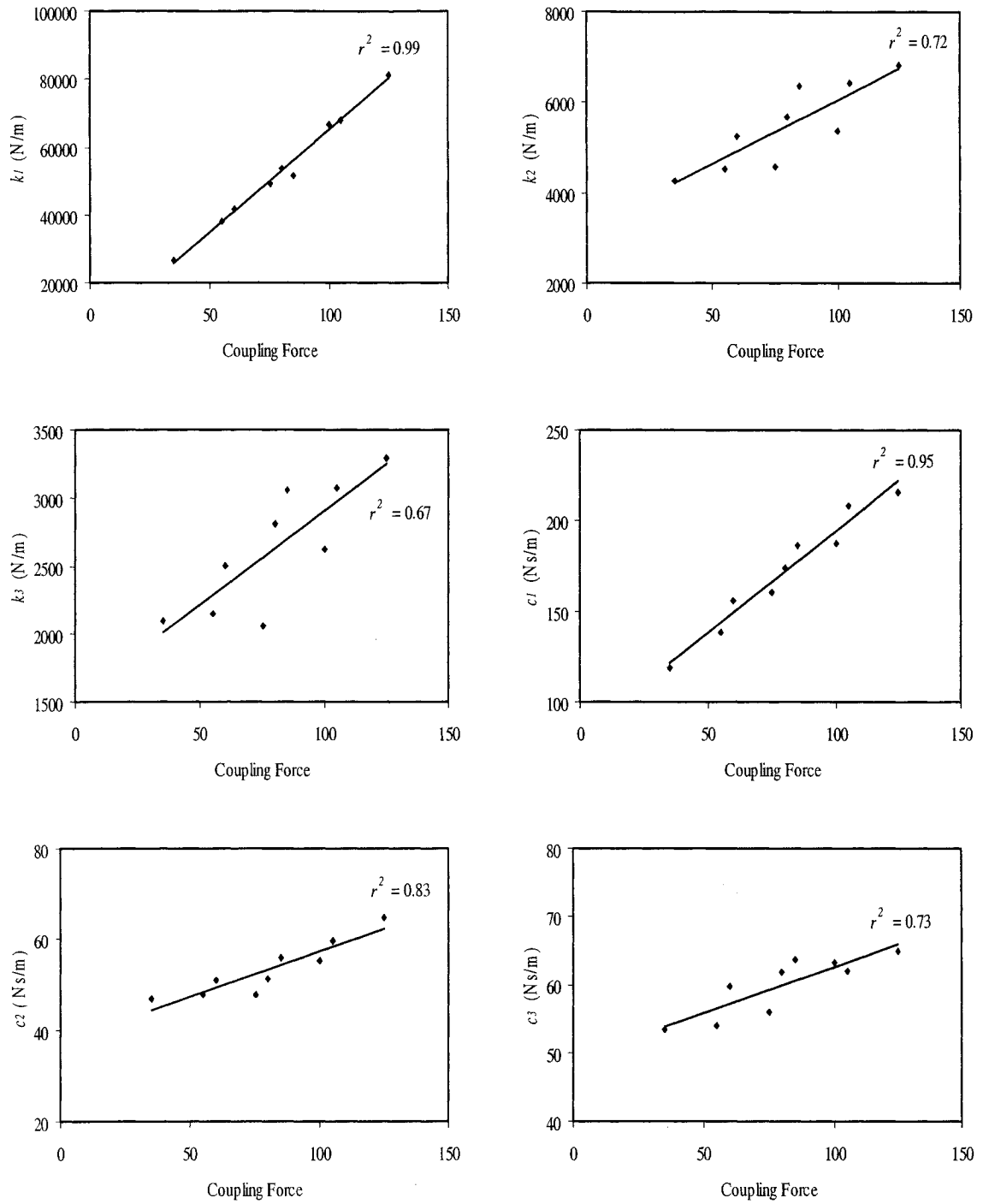
Figure 6.13: Linear correlations between model parameters (model *B)* and the coupling force ($z_h$-axis; posture *P1*).

Equations (6.15) and Figure 6.13 suggest relatively lower correlation factors for some of the model parameters than those obtained for model *A*, particularly for $k_2$, $k_3$ and

c3. In attempt to improve the estimations of the model parameters, multiple linear regressions between model parameters and both the grip and push forces ($F_g$ and $F_p$) as independent variables are performed. The results suggested relatively higher correlation factors, as it is evident from the following linear regression formulations and the correspondent r2 values:

$$k_1 = 4685 + 644\ F_g + 581\ F_p;\ r^2 = 0.99$$
$$k_2 = 3186 + 7.17\ F_g + 41.6\ F_p;\ r^2 = 0.98$$
$$k_3 = 1510 + 2.56\ F_g + 2.9\ F_p;\ r^2 = 0.96$$
$$c_1 = 81.7 + .854\ F_g + 1.29\ F_p;\ r^2 = 0.99$$
$$c_2 = 37.3 + .117\ F_g + .251\ F_p;\ r^2 = 0.92$$
$$c_3 = 49 + .06\ F_g + .181\ F_p;\ r^2 = 0.88$$

(6.16)

The above formulations suggest that consideration of model parameters as functions of grip and push forces would be desirable than that based upon functions of the coupling force. The resulting model could permit improved prediction of the biodynamic responses as functions of the hand grip and push forces.

### 6.4.3 Four-mass and three-DOF model (structure $D$, $z_h$-axis))

The parameters of the four-mass and three-DOF model structure $D$, shown in Figure 6.3(d), are identified corresponding to each $F_g/F_p$ combination. Similar to the model structures $A$ and $B$, some of the model parameters revealed low sensitivity to alterations in the hand forces, particularly the coupling force. These include $m_1$, $m_3$, $k_2$, $k_3$, and $c_3$. The variations in the remaining identified parameters with the hand forces are summarized in Table 6.6.

272

Table 6.6: Variations in the hand-arm model (structure $D$) parameters with hand forces under $z_h$-axis vibration. ($m_1= .023$ kg; $m_3= 1.5$ kg; $k_2$=6000 N/m; $k_3$=8000 N/m; and $c_3= 5$ Ns/m)

| $F_g$ (N) | $F_p$ (N) | Coupling Force (N) | $k_1$ (N/m) | $k_4$ (N/m) | $c_1$ (Ns/m) | $c_2$ (Ns/m) | $c_4$ (Ns/m) | $m_2$ (kg) | $m_4$ (kg) |
|---|---|---|---|---|---|---|---|---|---|
| 10 | 25 | 35 | 24575 | 3506 | 121 | 23 | 113 | 1.54 | 1.06 |
| 10 | 50 | 60 | 38448 | 2581 | 170 | 31 | 108 | 1.51 | 0.67 |
| 10 | 75 | 85 | 50225 | 1807 | 214 | 43 | 97 | 1.45 | 0.24 |
| 30 | 25 | 55 | 36910 | 3340 | 139 | 32 | 107 | 1.45 | 0.99 |
| 30 | 50 | 80 | 53157 | 2335 | 182 | 41 | 101 | 1.4 | 0.53 |
| 30 | 75 | 105 | 69322 | 2006 | 221 | 55 | 80 | 1.37 | 0.24 |
| 50 | 25 | 75 | 47244 | 3062 | 161 | 33 | 108 | 1.44 | 1.01 |
| 50 | 50 | 100 | 66259 | 2696 | 181 | 48 | 96 | 1.36 | 0.67 |
| 50 | 75 | 125 | 83550 | 1831 | 214 | 64 | 75 | 1.33 | 0.2 |

In an attempt to relate the identified model parameters with the hand-handle coupling force, linear correlation analyses were performed between the model parameters and the coupling force. The results generally revealed linear variations in the model parameters with the $CF$ with correlation factors in the 0.64 to 0.98 range, as shown in Figure 6.14. Some of the trends observed from regression relationships could be physically explained, while others could be taken as empirical relations. The stiffness coefficient $k_1$ increases with the increase in coupling force, suggesting higher stiffness due to hand-handle coupling with increase in hand forces ($r^2= 0.98$). The damping coefficients ($c_1$ and $c_2$) also increase with the coupling force which could indicate more energy dissipation in the hand-arm system as the coupling between the hand and the handle increases. The contribution due to the mass and elasticity ($m_4$, $k_4$, $c_4$) near the support diminishes with increase $CF$ for the flexed elbow posture. The model parameters could be described as a function of the coupling forces ($CF$) on the basis of the regression relationships, as:

$k_1 = 656.15 * CF - 303.85, \ r^2 = 0.98;$

$k_4 = -18.3 * CF + 4040, \ r^2 = 0.64;$

$m_2 = -.0023 * CF + 1.62, \ r^2 = 0.85;$

$m_4 = -.01 * CF + 1.42, \ r2 = 0.64;$

$c_1 = 1.1 * CF + 9.9, \ r^2 = 0.77;$

$c_2 = .456 * CF + 4.54, \ r^2 = 0.95$

$c_4 = -.43 * CF + 133.1, \ r^2 = 0.85$ 　　　　　　　　　　　　　(6.17)

The above relations reveal relatively lower correlation factors for some of the model parameters with regards to the coupling force. In an attempt to improve the model predictability, multiple linear regressions were also performed to study the variations in model parameters with variations in $F_g$ and $F_p$ as independent variables. Higher correlations factors were obtained than those with the coupling force. The multiple linear regression relations for different model parameters with the grip and push forces are obtained as:

$k_1 = -219 + 698 \, F_g + 629 \, F_p, \ r^2 = 0.99;$

$k_4 = 4071 - 2.54 \, F_g - 28.4 \, F_p, \ r^2 = 0.94;$

$m_2 = 1.61 - .0031 \, F_g - .0019 \, F_p, \ r^2 = 0.93;$

$m_4 = 1.44 - .00075 \, F_g - .0159 \, F_p, \ r^2 = 0.98;$

$c_1 = 89.6 + .433 \, F_g + 1.52 \, F_p, \ r^2 = 0.95;$

$c_2 = 4.42 + .395 \, F_g + .496 \, F_p, \ r^2 = 0.96;$

$c_4 = 133 - .316 \, F_g - .505 \, F_p, \ r^2 = 0.89$ 　　　　　　　(6.18)
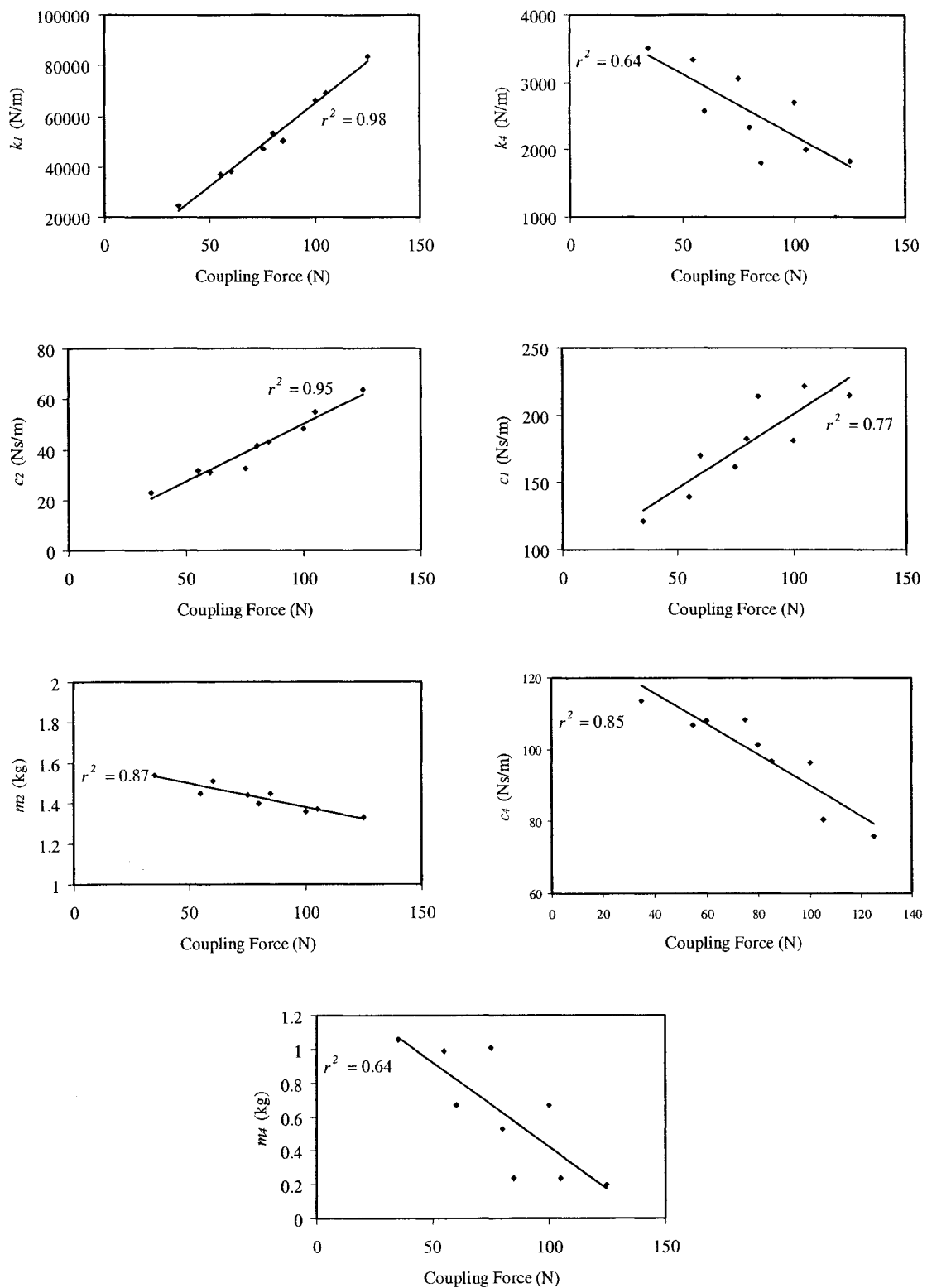
Figure 6.14: Linear correlations between model parameters (model $D$) and the coupling force ($z_h$-axis; posture $P1$).

A comparison of the relations expressed in equations (6.17) and (6.18) suggests that application of linear multiple regressions with $F_g$ and $F_p$ as independent variables would yield higher correlation factors for the model parameters. The consideration of mechanical-equivalent model parameters as function of grip and push forces could thus enhance the model prediction ability over a wide range of hand forces.

### 6.4.4 Three-mass and two-DOF model (structure $B$, $x_h$-axis)

The parameters of the three-mass and two-DOF model structure $B$ under $x_h$-axis vibration are identified in a similar manner corresponding to different $F_g/F_p$ combinations. The results attained from solution of the minimization problem for each grip and push force combination revealed considerable variations in the model parameters with hand forces. The parameters $m_2$ and $c_3$, however, formed exceptions and revealed insensitivity to variation in hand forces. Table 6.7 summarizes the variations in the remaining identified parameters of model $B$ with the hand forces. The results suggest that all the parameters could be considered relatively insensitive to variations in the coupling force. The variations in the stiffness and damping parameters with coupling force reveal linear increase in the parameters with coupling force, as shown in Figure 6.15. The correlation factors are lower and range from 0.39 to 0.83.

Table 6.7: Variations in the hand-arm model (structure $B$) parameters with hand forces under $x_h$-axis vibration. ($m_2$= .3 Kg ; and $c_3$= 15 Ns/m ).

| $F_g$ | $F_p$ | Coupling Force | $m_1$ | $m_3$ | $k_1$ | $k_2$ | $k_3$ | $c_1$ | $c_2$ |
|---|---|---|---|---|---|---|---|---|---|
| (N) | (N) | (N) | (kg) | (kg) | (N/m) | (N/m) | (N/m) | (Ns/m) | (Ns/m) |
| 10 | 0 | 10 | .025 | .207 | 43602 | 4442 | 100 | 132 | 9 |
| 10 | 25 | 35 | .023 | .263 | 70159 | 4717 | 326 | 151 | 15 |
| 10 | 50 | 60 | .019 | .326 | 74839 | 5533 | 799 | 165 | 29 |
| 30 | 0 | 30 | .029 | .217 | 92917 | 7288 | 100 | 189 | 12 |
| 30 | 25 | 55 | .029 | .232 | 119053 | 6719 | 187 | 203 | 16 |
| 30 | 50 | 80 | .026 | .325 | 153258 | 7118 | 944 | 219 | 26 |
| 50 | 0 | 50 | .038 | .224 | 128465 | 9731 | 100 | 201 | 18 |
| 50 | 25 | 75 | .034 | .237 | 156273 | 8783 | 310 | 225 | 19 |
| 50 | 50 | 100 | .0266 | .31 | 206283 | 8991 | 1005 | 250 | 25 |

Owing to the low correlation factors between the model parameters and the coupling force, linear multiple regressions have been performed considering the grip and push forces as the independent variables. The analyses resulted in following regression relationships for different model parameters in grip and push forces:

$$m_1 = .0232 + .000263 \, F_g - .000136 \, F_p, \quad r^2 = 0.91;$$

$$m_3 = .214 - .000208 \, F_g - .00209 \, F_p, \quad r^2 = 0.89;$$

$$k_1 = 12257 + 2520 \, F_g + 1129 \, F_p, \quad r^2 = 0.96;$$

$$k_2 = 3803 + 107 \, F_g + 1.21 \, F_p, \quad r^2 = 0.95;$$

$$k_3 = -25 + 1.58 \, F_g + 16.3 \, F_p, \quad r^2 = 0.88;$$

$$c_1 = 118 + 1.90 \, F_g + .742 \, F_p, \quad r^2 = 0.94;$$

$$c_2 = 9.7 + .0773 \, F_g + .269 \, F_p, \quad r^2 = 083 \tag{6.19}$$

The above relationship reveal considerably higher correlation factors ($r^2$) of linear multiple regressions of $F_g$ and $F_p$ with the model parameters, when compared to those obtained from regressions of $CF$. The correlation factors range from 0.83 to 0.96. The two-DOF model coupled with linear multiple regression relationships could thus provide accurate prediction of the biodynamic response as a function of hand forces.
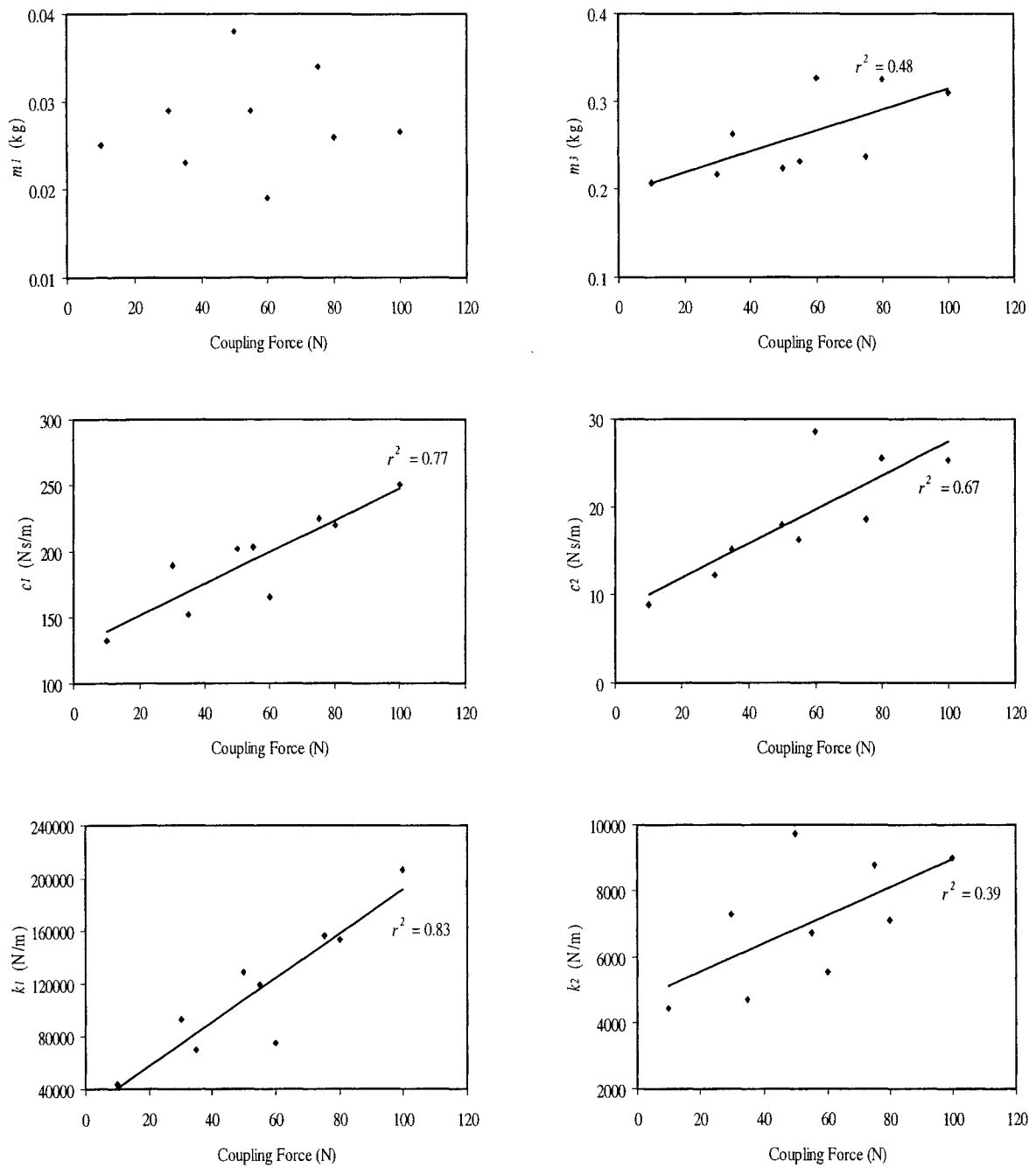
Figure 6.15: Linear correlations between model parameters (model $B$) and coupling force (40 mm handle, $x_h$-axis, posture $P1$)

## 6.4.5 Three-mass and three-DOF mode (structure $C$, $x_h$-axis)

The parameters of the three-mass and three-DOF model structure $C$ are identified corresponding to each $F_g/F_p$ combination in a similar manner to satisfy the measured biodynamic responses under $x_h$-axis vibration. An examination of the range of identified parameters over the range of hand forces considered revealed relatively low sensitivity of parameters $m_3$, $k_4$, $c_1$, $c_3$ and $c_4$ to variations in coupling force. Table 6.8 summarizes the variations in the remaining parameters with varying hand forces. Figure 6.16 illustrates the linear correlation of the model parameters with the coupling force. The figures show nearly linear increase in stiffness parameters ($k_1$, $k_2$ and $k_3$) with the coupling force, suggesting increasing stiffness of the hand arm system. The corresponding correlation factors tend to very low for $k_1$ (0.23) and $k_3$ (0.23), and somewhat reasonable for $k_2$ (0.78). The damping constant $c_2$ and $m_2$ also increase slightly with the coupling force with $r^2$ values being 0.79 and 0.39. The mass near the support $m_4$ decreases with coupling force in a linear manner ($r^2 = 0.74$), as observed in case of model $D$ under $z_h$-axis.

Owing to the relatively lower correlation factors of the linear regressions in $CF$, multiple regressions in grip and push forces were also attempted. The results revealed similar degree of correlation of various model parameters with the grip and push forces. It is thus concluded that the three-mass and three-DOF model (structure $C$) can provide a reasonable prediction of the biodynamic responses over the range of grip and push forces. The model structure $B$ is thus considered adequate for general application over range of hand forces $x_h$-axis vibration.

Table 6.8: Variations in the hand-arm model (structure $C$) parameters with hand forces under $x_h$-axis vibration. ($m_3$= .026 kg; $k_4$= 6000 N/m; and $c_1$= 500 Ns/m)

| $F_g$ (N) | $F_p$ (N) | Coupling Force (N) | $k_1$ (N/m) | $k_2$ (N/m) | $k_3$ (N/m) | $c_2$ (Ns/m) | $m_2$ (kg) | $m_4$ (kg) |
|---|---|---|---|---|---|---|---|---|
| 10 | 0 | 10 | 166452 | 52804 | 3004 | 165 | 0.04 | 0.407 |
| 10 | 25 | 35 | 197429 | 106072 | 3680 | 184 | 0.04 | 0.36 |
| 10 | 50 | 60 | 210475 | 123245 | 4741 | 193 | 0.04 | 0.337 |
| 30 | 0 | 30 | 350566 | 115697 | 6305 | 220 | 0.06 | 0.325 |
| 30 | 25 | 55 | 493091 | 134981 | 5445 | 237 | 0.06 | 0.331 |
| 30 | 50 | 80 | 454723 | 182236 | 6879 | 287 | 0.06 | 0.29 |
| 50 | 0 | 50 | 417331 | 152871 | 9203 | 219 | 0.08 | 0.291 |
| 50 | 25 | 75 | 509657 | 180995 | 8515 | 246 | 0.08 | 0.3 |
| 50 | 50 | 100 | 305952 | 354790 | 9114 | 337 | 0.08 | 0.27 |
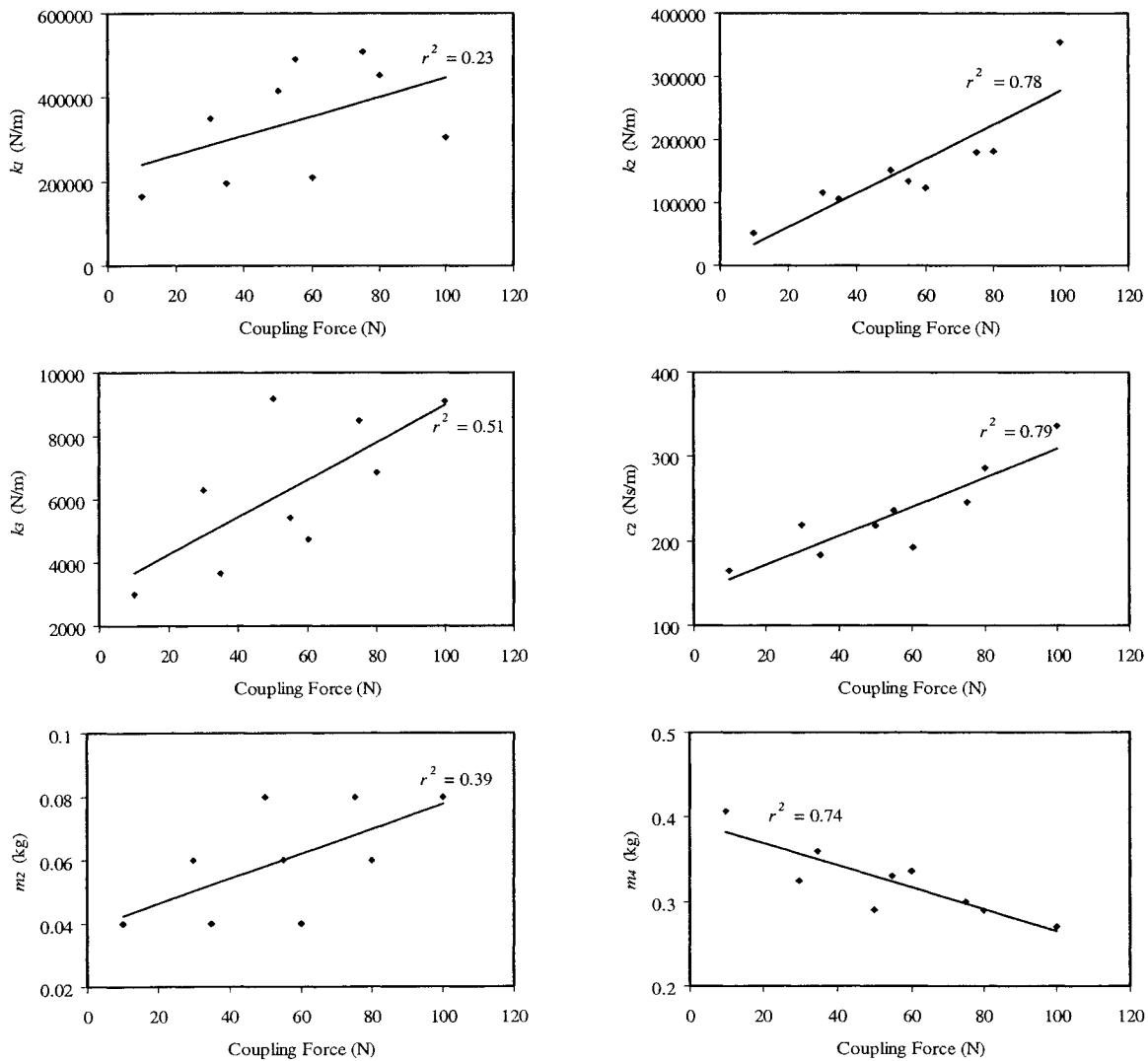


Figure 6.16: Linear correlations between model parameters (model $C$) and coupling force (40 mm handle, $x_h$-axis, posture $P1$)

280

## 6.5   Model Parameters as a Function of Hand-Arm Posture

The significant effects of variations in the hand-arm posture on the biodynamic responses have been clearly observed from the measured data. The postural effects on the measured *DPMI* and absorbed power were observed to be far more significant under exposure to $z_h$-axis vibration than those under $x_h$-axis vibration. The applicability of the proposed model structures for characterizing the biodynamic response of the extend arm posture (posture *P2*) is thus examined. Moreover, only the two-mass and two-DOF model structure (*A*) is attempted, since this structure provided highest correlation factors between the coupling force and the model parameters.

The optimization problem defined previously (equation (6.11)) is solved for each combination of hand forces $(F_g/F_p)$ in conjunction with the corresponding measured data acquired for the extended arm posture. The resulting model parameters, considered valid for a particular hand force combination and the extended arm (posture *P2*), are summarized in Table 6.9. The results suggested only slight variations in parameters $k_3$ and $c_1$. These parameters were thus held fixed during the parameter identification task.

Table 6.9: Variations in the hand-arm model (structure A) parameters with hand forces under $z_h$-axis vibration and posture P2 ($k_3$= 1000 N/m; and $c_1$= 750 Ns/m).

| $F_g$ (N) | $F_p$ (N) | Coupling Force (N) | $k_1$ (N/m) | $k_2$ (N/m) | $c_2$ (Ns/m) | $c_3$ (Ns/m) | $m_2$ (kg) | $m_3$ (kg) |
|---|---|---|---|---|---|---|---|---|
| 10 | 25 | 35 | 186553 | 26616 | 114 | 222 | .03 | 2.96 |
| 10 | 50 | 60 | 234012 | 44817 | 153 | 278 | .0322 | 2.82 |
| 10 | 75 | 85 | 314088 | 65066 | 170 | 300 | .036 | 2.76 |
| 30 | 25 | 55 | 224693 | 46393 | 136 | 260 | .0271 | 2.86 |
| 30 | 50 | 80 | 314070 | 64739 | 171 | 290 | .0423 | 2.76 |
| 30 | 75 | 105 | 351292 | 96121 | 225 | 321 | .0416 | 2.65 |
| 50 | 25 | 75 | 276749 | 65610 | 156 | 272 | .0318 | 2.8 |
| 50 | 50 | 100 | 348494 | 86279 | 207 | 282 | .049 | 2.75 |
| 50 | 75 | 125 | 404966 | 103260 | 214 | 326 | .0496 | 2.67 |

Linear regressions are performed to examine the variations in model parameters with the coupling force. Figure 6.17 shows the correlations between $CF$ and the model parameters. The results suggest nearly linear variations in the model parameters with the coupling force. The correlations factors between models parameters and $CF$ vary from 0.75 to 0.98. The parameters could thus be estimated as a function of the hand forces from the linear relations obtained from regression analyses and expressed as;

$m_2 = .0002 * CF + .02, \quad r^2 = 0.75;$

$m_3 = -.0033 * CF + 3.04.02, \quad r^2 = 0.91;$

$k_1 = 2515.4 * CF + 93756, \quad r^2 = 0.98;$

$k_2 = 897.35 * CF - 5243, \quad r^2 = 0.97;$

$c_2 = 1.275 * CF + 69.67, \quad r^2 = 0.91;$

$c_3 = 1.044 * CF + 200, \quad r^2 = .084$ (6.20)

The identified parameters of the model structure ($A$) on the basis of the data acquired for the extended arm posture ($P2$) are compared with those identified for the bent elbow posture ($P1$) in Table 6.4. The parameters of the identical model structure ($A$) alone are considered. The comparison revealed important trends for some of the model parameters in view of the two postures considered. General conclusions and trends, however, could not be derived considering the availability of data for only two postures. The most significant effect of the posture could be observed in the mass parameters. The model mass $m_3$ for the extended arm posture ($P2$) is considerably higher than that for the bent elbow posture ($P1$). The total model mass for posture $P2$ is higher than that for posture $P1$, which conforms to the experimental observations of notable difference in the apparent masses for the two postures at low excitation frequencies.
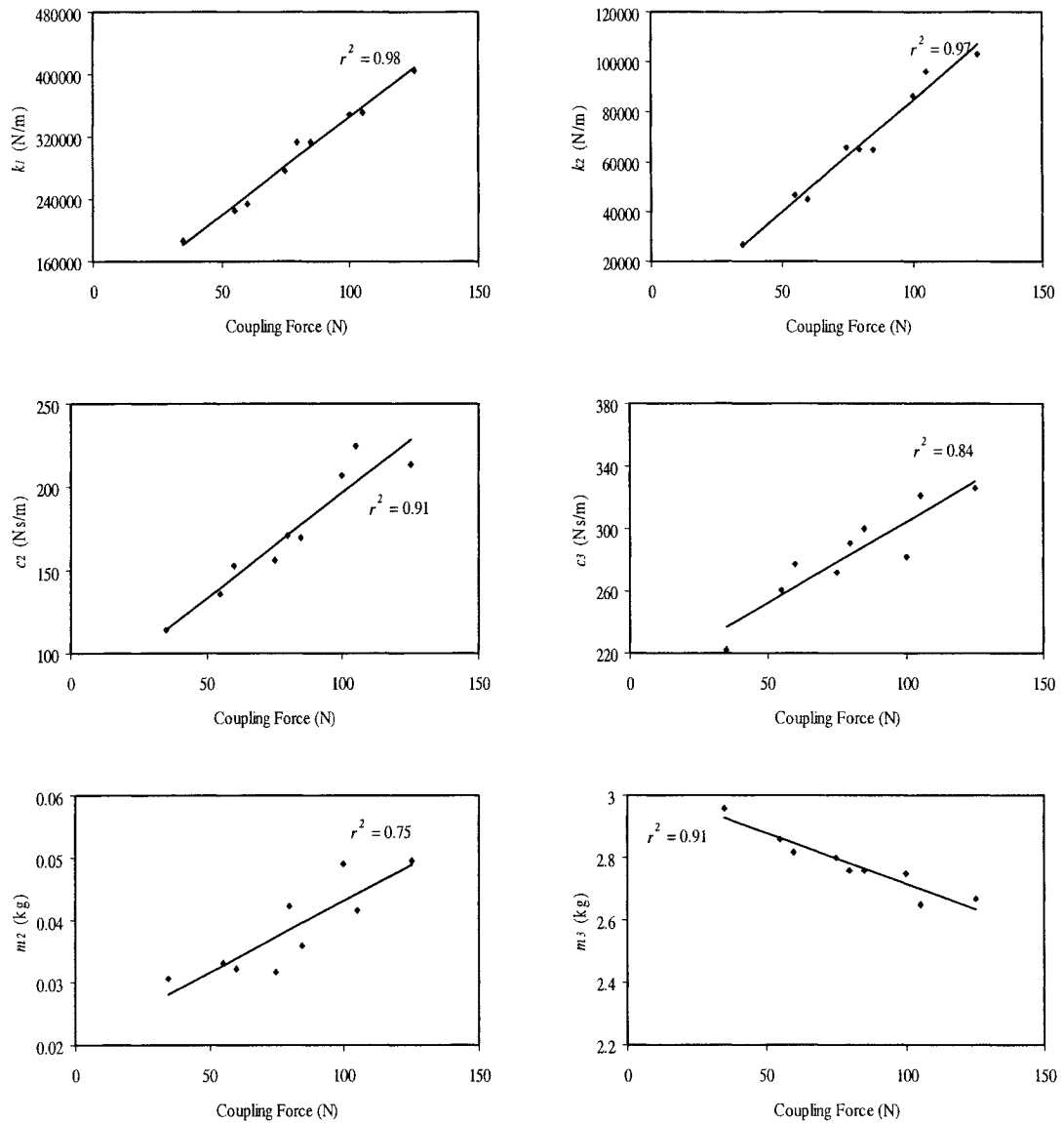
Figure 6.17: Linear correlations between the model parameters (model $A$) and the coupling force ($z_h$-axis, posture $P2$)

The two models exhibit identical value of damping $c_1$, near the handle contact, while the damping constant $c_3$ for posture $P2$ is remarkably higher than that for the posture $P1$ model. The model corresponding to $P2$ would thus yield higher power dissipation. This particular observation also conforms to the measured absorbed power data, which is considerably higher with the extended arm posture. The stiffness constant

283

in the vicinity of the support ($k_3$) is identical for both postures, while other stiffness constants are comparable, higher total mass would thus lead to lower resonant frequency of the hand-arm model under extended hand-arm posture, as observed from the measured data. Table 6.10 summarizes the comparisons between the model parameters identified for the two considered postures obtained from the generalized model (structure $A$).

Table 6.10: Comparison between model parameters under postures $P1$ and $P2$ for different hand force combinations (model $A$, $z_h$-axis)

| $F_g/F_p$ (N) | 10/25 | | 30/50 | | 50/75 | |
|---|---|---|---|---|---|---|
| Posture | $P1$ | $P2$ | $P1$ | $P2$ | $P1$ | $P2$ |
| $m_2$ (kg) | 0.031 | 0.03 | 0.043 | 0.0423 | 0.061 | 0.0496 |
| $m_3$ (kg) | 1.26 | 2.96 | 1.26 | 2.76 | 1.26 | 2.67 |
| $k_1$ (N/m) | 215414 | 186553 | 292648 | 314070 | 371448 | 404966 |
| $k_2$ (N/m) | 33468 | 26616 | 73258 | 64739 | 104059 | 103260 |
| $k_3$ (N/m) | 1000 | 1000 | 1000 | 1000 | 1000 | 1000 |
| $c_1$ (Ns/m) | 750 | 750 | 750 | 750 | 750 | 750 |
| $c_2$ (Ns/m) | 124 | 114 | 200 | 171 | 250 | 214 |
| $c_3$ (Ns/m) | 77 | 222 | 77 | 290 | 77 | 326 |

## 6.6 Models Validations

The generalized hand-arm model is further examined in view of its vibration properties and its ability to predict the biodynamic responses of the hand-arm system. The model validity is examined under three different hand force combinations. Since the baseline model was developed for 30 N grip and 50 N push forces, the hand forces other than the baseline values are thus considered. Three-DOF with four masses (model $D$) and two-DOF with three masses (model $B$), representing the hand-arm system exposed to $z_h$- and $x_h$-axes vibration, respectively, are chosen for assessing their validity over a range of hand forces. The vibration properties of the models are assessed in terms of natural frequencies and damping ratios corresponding to single hand force combination.

284

The parameters for the four mass three-DOF model under $z_h$-axes vibration, $F_g=$ 50

N and $F_p=$ 50 N, can be obtained from equations (6.19). The static deflection of this

model when exposed to 50 N push force is in the order of 0.035 m. Eigenvalue problem

was formulated and solved to identify natural frequencies and damping ratios of the

hand-arm model with model parameters computed from regressions functions. The

analyses revealed model natural frequencies as 9.8, 23.8 and 36.8 Hz, while the

corresponding frequencies of damped oscillations were obtained as 9.16, 19.09 and 33.7

Hz, for the three-DOF model ($D$). The corresponding damping ratios were obtained as

0.61, 0.38 and 0.39, respectively. The frequencies of damped oscillations of the hand-arm

model directly relate to the maxima and minima in apparent mass magnitude response, as

shown in Figure 6.18.
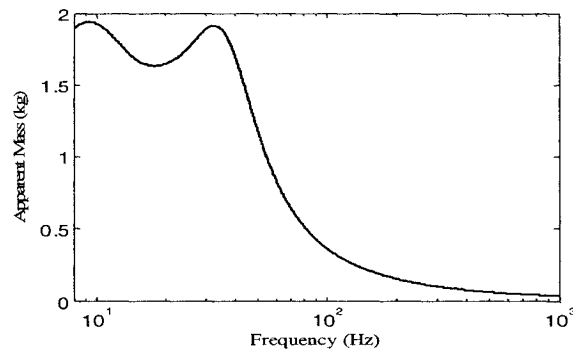


Figure 6.18: Apparent mass response of the hand-arm system model $D$ ($F_g=50$ N, $F_p=50$ N, posture $P1$, $z_h$-axis).

Figure 6.19 illustrates the comparisons of the biodynamic responses ($DPMI$ and

absorbed power) derived from model ($D$) under $z_h$-axis vibration with the measured data.

The comparisons are presented for three hand force combinations. The model exhibits

good prediction of both biodynamic responses, $DPMI$ and absorbed power for the hand

force combinations considered. Some deviations, however, are observed in the $DPMI$

response at frequencies above 200 Hz, under higher hand forces.
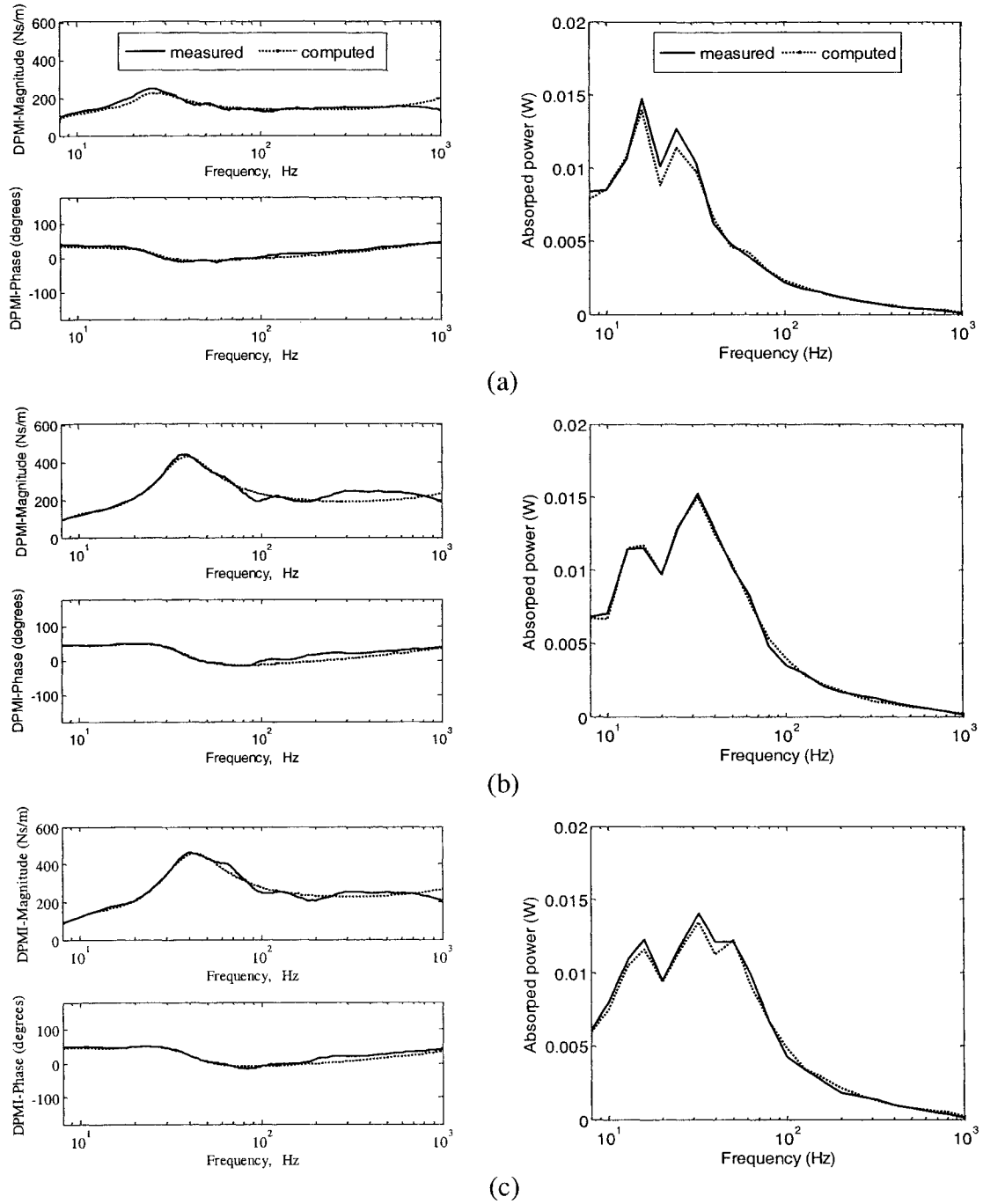
Figure 6.19: Comparisons of hand arm model ($D$) responses with the mean measured data under different combinations of $F_g/F_p$: (a) 10/25; (b) 50/50; and (c) 50/75 (Model $D$, $z_h$-axis, 40 mm handle, and posture $P1$).

The results suggest that the model can accurately predict the *DPMI* magnitude and phase responses in the entire frequency range for different grip and push forces. The model, particularly, yields good prediction of the peak *DPMI* magnitude and the

corresponding frequency. The absorbed power prediction ability of the model is also reasonably good, as observed in the figure, although some errors are evident under light and high hand forces.

Two-DOF model (model $B$) of the hand-arm system is considered for examining its validity under $x_h$-axis vibration coupled with 40 mm handle and posture $P1$. The model would yield static deflection in order of 0.06 m under the application of a 50 N static push force. Assuming $F_g$=50 N and $F_p$=50 N, the model parameters could be obtained from equation (6.20). The model parameters are employed to solve the eigenvalue problem to identify its natural frequencies and damping ratios. The natural frequencies of the model were attained as 28 and 131 Hz, while the corresponding damped frequencies as 26 and 108 Hz. The both vibration modes were found under-damped with damping ratios of 0.37 and 0.56. The apparent mass magnitude response, shown in Figure 6.20, suggests presence of peak magnitudes in the vicinity of the identified frequencies.
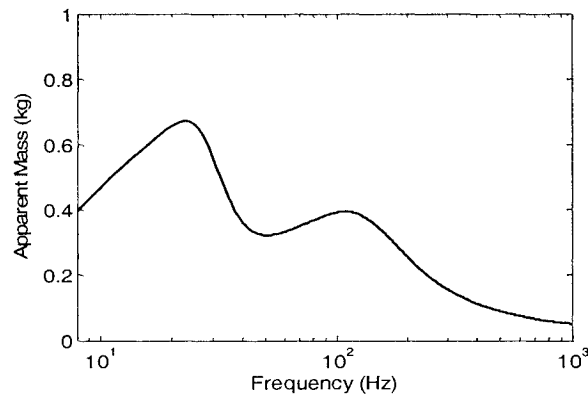


Figure 6.20: Apparent mass of hand-arm system computed from the model parameters (model $B$, $F_g$= 50 N, $F_p$=50 N, posture $P1$, $x_h$-axis).

The validity of the model is examined by comparing its responses with the mean measured data in terms of *DPMI* and absorbed power under three different hand force

287

combination. Figure 6.21 illustrates comparison of the mean measured data with the computed biodynamic responses under three different hand force combinations.



(a)

(b)

(c)
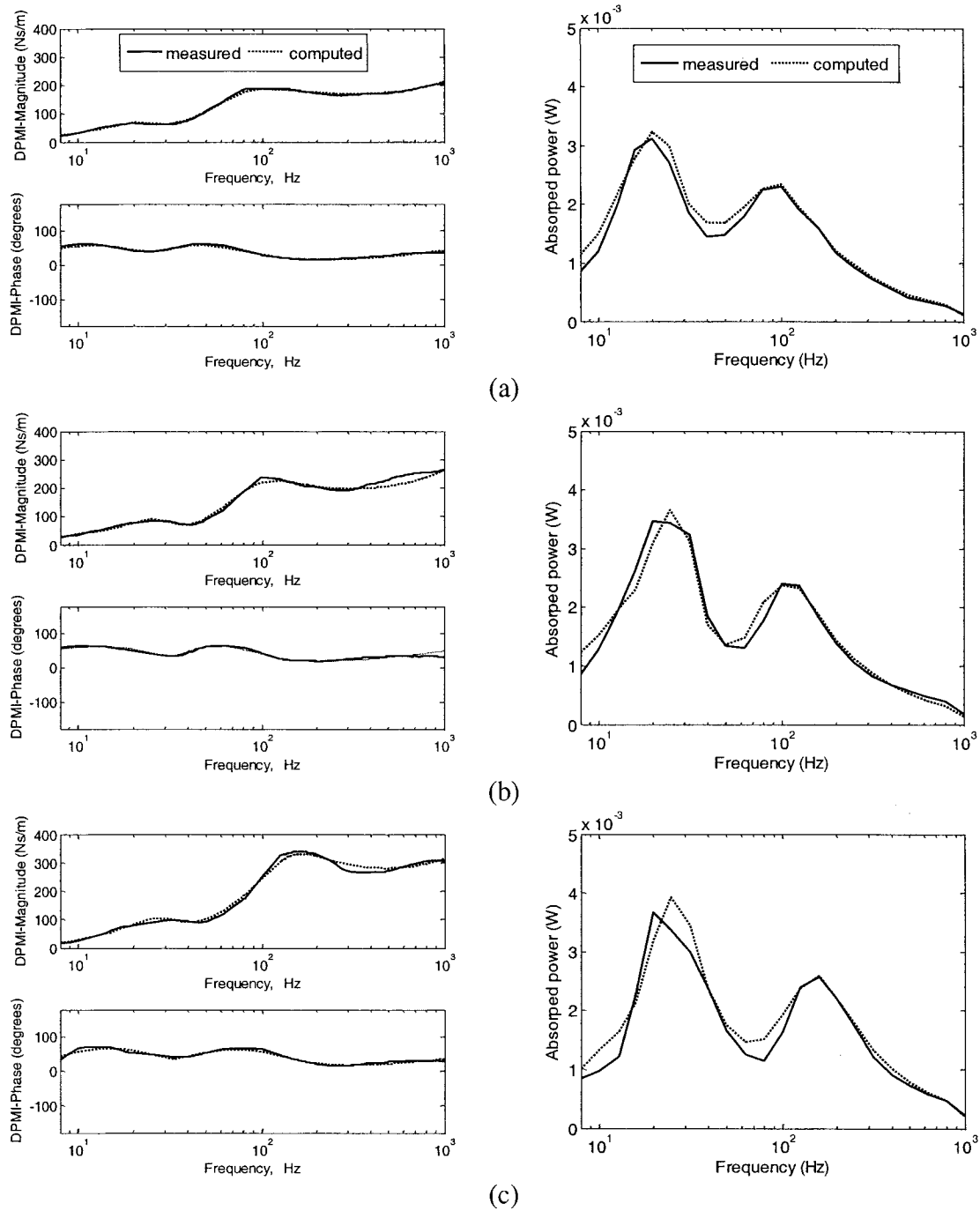
Figure 6.21: Comparisons of the hand arm model (*B*) responses with the mean measured data under different $F_g/F_p$ combinations: (a) 10/25; (b) 30/00; and (c) 50/50 (Model *B*, $x_h$-axis, 40 mm handle, posture *P1*).

The model responses in *DPMI* compare reasonably well with the mean measured data under the hand force combinations. Some deviations in the magnitude response are observed at frequencies above 100 Hz. The model also yields excellent prediction of the *DPMI* phase response. Relatively large deviations, however, are observed between the computed and measured absorbed power. The model results, however, show trends very similar to those observed in the measured data. The prediction error tends to higher under the highest hand force level considered in the study ($F_g = 50$ N, $F_p = 50$ N).

## 6.7 Summary and Conclusions

Although a number of biodynamic models have been proposed in the literature to characterize the biodynamic responses of the human hand-arm system exposed to vibration, the methodology used for estimating the model parameters has often relied on data measured under various conditions. While the driving-point mechanical impedance has been most widely used to estimate the model parameters, none of the proposed models have attempted to combine both the magnitude and phase of *DPMI* response with the absorbed power under representative hand forces. In this chapter, a new approach of modeling the hand-arm system has been proposed by using both the *DPMI* and absorbed power responses as the target functions. A conceptual mistake has been corrected concerning the number of DOF of the reported models. Consequently, the resonant frequencies of the system are related to the of the apparent mass magnitude peaks.

The mean values of measured impedance magnitude and phase response, and absorbed power were utilized to derive two- and three-DOF lumped parameter models of the human hand-arm system exposed to $z_h$- and $x_h$-axes vibration. The model parameters were identified through solution of a constrained optimization problem, which resulted in

different model parameters depending on the axis of vibration, structure of the model, hand-arm posture. The models, in general, showed reasonably good agreement with the measured responses. Three-DOF model with four masses and two-DOF model with three lamped masses yield similar trends and comparable level of accuracy. The model parameters are further identified as functions of both the grip and push forces. On the basis of the results, model structure $D$ (Three-DOF and four masses) and structure $B$ (two-DOF and three masses) are suggested for accurate prediction of the biodynamic responses under $z_h$- and $x_h$-axes vibration, respectively. The results suggest that the model can provide a reasonably good prediction of the driving-point mechanical impedance and absorbed power characteristics of the hand-arm system under $z_h$- and $x_h$-axes vibration. The vibration properties of the proposed models could be considered appropriate in view of the practical issues and related to model implementation, namely static deflection, damping ratio and damped frequencies.

CHAPTER 7

CONCLUSIONS AND RECOMMENDATION FOR FUTURE WORK

7.1    General

Prolonged exposure to hand-transmitted vibration has been associated with several diseases and disorders among the operators of power tools, collectively known as hand-arm vibration syndrome (HAVS). The vascular effects or vibration white finger (VWF), which appears as episodes of fingers blanching together with tingling and numbness in the exposed hand, have been studied and documented more than the other components. The risk of developing HAVS has been reported to depend on several physical and biodynamic factors such as magnitude and axis of vibration, frequency of vibration, the duration of vibration exposure, the mechanical coupling between the hand and the handle and on the hand-arm posture of power tools operators. Various epidemiological studies have reported high prevalence rates of VWF symptoms among the operators of hand-held power tools. These high prevalence rates promoted several clinical studies to establish the cause-effect relationships, and engineering studies to improve work place environment and minimize the hazardous consequences. These studies have primarily focused on dynamic response characterization of the hand-arm and development of mechanical-equivalent models of the human hand-arm.

The characterizations of the biodynamic responses ($DPMI$ or/and absorbed power) of the human hand-arm system to hand transmitted vibration forms an essential basis to effectively evaluate vibration exposures, vibration response of the coupled hand-tool

291

system and to investigate the potential injury mechanisms. Despite the fact that the biodynamic responses of the hand-arm system have been measured in many studies under carefully controlled test conditions, considerable differences are known to exist among the data and the conclusions regarding the influence of different contributory factors reported by different investigators. Such differences in the reported data and conclusions could be attributed to complex nature of the hand-arm system and other factors related to differences in the experimental setup, measurement systems, and dynamic characteristics of the handle. There is thus a need for additional data measured under comparable and representative conditions to help identify definite trends and to gain an insight into the coupling influences among the different factors. On the other hand, it has been reported that the mechanism leading to WFV disorders may be related to local concentration of hand-handle contact pressure and thus the impaired blood flow, it was hypothesized that local concentration of contact pressure together with the hand-transmitted vibration may be related to causation of the VWF.

7.2   Major Contributions of the Dissertation Research

The primary focus and major contributions of this thesis research include: (i) thorough analyses of different definitions of the hand forces, a methods of measuring the static contact force at the tool handle–hand interface, and to identify a relationship to obtain an estimate of the contact force from the measurable hand grip and push forces; (ii) study the influence of handle size, grip and the push forces on the hand-handle interface peak pressure and distribution in view of sustain pressure (SP) and pressure discomfort (PDT) thresholds; (iii) characterization of biodynamic responses in terms of DPMI and absorbed power through measurements, and analyses of the influence of

different contributory factors; and (iv) development of mechanical-equivalents models of the hand-arm system which could be applied under a wide range hand forces. The major highlights and contributions of this dissertation research are summarized in the following sections.

### 7.2.1  Definition and measurement of static contact force

Owing to the strong dependence of the health risks associated with vibration exposure of the human hand and arm on the hand forces imparted on the tool, a laboratory study was performed to measure the contact force at the tool handle–hand interface. The measured data were analyzed to identify the relationships between the contact force and the relatively easily measurable hand grip and push forces as a function of the handle size. A simulated tool handle fixture was realized to measure the grip and push forces using force sensors integrated within the handle and a force plate. The contact force was derived through integration of the interface pressure over the contact area. These were measured using a capacitive pressure-sensing grid at the laboratory of the Institut de recherche Robert-Sauvé en santé et en sécurité du travail du Québec (IRSST) and at the US National Institute for occupational health and safety (NIOSH). The hand–handle interface pressure data were analyzed to derive the contact force, as functions of the constant magnitudes of the grip and push forces, and the handle size. The measurements were performed with 10 male subjects and three circular cross-section at NIOSH laboratory and 7 male subjects and six handles of different sizes and shapes at IRSST laboratory under different combinations of grip and push forces. The study resulted in a regression relationship for estimating the hand-handle contact force from the measurable grip and push forces.

293

### 7.2.2 Pressure distribution at hand-handle interface

The distribution of localized pressure peaks over the hand surface were investigated through measurements performed under applications of different combinations of hand grip and push forces. Three different cylindrical handles of 30, 40 and 48 mm were used to measure the hand-induced forces and distributed pressures using a capacitive pressure-sensing mat wrapped around the handle. The hand-handle pressure distributions acquired at the NIOSH laboratory were analyzed using the *EMED* software to determine the magnitude of peak pressures and their locations, and mean pressures within specified regions of palm and fingers as functions of the grip and push forces and handle size. The study provided an elaborate methodology to assess the pressure distributions in relation of *SP* and *PDT*, and proposed relations to determine the pressure peaks from the measurable grip and push forces. The hand surface was divided into 5 zones to study the localized peak pressures and contact forces developed within each zone. The measured data were further analyzed to identify the magnitudes and locations of localized pressure peaks occurring at the hand surface in view of the *SP* and *PDT*.

### 7.2.3 Driving-point mechanical impedance (*DPMI*) of the human hand-arm system

The driving-point mechanical impedance has been investigated and employed to characterize the biodynamic response of the hand-arm system. Even though the *DPMI* does not directly relate to tissue loading and dynamics of the musculoskeletal structure of the hand-arm system, the *DPMI* modulus and phase fully describe the overall mass-spring-damper-like behavior of the hand-arm system. The *DPMI* can thus be effectively applied to estimate the amount of mechanical energy dissipated by the hand-arm structure under a specified hand tool vibration spectrum. The reported *DPMI* data with the effects

of contributory factors differ remarkably. An extensive study was thus undertaken to measure the *DPMI* response of the seven male subjects under relatively wide realistic test conditions. Six instrumented cylindrical handles with different sizes and shapes were designed and instrumented to provide measures of the static and dynamic hand-handle forces and acceleration at the driving point. The handle were mounted, independently, on an electrodynamic shaker system through a support fixture and two force transducers to measure the static and dynamic push force. The handle and the support structure were oriented in two different arrangements to simulate the $z_h$- and $x_h$-axes of vibration to study the biodynamic response of the human hand-arm exposed to vibration along these two axes. The *DPMI* was measured under two levels of broadband random excitations in the 8–1000 Hz frequency range and nine different grip and push forces combinations. Same test conditions have been repeated under two hand-arm postures to study the influence of the posture and its conjunctions with other contributory factors on the *DPMI* responses. The experiments were performed at the IRSST laboratory. ANOVA analyses have been performed to examine the influence of different contributory factors on the *DPMI* magnitude response in different frequency bands.

The major contribution of this component of the study includes the analyses of various contributory factors on the *DPMI* responses, namely, handle geometry, handle size, hand-arm posture, vibration level, and hand grip and push forces. The study also presented correlations of the *DPMI* magnitude response with the hand-handle coupling and contact forces.

### 7.2.4 Absorbed power by hand-arm system

It has been reported that the absorbed power by the human hand-arm system exposed to vibration could be a better estimate of the exposure than the frequency-weighted acceleration, as recommended in the ISO 5349-1 for the risk assessment of hand-transmitted vibration. Unlike the *DPMI*, which is almost independent of the vibration magnitude, significantly higher magnitudes of absorbed power are obtained under higher vibration magnitudes. Many studies have reported strong effects of different contributory factors on the absorbed power, such as the intensity, frequency and direction of vibration, as well as the grip and push forces exerted on the handle. However, their findings are somewhat contradictory, the differences in the reported absorbed power data could be observed not only in the absorbed power values, but also in relation to other intrinsic and extrinsic factors. The absorbed power by the hand-arm system for seven male subjects has been measured under the same test conditions of the *DPMI* measurements. Inter-subject variability and the coefficient of variation of the measured individual total absorbed power and the absorbed power in the one-third octave band has been computed. The analyses of the mean measured data have been performed to study the influence of different contributory factors on the total absorbed power and on the absorbed power in the one-third octave bands under vibration along the $z_h$- and $x_h$-axes in the of 8-1000 Hz frequency range. The results and conclusion were supported by statistical analyses.

The major contributions of this work involved the analyses of power absorption data in light of various intrinsic and extrinsic factors. These included the handle size and geometry, the vibration levels, hand forces (grip, push, coupling and contact) and hand-arm posture. The results data analyses in the different frequency bands suggested

296

vibration frequency range for potential applications in define an adequate frequency-weighting.

### 7.2.5 Development of mechanical-equivalent biodynamic models

Biodynamic models of human hand and arm have been proposed to characterize the vibration amplitude and power flow in the coupled hand, tool and work piece system. The applications of mechanical equivalent or biodynamic models of the human hand and arm offer considerable potential to carry out assessments through both analytical and experimental analyses, where the involvement of human subjects could be considerably reduced. However, none of reported model could be successfully applied to study the coupled hand-tool system behavior under different conditions. Moreover, the models are considered valid only in the vicinity of the selected test condition and hand forces. The major contributions of this work involved a correction of conceptual mistake concerning the number of DOF of the reported models. Consequently, the resonant frequencies of the model could be related to the of the apparent mass magnitude peaks. A new approach of modeling the hand-arm system has been proposed by using both the *DPMI* and absorbed power responses as the target functions, over a wide range of hand forces. The proposed models are thus considered valid over a range of hand forces.

### 7.3 Major Conclusions

From the results of the experimental and analytical studies on the static contact force and pressure distributions at hand-handle interface and hand-arm biodynamic responses to vibration, the following major conclusions are drawn:

- The hand-handle interface contact force varies as a linear combination of the grip and push forces and the handle diameter. The hand–handle contact force for a

297

given handle size could be derived from a linear combination of the grip and push forces, where the contribution due to grip force is considerably larger. The variations in push force tend to cause a constant shift in the contact force over the entire range of grip forces. The rate of change of contact force with respect to push force was observed to be comparable for all handle sizes and shapes, suggesting that the contact force is relatively less sensitive to handle size and shape. The rate of change of contact force with respect to grip force, however, tends to be much higher for smaller handles.

- The dependence of the grip force and consequently the contact force on the handle diameter can be accurately described by a linear function in handle diameter. A relationship is formulated to characterize the hand contact force on the basis of the linear combination of grip and push forces in conjunction with linear variations in the handle size.

- The proposed linear relationship could be conveniently applied to obtain good estimate of hand-handle contact force from the directly measurable grip and push forces.

- The magnitudes and distribution of hand-handle interface pressure during a gripping and pushing task vary considerably with the applied grip and push forces, and the handle diameter. The pressures of considerable magnitudes develop within the hand-handle interface, under high grip and/or push forces. Application of high grip and push forces causes the peak pressures to exceed the discomfort threshold values, specifically for the thenar eminence, when a large size handle is used.

- The peak pressure for a given handle size could be estimated from a linear combination of the directly measurable grip and push forces, where the weighting of the grip force is considerably higher than the push force. A large size handle yields higher magnitude of interface peak pressure, while the small handle causes higher contact force, suggesting more uniform pressure distribution over the smaller size handles. Owing to the difficulties associated with measurement of the interface pressures, the proposed relationships could be conveniently applied to obtain an estimate of the mean values of peak pressures on the basis of directly measurable grip and push forces.

- The locations of localized pressure peaks in the operator's hand vary considerably with handle size and applied grip/push forces. The large size handle considered in this study causes the pressure peaks to occur in the lateral side of the palm for the entire range of grip and push forces considered.

- The proportions of hand-handle contact force developed within different hand zones also vary linearly with grip and push forces, and strongly depend upon the handle size. The results show that the contact force developed in the vicinity of proximal phalanges of the digits and the palm is generally attributed to the push force, while forces at the fingers surface are caused by the gripping action.

- In spite of the considerable variations observed in the biodynamic responses in terms of *DPMI* and absorbed power among the individuals under both vibration axes considered in this research work, definite trends in the responses could be observed with regards to the variations in the main factors considered in the study.

- The biodynamic responses of the hand arm system exposed to vibration is dependent upon many contributory factors such as, vibration axis, excitation frequency, grip and push forces, handle size and shape, and hand arm posture. The influences of different contributory factors, however, are coupled in a complex manner, as observed from two-way interactions of different factors, e.g. the effect of hand-arm posture is more evident under $z_h$-axis vibration than that of $x_h$-vibration.

- The *DPMI* responses vary considerably with variations in the grip and push forces combination and handle size. An increase in either the grip or the push force resulted in higher peak magnitude of *DPMI* and the corresponding frequency under both $x_h$- and $z_h$-axes vibration, suggesting the stiffening of the hand-arm system.

- The magnitude of *DPMI* and absorbed power under $z_h$-axis vibration are better correlated with the coupling force, defined as the direct sum of grip and push forces, at frequencies below 200 Hz, while at frequencies above, the correlation was better with the contact force.

- The handle size revealed a considerable influence on the *DPMI* magnitude response, particularly near the frequencies of peak magnitudes and at high frequency under both considered vibration axes. A larger handle caused remarkably higher *DPMI* magnitude at higher frequencies. A larger handle also causes high interface pressure peaks.

- Hand-arm posture has obvious influence on the biodynamic responses of the hand-arm system exposed to vibration, specifically under $z_h$-axis vibration. The

posture with extended forearm (180° elbow flexion) yields relatively stronger coupling with the vibrating handle at low frequencies. The low frequency apparent mass magnitude of the hand-arm under this posture is approximately three times than that measured with the bent forearm posture (90° elbow flexion). The influence of variations in the push and grip forces on the impedance magnitude and absorbed power, specifically at low frequencies, is more obvious under the extended-arm posture, than those under the bent-elbow posture.

- The extended arm posture yields considerably larger absorption power than the bent elbow posture, and causes transmission of significant vibration to the upper body.

- Depending on the axis of vibration, handle size, vibration level, and grip and push forces, the total power absorbed by the extended hand-arm posture could be up to 96 % higher than that of the hand-arm posture with the bent elbow.

- The absorbed power results suggest that 75 to 89 %, 90 to 95% and 96-98% of the total power is dissipated in the 8-50 Hz, 8-100 Hz and 8-200 Hz frequency ranges, respectively, irrespective of the excitation magnitude, handle size and hand forces under $z_h$-axis vibration. While the results show 55 to 63 %, 65 to 81% and 86-92% of the total power is dissipated in the 8-50 Hz, 8-100 Hz and 8-200 Hz frequency ranges, respectively, irrespective of the excitation magnitude, handle size and hand forces under $x_h$-axis vibration.

- The frequency-weighting defined in the current standard (ISO-5349-1) emphasizes the importance of transmitted vibration up to 16 Hz, it suppresses the vibration at frequencies above 16 Hz at a rate of dB/decade. The results obtained

in this study suggest that the weighting function may provide an underestimate of the injury potential, and should be different for exposure under different axis of vibration. The cut-off frequency of the recommended weighting function in the order of 50 Hz and 100Hz for $z_h$- and $x_h$-axes vibration, respectively, may better represent the power dissipation properties of the human hand and arm exposed to hand-transmitted vibration.

- A new approach of modeling the hand-arm system has been proposed by using both the *DPMI* and absorbed power responses as the target functions to improve the validity and capability of the analytical model. A conceptual mistake has been corrected concerning the number of DOF of the reported models. Consequently, the resonant frequencies of the system are related to the apparent mass magnitude peaks.

- The proposed model can effectively be applied for practical ranges of hand forces, the model parameters could be identified as functions of both the grip and push forces. The proposed models for $z_h$- and $x_h$-axes of vibration showed reasonably good agreement with both the measured responses, *DPMI* and absorbed power. The vibration properties of the proposed models could be considered appropriate in view of the practical issues related to model implementation, namely static deflection, damping ratio and damped frequencies.

- The absorbed power under $z_h$-axis vibration is much higher than that under $x_h$-axis. It is recommended to orient the power tools, if the work permits, such that the dominant vibration occurs along the $x_h$-axis. Extended arm posture also yields higher absorbed power than the posture with the bent elbow. Working with the

bent elbow posture is thus recommended, whenever the work environment permits.

## 7.4 Recommendations for Future Research Work

Characterization of human responses to vibration and understanding of the injury mechanisms would require extensive efforts at the fundamentals levels. The future directions in this field may include some of the following tasks:

- Measurements of the blood flow to the fingers, under vibration, with the conjunction of the hand-hand interface peak pressure data could provide considerable knowledge on the mechanism causing the onset of VWF syndrome at fingers tips.

- The hand-arm models, proposed in this dissertation, could be utilized in conjunction with models of the power tools and field measured vibration data to study the influence of different operating and design parameters, and to design effective vibration isolators.

- Performing the measurement of vibration transmissibility to different parts of the hand-arm system such as the wrist, elbow and shoulder joints. Could help understand the transmission of vibration to the upper body, particularly under different postures.

- The vibration transmissibility data would also contribute to more effective mechanical and bio-mechanical models of the hand-arm system.

- Measurements of contact force and pressure distribution under dynamic conditions could provide considerable insight into potential mechanism causing impaired blood flow to fingers.

303

- Apply more than two hand-arm postures in the measurement of hand-arm biodynamic response and study the effects of typical operating postures on the *DPMI* and dissipated power responses. This would also permit the development of hand-arm analytical models generally applicable for different hand-arm postures.

- Application of different vibration spectra, such as sinusoidal, constant velocity random excitations and typical power tools spectra should be undertaken to study the influence of vibration type on the hand-arm system biodynamic response, particularly the non-linear behavior of the hand-arm system. Further investigations on the conjunctions of vibration type with other contributory factors are also suggested.

- Further research work on the handle design would be desirable to seek more uniform hand-handle interface pressure distribution.

- Further investigations may be conducted to study the influence of tool weight and work posture on the hand-arm biodynamic response to vibration.

- More research work may be performed on the optimal hand-arm posture for operators of different power tools under variations in the work conditions.

- Studies are needed to measure and determine the dynamic response of the hand-arm muscles, and its relationships with the hand-arm biodynamic response, interface hand-handle pressure distribution and its associations with fatigue and stress experienced by the operator. Such investigations would permit identification of safer operating work conditions.

# REFERENCES

Abrams, C.F. 1971: Modeling the vibration characteristics of the human hand by the driving point mechanical impedance method, PhD Thesis, North Carolina State University, USA.

ACGIH 1990: American Conference of Government Industrial Hygienists. *Threshold Limit Values for Vibration.* Ohio, USA.

ACGIH 1998: American Conference of Government Industrial Hygienists. *Threshold Limit Values for Chemical Substances and Physical Agents & Biological Exposure Indices.* Ohio, USA.

Amis, A.A. 1987: Variation of finger forces in maximal isometric grasp tests on a range of cylindrical diameters. *Journal of Biomedical Engineering,* 9, pp. 313-320.

ANSI-S3.34, 1986: Guide for the Measurement and evaluation of human exposure to vibration transmitted to the hand, *American National Standards Institute,* New York, USA.

Armstrong, T.J., Buckle, P., Fine, L.J., Hagberg, M., Jonsson, B., and Kilbom, A. 1993: A conceptual model for work-related neck and upper-limb musculoskeletal disorders, *Scandinavian Journal of Work, Environment and Health,* 19, pp.73–84.

Ayoub, M. and Lo Presti, P. 1971: The determination of an optimum size cylindrical handle by use of electromyography, *Ergonomics,* 4(4), pp. 503-518.

Banister, P. A. and Smith, F. W. 1972: Vibration induced white fingers and manipulative dexterity, *British Journal of Industrial Medicine,* 29, pp. 264-267.

Bendat, J. and Piersol A.G. 1986: Random data; analysis and measurement procedures, *John Wiley & Sons,* second edition, New York, USA.

Bernard, D. 1990 : Etude de la masse du systeme main-bras et de l'activite musculaire correspondante lors d'une simulation de brise-breton, *Institue National de Recherche et de Sécurité,* Report MAV-DT-140/DB.

Bernard, B.P. 1997: Musculoskeletal disorders and workplace factors: a critical review of epidemiologic evidence for work-related musculoskeletal disorders of the neck, upper extremity, and low back, *United States Department services,* Cincinnati, USA.

Björing, G., Johansson, L. and Hägg, G. M. 2002: Surface pressure in the hand when holding a drilling machine under different drilling conditions, *International Journal of Industrial Ergonomics,* 29, pp. 255-261.

305

Blackwell, J.R., Kornatz, K.W., Health, E.M., 1999. Effect of grip span on maximal grip force and fatigue of flexor digitorum superficialis. *Applied Ergonomics*, 30, pp. 401-405.

Bovenzi, M. 1990: Medical aspects of the hand-arm vibration syndrome. *International Journal of Industrial Ergonomics*, 6, pp. 61-73.

Bovenzi, M. 1993: Digital artery responsiveness to cold in healthy men, vibration white finger and primary Raynaud's phenomenon. *Scandinavian Journal of Work, Environment and Health*, 19, pp. 271–276.

Bovenzi, M. 1997: Hand-transmitted vibration. *In: Encyclopedia of Occupational Health and Safety*, 4th Edition. ILO, Geneva, Vol II, pp 50.7-50.12.

Bovenzi, M., Lindsell, C.J. and Griffin M.J. 2000: Acute vascular responses to the frequency of vibration transmitted to the hand, *Occupational and Environmental Medicine*, 57 , pp. 422–430.

Brammer A. 1984: Exposure of the hand to vibration in industry. Publication No. NRCC 22845, *National Research Council*, Ottawa, Canada.

BSI 6842, 1987: British standard guide to the measurement and evaluation of human exposure to vibration transmitted to the hand, *British Standards Institution*, London, England.

Bullinger, H.-J.,.Muntzinger, W.F and Lauster,P. 1989: Numeric simulation of hand-transmitted vibrations. *Advances in Industrial Ergonomics & Safety I* (A. Mital (editor), London: Taylor & Francis, pp. 575-582.

Burström, L. and Lundström, R. 1988: Absorption of vibration energy in the human hand-arm exposed to sinusoidal vibration, *International Archives of Occupational Environmental Health*, 61, pp. 213-216.

Burström, L. and Lundström, R. 1989: Energy absorption in the human hand-arm while exposed to vibration; *Proceeding of the 5$^{th}$ International Conference on Hand-Arm Vibration*, Kanazawa, Japan.

Burström, L. and Lundström, R. 1992: Determination of mechanical energy absorption in the human hand-arm whilst exposed to vibration; *Proceeding of the 6$^{th}$ International Conference on Hand-Arm Vibration*, Bonn, Germany.

Burström, L. 1990: Measurements of the impedance of the hand and arm. *International Archives of Occupational and Environmental Health*, 62, pp. 431–439.

Burström, L. 1990: Absorption of vibration energy in the human hand and arm, Ph.D. Thesis, Luleå University of Technology, Luleå, Sweden.

Burström, L. 1994: The influence of individual factors on the absorption of vibration energy in the hand and arm. *Journal of Low Frequency Noise and Vibration*, 13(4), pp. 115-122.

Burström, L. and Lundström, L. 1994: Absorption of vibration energy in the human hand and arm, *Ergonomics*, 37(5), pp. 879-890.

Burström, L. 1997: The influence of biodynamic factors on the mechanical impedance of the hand and arm. *International Archives of Occupational Environmental Health*, 69, pp. 437-446.

Bylund, S.H., Burström, L. 2003: Power absorption in women and men exposed to hand-arm vibration, *International Archives of Occupational Environmental Health*, 76, pp. 313-317.

Chaffin, D.B. and Anderson, B.J. 1984: *Occupational Biomechanics, John Wiley $ Sons*, New York.

Chen, Y., 1991: An evaluations of hand pressure distribution for a power grasp and forearm flexor muscle contribution for a power grasp on cylindrical handles. Ph.D. thesis, University of Nebraska, Nebraska.

Cherian, T. 1994, Control of hand-transmitted vibration through development and analysis of a human hand-arm-isolator model, MSc Thesis, Concordia University, Montreal, Canada.

Cherian, T., Rakheja, S. and Bhat, R.B. 1996: An analytical investigation of an energy flow divider to attenuate hand-transmitted vibration, *International Journal of Industrial Ergonomics*, 17, pp. 455-467.

Chetter, I. C., Kent P. J. and Kester R. C. 1997: The hand arm vibration syndrome: a review, Cardiovascular Surgery, 6, pp. 1-9.

Chiang, H., Ko, Y., Chen, S., Yu, H., Wu, T., and Chang, P. 1993: Prevalence of shoulder and upper-limb disorders among workers in the fish-processing industry, *Scandinavian Journal of Work, Environment and Health*, 19, pp.126–131.

Cronjäger, L. and Hesse, M., 1989: Hand-arm system response to stochastic excitation, *Proceeding of the 5th International Conference on Hand-Arm Vibration*, Kanazawa, Japan.

Cundiff, J. S. 1976: Energy dissipation in human hand-arm exposed to random vibration, *Journal Acoustic Society of America*, 59, pp. 212-214.

Daikoku, M. and Ishikawa, F. 1989: Mechanical impedance and vibration model of hand arm system, *Proceeding of the 5th International Conference on Hand-Arm Vibration*, Kanazawa, Japan.

Danuta, R. 2003: Maximum Handgrip, Force in Relation to Upper Limb Posture -A Meta-Analysis, *AIHA Journal*, 64(5), pp.609-617.

Donati, P., Bitsh, J. and Bernard, D. 1992: Measurement of the apparent mass and loads on muscles of the hand and arm during simulated breaker operation. *Proceeding of the 6th International Conference on Hand-Arm Vibration*, Bonn, pp. 411-423.

Dong, R., Rakheja, S., Schopper, A.W., Han, B. and Smutz W.P. 2001: Hand-transmitted vibration and biodynamic response of the human hand-arm: a critical review, *Critical Reviews in Biomedical Engineering*, 29(4), pp. 393–439.

Dong, R., Schopper, A.W., McDowell, T. W., Welcome, D. E., Wu, J. Z., Smutz W.P., Warren, C. and Rakheja, S. 2005: Vibration energy absorption (VEA) in human fingers-hand-arm system, *Medical Engineering & Physics*, 26 (6), pp. 483-492.

EN-420, European Committee for Standardization, 1994. General requirements for gloves. European Committee for Standardization.

Engstrom, K. and Dandanell, R. 1986: Exposure conditions and Raynaud's phenomenon among riveters in the aircraft industry. *Scandinavian Journal of Work Environment Health*, 12, pp. 293–295.

Fellows, G. L. and Freivalds, A. 1991: Ergonomics evaluation of a foam rubber grip for tool handles, *Applied Ergonomics*, 22, pp. 225-230.

Fransson, C. and Winkel, J. 1991: Hand Strength: The influence of grip span and grip type. *Ergonomics*, 34 (3), pp. 881-892.

Fransson-Hall, C. and Kilbom, A. 1993: Sensitivity of the hand to surface pressure, *Applied Ergonomics*, 24, pp. 181-189.

Fridén, J. 2001: Vibration damage to the hand: clinical presentation, prognosis and length and severity of vibration required, *The Journal of Hand Surgery*, 26B, pp. 471-474.

Freivalds., A. 2004: Biomechanics of the Upper Limbs Mechanics, Modelling and Musculoskeletal Injuries, *CRC press*.

Gemme, G. and Taylor W. 1983: Foreword: Hand-arm Vibration and the central autonomic nervous system, *Journal of Low Frequency Noise and Vibration*, Special Volume: 1-12.

Gemne G. and Saraste, H. 1987: Bone and joint pathology in workers using hand-held vibrating tools: An overview, *Scandinavian Journal of Work, Environment and Health*, 13, pp. 290–300.

Gemne, G., Diagnostics of hand-arm system disorders in workers who use vibrating tools. *Occupational and Environmental Medicine*, 1997, 54: 90-95.

Gierke V. H. 1971: Guide of the evaluation of human exposure to hand-transmitted vibration. *International Standard Organization*, ISO/TC 108, Geneva, Switzerland.

Griffin, M.J. 1990: Handbook of Human Vibration, *Academic Press*, London.
Griffin, M.J. 1998: Evaluating the effectiveness of gloves in reducing hazards hand-transmitted vibration. *Occupational and Environment Medicine*, 55, pp. 340-348.

Girden, E.R. 1992: ANOVA: repeated measures, *Sage Publications*, Newbury Park, California.

Gurram, R. 1993: A study of vibration response characteristics of the human hand-arm system, Ph.D. Thesis, Concordia University, Montreal, Canada.

Gurram, R., Rakheja, S. and Brammer, A.J. 1995: Driving-point mechanical impedance of the human hand-arm system: Synthesis and model development, *Journal of Sound and Vibration*, 180, pp. 437-458.

Gurram, R., Rakheja, S. and Gouw, G.J. 1995: A study of hand grip pressure distribution and EMG of finger flexor muscles under dynamic loads. *Ergonomics*, 38(4), pp. 684-699.

Hall, N.B., Bennett, E.M. 1956: Empirical assessment of handrail diameters, *Journal of Applied Psychology*, 40, pp. 381-382.

Hartung, E. Dupuis H. and Schäfer M. 1993: Effects of grip and push forces on the acute response of the hand-arm system under vibrating conditions. *International Archives of Occupational and Environmental Health*, 64, pp. 463-467.

Hempstock, T.I. and O'Connor, D.E. 1989: Measurement of impedance of hand arm system. *Proc. Inst. of Acoustics*, 11(9), pp. 483-490.

Hill. E. C. , Langis J. W., Petherick J. E., Campbell D., Haines T. , Andersen J., Conley K. K., White J., Lightfoot N. E. and Bissett R. J. 2001: Assessment of Hand-Arm Vibration Syndrome in a Northern Ontario Base Metal Mine, *Chronic Diseases in Canada*, 22, pp. 88-92

ISO 10819, 1996: Mechanical vibration and shock – Hand-arm Vibration – Method for the measurement and evaluation of the vibration transmissibility of gloves at the palm of the hand, *International Standard Organization*, Geneva, Switzerland.

ISO 8727, 1997: Mechanical vibration and shock, Human exposure, Biodynamic coordinate systems, *International Standard Organization*, Geneva, Switzerland.

ISO 10068, 1998: Mechanical vibration and shock – Free, mechanical impedance of the human hand-arm system at the driving point, *International Standard Organization*, Geneva, Switzerland.

ISO 5349-1, 2001: Mechanical vibration – Measurement and evaluation of human exposure to hand-transmitted vibration- Part 1: General guidelines, *International Standard Organization*, Geneva, Switzerland.

ISO/WD 15230, 2004: Definition and guidelines for the measurement of the coupling forces for operators exposed to hand-arm vibration, *International Standard Organization*, Geneva, Switzerland.

Iwata, H., Dupuis, H. and Hartung, E., 1972: Ubertrang von horizontalen sinusschwingungen auf die oberen extremitaten bei halbpronationsstellung und reaktion des m biceps. *Int. Arch. Arbeitsmed*, 30, pp. 313-327.

Jahn, R. and Hesse, M. 1986: Applications of hand–arm models in the investigation of the interaction between man and machine, *Scandinavian Journal of Work, Environment and Health*, 12, pp. 343–346.

Jandak, Z. 1989: Energy transfer to the hand-arm system at exposure to vibration, *Proceeding of the 5th International Conference on Hand-Arm Vibration*, Kanazawa, Japan, 1989.

Jandák Z. 1998: Driving-point mechanical impedance of the hand-arm system at exposure to stochastic vibration, *Proceeding of the 8th International Conference on Hand-Arm Vibration*, Umeå, Sweden, pp. 369-375.

Johansson, L., Kjelberg, A., Kilbom, A. and Haag, G. M. 1999: Perception of surface pressure applied to the hand, *Ergonomics*, 42(10), pp. 1274-1282.

Kattel, B.P., Fredericks, T.K., Frenandez, J.E. and Lee, D.C. 1996: The effect of upper extremity posture on maximum grip strength, *International Journal of Industrial Ergonomics*, 18, pp. 423-429.

Kattel, B.P. and Fernandez, J. E. 1999: The effect of rivet gun on the hand-arm vibration, International Journal of Industrial Ergonomics, 23, pp. 595-608.

Kaulbars, U. 1996: Measurement and evaluation of coupling forces when using hand-held power tools, *Central European Journal of Public Health*, 4(1), pp. 57-58.

Kilbom, A. Makarainen, M. Sperling, L. Kadefors R.and Liedberg L. 1993: Tool design, user characteristics and performance: a case study on plate-shears, *Applied Ergonomics*, 24, pp. 221–230.

310

Kinne, J. and Melzig-Thiel, R. 1996: Derivation of mean impedance curves as a basis for mechanical models of the human hand–arm system. *Central European Journal of Public Health*, 40, pp. 53–56.

Kihlberg, S. 1995: Biodynamic response of the hand-arm system to vibration from an impact hammer and a grinder, *International Journal of Industrial Ergonomics*, 16, pp. 1-8.

Kong Y.K. and Lowe B.D. 2005: Optimal cylindrical handle diameter for grip force tasks, *International Journal of Industrial Ergonomics*, 35(6), pp.495-507.

Kuorinka, I. and Forcier, L. 1995: Work-related Musculoskeletal Disorders (WMSDs): A Reference Book for Prevention, *Taylor & Francis.*, London, England.

Kurozawa Y, Nasu Y, Hosoda T, Nose T. 200: Long term follow up study on patients with vibration induced white finger (VWF). *Journal of Occupational and Environmental Medicine*, 44(12), pp.1203-1206.

Kuzala, E. A., and Vargo, M. C. 1992: The relationship between elbow position and grip strength, *American Journal of Occupational Therapy*, 46, pp. 509-512.

Lee, Y.H. and Jiang, M.S. 1999: An ergonomic design and performance evaluation of pipettes. *Applied Ergonomics*, 30, pp. 487–493.

Li, K.W. 2002: Ergonomic design and evaluation of wire tying hand tools, *International Journal of Industrial Ergonomics*, 30 (3), pp. 149-161.

Lidström, I.M. 1977: Vibration injury in rock drillers, chiselers, and grinders. In: *Some views on the relationship between the quantity of energy absorbed and the risk of occurrence of vibration injury*, pp. 77–83.

Louda, L., Hartlova, D., Muff, V., Smolikova, L., and Svoboda, L. 1994: Impulsive vibration and exposure limit, *Nagoya Journal of Medical Science*, 57, pp. 165-172.

Lundström, R. and Burström, L. 1989: Mechanical impedance of the human hand-arm system, *International Journal of Industrial Ergonomics*, 3, pp. 235-242.

Mansfield, N. J. and Griffin, M. J., 1998: Effect of Magnitude of vertical whole-body vibration on absorbed power for the seated human body, *Journal of Sound and Vibration*, 215 (4), pp. 813-825.

Marley, R.J., DeBree T.S., and Wehrman, R. 1993: Grip strength as a function of forearm and elbow posture on maximum grip strength, *Second Industrial Engineering Research Conference Proceeding*, Los Angeles, USA, pp. 525-529.

McConnel, K.G. 1995: Vibration Testing: Theory and Practice, *John Wiley & Sons*, New York, USA.

Meagher, S.W. 1987: Tool design for prevention of hand and wrist injuries, *Journal of Hand Surgery*, 12(A), pp. 855-857.

Mendenhall, W. and Sincich, T. 1984: Statistics for the engineering and computer sciences, *Dellen Publications Co.*, San Francisco.

Mirbod, S. and Inaba, R. 1992: A study on the vibration-dose limit for Japanese workers exposed to hand-arm vibration, *Industrial Health*, 30, pp. 1–22.
Mishoe, J.W. and Suggs, C.W. 1977: Hand –arm vibration. Part II. Vibrational responses of the human hand, *Journal of Sound and Vibration*; 53, pp. 545-558.

Miwa, T. 1986: Evaluation methods for vibration effect: part 6. Measurements of unpleasant and tolerance limit levels for sinusoidal vibrations, *Industrial Health*, 6, pp. 18-27.

Miyashita, K., Shiomi, S., Itoh, N. Kasamatsu, T., and Iwata, H. 1983: Epidemiological study of vibration syndrome in response to total hand-tool operating time. *British Journal of Industrial Medicine*, 40, pp. 92–98.

Miyashita, T., Miura, H., Futatsuka, M., 1990: Hand-arm vibration, noise, temperature and static load: An experimental study of peripheral circulation while operating chain saws, *Kurume Medicine Journal*, 37, pp. 73-83.

Moore, J.S. 1992: Carpal tunnel syndrome, *Occupational Medicine*: State of the Art Reviews 7(4), pp.741-763.

Moore, J.S. and Garg, A. 1994: Upper extremity disorders in a pork plant: relationship between task risk factors and morbidity, *American Industrial Hygiene Association Journal*, 55, pp.703–715.

Moustafa, A.K. Reynolds D.D. 2004: Mechanical Impedance Characteristics of the Hand and Arm, *Proceeding of the 10th International Conference on Hand-Arm Vibration*, Las Vegas, USA.

Muralidhar, A. and Bishu, A. A. 2000: Safety performance of gloves using the pressure tolerance of the hand, *Ergonomics*, 43(5), pp. 561-572.

Nathan, P.A., Meadows, K.D. and Doyle, L.S., 1988: Occupation as a risk factor for impaired sensory conduction of the median nerve at the carpel tunnel. *Journal of Hand Surgery*, 13, pp. 167-170.

Necking, L. E., Lundborg, G., Lundström, R., Thornell, L. and Fridén, J. 2004: Hand muscle pathology after long-term vibration exposure, *Journal of Hand Surgery*, 29(5), pp. 431-437.

Nelson, C.M. and Griffin, M.J. 1993: Comparison of predictive models for vibration-induced white finger, *Proceeding Of the 6th International Conference On Hand-Arm Vibration*, Bonn, pp. 875-883.

Nerem, R.M. 1977: Vibration enhancement of blood-arterial wall macromolecule transport, *Proceeding of the International on Hand-Arm Vibration Conference*, pp. 37-41.

Nilsson, T., Hagberg, M., Burstrom, L. Kihlberg, S. and Lundström, R., 1993. Risk assessment of impaired nerve conduction at the carpel tunnel in relation to vibration exposure among platters and assemblers. *Proceeding of the 6th International Conference on Hand-Arm Vibration*, Bonn, Germany, pp. 395-402.

Nilsson, T. and Lundström, R. 2001: Quantitative thermal perception thresholds relative to exposure to vibration, *Occupational and Environmental Medicine*, 58, pp. 472-478.

NIOSH 1989: Criteria for a recommended standard, Occupational exposure to Hand-Arm Vibration. *National Institute for Occupational Safety and Health*, pp. 89-106.

NIOSH 1997: Musculoskeletal disorders and workplace factors: A critical review of epidemiologic evidence for work-related musculoskeletal disorders of the neck, upper extremity, and low back, *National Institute for Occupational Safety and Health*, Publication No. 97–141, Cincinnati, OH: U.S

NRC and IOM 2001: Musculoskeletal Disorders and the Workplace: Low Back and Upper Extremities, *National Academy Press*, Washington, DC.

Palmer, K., Griffin, M., Syddall, H., Pannett, B., Cooper, C. and Coggon D. 2001: Risk of hand-arm vibration syndrome according to occupation and sources of exposure to hand-arm transmitted vibration: a national survey. *American Journal of Industrial Medicine*, 39 (4), pp. 389-396.

Pelmear, P.L., Leong, D., Taylor, W., Nagaligam, M. and Fung, D. 1990: Hand-arm vibration syndrome health effects and safety standards. *Proceeding Of the 5th International Conference On Hand-Arm Vibration*, pp. 63-66.

Pelmear, P.L., Kusiak R. and Leong, D. 1995: Hand-arm vibration syndrome associated with impact vibration, *Journal of Low Frequency Noise and Vibration*; 14(2), pp. 73-79.

Pelmear, P., Taylor, and Wasserman, D.E. 1998: Hand-Arm Vibration: A Comprehensive Guide for Occupational Health Professionals-2nd Edition, *OEM Medical Publishers*, Beverly Farms, MA.

Pradko, F., Lee, R. A. and Greene, J. D. 1965: Human vibration-response theory, *American Society of Mechanical Engineering*, Paper No. 65-WA/HUF-19.

Pyykkö, I., Farkkila, M., Toivanen, J., Korhonen, O. and Hyvarinen, J. 1976: Transmission of vibration in the hand-arm system with special reference to changes in compression force and acceleration. *Scandinavian Journal of Work Environment and Health*, 2: 87-95.

Pyykkö, I. 1986: Clinical aspects of the hand-arm vibration syndrome. Scandinavian Journal of Work, *Environment and Health*, 12, pp. 439-447.

Radwin, R.G., Armstrong, T.J. and Chaffin, D.B. 1987: Power hand tool vibration effects on grip exertions, *Ergonomics*, 5, pp. 833-855.

Rakheja, S., Wu, J.Z., Dong, R.G., Schopper, A.W. and Boileau, P.E. 2002: A comparison of biodynamic models of human hand-arm system for applications to hand-held power tools, *Journal of Sound and Vibration*, 249, pp. 55-82.

Rakheja, S., Gurram, R., Gouw G.J. 1993: Development of linear and nonlinear hand-arm vibration models using optimization and linearization techniques, *Journal of Biomechanics*, 26(10), pp. 1253-60.

Reidel, S. 1995: Consideration of grip and push forces for the assessment of vibration exposure, *Central European Journal of Public Health*, 3, pp. 139-141.

Rempel, D.M., Harrison, R.J. and Barnhart, S. 1992: Work-*related cumulative trauma disorders of the upper extremity, Journal* of American Medical Association, 267, pp. 838-842.

Reynolds D.D. and Soedel, W. 1972: Dynamic response of the hand-arm system to sinusoidal input, *Journal of Sound and Vibration*, 21, pp. 339-353.

Reynolds, D. D. 1977: Hand-arm vibration; a review of three years research, *Proceeding of the 2th International Conference on Hand-Arm Vibration*, Cincinnati, pp. 99-128.

Reynolds D.D. and Keith R. H. 1977: Hand-arm vibration. Part I: Analytical model of the vibration response characteristics of the hand, *Journal of Sound and Vibration*, 51, pp. 237-253.

Reynolds, D.D. and Angevine, E.N. 1977: Hand-arm vibration. Part II: Vibration transmission characteristics of the hand and arm, *Journal of Sound and Vibration*, 51, pp. 255-265.

Reynolds, D.D. and Falkenberg, R.J. 1984: A study of hand vibration on chipping and grinding operators, Part II: Four-degree-of-freedom lumped parameter model of the vibration response of the human hand. *Journal of Sound and Vibration*, 95, pp. 499-514.

Roquelaure, Y., Mechali, S., Dano, C., Fanello, S., Benetti, F., Bureau, D., Mariel J., Martin Y-H., Derriennic F., and Penneau-Fontbonne, D. 1997: Occupational and personal

risk factors for carpal tunnel syndrome in industrial workers, *Scandinavian Journal of Work, Environment and Health*, 23, pp. 364–369.

Rosecrance, J. C. and Cook, T. M. 1998: Upper extremity musculoskeletal disorders: occupational association and a model for prevention, *Central European Journal of Public Health*, 4(3), pp. 214-231.

Schäfer, N. Dupuis H. and Hartung, E. 1984: Acute effects of shock-type vibration to the hand-arm system, *International Archives of Occupational Environment Health*, 55, pp. 49–59.

Sörensson, A. and Lundström, R. 1992: Transmission of vibration to the hand, *Journal of Low Frequency Noise and Vibration*, 11, pp. 143-144.

Sörensson, A. and Burström, L. 1996: Energy absorption of vibration in the hand for higher frequencies, *Journal of Low Frequency Noise and Vibration*, 15 (2), pp. 71-79.

Sörensson, A. and Burström, L. 1997: Transmission of vibration energy to different parts of the human hand-arm system, *Journal of Occupational and Environmental Health*, 70, pp. 199-204.

Sörensson, A. 1998: Energy absorption and transmission in hand and arm of during high frequency vibration and impact, Ph.D. Thesis, Luleå University of Technology, Luleå, Sweden.

Taylor, W., Wasserman, D., Behrens, V, Reynolds, D. and Samueloff, S. 1984: Effect of the air hammer on the hands of stone cutters, *British Journal of Industrial Medicine*, 41, pp. 289-295.

Thomson, W.T 1993: Theory of vibration with applications, *Prentice Hall*, Englewood Cliffs, NJ, USA.

Toppila, E., Starck, J. and Pyykkö, I., 1997: Transmission of vibration from the handle to hand, effect of biodynamic factors, *Advance in Occupational and Ergonomics Safety II*, pp. 507-511.

Turner, J.R and Thayer, J.F. 2001: Introduction to analysis of variance: design, analysis, & interpretation, *Sage Publications*, Thousand Oaks, California.

Walker, D., Jones, B. and Ogston, S. 1986, Occurrence of white finger in gas industry, *Scandinavian Journal of Environment and Health* 12, pp. 301-303.

Welcome, D., Rakheja, S. Dong, Wu J. Z. and Schopper A.W. 2004, An investigation on the relationship between grip, push and contact forces applied to a tool handle, *International Journal of Industrial Ergonomics*, 34 (6), pp. 507-518.